Targeted Copper (II) Compounds with Selective Anti – Cancer and Anti-Microbial Activity

A thesis submitted to Maynooth University in fulfilment of the requirements for the degree of

Doctor of Philosophy

by

Stephen Barrett, B.Sc. (Hons)

Department of Chemistry,

Maynooth University,

Maynooth,

Co. Kildare, Ireland

October 2021

Research supervisor: Dr Diego Montagner

Co – Supervisor: Dr Tobias Krämer

Head of Department: Prof. A. Denise Rooney

To my parents

True success is not the absence of failure,

It is the refusal to surrender.

Table of Contents

Acknowledgements

The completion of this thesis would not have been possible without the help of several people in my life. First and foremost, I would like to thank my supervisor Dr. Diego Montagner for his constant support, encouragement, and generosity of his time. Diego I couldn't have asked for a better mentor and friend during this project. It has been an absolute honour to work with you over the last four years. To my Co- Supervisor Dr. Tobias Krämer thank you also for being an inspiration and helping me overcome many difficult problems and learn new skills.

I would like to thank the Department of Chemistry in Maynooth as a whole for awarding me a graduate teaching fellowship which allowed me to opportunity to complete my PhD. Thank you to the heads of department during my time here, particularly Prof. Denise Rooney and Dr. Jennifer McManus. Thank you both for allowing me to carry out my research at Maynooth University. Thank you to all academic staff in the Chemistry Department for being there to help me throughout my PhD. Especially to Dr. Trinidad Velasco Torrijos for your valuable input and advice to many chemistry problems and for my cat! I would also like to thank all the collaborators I have worked with over the last four years including Prof. Kevin Kavanagh of the Department of Biology Maynooth, Prof. Valentina Gandin of the Department of Pharmacy in University Padova and Prof. Andrew Kellet from the Department of Chemistry DCU.

Thank you to all the technical and admin staff in the Department of Chemistry Maynooth for all your help over the years, particularly Barbara, Ria, Ken and Noel and of course Donna and Carol for all your help throughout my 10 years here.

I would like to thank all the postgraduates I have worked with past and present for making my time here very memorable and for all the coffee and pints. Especially to Luke M , Amanda and Conor Gero. To Dr. Ross Driver for your knowledge and patience when I started and for all the lovely brews and to Abby for all your love and friendship over the last years.

To all my friends from home particularly Gavin, Alan, Mick, Harry, Dan, Dolly, and the Yeti and all of "gamblor" for the countless laughs and variety of fun you provided me with during my PhD but also during my life in general. I couldn't ask for a better bunch of friends.

To Harlei for not only your relentless patience, but for your knowledge. Thank you for being there when no one else was and for the countless coffees and pints and for our trip to China,

but most of all for being my friend. You are a true shining star in an often-dark world. Thank you so much for your friendship and kindness and long may it continue.

Finally, I would like to thank my family. My mother Mary and father Andy for their continuing support throughout this journey and many potholes they lifted me out of. I thank both of you from the bottom of my heart for all your love and support. Dad you may be gone now but you're never forgotten, thank you for believing in me and for the many memories I have. May you rest in peace.

Declaration

I declare that the work presented in this thesis was carried out in accordance with the regulations of Maynooth University. The work is original, except where indicated by reference, and has not been submitted before, in whole or in part, to this or any other university for any other degree.

Signed: __ *Stephen Barrett*   Date: 28-10-21

Stephen Barrett, B.Sc. (Hons)

Abstract

The selectivity for cancer cells has always been one of the major challenges for anticancer drugs and, in particular, for metal-based agents, such as cisplatin. Despite the great success of the anticancer drug of cisplatin and of a few other Pt(II) compounds, such as carboplatin and oxalilplatin, the lack of selectivity, the high toxicity and the resistance mechanisms are limiting their use. There are several strategies that could be implemented to overcome the lack of selectivity and one of these is the use of specific vectors whose receptors are overexpressed in the cancer cells with respect healthy tissues (i.e. sugars and carbohydrates in general). Two very important vectors whose receptors are overexpressed are estrogens and biotin.

In this thesis we report the synthesis and characterisation of a plethora of completely novel Copper (II) based compounds whose coordination sphere has been modified to accommodate estrogens (Chapter 2) and biotin (Chapter 3), with the aim to enhance the tumour selectivity. The complexes have been successfully synthesised and characterised and their application as anticancer agents have been evaluated. The rationale for the use of Copper instead of Platinum is due to Copper being much less toxic than Platinum, being and endogenous metal, and for this reason it is more tolerable within the body. There are several examples of Copper based complexes with anticancer properties and it is interesting to note that Copper complexes show a different mechanism of action with respect Pt based ones. Copper, being a redox active metal with two available oxidation states in physiological conditions ($E^0_{Cu(II)/Cu(I)}$ = + 0.15 V) can interfere with the cellular redox stress and produce ROS (Reactive Oxygen Species) that can alter the cellular redox environment. In fact, mitochondria, where the cellular respiration process happens, are considered an important target for Cu complexes. The new complexes have been tested against a large panel of cancer cell lines, cells which both overexpress these corresponding receptors (estrogens or biotin) and ones which do not and very promising and interesting results are obtained. For some complexes the redox stress, the ROS production and the mechanism of cell death are reported. While mitochondria are considered the most important target of Copper based compounds, the mitochondrial and nuclear DNA also play a very important role. Depending on the nature of the ancillary ligands, Cu species can bind to the DNA forming several adducts. In Chapter 4 are described a series of novel Cu(II) species, containing different planar aromatic ligands (derivatives of DPPZ, dipyrido-phenazine), that can act as DNA intercalators, with the aim to investigate the role of the substituents (electron withdrawing or electron donating groups) on the biological properties. These complexes are synthesised

and characterised and their interaction with DNA is explored. A detailed and comprehensive theoretical characterisation is also reported. These complexes show very interesting antimicrobial properties against MRSA strain and antifungal activity against Candida Albicans.

Abbreviations

°C = Degrees Celsius

(CH3)2CO = Acetone

2008 = Human cervical

A3780 = Human ovarian cancer

A431 = Human epidermoid carcinoma

Ac = Acetyl

Aq = Aqueous

Ar = Aromatic

Atm = Atmospheric pressure

ATR = Attenuated Total Reflection

Boc = t-butyloxycarbonyl

BT-474 = Invasive ductal breast cancer

C. albicans = Candida albicans

$CDCl_3$ = Deuterated chloroform

CEM = T cell leukemia

CEM-VLB = Drug resistant leukemia

CEM-VLBb = Multi drug resistant T cell leukemia

$CHCl_3$ = Chloroform

COSY = Correlation Spectroscopy

d = doublet

d5-Pyridine = Deuterated pyridine

DCM = Dichloromethane

dd = doublet of doublet

DEPT = Distortionless enhancement by polarization transfer

DIPEA = Diisopropylethylamine

DMF = Dimethylformamide

DMSO = Dimethylsulfoxide

DNA = deoxyribonucleic acid

dppn = benzo[i]dipyrido[3,2-a:2′,3′-h] quinoxaline

dppz = dipyrido[3,2-a:2',3'-c] phenazine

dpq = dipyrido[3,2-d:2',3'-f] quinoxaline

DU145 = Human prostate cancer

E. coli = Escherichia coli

e.g., = Exempli gratia (Latin for 'for example')

EE = ethisterone

Equiv = Equivalents

ES = ethynylestradiol

ESI = Electrospray ionisation

Et2O = Diethyl ether

EtBr = Ethidium Bromide

EtOAc = Ethyl acetate

EtOH = Ethanol

FDA = food and drug agency

G. mellonella = Galleria mellonella

hrs = Hours

HCl = Hydrochloric acid

HCT-15 = Human colon carcinoma

HMBC = Heteronuclear Multiple Bond Correlation

HPLC = High Performance Liquid Chromatography

HR-MS = High Resolution Mass Spectrometry

HSQC = Heteronuclear Single Quantum Coherence

HT1080 = Human fibosarcoma

HT-29 = Human colorectal adeenocarcinoma

i.e., = Id est (Latin for 'that is')

IR = Infrared spectroscopy

K = Kelvin

LNCaP = Human prostate cancer

m = multiplet

M21 = Human melanoma

MCF-7 = Huaman breast cancer

MDA-MB-468 = Triple negative breast cancer

MeCN = Acetonitrile

MeOD = Deuterated methanol

MeOH = Methanol

mg = Milligram

MIC = Minimal Inhibitory Concentration

min = Minutes

mL = Millilitre

mm = Millimetre

MRSA = methicilin resistant Staphylcoccus aureus

NEt3 = Triethylamine

nm = Nanometre

NMR = Nuclear Magnetic Resonance

OH = Hydroxy group

PC3 = Human prostate cancer

Pd/C = Palladium on activated carbon

Pet Ether = Petroleum ether

phen = 1,10-phenanthroline

Rf = Retention Factor

RNA = ribonucleic acid

ROS = reactive oxygen species

rt = Room temperature

S. aureus = Staphylococcus aureus

SAR = Structure Activity Relationship

sat. = Saturated

sec = Seconds

t = triplet

TBTU = O-(Benzotriazol-1-yl)-N, N,N',N'-tetramethyluronium tetrafluoroborate

TFA = Trifluoroacetic acid

THF = Tetrahydrofuran

TLC = Thin Layer Chromatography

TOF = Time of Flight

μm = Micrometre

1   Chapter 1: Introduction

1.1   The role of metals in medicine

The role of metals in medicine is a very ancient tradition. Copper, Zinc and Gold have all infamously been used by our ancestors. The practice of using Copper and Zinc dates back as far as 3000 BC in Egypt. With Copper being used to sanitise water systems and Zinc being used in ointments to treat wounds. Gold has also played an important role in medicinal history, in ancient Chinese culture. Gold has been used to treat a range of ailments from around 3,500 years ago. The famous Egyptian medical papyrus known as *Papyrus Ebers* from 1500 BC describes the use of copper to treat inflammation and iron to treat anaemia. This document is the first known written account of the use of metals in medicine. Around 1500 AD Paracelsus, the Swiss doctor and alchemist was the first to recommend mineral substances such as mercury, arsenic and antimony salts for the treatment of human diseases, those of which included cancer. In the early 17th century, Nicholas Culpeper marketed his gold-based therapeutic elixir, better known as "Goldwasser" or "Aurum Potabile" which was considered an effective treatment of the loss of "vital spirit", such as melancholy states or weakness.

From the beginning of the 20th century, metal-based compounds have demonstrated a growing role of importance within the medicinal field. *Ehrlich et al.* in 1909 discovered the activity of the arsenic containing compound arsenphenamine against syphilis, which was then subsequently marketed under the name of salvarsan.[1] During the same period, Koch was working with gold cyanide for the treatment of tuberculosis (Figure 1.0). In 1912, antimony-based compounds were introduced for the treatment of leishmaniosis [2] and an iron chelating compound, deferoxamine, was brought to light for the treatment of malaria. In 1965 the discovery of cisplatin by chance by Barnett Rosenberg would pave the way for metal-based compounds as viable chemotherapy options as their pharmacokinetics and mechanism of action were very different than any organic and biological drug available. The development of metal-based therapeutics has played a huge role in anti-tumour medicines. Metal based compounds offer great versatility not often displayed by their rival organic or biological counterparts. This can be due to a number of effects displayed by the metal complex. Ligand exchange is possible within the cell or within the biological system, increasing potency and the duration of the therapeutic effect. The various oxidation numbers displayed by the metal centre can encourage the generation of ROS through redox in the cell which in turn can have a combined therapeutic effect.[3]
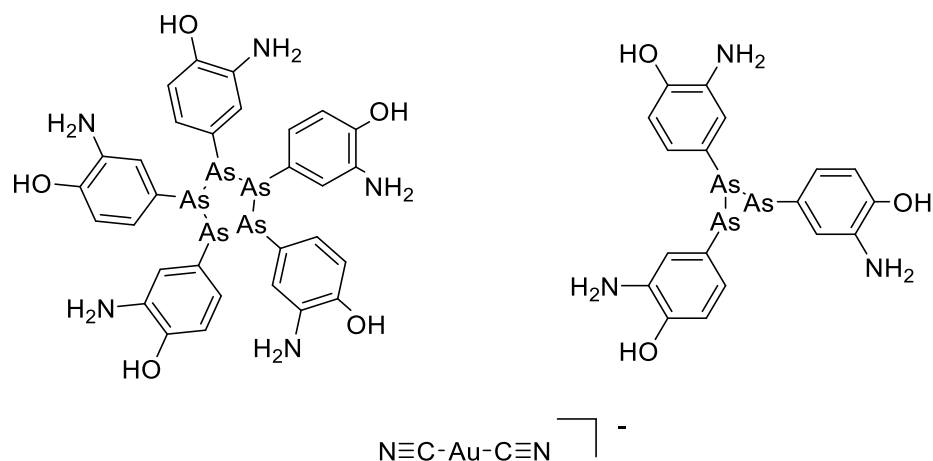
Figure 1.0: Structures of pentamer and trimer of the arsenic drug salvarsan and also the gold complex dicycano aurate by Koch *et al.*

It has also been displayed the combined pharmacological effect of the ligand and the metal centre has a far higher therapeutic effect than either the free metal or free ligand alone.[4] Other aspects influencing the activity of the metal complexes are the coordination number, the electric charge and the hydrophilicity or lipophilicity. Most often, the metal-based drugs are prodrugs, therefore only becoming active after undergoing ligand exchange or reduction within the cellular medium. After this initial step, the metal-based drug is now free to interact with its target.

With this in mind grave thought must be considered when developing metal based drugs as metal intoxication or metal poisoning is a serious drawback.[5] Despite this issue, metal-based compounds have considerable advantages over organic based molecules and these differences can be exploited to design new metal-based therapeutics. In conclusion the variables which are responsible for the activity of the metal-based drugs are vast and therefore both *in vitro* and *in vivo* studies are necessary in order to understand their mode of action and pharmacological target. There are currently several metal complexes used for the treatment of different diseases: gold complexes have been used since 1935 in the treatment of rheumatoid arthritis, first in polymeric form and later in the form of monomers such as auranofin. Unlike other gold complexes with anti-arthrosis properties which are for parenteral use, auranofin is administered orally and is currently used in phase I and II clinical trials alone or as a combination therapy for the treatment of ovarian cancer, chronic lymphocytic leukaemia and lung cancer.[6]

Silver complexes (e.g., silver sulfadiazine) and antimony (e.g. N-methylglucamine antimony) are used as anti-infective agents. For over two centuries bismuth compounds have been

indicated for the treatment of pathological conditions at the gastrointestinal level, in particular they have proved to be a safe, effective, economical and practical method for the eradication of Helicobacter pylori in patients suffering from chronic gastritis.[7] In addition to therapeutic use, metal-based compounds also play a crucial role in radiological diagnostics and radiopharmaceuticals. Doping can be carried out using Barium in the form of barium sulphate which is consumed as an oral solution by the patient and used as a contrast agent. MRI (Magnetic Resonance Imaging) extensively exploits the paramagnetic characteristics of the Gd^{3+} ion which gives rise to incredibly detailed images of the cardiovascular system, organs, and the brain. The structure of gadoteric acid is shown in figure 1.1. All in all, there is great versatility available from metals across a wide range of techniques in the medicinal chemistry field. Daily uses range from high-definition imaging of sites within the body to the treatment of many pathogens and diseases.
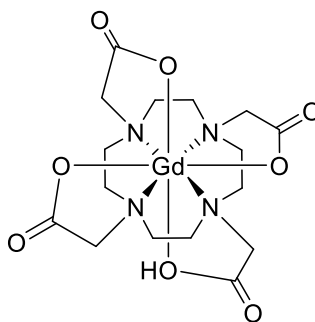
Figure 1.1: Structure of Gadoteric acid commercially known as *Dotarem*.

1.1.1   Cisplatin

The most famous of all metal – based anti-cancer drugs is cisplatin or *cis* - diamminedichloridoplatinum(II) (Figure 1.2). The compound was first synthesized in 1844 by the Italian chemist and physician Michele Peyrone and was for a very long time known as Pyrones salt.

$$H_3N \diagdown \qquad \diagup Cl$$
$$Pt$$
$$H_3N \diagup \qquad \diagdown Cl$$
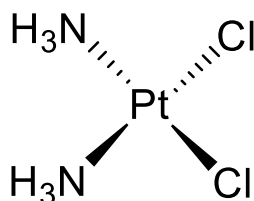
Figure 1.2: Molecular structure of Cisplatin.

It was only in 1965 that the anti-tumour activity of cisplatin was discovered by Barnett Rosenberg a physicist at Michigan State University. Rosenberg studied how an electric field can influence cell replication and conducted his experiments with *Escherichia coli* bacteria. The bacteria were subjected to repeated applications and removal of an alternating current generated by two platinum electrodes in an aqueous solution of NH_4Cl. It was observed that the bacteria had become very elongated, about 300 times their normal length and that cell division was strongly inhibited (Figure 1.3). Rosenberg showed that this phenomenon was not due to the presence of the electric field, but to the formation of electrolysis products by platinum electrodes. The inhibitory activity of bacterial growth was in fact attributed to the formation of a compound: *cis*-diaminodichloroplatinum (II), now more commonly referred to as cisplatin. Subsequently the study of this effect on tumour cells was further probed with the use of two murine models of tumours: sarcoma 180 and leukaemia L1210. *In vivo* studies showed that among all the proposed platinum complexes, the most effective and the least toxic was cisplatin.[8]
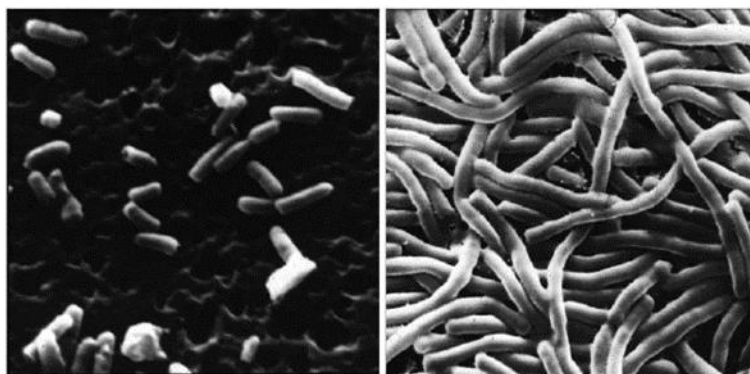
Figure 1.3: Elongation of the bacteria during the experiment conducted by B. Rosenberg *et al.* 1969.[8]

 In 1979 the FDA approved the clinical use of cisplatin as an antineoplastic drug: since then, it has become one of the most used drugs in chemotherapy regimens. Cisplatin is recognized as one of the most effective anticancer drugs available today and is on the World Health Organization's List of Essential Medicines. It is active against a broad spectrum of cancers ranging from numerous solid tumours to lymphomas. In testicular carcinomas and ovarian carcinomas particularly, up to 45 % and 30 % of complete remission have been achieved respectively when used as the single therapeutic agent.[9, 10] First line mono-chemotherapy using cisplatin is extremely effective in the treatment of particularly resistant tumours such as melanoma and breast cancer.[11] and contributes significantly to the regression of some cerebral neoplasms and bladder cancers.[12] Cisplatin has also displayed excellent results in the clinical treatment ofadrenal cortical carcinoma, head, neck and lung cancers.[10] Unfortunately, during the clinical trial studies, problems with cisplatin arose regarding the toxicity of the compound and the platinum core.[13] This in turn leads to limitations on dosage and the prolonged use of the drug as a single treatment. More interesting is cisplatin's synergistic action with other cytotoxic drugs, most notably vinblastine and again antimetabolites such as 5-fluorouracil and methotrexate and, most recently, paclitaxel (Figure 1.4). Platinum-based chemotherapy, together with gemcitabine and bevacizumab is now the first-line treatment for adult patients with non-small cell lung cancer.[14]
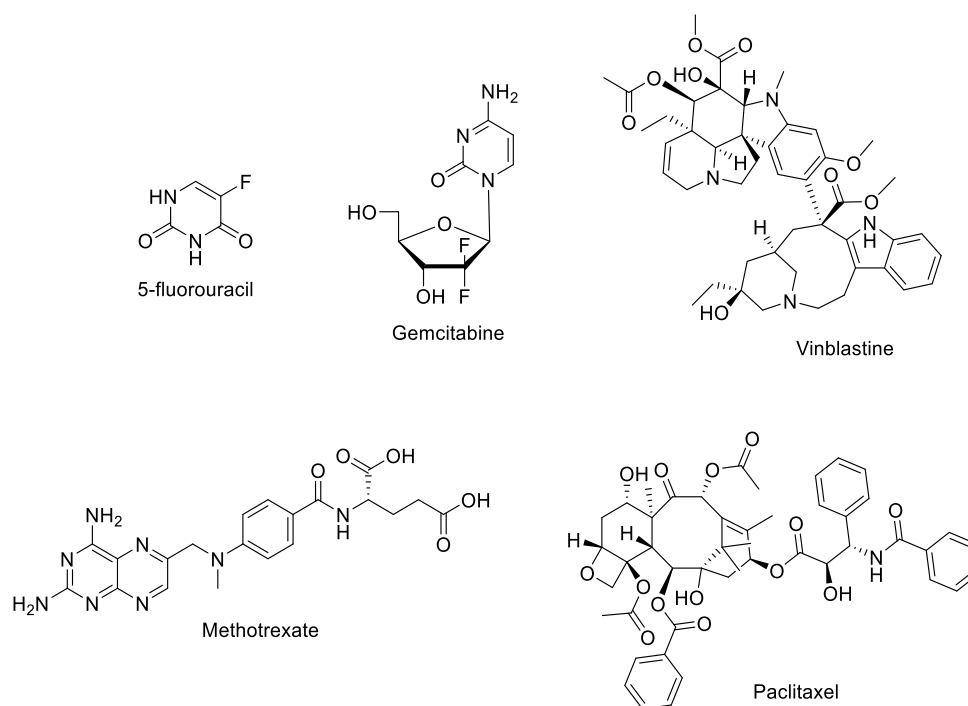
Figure 1.4: Structure of FDA approved chemotherapy drugs.

1.1.2   The Chemistry and mechanism of Action of Cisplatin

Platinum is a transition metal which resides in group 10 of the periodic table. There are three common oxidation states: Pt (0) or platinum metal, Pt (II) and Pt (IV); their respective complexes display tetrahedral geometry, square planar and octahedral geometry. Cisplatin is a square planar coordination complex of Pt (II), with two chlorines and two ammonia in the cis position.

Cisplatin performs its cytotoxic action as a result of stable covalent binding to the DNA nucleobases, with formation of intra and inter-strand adducts which prevent DNA replication resulting in cell death. Its mechanism of action is therefore substantially comparable to that of alkylating agents, although from a chemical point of view the reactions described should be more correctly defined as platination reactions and not alkylation reaction.[15] There are mainly three different routes of drug entry into the tumour cell: the prominent path is represented by passive diffusion through the cell membrane.[16] Another type of transport is represented by protein carriers, such as OTCs (organic cation transporter) involved in the transport of endogenous cations. Finally, the third type involves the use of protein carriers such as hCTR1 (human copper transporter 1) involved in the transport of endogenous copper and other metals. The efflux from the cell is mediated instead by two ATPases displayed in (Figure 1.5), ATP7A and ATP7B and by the MRP (Multidrug Resistance Protein). The MRP

family of proteins contains at least six members: MRP1 and five of its homologues; these are membrane proteins, in turn belonging to the ABC superfamily (ATP binding cassette).[17]
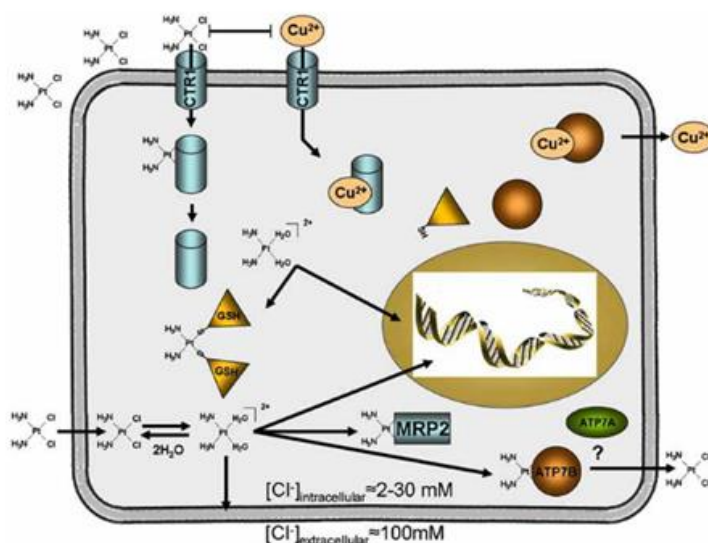
Figure 1.5: Schematic depiction of cisplatin uptake, cell efflux and DNA binding J. Castilla *et al*.[18]

Cisplatin is administered intravenously; it circulates in the neutral form within the plasma where the concentration of chloride ions is higher than 100 mM. It will then cross the cell membrane *via* the mechanisms illustrated above (figure 1.2). Inside the cell, the decreased concentration of chloride ions (3-4 mM) will determine the hydrolysis of cisplatin and the chlorine atoms are replaced by water or by the OH$^-$ ion in a complex multi-stage reaction that leads to formation of mono-aqua species *cis* - $[Pt(NH_3)_2Cl(OH_2)]^+$ and the diaqua species, *cis* - $[Pt (NH_3)_2(OH_2)_2]^{2+}$. [19] These newly formed complexes are slightly acidic in nature and can still slowly dissociate, creating a mixture of water-soluble hydroxides, hydroxy-complexes and even dimers (Figure 1.6).

The aqueous species which form during this process are considered to be the reactive forms of cisplatin: these species, in fact, can easily react with substrates which display nucleophilic characteristics, being very electrophilic and possessing excellent leaving groups.
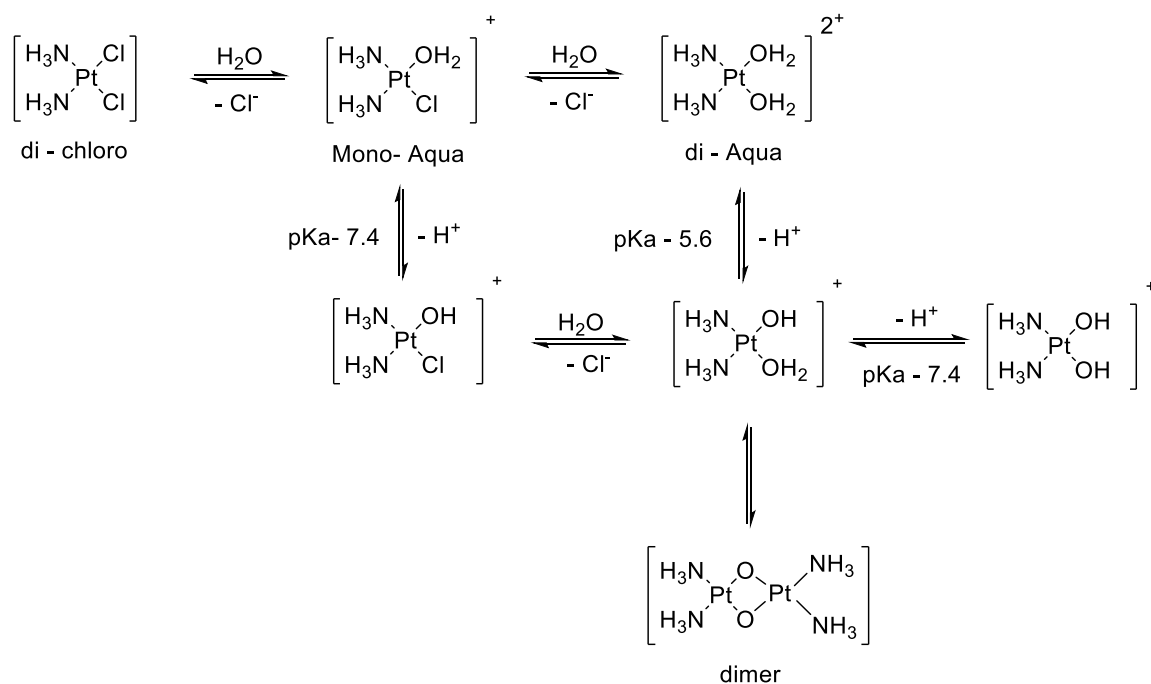
Figure 1.6: Equilibrium of cisplatin hydrolysis and formation of hydrated complexes in aqueous solution.

The main target of cisplatin is the nuclear DNA; however, the biological effects of cisplatin are not only due to the DNA binding. It also interferes with RNA, proteins, and other macromolecules of crucial biological importance. Usually, DNA is almost inaccessible for drugs, as it is folded back on itself and around proteins known as histones. However, when transcription of a protein or replication begins, the DNA is momentarily exposed and can be attacked.

The target groups in the DNA are usually secondary or tertiary nitrogen bases, especially the purine ones (adenine and guanine) due to the nucleophilicity of the imidazol portion. The nitrogen in the 7 position (N7) of guanine represents the preferential site of binding, as it is placed within the major groove of the DNA it is sterically more exposed than nitrogen in position 3; a covalent coordination bond is therefore formed with the free doublet of nitrogen atoms (Figure 1.7).[18]
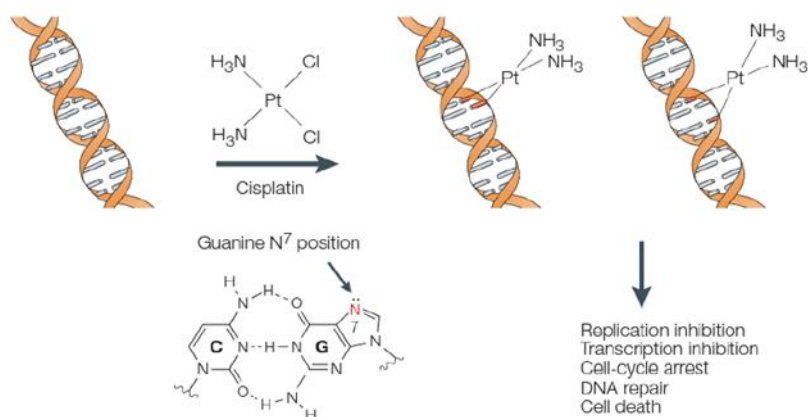
Figure 1.7: Binding of Cisplatin to the N7 position on the Guanine Wang *et al.*[19]

Overall the total amount of cisplatin that manages to enter the cell and interact with the DNA is a very small percentage, about 1 %.[20] The drug in most cases forms intra-strand bonds between adjacent guanines or between guanine and adenine; very small amounts can form inter-strand bonds between two guanines placed on opposite filaments.[8] The formation of intra-strand bonds is mostly responsible for the cytotoxic effect. It is hypothesized that this is due to the distortion of the DNA helix to 35°. These DNA distortions prevent replication and transcription as enzymes associated with these functions are unable to function as required as the cis platinum has now been bound causing the damage just described. All this leads to the activation of a cascade of apoptotic events eventually resulting in cell death.[20] The adducts that are formed are further stabilized by the formation of a link between an amino group of the aqueous form of cisplatin and the nucleotide phosphate group (Figure 1.8).
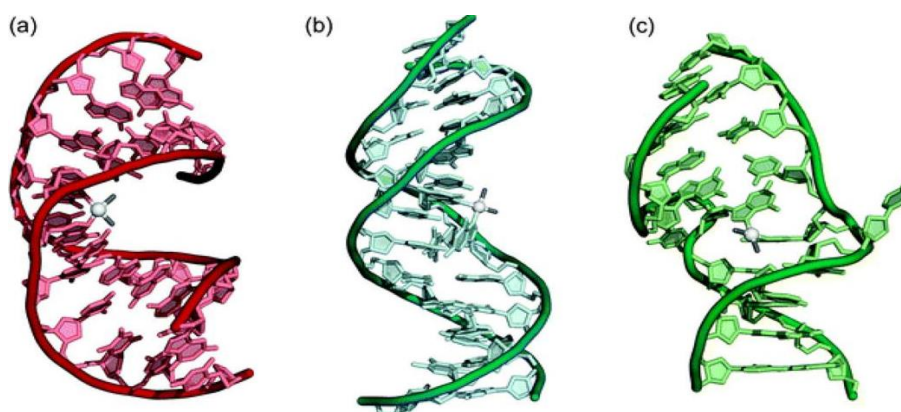
Figure 1.8: Structure of cis-platinum-DNA adducts: (A) DNA in the double-stranded form associated with a cis-platinum molecule;(B) intra-strand adducts; (C) inter-strand adducts. Johnstone *et al.*[21].

1.1.3   Limitations of using Cisplatin

In recent years, many limitations and drawbacks in the use of cisplatin have started to spring up.[22] Cisplatin is responsible for multiple off-target toxicity that can not only seriously affect the patient's quality of life, but also lead to drug dose reductions or the selection of combination chemotherapy. These main side effects of cisplatin are nephrotoxicity, neurotoxicity, and ototoxicity.

Nephrotoxicity

Nephrotoxicity or toxicity within the kidneys is a toxic effect which can arise from treatment with cisplatin. This side effect appears to be dose-dependent and is attributable to the administration of high concentrations of the drug and the consequent activity on transporters.[23] and renal enzymes through the formation of a chelate between platinum and some residues present in renal proteins.[24] This results in damage to the epithelial cells of the renal tubules followed by degeneration of the tubules themselves, disappearance of the brush haem, necrosis, and mineralization. Eventually, this results in acute renal failure or, in many cases, chronic syndrome in which electrolytes are lost[25] and inflammatory pathogenesis involving lymphocytes.[26] Symptoms include hyperazotemia, hypercreatininemia with progressive reduction of creatinine clearance and hyperuricemia. Maintaining hydration of the patient can greatly reduce the severity of these symptoms: Cisplatin can be administered in conjunction with osmotic diuretics[27] or the tyrosine kinase inhibitor, imatinib. Oral co-administration of imatinib and cisplatin in murine models has been shown to reduce the renal accumulation of cisplatin and consequently nephrotoxicity. It should be remembered, however, that nephrotoxicity is progressive after several doses and is only partially reversible.[27]

Ototoxicity

Ototoxicity is another toxic drawback of cisplatin which manifests itself with tinnitus, i.e., whistles, buzzing, rustling, or ear pulsations, associated with possible loss of hearing, which can be unilateral or bilateral. It arises as a result of apoptosis of auditory sensory cells, [28] due to the production of reactive oxygen species (ROS). It may be reversible or persistent, depending on the patient's age, cumulative doses, total number of therapy courses carried out, and deterioration of kidney function.[29] The incidence of this effect is related to the total dose of cisplatin administered and the peak concentration of the drug in the serum at the time of administration.

In addition to the adverse effects listed, nausea and vomiting are also very frequent and can manifest themselves with such intensity that the patient sometimes is reluctant to continue or refuses treatment. Acute nausea and vomiting (with onset of 1 to 24 hours after therapy) has been identified, and late onset (24 to 120 hours after therapy) which can persist for several days with a tendency to accrue is also known to occur. To reduce these effects, however, it is possible to combine the therapy by using antagonists of serotonin receptors, known as antiemetics.[10]

Another indicative side effect of high dose cisplatin treatment is myelosuppression, which results in a reduced hematopoiesis determinant of possible anemia, leukopenia, or platelets, respectively characterized by reduced amounts of hemoglobin in the blood, reduced number of leukocytes and predisposition to infection, reduced number of platelets and increased risk of hemorrhages. Chemotherapy-induced cardiotoxicity characterized by prolongation of the QT interval has also been verified, following treatment with cisplatin, so the use of the drug in subjects with congenital syndrome of the prolonged QT interval is to be avoided. On the other hand, the induction of hepatotoxicity characterized in mice by an increase in lipid peroxidation has been less studied, resulting in an alteration in the functionality of the antioxidant liver enzymes.[10]

Neurotoxicity

Neurotoxicity is a side effect of the drug which has led to increased clinical importance and may even become the limiting factor in the continuation of this therapy. Neurotoxicity induced by cisplatin is completely dependent dose and can manifest itself with the onset of several symptoms including paresthesia, the loss of sensitivity or tingling in the limbs or in other body parts. It can also include areflexia, which is, the total loss of reflex, and loss of proprioception, which is one's spatial awareness ability or perception and recognition of the position of one's body in an area. The disorder can deteriorate to the point of manifestations of ataxia and will limit the patient's ability to move and live independently. It tends to be more severe and to arise more quickly in elderly and debilitated subjects, or in patients previously treated with other neurotoxic drugs. Confirmed and symptomatic forms appear in almost 50 % of cases and tend to persist for long periods of time after suspension of therapy. Useful substances in the treatment of neurotoxicity from cisplatin are antioxidants such as melatonin, vitamin E selenium, nitric oxide modulators and diuretics.[30] One way that has recently seen loads of interest is the use of another metal, that can be endogenous and less toxic, such as Copper.

1.2 Copper in biological systems

Copper is an essential endogenous transition metal existing at around 2.0 mg / Kg in the human body, it is the third most abundant metal found in the human body after iron and zinc.[31] Copper is the 29th element in the periodic table and has electronic configuration $[Ar]3d^{10}4s^1$. The element resides in group 11, above silver and gold. The most common oxidation states for copper in the biological systems are cuprous Cu^+ and cupric Cu^{2+}; with Cu^{1+} mostly responsible for reducing intracellular environment, and the latter plays a more dominant role in the oxidizing extracellular environment. Cu^{3+} and Cu^{4+} are rarely found, although there have been recent theoretical investigations into complexes containing these oxidation states.[32]

Cu (II) is the most stable oxidation state and while Cu(I) readily undergoes oxidation and dismutation. Due to the easy interconversion or rapid oxidation / reduction between the two oxidation states, copper has been identified as an essential trace element for all organisms which have an oxidative metabolism. Furthermore, functions including angiogenesis, the response to hypoxia and neuromodulation are all hugely important biological processes associated with the element.

Copper is also an important fundamental co-factor for the structural and catalytic properties of a wide variety of enzymes which take part in important biological functions necessary for cell growth and development. These include cytochrome C oxidase (involved in the electron transport chain at the level of mitochondrial), superoxide dismutase (important in detoxification from reactive oxygen species (ROS)) and lysyl-oxidase (necessary for cross-linking elastin and collagen).[33] Copper Amine Oxidases (CAOs) which make up a class of enzymes containing Cu^{2+} generate hydrogen peroxide and ammonia as by-products. The aberrant expression of these enzymes is linked to inflammation, fibrosis and carcinogenicity.[34]

Although the bio essential attributes of copper have long been established,[3] in the last decade, copper has been formidably identified as playing an ever-increasing role in human health and well-being, and it has transitioned from a relatively unknown element, associated with a few rare conditions, to an element of huge importance in the pathology of several significant neurological diseases. This prominence has largely arisen as a consequence of very fast advances in understanding of copper homeostasis at a molecular level and a modern interest in "bioinorganic Chemistry". It is important to note that copper can become toxic if present in high concentrations. It is known that the bivalent ion is particularly poisonous to

small organisms; For example, immersing some bacteria and microorganisms in a copper vessel containing water has proved fatal. In addition, copper-based compounds are known to prevent the growth of algae.[34]

One of the main mechanisms of action proposed to explain copper-induced cellular toxicity comes from the tendency of copper-induced ions to participate in the formation of reactive oxygen species (ROS), both in the form of cupric copper and cuprous copper. In the presence of superoxide anion ($^\bullet O^{2-}$) or reducing agents such as ascorbic acid or reduced glutathione (GSH), Cu(II) can be reduced to Cu(I), which is then able to catalyze the formation of hydroxyl radical (OH$^\bullet$) from hydrogen peroxide (H_2O_2) via the Fenton and Haber-Weiss reaction (Figure 1.9).[35]

Fenton Reaction

$$Cu(I) \; + \; H_2O_2 \longrightarrow Cu(II) \; + \; OH^- \; + \; HO^\bullet$$

Haber - Weiss reaction (super oxide driven Fenton reaction)

$$Cu(I) \; + \; H_2O_2 \longrightarrow Cu(II) \; + \; OH^- \; + \; HO^\bullet$$

$$O_2 \qquad\qquad\qquad O_2^{-\bullet}$$

Harber - Weiss net reaction

$$O_2^{-\bullet} \; + \; H_2O_2 \longrightarrow O_2 \; + \; HO^- \; + \; HO^\bullet$$
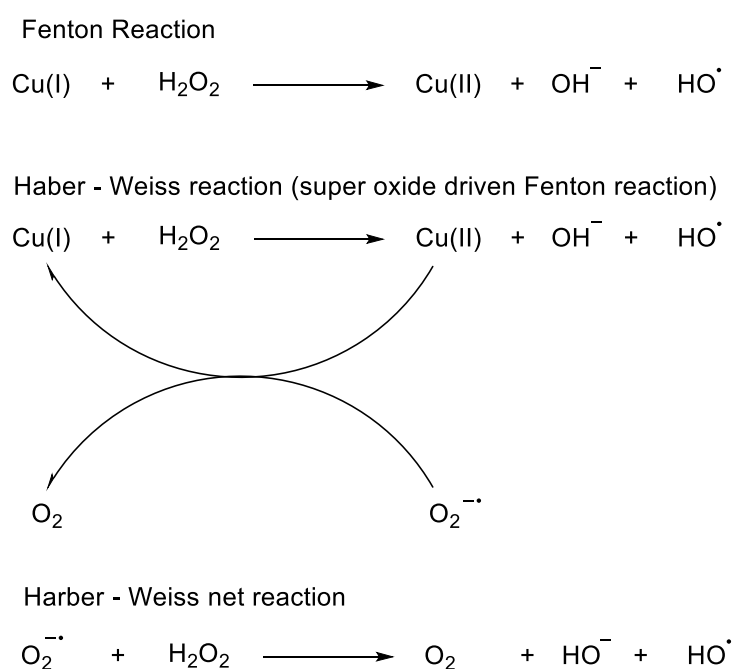
Figure 1.9: Fenton and Harber – Weiss reactions.

1.2.1 Copper dependent enzymes

As stated previously, copper is an essential cofactor and a structural component in a number of important enzymes within animals (Table 1) and plants. Mostly of these enzymes are involved in redox reactions. [36] Many enzymes utilize the high redox potential of the Cu $^{2+}$/Cu$^+$ system for oxidation reactions. Some classic examples are superoxide by superoxide dismutase and catechols by tyrosinase. Other well researched copper-dependent enzymes participate in biological processes such as the metabolism of energy (e.g. cytochrome c oxidase), antioxidative defence (e.g., Zn,Cu-superoxide dismutase) and iron metabolism (e.g., ceruloplasmin).[3] Copper-dependent enzymes can be broken into three categories. These are classified as type 1, 2 or 3 copper enzymes, type 1 are known as

"blue copper sites".[36] Mostly, copper containing enzymes have only one type of copper centre, however in some enzymes (e.g., cytochrome c oxidase, ceruloplasmin,) more than one copper centre has been observed. Blue copper sites, also known as type 1 sites, solely preform single electron transfer.[36, 37] Type 2 copper sites lack unique features in their UV/Vis and EPR spectra. These function by catalytically activating the enzyme substrates via direct interaction other than utilising electron transfer.[36] Type 3 copper sites are binuclear. These type 3 copper sites are constituted of two copper ions in close space and proximity, each copper atom is coordinated by three histidine. These can be reversibly bridged by dioxygen. Type 3 copper sites are responsible for the activation and transport of oxygen. [36]

Table 1.0: Mammalian copper – dependent enzymes. [38]

Enzyme	Function
Cytochrome *c* oxidase	Oxidative phosphorylation
Cu,Zn superoxide dismutase (SOD1)	Superoxide detoxification, signalling
Ceruloplasmin (Cp)	Ferroxidase
Lysyl oxidase (LOX)	Crosslinking of collagen and elastin
Tyrosinase	Melanin synthesis
Dopamine-β-monoxygenase (DβM)	Norepinephrine synthesis
Peptidylglycine α-amidating enzyme (PAM)	Activation of peptide hormones
Copper amine oxidase	Deamination of amines
Hephaestin	Ferroxidase
Coagulation factors V and VIII	Blood clotting

1.2.2   Cytochrome *c* Oxidase

Cytochrome *c* Oxidase is part of a family of heme-copper oxidases which are the terminal oxidases within the respiratory chain. It exists within the mitochondrial inner membranes where it is responsible for the catalysis of a single electron transfer from cytochrome *c* to dioxygen in what is known to be the final step in a process known as mitochondrial oxidate phosphorylation.[37] Cytochrome *c* oxidase in mammals in is referred to as a multimeric protein complex. It is made up of 13 subunits which are encoded by both the nuclear and mitochondrial genome. Complex IV or cytochrome *c* oxidase is ultimately the product of cytochrome *c* reductase or complex III meaning it is the reduced form of this enzyme. This reduction occurs via the heme-C in cytochrome *c* reductase in where it is responsible for

taking the electron from the cytochrome *c* reductase and then giving the electron becoming cytochrome *c* oxidase.

The electron initially is moved from the heme C to the copper cofactor or Cu(A), this delivery site is known as cytochrome c oxidase subunit (II).[39] It then moves to cytochrome A and ultimately it ends up at the binuclear centre known as cytochrome A3 and Cu(B). The bi nuclear complexed is sometimes referred to as the oxygen splitting complex. This is due to electrons from Cu(B) being transferred to molecular oxygen (O_2). It is at this point the O_2 will be split into H_2O. the reaction scheme for this is given below (Figure 1.10).
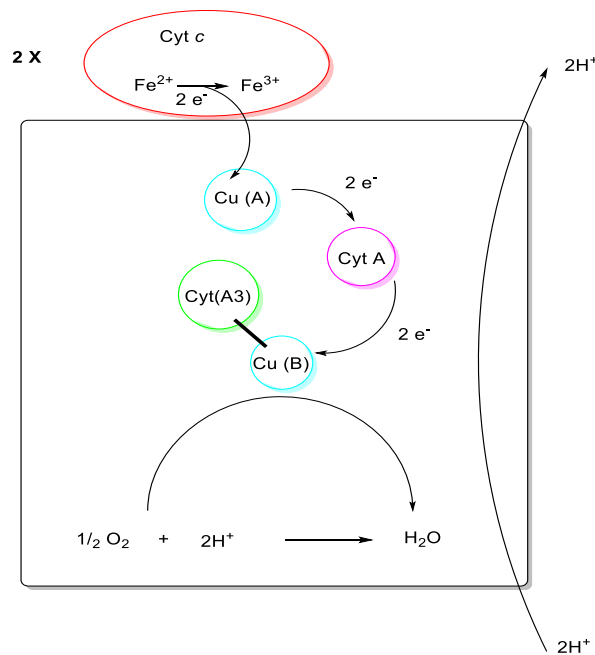
Figure 1.10: Electron flow within the cellular matrix.

In total four electrons from cytochrome *c* are required to fully reduce O_2 to H_2O, therefore four cytochrome *c* oxidase are required to carry out each conversion of O_2 to H_2O as each cytochrome *c* oxidase can only deliver a single electron at a time. The enzyme is also responsible for the movement of two protons from the cellular matrix into the intermembrane space. It has been demonstrated in the past that the copper (B) part of the enzyme is strongly inhibited by Lewis bases or nucleophiles, particularly the cyanide, and azide anions and also carbon monoxide.[40] Inhibition of complex IV or any of the complexes I – IV will lead to an inability to pump protons across the membrane and ultimately death. Deficiency of cytochrome *c* oxidase is very often a common cause of defects in the respiratory chain in humans. Pathological aspects can range from cardiomyopathy, metabolic acidosis, neurodegeneration to weakness.[41]

1.2.3   Copper, Zinc superoxide dismutase (SOD1)

Of the three known families of superoxide dismutase the copper, zinc superoxide dismutase enzyme (SOD1) is the most commonly used one by eukaryotes. The cytoplasmic matrix in almost every eukaryote cell contains the SOD1 enzyme. The enzyme these days can be purchased commercially and has a molecular mass of around 32,500.[42] The role of the SOD1 system is to catalyse the conversion of the potentially toxic super oxide anion and convert it into the less toxic species hydrogen peroxide and molecular oxygen (Figure 1.11). Once superoxide is protonated it can destroy DNA and enzymes in the body *via* oxidative damage.[43]

$$2O_2^{\bullet -} + 2H^+ \rightleftharpoons H_2O_2 + O_2$$
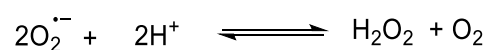
Figure 1.11: Equilibrium conversion between superoxide and hydrogen peroxide and molecular oxygen.

The copper ion at the enzymes active site is responsible for catalysing the reaction and the zinc ion is present for support and structural stabilization. There are three different types of super oxide dismutase. The copper, zinc superoxide dismutase (SOD1) is found in the cytoplasm of the cells which is composed of around 80% water. The protein is folded so as the solvent exposed exterior is mostly composed of hydrophilic amino acids with the hydrophobic amino acids on the interior and away from the polar solvent.[44] Kaur *et al*.[45] has recently discovered a mutation occurring in SOD1 which is linked to the genetic disease amyotrophic lateral sclerosis (ALS).
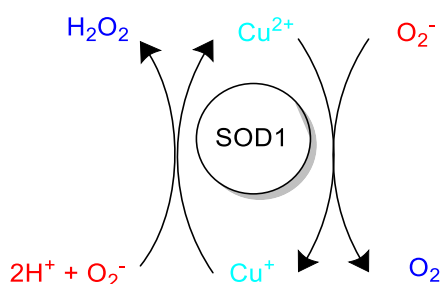
Figure 1.12: Generic scheme of the reaction catalysed by SOD1.

The cycle consists of two different redox reactions (Figure 1.12). On the right-hand side, the super oxide is oxidised to molecular oxygen and the copper is reduced from Cu^{2+} to Cu^+. This

happens *via* direct coordination of Cu^{2+} atom to superoxide and therefore the reaction occurs in the inner sphere. On the left-hand side, the superoxide is reduced to hydrogen peroxide and the Cu$^+$ is oxidised back to Cu^{2+}. However, in this case there is no coordination of the superoxide to the Copper centre and therefore is proceeds *via* outer sphere.[46] The superoxide dismutase is a dimer which is composed of two identical subunits, each containing 151 amino acid residues. These are arranged in 8 beta sheets and 3 exterior loops. Each subunit has an active site with superoxide molecules will bind too and be either oxidised or reduced in the redox reaction.[47] The two subunits line up along the same axis and are orientated opposite each other.[48] This leads to the active sites on the subunits pointing in different directions. One of the most important aspects of superoxide dismutase is the funnel shape which leads to the active site.[49]

 Within this "funnel" are the two metal cations zinc and copper along with the amino acids histidine and arginine which are also positively charged (Figure 1.13). It is these that attract the negatively charged superoxide molecules. The copper atom is exposed within the funnel so as the super oxide anion can bind to it directly, due to Cu^{2+}. The zinc atom is buried within the protein and does not play a direct role in the catalysis of the dismutase reaction. It is mostly there as a structural scaffold for the protein.[50]
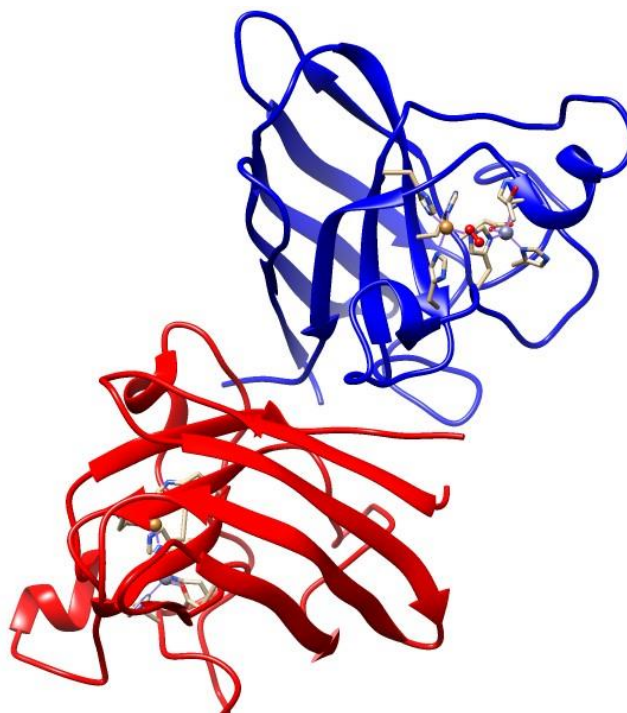
Figure 1.13: Ribbon diagram of the reduced form of Cu,Zn SOD with two subunits differentiated in blue and red. Active site side chains and metal cofactors are shown with superoxide bound.[51]

1.3   Copper in Disease

The role of copper in the homeostasis process is of fundamental importance as a deficiency or an excess of this element can very much compromise the state of health of the organism itself. In fact, the alteration of copper homeostasis can lead to serious disorders, in particular neurological and neurodegenerative disorders. The most common neurological diseases related to this metal are Wilson's disease and Menkes disease.

Wilson's disease, also known as hepatolenticular degeneration, is caused by a mutation in the gene coding for ATP7B, resulting in a deficit in biliary copper excretion and therefore excessive accumulation of copper in the liver. This disease leads to liver problems with possible cases of hepatomegaly, acute hepatitis, or cirrhosis.[52] Menkes disease is a genetic disease, caused by several mutations in the gene coding for ATP7A, a copper transporter responsible for excretion of copper from the cell. It involves a decrease in the absorption of copper at the intestinal level, which is reflected in different clinical conditions such as low muscle tone, mental retardation, developmental delay, premature death.[53]

In addition to this, and in recent years it has been demonstrated that altered metal ion homeostasis may be involved in the progression of neurodegenerative diseases.[54] Metal-protein interactions seem to play a critical role in protein aggregation and involve aggregated protein accumulation, oxidative damage to the brain, and loss of neuronal cells, as is the case with aging. Copper is in fact involved in prion disease where, along with other metals, it favours the assembly of the β-amyloid protein and is involved in Alzheimer's neuropathology which leads to senile dementia.[55] Parkinson's disease is another neurodegenerative disease involving copper. An accumulation of iron and decreased levels of copper in the brain are common in patients with Parkinson's disease. This discovery became very important as both metals are involved in the generation and propagation of free radicals, along with having a role in the precipitation of proteins due to their redox properties. Copper can induce aggregation of α-synuclein, a protein that may be involved in the pathogenesis of Parkinson's disease, although this reaction has only been observed in the presence of a higher concentration of copper than that found in normal tissues.[53] In Parkinson's disease, fluctuations in copper levels within the central nervous system cause the death of neuronal cells. In this regard, recent clinical studies hypothesize the therapeutic use of copper-based compounds as agents modifying the course of the disease. [56]

Metabolic profiling has shown that people containing a very low level of serum zinc also have a very high level of copper.[57] Bredesen *et al.* stated that they did not fully understand why

people often have these high copper – low zinc ratios. Copper and zinc are competitive in their absorption. Very often too much of one is associated with too little of the other. Mostly in modern society people suffer from zinc deficiency. It is understood that both copper and zinc will compete for absorption.[58] Often medications for acid reflux inhibit the absorption of zinc, this is known as drug induced copper deficiency.

The use of anti-copper drugs including Zinc, tetrathiomolybdate and penicillamine can lead to possible copper deficiency, which will usually manifest itself first as a low ceruloplasmin level and eventually it is followed by pancytopenia. In the mid to late 2000s copper was also identified as a major component in Creutzfeldt Jakob (prion) disease.[59, 60] Aside from this the coordination surroundings and structural frameworks of Cu^{2+} complexes within both the amyloid precursor protein (APP) and prion protein are now extremely well documented and have been characterized in many separate structural and bio physical studies.[60, 61] In the subsequent section the purposeful use of tetrathiomolybdate to promote copper deficiency as a therapeutic tool will be discussed.

In 1971 Folkmann *et al.* identified that the growth of a solid tumour is dependent on angiogenesis, [62] and thus this would most likely become a major hurdle of cancer as most adults do not have huge requirements for angiogenesis with exception of wound healing.[63] Over the last thirty years, there has been an explosion of interest in angiogenic promoters and inhibitors, and also in pathways to inhibit angiogenesis as a possible method of cancer treatment.[64] Since the early 80s there has been an increasing interest in coppers role in angiogenesis. Rabbit cornea models have demonstrated that copper is directly involved in the stimulation of angiogenesis.[65] Along with this Ziche *et al.* demonstrated that acute copper deficiencies in animals have shown to strongly inhibit the response to many usually angiogenic stimuli when placed in the cornea.[66] In the early 90s research by Brem *et al*. showed that animals displaying a copper deficiency experienced reduced growth and invasive characteristics of tumours which had been placed within their brains.[67]

A group at Michigan University have demonstrated that tumour growth can be inhibited by treatment with tetrathiomolybdate in animal models and also in patients.[68] When administered with food, the tetrathiomolybdate complex is not absorbed, this induces the animal or patient into a negative copper balance. If administered between meals, tetrathiomolybdate is fully absorbed, it then forms a complex with the copper ions and serum albumin, leading to an elevation of serum copper due to the slow clearing of the complex.

1.3.1   Copper in medicine

For thousands of years the healing properties of copper have been known.[69] The use of copper is heavily recorded by the ancient Egyptians as far back as 3000 BC both an antiseptic and to sterilise water for drinking and wound treatment.[70] Sections of the *Papyus Ebers* dating from 1500 BC have described the use of copper infused oils and ointments.[71] Copper bracelets have long been worn by those suffering from arthritis and are still worn today. The therapeutic effects of copper-based medications are certainly not without historic reference, because of this there has been a major interest in copper-based medications to treat a variety of illnesses over the last couple of decades. Copper (II) is especially an attractive metal for the design of modern drugs to treat a variety of illnesses. This comes down to a number of factors. Firstly, the metal can display a number of geometries and coordination numbers and is often a more versatile option than other metals. The redox properties of the copper centre can very easily be exploited in the body for desired effects giving a dual like effect of the organic drug component and the metal centre itself. More will be discussed about this later in the thesis. Moreover, copper does exist in the human body as the third most abundant trace element and therefore toxicity issues around copper containing drugs are very much limited in comparison to their platinum, gold, or lithium.

1.3.2   Copper - based non-steroidal anti-inflammatory drugs (NSAIDs)

With the above in mind it has led to an array of copper (II) based NSAIDs.[72] All of which have demonstrated magnified anti – inflammatory activity along with very low gastrointestinal toxicity in comparison to their copper free predecessors. [70] Although there is a long and well researched history of copper based NSAIDs, they have not to date made a huge mark on the market. Despite such huge interest very little is known about their pharmacology and mechanism of action. Not a single Copper (II) based anti-inflammatory has been authorised for use by the FDA or EMA. There is however an ethanol-based gel containing copper salicylate available for purchase for the application of topical temporary pain relief (Alcusal ©). Also available is a copper (II) dimer of indomethacin (IndoH/1- (4-chlorobenzoyl)-5-methoxy-2-methyl-1H-Indole-3- acetic acid possessing very low toxicity and be commercially purchased in South Africa, Australia and New Zealand as an oral medication for veterinary use (Figure 1.14).[73] These copper (II) drugs display very low toxicity and are of huge interest., mainly due to the fact that several commercially available anti – inflammatory drugs including NSAIDs are associated with undesired side effects including GI ulceration, exacerbation or hypertension and renal insufficiency and failure.[74]
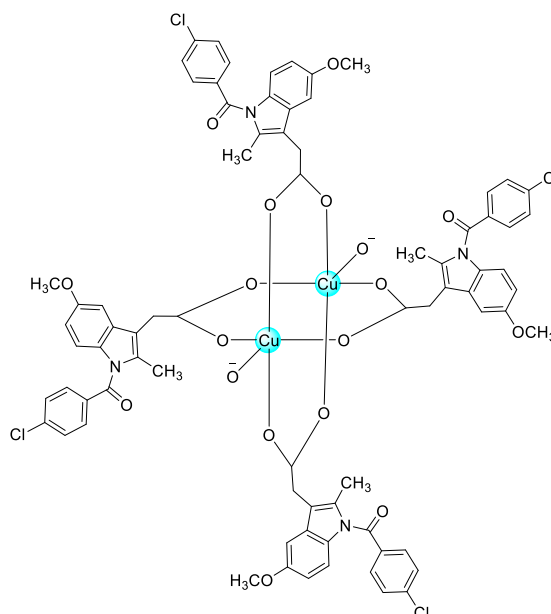
Figure 1.14: Di-nuclear copper (II) compound available as veterinary medication.[73]

In 1976 Sorenson *et al.* had shown that these copper (II) complexes (Figure 1.15) of anti-inflammatory drugs were vastly more active that both the copper salt precursor and the free ligand for of the NSAID.[75] He proposed that the pharmacological activity displayed was most likely due to the intrinsic physio – chemical ability of the complex itself rather than a combination of both the free copper salt and ligand. This was deduced on the fact the amount of copper present in the actual complex itself was not enough to have such anti – inflammatory activity.[76]   Sorenson showed that the copper (II) complex of salicylate displayed anti – inflammatory properties 30 times greater than those displayed by the control aspirin.[70] Interestingly enough copper (II) complexes of many non anti – inflammatory agents also displayed anti – inflammatory activity.[70]
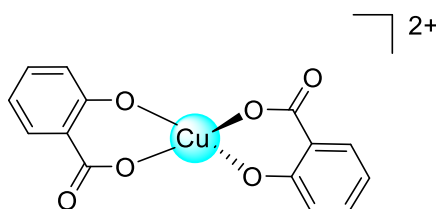
Figure 1.15: Copper(II) complex of salicylic acid - [Cu(Salicylate)] [2+] Sorenson *et al.*[75]

1.3.3   Copper based anti – ulcer treatments

Although there are many reports of copper compounds to treat ulcers there are to date no commercially obtainable compounds that serve this purpose. In 2009 Tuorkey *et al.*[77] demonstrated significant decrease in gastric juice in rats after the administration of a copper

nicotinate complex. The complex was first synthesised in 1987 by Goher *et al*.[78] After the studies concluded it was deemed that the copper (II) nicotinate complex did display anti-ulcer properties 2 -3 times that of the aspirin (Figure 1.16).
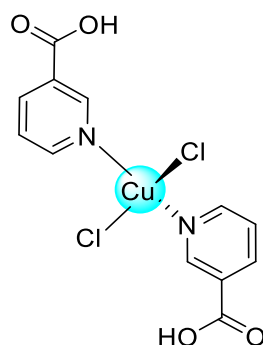
Figure 1.16: Copper complex produced by Goher *et al*.[78] demonstrated anti-ulcer capabilities.

1.3.4   Copper compounds with anti – parasitic properties

There have been numerous copper (II) complexes reported in past literature which displayed the ability to inhibit *Leishmania* parasites, many of these have shown both potency and selectivity. Copper (II) compounds with coordinated (dtmp) or 5,7-dimethyl-s-triazolo [1,5-a] pyrimidine, synthesised by Cabellero *et al.* (Figure 1.17) were well researched and displayed anti parasitic effects.[79] These complexes were screened against *L. braziliensis* and *L. infantum* with the complex shown below displaying IC$_{50}$ values in the micro molar range for *L. braziliensis* and *L. infantum* respectfully. (39.6 & 10.3 µM). selectivity was also displayed in both cases but much more in respect to the *L. braziliensis*.
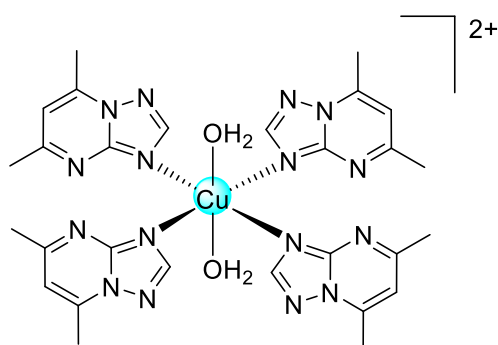
Figure 1.17: Complex prepared by *Cabellero et al.*[79]

BenzCo is a Copper (II) complex of limonene – thosemicarbazone that has been prepared by Britta *et al.* (Figure 1.18). The effects of it were studied on L. *amazonesis* concluding the compound had powerful anti-leishmanial properties.[80] The effects of this particular compound have been studies in great detail, and it was established not only was it effective against the parasite, but it was effective against many stages of the parasite, specifically leishmania promastigotes.
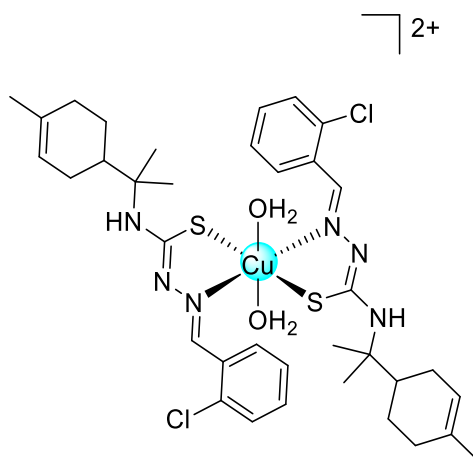
Figure 1.18: Molecular structure of *BenzCo*.[80]

1.3.5   Copper compounds with anti – convulsant activity

Copper (II) complexes investigates by Sorenson *et al.* as early as 1973 displayed very desirable anti – convulsant activity in the µM / Kg range in rodent models.[81] Some of the complexes displayed very fast onset also as fast as 30 minutes and the therapeutic effect continued to last up to 8 hours. Other compounds that were investigated had a very delayed onset of actions, but the effects lasted up until 24 hours. Almost all the complexes examined in this study were found to be very effective when administered in a pentylenetetrazol induced seizure case.[76] Sorenson *et al.* screened a huge array of copper compounds as anti – convulsants, [82] The most effective of these proved to be two Bis compounds. A *Bis* - 3,5-diisopropyl salicylic acid and a *Bis*- Amobarbital complex of copper (II) chloride (Figure 1.18). The assays showed that the copper (II) complex of the barbiturate was far more effective than its salt form sodium amobarbital and also the copper (II) chloride salt.[82] Also, since it is known that neither diisopropyl salicylic acid nor the copper chloride salt display anti-convulsant properties, Sorenson concluded that the existent of the anti – convulsant activity was indeed from the copper complex of the parent molecule.
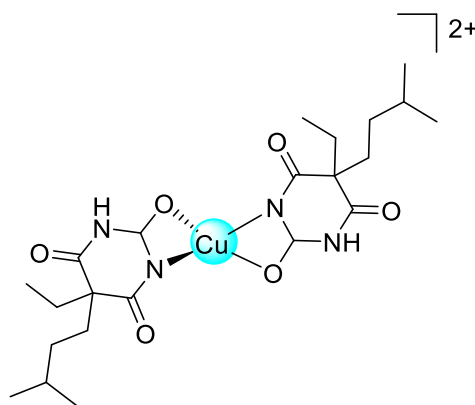
Figure 1.18. Sorensons *et al* Bis amobarbital copper (II) compound.

1.3.6 Anti-microbial activity of copper

Given major advances in the development of antimicrobial medicines, infectious diseases still rank in the top five causes of death in developing countries and socio economic populations around the globe accounting for around 13 million fatalities annually.[83] Infectious disease isn't only a cause for concern in socio economic populations, in developed countries it is estimated that approx. 1.4 million people are prone to clinically – acquired infections, this risk is increased by up to 2000 % in poorly developed countries.[84]

Based on this, it is no surprise there has been a huge investigation into the anti-microbial activity of copper containing compounds, especially copper – phenanthroline compounds. In 1978 Sigman *et al*. began testing on these famous copper – phenanthroline coordination complexes and discovered they were playing a significant role in DNA cleavage.[85] More will be discussed in the next section and the following chapters about Sigmans work. One of the largest screenings of copper - phenanthroline complexes against bacteria was done in 2013 by Neville *et al*. the general structure for these compounds is given (Figure 1.19).
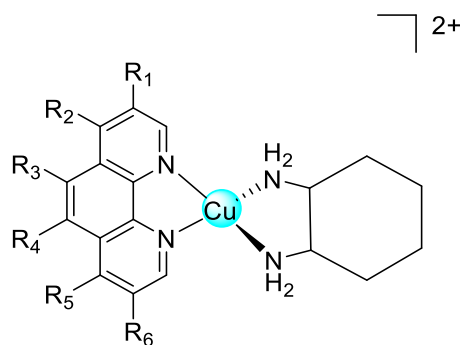
Figure 1.19: General structure of Nevilles copper(II) – phenanthroline complexes , R1 – 6 represent functionalised positions.[86]

The complexes were examined for their capacity to inhibit the growth of liquid cultures of *S. aureus*, *E. coli*, *P. aeruginosa* and *S. cerevisiae* at a concentration of ≤ 20 μM. Although significant inhibition was not demonstrated in cases of *P. aeruginos*a and *S. cerevisiae*, which Neville *et al.* speculated it was most likely due to molecular size exclusion as the outer membrane permeability of *P. aeruginosa* is comparatively smaller than that of *E. Coli* and *S. aureus*. This would mean that there would be restricted rate of uptake and effective efflux. Again with *S. cerevisiae* only mild inhibition was seen by Neville *et al.* it was discovered in this case that the cell wall of *S. cerevisiae* excluded molecules of a size 620 – 760 g mol^{-1}. It was however determined that this was most likely not the primary mechanism of resistance in this bacterium.[86] There appeared to be efflux mechanisms specifically associated with *S. cerevisiae* at play in this case.[87]

Bacteria are well known to sequester copper, practice efflux mechanisms and utilise enzymes for detoxification for the homeostasis of copper both inside and outside the cell.[88] Because of this, coordination complexes of copper have become vastly interesting as a delivery method in order to allow for the transition of the copper itself across the bacterial cell wall and onto important targets such as DNA. Upon complexation, the organic ligand can facilitate the uptake of the copper ion into the cell. In which case the usually lipophilic ligand has now disguised the hugely lipophobic character of the copper ion and thus the copper ion enters the cell.[89] In unison to the transition of the metal ion into the cell, sequestration of copper by the anionic groups present in the cell and various enzymes is prevented.

In a situation where the copper ion is complexed to a known biologically active organic ligand often there is a dual effect or synergistic effect leading to greater therapeutic effects than if both the free ligand and copper salt were present separately as shown by Sigman *et al*. [90] This is particularly important in copper based anti-cancer agents which will be discussed in the following section and in subsequent chapters of this thesis.

1.3.7   Copper based anti – cancer compounds

Given the commercial success of cisplatin it has significant drawbacks as a medicine. Not only are there a huge amount of off target interactions with cisplatin but selectively is incredibly low with only around 1% of the drug reaching its actual target the DNA.[20] This issue coupled with the very evident toxicity issues around using the drug have given rise to incredible research interest in metal-based alternatives for cisplatin, oxaliplatin and carboplatin.

Copper has come to major prominence as an extremely viable candidate as this metal ion boasts many advantages. These include but are not limited to the variable coordination numbers displayed by copper complexes. These give rise to a multitude of geometries which in turn can be exploited for various interactions. Copper salts are significantly less toxic than those of platinum, reducing the dose dependant side effects hugely. However, it is worth noting that copper can be toxic due to its redox activity and its affinity for binding sites which should be binding other metals. The variation in coordination number also allows for a multitude of ligands to be complexed to both copper (I) & copper (II) centres. There are very few examples of copper (III) complexes reported, [91] however the coordination chemistry of copper compounds is dominated by copper (II) complexes. Both oxidation states of the metal offer significant properties with copper (I) showing a preference for soft donor atoms such as Sulfur. The most common coordination number displayed by copper (I) is four, giving rise to a tetrahedral geometry in these complexes, however small numbers of two and three coordinate complexes have been identified giving rise to linear and trigonal geometries (Figure 1.20).[92]

Copper (I)

Linear
CN = 2

Trigonal
CN = 3

Tetrahedral
CN = 4
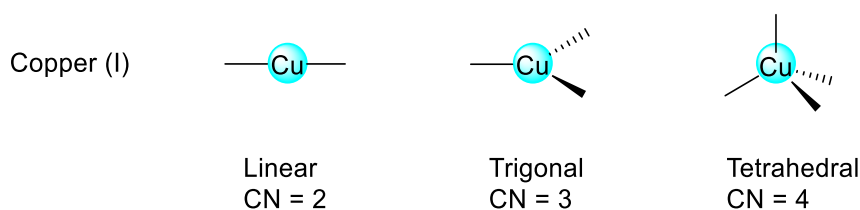
Figure 1.20: Geometries and coordination numbers (CN) of copper (I) complexes.

The stability of both species copper (I) and copper (II) present in coordination compounds, is different from that of their free ions. What emerges is that Cu(I) is stabilized in coordination compounds in both aqueous and atmospheric environments. This feature is mainly dependent upon the nature of the ligand and is given by high values of solid ion lattice energy and solvation energy for the copper (I).[93] Copper (II) complexes display a coordination

number of four, five or six leading to geometries of distorted tetrahedral, trigonal bi-pyramidal and octahedral (Figure 1.21). This allows for a selection of ligands to be complexed from mono to hexadentate chelates, offering a huge variety of options to attach to the metal ion. The most common donor atoms in a copper (II) system tend to be (O, S, N and halides).[94]

Tetrahedral
CN = 4

Tirgonal bi-Pyrimidal
CN = 5

Octahedral
CN = 6
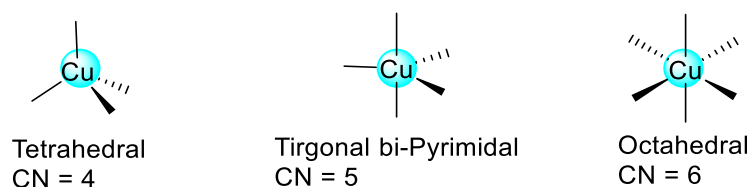
Figure 1.21. Geometries and coordination numbers (CN) of copper (II) complexes.

The biological activity of copper complexes with   N,N-donor ligands ,in particular those containing 2,2'-Bipyridine (*BIPY*) and 1-10 phenanthroline (*phen*), have been studied since the 1970s by Sigman *et al*. and collaborators, and again revised in the 1990s where it is still the subject of much scientific research.[95] The very first complexes evaluated by Zelenko *et al*. for cytotoxic properties were ones of Copper (II) phenanthroline initially synthesized by Sigman.[96] The reaction between 1,10-phenantroline and various copper salts leads to the formation of stable *bis* – phenanthroline copper complexes. Studies have shown that the complex $[Cu(phen)_2]^+$ (Figure 1.22) is capable of inducing oxidative damage at the level of both DNA and RNA which is mediated by interaction with the sugar portion of the two nucleotides.[96] The presence of reducing molecules at a cellular level such as L-ascorbate, NADH, GSH or other thiols mediate the formation of free hydroxyl radicals through the oxide reaction oxidizing copper(I) to copper (II).

DNA cutting activity by $[Cu(phen)_2]^{+/2+}$ is thought to occur following a multi-step mechanism: (i) $[Cu(phen)_2]^{2+}$ is reduced in solution to $[Cu(phen)_2]^+$; (ii) $[Cu(phen)_2]^+$ binds to the DNA in a non-covalent manner; (iii) $[Cu(phen)_2]^+$ is then oxidized to $[Cu(phen)_2]^{2+}$ by H_2O_2 produced *in situ;* (iv) Cu-"oxo" and / or Cu-"hydroxyl" species are formed during oxidation, the exact nature of which is unknown; (v) an oxidative attack mediated by this complex leads to a cut of DNA.[96, 97]
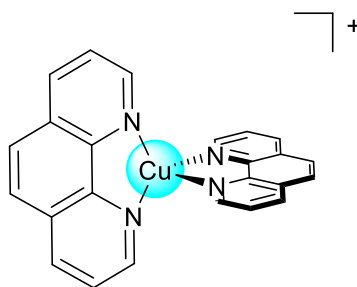
Figure 1.22: *Bis*-[Cu (Phen)$_2$] in its reduced form

Zhou *et al*. have reported that [Cu(phen)$_2$]$^{2+}$ induces apoptosis in the bel-7402 cell line (liver cancer) mediated by a cell cycle block in phase G1.[98] More recently, Cai *et al*. and collaborators have shown that the apoptosis induced by [Cu(phen)$_2$]$^{2+}$ in this cell line is attributable to a high intracellular accumulation of copper, mediated by the intercalation of the phen ligand into the DNA. [99, 100] The same complex demonstrates a high cytotoxicity towards the lines HL60 (human promyelocytic leukemia) and GSC-7901 (human gastric tumor), being able to inhibit the growth of treated cells by about 90%.[100] Despite the very interesting results, the use of the copper complex with bis-phenanthroline shows some limitations, namely its formation is disadvantaged in a physiological environment due to the association of the second molecule of phenanthroline and also the complex shows a lower selectivity at the atomic level of DNA. [100] [101]

To improve the stability of these complexes, two different strategies have been put in place forward during synthesis of these compounds (i) the introduction of a chain which acts as a bridge between the two phenanthroline scaffolds in order to ensure the chelating action. (ii) the use of a Cu-(phen) portion to which other ligands are coordinated (such as amino acids or several mono dentated chelating moieties.[97] Pitie *et al.* have modified the phen scaffold by introducing a serinolic bridge (abbreviated with the term Clip) which bridges the two phenanthroline scaffolds in position 2, (Figure 1.23) leading to the formation of the complex [Cu(2-Clip-phen)]$^{2+}$, or in position 3, with the formation of the complex [Cu(3-Clip-phen)]$^{2+[97]}$.
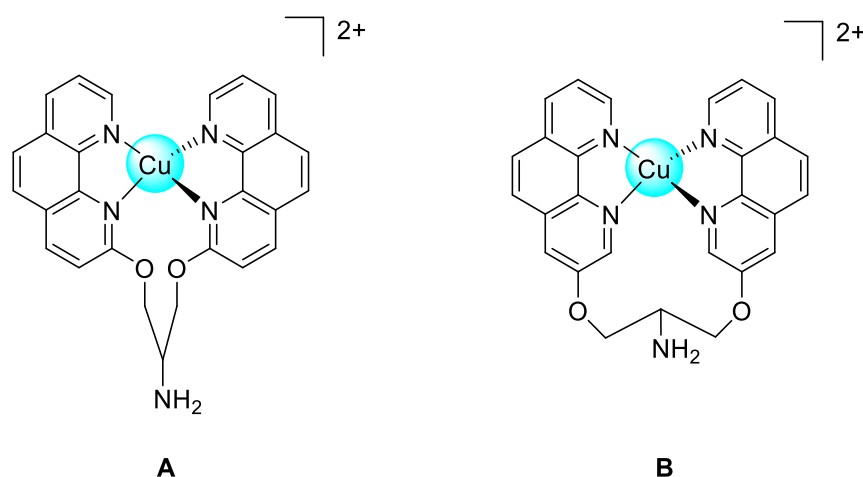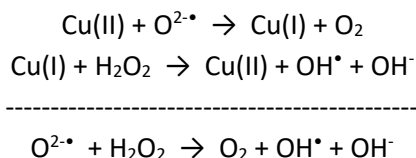
Figure 1.23: [Cu(2-Clip-phen)]$^{2+}$ (**A**) and [Cu(3-Clip-phen)] $^{2+}$ (**B**) prepared by Pitie *et al.*

These changes have made it possible to obtain important advantages: (i) the bridging of the phenanthroline scaffolds ensures that both phenanthroline ligands coordinate the metal; (ii) the [Cu(2-Clip-phen)]$^{2+}$ and [Cu(3-Clip-phen)]$^{2+}$ complexes cut DNA 60 times more effectively than [Cu(phen)$_2$]$^{2+}$ respectively by a mechanism similar to that described for the complex [Cu(phen)$_2$]$^{2+}$. [97]

The cause of the increased DNA cutting activity is not fully understood to date, but it is assumed to arrive from the structural characteristics of the compound rather than its electronic properties.[97] It has been proposed that the amino group on the complex [Cu(3-Clip- phen)]$^{2+}$ can become protonated which then favors the interaction with the polyanionic structure of DNA by forming a hydrogen bond with the oxygen atom on the phosphate chain.[102]

One of the main mechanisms of action proposed to explain copper-induced cellular toxicity comes from the tendency of copper-induced ions to participate in the formation of reactive oxygen species (ROS), both in the form of cuprous copper and cupric copper. In the presence of superoxide anion ($\bullet O^{2-}$) or reducing agents such as ascorbic acid or reduced glutathione (GSH), Cu(II) can be reduced to Cu(I), which is able to catalyze the formation of the extremely destructive hydroxyl radical (OH$\bullet$) from hydrogen peroxide (H$_2$O$_2$) via the Haber-Weiss reaction shown below:[35]

$$Cu(II) + O^{2-\bullet} \rightarrow Cu(I) + O_2$$
$$Cu(I) + H_2O_2 \rightarrow Cu(II) + OH^{\bullet} + OH^-$$
$$\text{--}$$
$$O^{2-\bullet} + H_2O_2 \rightarrow O_2 + OH^{\bullet} + OH^-$$

The hydroxyl radical, being highly reactive, can interfere with almost any biological molecule by tearing a proton from a carbon bound to the aminic group to form a radical protein and an unsaturated fatty acid which in turn forms a lipid radical. All this causes oxidative damage to cells.[103] This, along with the effect from the ligand, leads to a "dual effect" of both intercalation and the ROS cleaving the phosphate diester backbone of the DNA.

A series of drugs containing copper registered under the name Casiopeinas® (Cas) were developed by Ruiz-Azuara group.[104] These mixed copper complexes have a general formula [Cu(N-N)(A-A)](NO$_3$)$_2$ where N-N represents diamine neutral ligand, such as phenanthroline or bipyridine, and A-A denotes the donor N-O or O-O ligands, such as amino acids or acetylacetonates.[55, 104] Experiments conducted in rats show that one of the most promising complexes had very high antitumor activity towards the cell line of glioma C6, this was evidenced by a significant decrease in tumor volume, mitosis index and proliferation, against limited systemic toxicity.[105] In C6 cell cultures, it has been observed that this compound (Figure 1.24) promotes an increase in cell levels of ROS which, as a result, cause mitochondrial damage. This results in the activation of both caspase employed and independent of the apoptotic cell death waterfall.[105] In addition, the results of "COMET *assay"* carried out in peripheral blood lymphocytes and in the cell line of carcinoma of the uterine cervix HeLa, indicate massive DNA damage that appears to be strongly related to the nature of the chelating ligands.[105]
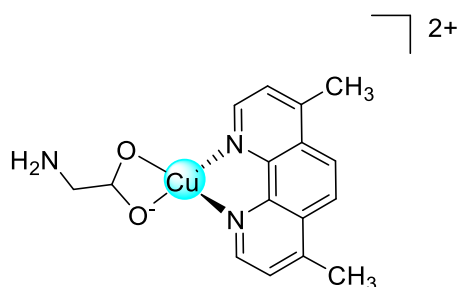
Figure 1.24: Structure of active copper (II) compound by Ruiz *et al.*

In a recent study it was compared to the different nuclease activity of copper (II) complexes containing different heterocyclic bases with N-donors: Phenanthroline (phen), dipyridoquinoxaline (DPQ), dipyridophenazine (DPPZ,) and benzodipyridophenazine (DPPN) (Figure1.25). The aim of the study was to assess whether the complexes containing the DPQ,

DPPZ and DPPN ligands, containing multiple extending aromatic systems, show a better DNA binding affinity than those with the phen analogue. The complex containing the phenanthroline ligand was less active towards DNA than those with DPQ and DPPZ; it has been observed that the complexes containing phen and DPQ have a better affinity of binding to the minor groove of DNA than the complexes containing DPPZ towards the major groove than the DNA itself. [106]

Phen   DPQ   DPPZ   DPPN
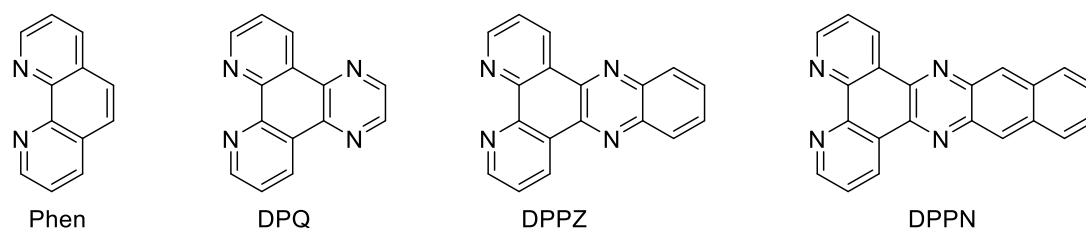
Figure 1.25: Structures of planar 1,10 N,N – donor ligands with increasing structural planarity.[106]

Charef *et al.* subsequently studied the nuclease activity of the copper (II) complex [Cu(DPQ)$_2$(DA)](CLO$_4$)$_2$ (DA = dodecylamine) (Figure 1.26). These findings showed that the complex was capable of strongly binding to DNA and RNA via intercalation. It seemed that the presence of a long aliphatic chain provided by the dodecylamine increased this hydrophobic interaction.[107]
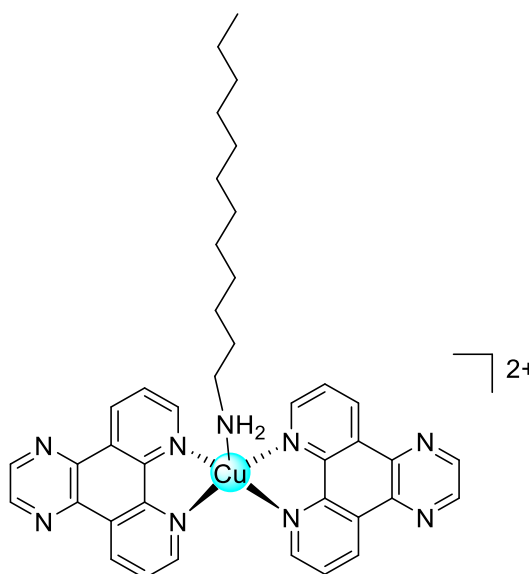
Figure 1.26: Complex prepared by Charef *et al*.

In 2017 four novel copper (II) complexes were characterized and examined by Tummalapalli *et al*. The generic molecular formula for this family of compounds is as follows [Cu(2-pytpy)(L)](NO_3)$_2$ · $2H_2O$(1-4), where 2-pytpy = 4-(2-pyridyl)-2,2: 6,2-terpyridine, L = bipyridyl (bipy), 1, 10 phenantroline, dipiridoquinossaline and dipyidophenazine(Figure 1.27). Various spectroscopic techniques were used to examine the DNA intercalation capacity of the different complexes and it was shown that the best ones are DPQ and DPPZ. Cytotoxic activity of the same complexes in liver cancer cells (HepG-2) was also evaluated and the copper complex with DPPZ ligand proved to be the most effective.[107]
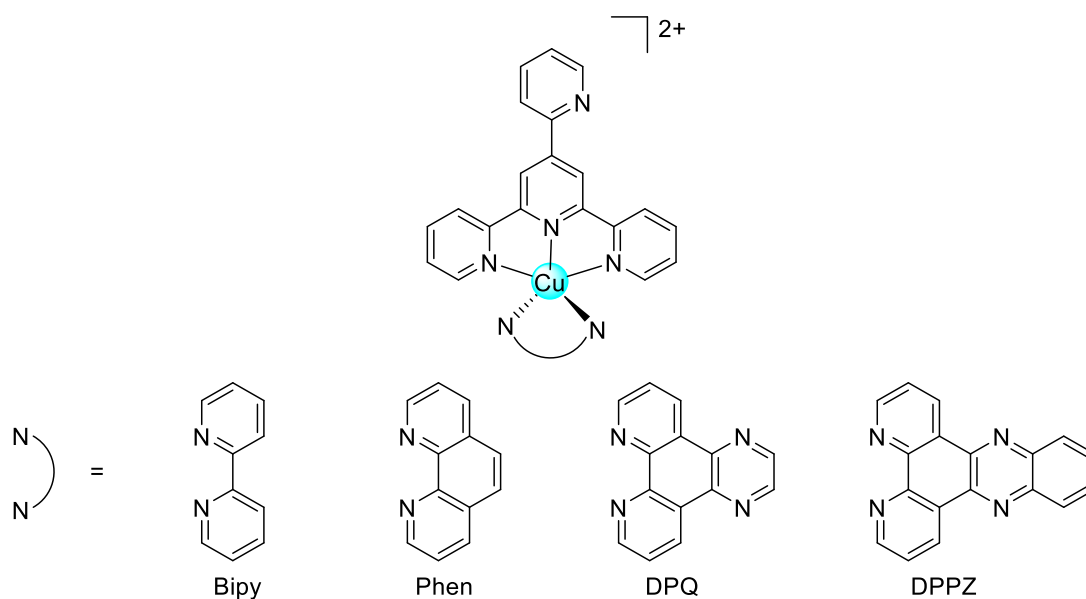
Figure 1.27: Copper (II) complexes synthesised by Tummalapalli *et al.*

This research leaned heavily on the 2014 research from Molphy *et al.* in which four complexes were synthesised and evaluated for biological activity (Figure 1.28). The starting scaffold was the same in each case with the synthesis of mono – phen copper (II) nitrate [Cu (Phen)($H_2O_2{}^{2+}$) and then beginning with dpq a family of four compounds were synthesised with increasing structural planarity. This study also concluded that intercalation was greatest with the complexes containing multiple aromatic systems (i.e. DPQ, DPPZ & DPPN). In addition to this, the cytotoxic activity was evaluated on ovarian cancer cells (SKOV3) and the most active compound was found to be the one containing the DPPN ligand. In fact, the action of [Cu(DPPN)(phen)]$^{2+}$ was very promising and comparable to that of doxorubicin, a chemotherapy intercalative drug currently in use.[108]
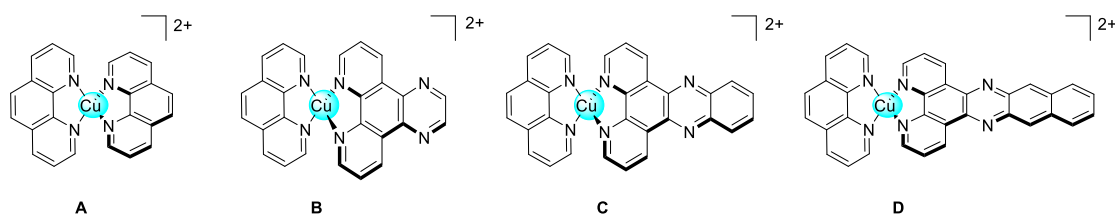
Figure 1.28: Structures of *Bis* – [Cu(Phen)]$^{2+}$ (**A**), [Cu (DPQ) (Phen)]$^{2+}$ (**B**),[Cu (DPPZ) (Phen)]$^{2+}$(**C**) and [Cu (DPPN) (Phen)]$^{2+}$ (**D**).[108]

1.4   Research aims

As already outlined in the preceding sections, there is huge need for the development of new drugs to fight bacterial infections and also to combat numerous cancers due to the global rise in drug resistance in both fields. The aim of the research described in this thesis is to develop novel copper (II) complexes which are both selective and active against these diseases.

The final metal complexes are formed of three major parts, as shown (Figure 1.29)

1) A low toxic endogenous metal centre such as copper.
2) A vector whose receptors are overexpressed in the tumoral tissues to increase the selectivity of the drug.
3) A planar aromatic ligand to target the nuclear DNA via intercalation.
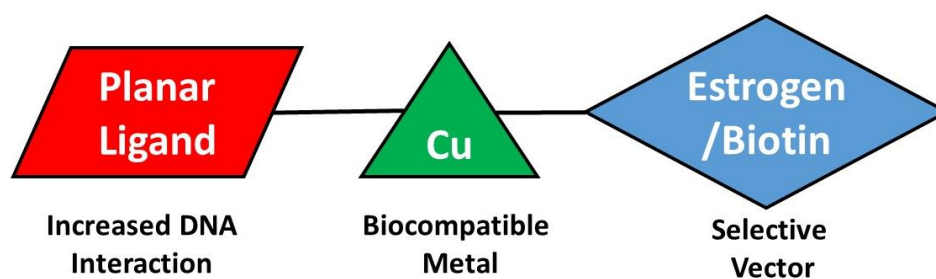
Figure 1.29: Schematic draw of the selective anticancer Cu(II) complexes synthesised in Chapter 2 and 3.

In order to design selective drugs, one strategy is to exploit the difference between cancer and healthy tissues and use vectors that could specifically target the cancer cell feature. Two families of complexes are described, with two different vectors:

(i)   Estrogens (Chapter 2).
(ii)   Biotin (Chapter 3).

The complexes described in Chapter 2 and 3 have been designed, synthetised, characterised with several techniques. Depending by the nature of the complexes, the DNA interaction was analysed. These families of compounds were then screened for anti-cancer activity, cellular uptake, antimicrobial properties, and mechanism of action in collaboration with Prof. Valentina Gandin from the Department of Pharmaceutical Science at the University Padua Italy, Prof. Andrew Kellett (Department of Chemistry, DCU Dublin City University) and Prof. Kevin Kavanagh (Department of Biology, Maynooth University). Some of the biological essays are performed completely by myself (i.e. antimicrobial properties) and others only in part (anticancer activity).

In the final chapter (Chapter 4) is reported the synthesis, characterisation, and DNA interaction of a family of copper (II) complexes tethering two planar aromatic ligands with different substituents, with the aim to analyse the effect of the functional group (electro-withdrawing or electro-donating) on the DNA interaction and antimicrobial activity. The synthesis and characterisation of these complexes are coupled with theoretical analyses, in particular regarding the UV-VIS and IR spectroscopical characterisation.

2   Chapter 2: Steroid derived copper (II) compounds

2.1   Introduction

2.2   Steroids and their role in medicine

In the 1950's, global research and development into steroid derived drugs exploded off the back of newly published reports on the pharmacological effects of the now infamous molecules cortisol and progesterone. Shortly after this, in 1952, it came the breakthrough in a lab synthesis of progesterone by Murray & Peterson *et al.*[109]

Steroids present themselves as a unique family of terpenoid lipids composed of four aliphatic basal rings. The rings are most often arranged in the 6-6-6-5 order as displayed below (Figure 2.0). Although steroids are naturally produced within the human body and in nature many synthetic analogues are available, since the 1950s around 300 steroidal drugs have been identified as treatments for various conditions,[110] making them second only to antibiotics in terms of medication by category. These compounds have been used as anti - inflammatory drugs to treat rheumatologic diseases such as lupus or rheumatoid arthritis. Recently, the drug design is looking at the use of steroids for many more illnesses[111] including allergy medications, leukaemia, interstitial lung disease, Cron's disease and prostate cancer to name a few. These wide range of illnesses are all treated by one of the two classifications of steroid hormones known as corticosteroids, or lab synthesised versions of natural steroids. The other classification being sex - steroids. Steroid hormones are responsible for the regulation of the metabolism, immune functions, and inflammation.
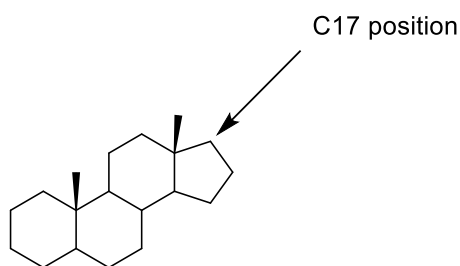
Figure 2.0: Generic structure of the steroid scaffold with the 17-position indicated

Many steroidal derived drugs are listed on the WHO list of essential medicines, particularly relevant, as mentioned above, for the treatment of anti-inflammatory conditions, autoimmune diseases, and fertility management.[112] Steroidal sex hormones are used currently to as treatment for male sexual organ dysfunction, gynecopathies and as a form of contraceptive medication.[113] To date, the two main routes to synthesise steroids on an industrial scale are the diosgenin pathway and the microbiological transformation route.[110]

In 1952 the total synthesis of a number of nonaromatic steroids was achieved by Woodward *et al.* with the synthesis comprised of twenty steps starting from 4-methoxytoluquinone.[114] Although an impressive achievement, it is not a realistic approach to industrial scale due to cost and yield. The demand for steroid drugs and steroidal precursors for the synthesis of these drugs is most certainly going to expand and grow, most likely due to the increased consumption of oral contraceptives as birth control. It is however worth noting that this rise in the popularity in steroids may open the door to the steroids being consumed in an abusive situation or by athletes seeking to improve performance. Health risks associated with the taking of unsupervised and unprescribed steroids can lead to liver cancer, heart attack and elevated levels of cholesterol in both females and males alike.

2.3   Hormone receptors

There are many different ways of delivering medication to the body in a specific and purposeful way. To date around 500 molecular structures have been identified which act as targets for drugs and most of these are receptors and enzymes, ion channels, nucleic acids, transport proteins and ribosomes. Multiple disciplines are involved in identifying these targets and it is known collectively as drug design. Hormones produce their effects on target tissues by binding to specific proteins called hormone receptors which are located in the target tissues only. The hormone receptors present on the cell membrane of these target cells are called membrane bound receptors and thus the receptors present inside the target cell are referred to as inter-cellular receptors, or nuclear receptors. Binding of a specific hormone to its receptor leads to the formation of a hormone receptor complex. Each receptor is specific to one hormone only and hormone – receptor complex formation leads to certain biochemical changes in the target tissue. Metabolism and hence physiological functions are regulated by these hormones that can be divided into four groups:

(i)   Peptide, polypeptide, protein hormones insulin, glucagon, pituitary hormones, hypothalamic hormones etc.

(ii)   Steroid's cortisol, testosterone, estradiol and progesterone Iodothyronines – thyroid hormones;

(iii)   Amino acid derivative – epinephrine;

(iv)   Hormones which interact with membrane bound receptors normally do not enter the target cell but generate second messengers. eg. Cyclic AMP, Ip3, Ca^{2+} etc which in turn regulate cellular metabolism.

Hormones which interact with intra cellular receptors (steroid hormones, iodothyronines etc) mostly regulate gene expression or chromosome function by the interaction of hormone – receptor complex with genome. Cumulative biochemical actions result in physiological and development effects.

2.3.1   Steroid hormone receptors as molecular targets

The steroid hormone receptors (SHRs) are ligand-dependent intracellular transcription factors that are known to influence the development and growth of many human cancers. These receptors pass signals from the steroid / hormone to the target gene *via* an interaction at the cellular level. In recent years, more and more evidence implicating SHRs and their coregulators in multiple pathophysiological conditions has sparked immense interest in understanding SHRs structure and cell biology which has resulted in exposing a unique window for novel steroid-based targeted therapies for cancer.[115]

As described earlier, the role of sex hormones in cancer progression within hormone sensitive tissues is very well established. For example, 60 - 70 % of breast cancers are considered as being hormone-dependent due to an overexpression of estrogen receptor (ER) proteins.[116] The overexpression of sex hormones in prostate cancer and colorectal cancers has also been very well documented.[116, 117] While the classical ER (ERα) is well-characterized, another, ERβ, has only recently been discovered.[118] Exploiting steroids such as estradiol as carriers or as agents able to disrupt the biological function of ERs, represents an attractive strategy for the rational design and development of anticancer agents.

2.3.2   Steroidal based ligands

In 2014 Zang *et al.* synthesised a new library of 11β-ether-17α-ethinyl-3,17ß-estradiol compounds which showed strong antagonist ER activity (Figure 2.1). These are a family of ethers and are of particular interest as they were highly active estrogen antagonists which were even more stable than previous substituents. Of these ligands ethers **1** & **2** bind very strongly to both the ERα and Erβ receptors.[119]
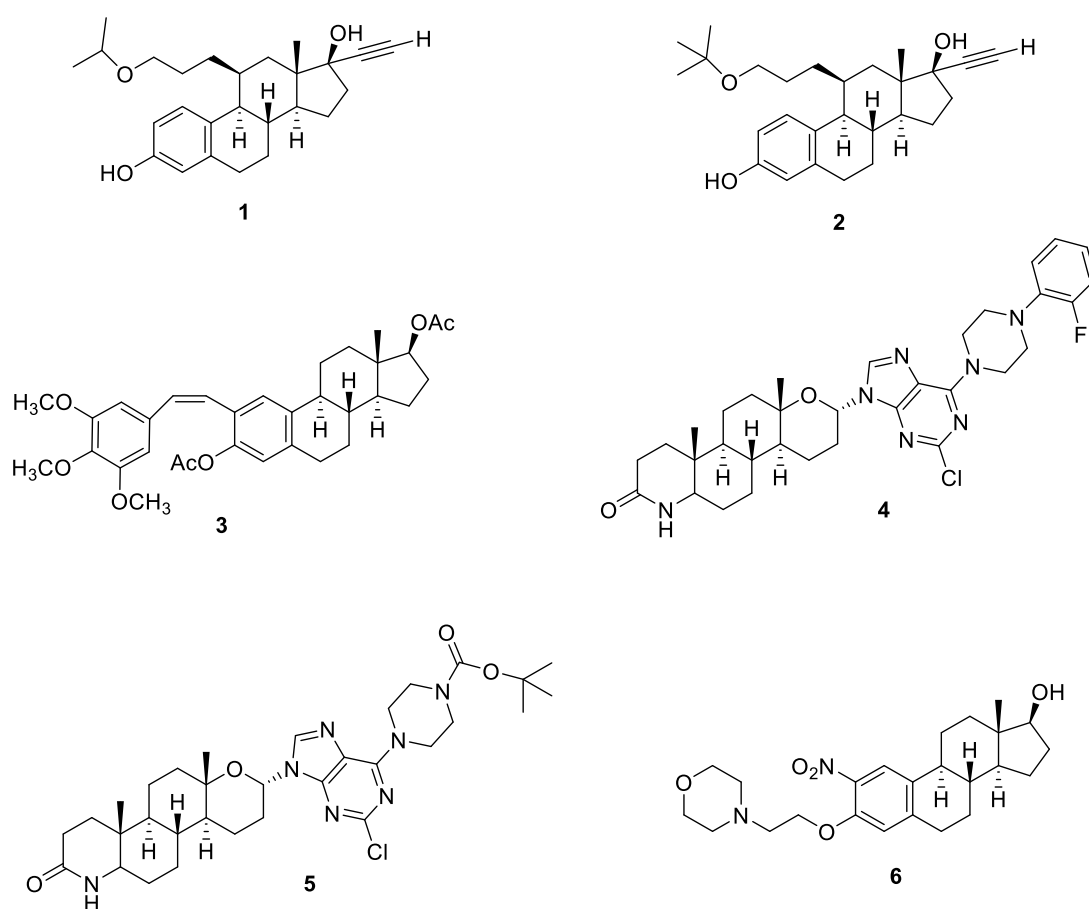
Figure 2.1: Steroidal – ether ligands.[119]

Combretastatin A4 analogues attached to a steroidal framework were reported to have anti-breast cancer properties. More recently, natural occurring compounds have increasingly been used in traditional medicines. The Combretastatin A4 molecule is known to induce apoptosis and act as an antiangiogenic agent.[120] Twenty-two different analogues were synthesized which included the Combretastatin A4 steroidal framework and among them, compound **3** (Figure 2.1) was the most active in both MCF-7 and MDA-MB-231 cells with an

IC_{50} of 7.5 µM and 5.5 µM.[121] The free Combretastatin A4 molecule is shown below (Figure 2.2).
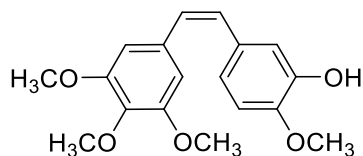
Combretastatin A4

Figure 2.2: Combretastatin A4 molecule.

More recently, Huang *et al*. reported two new libraries of novel C6-piperazine-substituted purine steroid–nucleosides and C6-cyclo secondary amine-substituted purine steroid-nucleoside analogues and were evaluated for their anticancer activity. [122] [123] [124] The nucleoside analogues displayed an important role in the development of antitumor drugs. Among them, the C6-aminopurine derivatives had a wide range of biological properties and displayed antitumor activity.[125] [126] [127] [128] [129] Of the C6-piperazine-substituted purine steroid–nucleosides analogues, compound **4** (Figure 2.1) showed the best results on the MCF-7 cell line.[130] However, compound **5** (Figure 2.1) displayed very moderate anticancer activity against the MCF-7 cell line.[131]

Bandyopadhyay *et al.* [29] published a series of 2- and 4-nitroestradiol derivatives. He showed that compound **6** (Figure 2.1), reduced the viability of ER-positive and ER-negative cells with similar efficacy. The cytotoxicity exhibited by **6** was slightly lower than 4-HT, with an IC_{50} value of approximately 2 µM in breast cancer cells. This data indicates that selective novel nitro-estradiol compounds effectively cause cytotoxicity in breast cancer cells and that the cytotoxicity may occur in an ER-independent manner.

2.3.3   Steroidal metal complexes

Dagorne *et al.* has published an extremely comprehensive review on the synthesis of transition metal steroid derivatives.[132] The work covers a huge volume of synthesis and modifications to many steroid conjugates and the synthesis of an array of transition metal derived steroidal compounds, many of which will be discussed below.

Some of the earliest reports of metal-based steroidal compounds were platinum (II)-steroid conjugates which date back to the early 1980s, but these early studies did not investigate their specific interactions with ERs. For example, Gandolfi *et al.* developed platinum(II)-estradiol conjugates, but despite the sound rationale behind their development, they were not found to be highly cytotoxic.[133] Estrogen conjugates modified in the 17α position have long since represented an attractive strategy as a delivery vector because it does not affect the affinity for the receptors.[134] [135] Zhang *et al.* synthesised a series of estrogen – derived complexes (Figure 2.3) using a squaramide structure as the metal core chelating moiety and these complexes were seen to be Erα agonists. In comparison to the free ligand (**7**) the binding affinity for all compounds **7- 10**) for Erα increased while the studies also showed the binding affinity for Erβ of (**7-10**) decreased.[136]
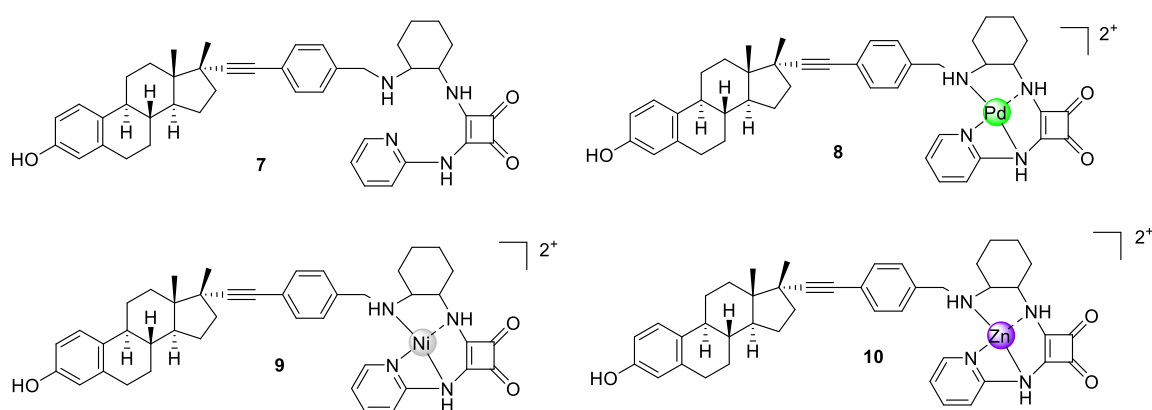
Figure 2.3: Novel estrogen conjugates developed by Zhang *et al*.[136]

More recently Vellé *et al*. compiled a series of four gold(I) complexes bearing *N*-heterocyclic carbenes and steroid derivatives (ethynylestradiol and ethisterone) with the generic formula [Au(R2 -imidazol-2-ylidene)(steroid)] and their antimicrobial activity was examined.[137]
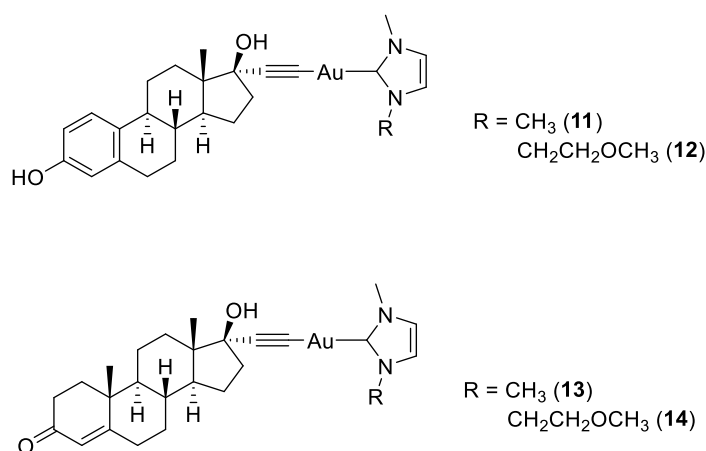

Figure 2.4: Family of compounds developed by Vellé *et al*.

As expected, both of the free steroid ligands (ethynylestradiol and ethisterone) were found to be inactive against *S. aureus* (Gram positive) and *E. coli* (Gram negative), and it pointed towards the presence of the metal centre being of fundamental importance for antimicrobial activity. The two carbene precursors which were the gold carbene chloride compounds were found to be the most active among the complexes which were tested, both in both Gram-positive and Gram-negative bacteria, displaying very low MIC_{50} values (average MIC_{50} : 4.1 and 5.85 mm for 1 and 2, respectively). Vellé *et al.* discovered that the presence of the estrogen seemed to slightly decrease the in vitro antimicrobial activity with respect to the two precursors of the carbene gold chloride complexes. However, it was discovered that complexes **11** and **12** (Figure 2.4) which had the estradiol moiety, were much more active than the corresponding testosterone species **13** and **14** (average MIC_{50} : 8.2 and 39.4 mm for **11** and **12**, and 95.0 and 69.2 mm for **13** and **14**, respectively).

Berube′ *et al*. have also conducted extensive research in trying to bring forward a lead platinum (II)-steroid conjugate. They proposed that the length of the spacer linking the steroid to the cytotoxic platinum(II) moiety played a crucial role in the biological activity of the complex with the optimal chain length consisting of either 11 or 12 carbons in length.[138] They have since advanced numerous examples of platinum(II)- estradiol conjugates with some exhibiting ER binding affinities similar to that of 17-β estradiol itself.[139] [140] [141] [142]

Over the past decade, Berube′ *et al.* have continued their work on steroids and managed to build a library of steroid derived compounds, including the development of a series of platinum (II)-estradiol complexes in which the estradiol was linked to the platinum centre *via* a N-substituted 2-aminoalkylpyridyl chelating derivative which included an aliphatic carbon chain spacer of varying length, (Figure 2.5).[143]

Berube's group found unsurprisingly that, while increasing the chain length, solubility decreased. This lead to the incorporation of a poly (ethylene glycol) linker which gave rise to increased solubility while also allowing the team to alter the spacer length. The complexes, bearing hexyl, octyl, undecyl, and tetradecyl spacers, which separate the cytotoxic platinum (II) core from the steroid nucleus (Figure 2.5), were screened against MCF-7 (ER+), MDA-MB-231 (ER−), MDA-MB-468 (ER−), and MDA-MB-436 (ER−) cell lines.
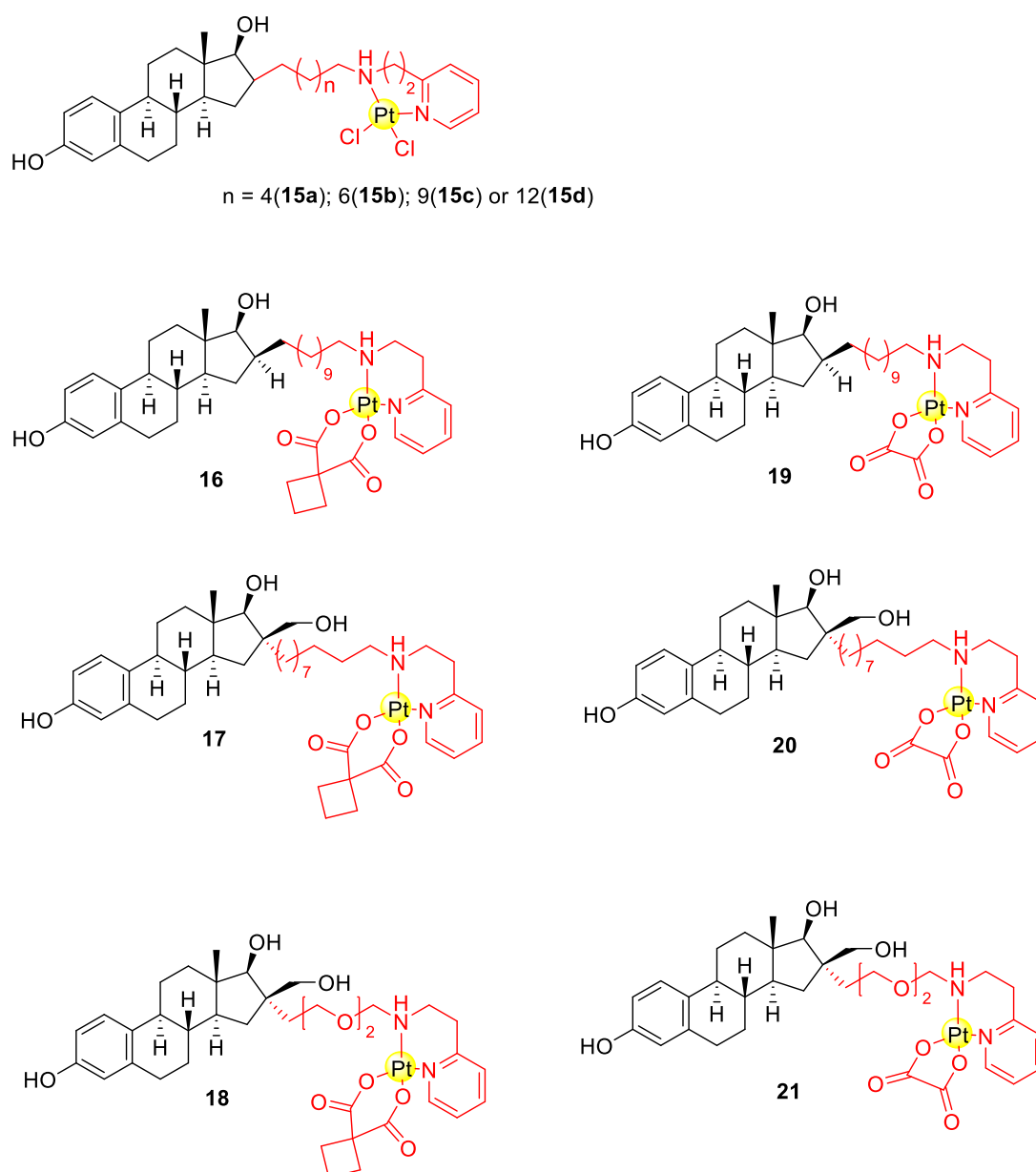
Figure 2.5: Molecular structures of platinum (II) derived – estrogen compounds (**15-21**).[143]

Complexes (**15 a-d**) showed very good ER binding affinity, similar to estradiol 17β. All were also significantly more cytotoxic than cisplatin (ranging between 4 and 9 times more potent) except against the MDA-MB-468 (ER−) cell line. There did not appear to be a direct correlation between alkyl chain length and cytotoxicity, though potency did vary slightly, with the complexes containing the 8 and 11 carbon chains (**15c** and **15d**) displaying the most potency. It required an 8-step synthesis to achieve these conjugates with yields in the region of 20 % which, although still very low, represented a significant improvement on the synthesis of some of their earlier related derivatives.[143]

Additional studies by Berube´ *et al*. looked at the efficacy of a series of estradiol-linked platinum (II) derivatives incorporating either the *O,O*-labile leaving ligand of carboplatin (**16 -21**), or that of oxaliplatin (**19 - 21**), Figure 2.5.[144] Six novel complexes were obtained, again with varying carbon chain linkers between the cytotoxic platinum core and the estradiol adduct for both carboplatin and oxaliplatin-based structures. The cytotoxicity of the complexes was then screened against the MCF-7 (ER+) and MDA-MB231 (ER−) cell lines and compared with cisplatin, carboplatin, and oxaliplatin. Interestingly, the group found that the carboplatin base had less effect on the inhibition of cancer cell proliferation, with IC_{50} values in the range 1.8 - 33 µM for the cisplatin derivatives and between 21 and 74 µM for the carboplatin analogues. Notably, the carboplatin analogues also resulted in a loss of ERα binding affinity. In these studies, the oxaliplatin based compounds were showed to be more promising, the compounds were maintaining ERα binding affinity and two of the three oxaliplatin compounds tested were displaying significantly lower IC_{50} values than that of cisplatin.[144]

The study by Berube and co-workers demonstrates the influence of the labile leaving ligands on not only the antiproliferative activity of the resulting conjugates but also on their ERα binding affinities.[144] The presence of the bulkier cyclobutane-1,1-dicarboxylate leaving ligand was clearly impacting on the biological profile of these complexes.

With an ever-growing prevalence of prostate cancer, Berube´ *et al.* proceeded to synthesise a family of platinum (II) compounds which were conjugated to a testosterone derivate in the 7α position. The testosterone was chosen on the rationale that it could promote androgen targeting. Six of these complexes were synthesised which included a 17β - acetyl testosterone linked to a cisplatin core *via* amino acid N-donor bridges (L- and D-2-pyridylalanine, L- and D-methionine, L-histidine and L-4-thiazolylalanine) (**22a-f**), [145] (Figure 2.6) below.

The group found that the stereochemistry presented by the amino acid had little to impact on the cytotoxicity. The pyridylalanine and thiazolylalanine complexes displayed the most cytotoxic activity (**22a, 22b & 22f)** against LNCaP, PC3, and DU145 androgen receptor positive and negative (AR+ and AR−) cell lines, displaying IC_{50} values lower than cisplatin across all cell lines. These complexes were further screened against additional AR+ and AR− cell lines: HT1080 HT-29, M21, MCF-7, MDA-MB-231, MDA-MB-468, CEM, CEM-VLBb, and CEM-VLB/CEM. All six of the compounds were again found to be significantly more cytotoxic than cisplatin against these cell lines with the exception of the multidrug resistant leukaemia CEM-

VLB and wild-type leukemia CEM-VLB/CEM cells. Compounds **22a** and **22f** were screened on HT-1080 tumours grafted onto chick chorioallantoic membrane and showed good antitumor activity while showing low toxicity toward chick embryos.[145]
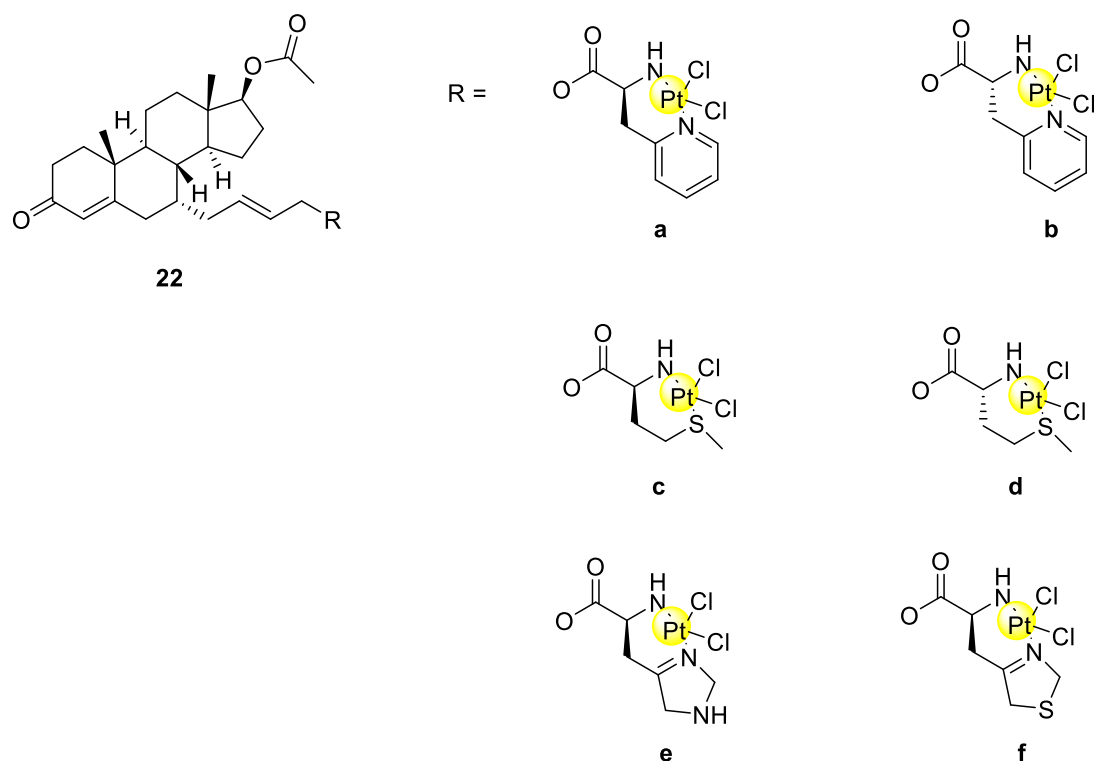
Figure 2.6: Molecular structures of testosterone coupled platinum (II) complexes prepared by Berube´.

In summary, from all the works published by Berube' (a pioneer in the use of estrogens-metal compounds) two important factors can be drawn. Firstly, that hormone receptor targeting is dependent on the cytotoxic metal core in this case platinum, secondly the nature of the linker separating the platinum core from the steroid is very important. With this in mind their studies lean towards the basis of a very strong design model for new hormone targeting cytotoxic metallodrugs. In 2006 Hannon *et al.* synthesised an estrogen platinum terpyridine conjugate [146] (Figure 2.7). The steroid was attached to the 4'-Ethynyl-terpyridine at the 17α position to yield the ligand 17α-[4'-Ethynyl-2,2':6',2''- terpyridine].
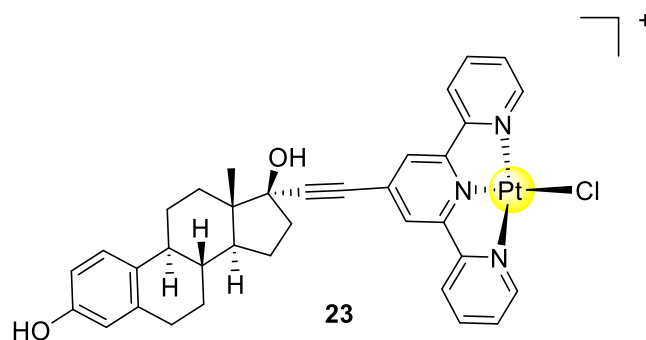
Figure 2.7: Hannon *et al.* estrogen platinum complex.[146]

Hannon *et al*. reported that the complex **23** did bind to serum albumin (a steroid transport protein) and to DNA simultaneously. This again demonstrates that steroid derived metal complexes can be bi-functional molecules. The crystal structure showed that it was unlikely to be able to intercalate the DNA. However it was more likely that the metal itself was coordinating to the bases in the major groove of the DNA.[146] When screened against MCF-7 cell lines where diethylstilbestrol was used as the control the IC_{50} for the complex was found to be 5 nM in comparison to that of the control at 0.1 nM.

Jaouen *et al* carried out some of the earliest work with metallo modified estradiol complexes in 2002.[147] Binding studies to the receptor were carried out and a relative binding affinity was established (RBA) this was measured in reference to the free estradiol ligand which was assigned a binding affinity of 100%. The two complexes which displayed the largest RBA were a rhenium and a ruthenium complex 13.5 and 16 % respectively (Figure 2.8)
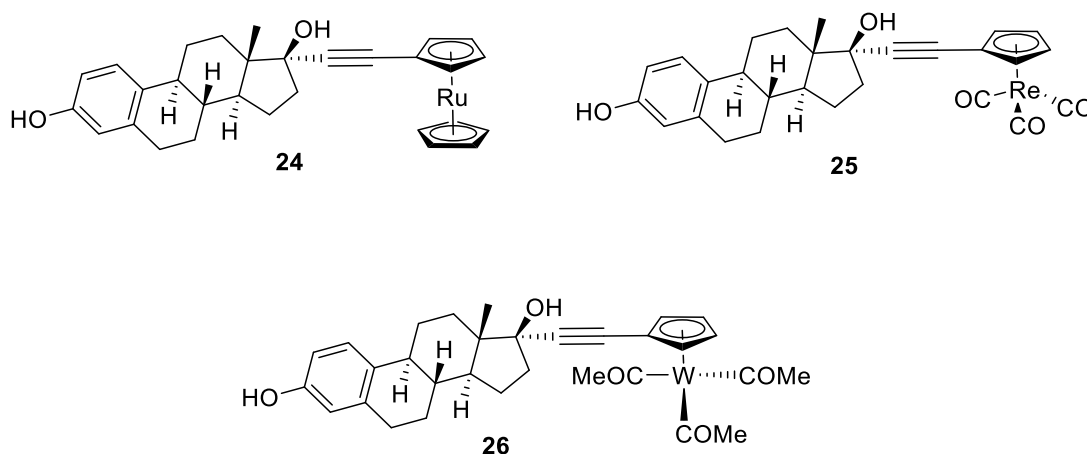

Figure 2.8: metallo-estrogen complexes from the Jaouen *et al*. group.

Jaouen also measured the lipophilic value of the complexes produced and they all had increased lipophilicity in comparison to the free estradiol ligand (3.3) with the three metal complexes showing very similar values (4.9, 5.3 & 5.3). The values are high enough for the

complexes to enter the cell but also remaining under 6 which means they arrive in the region for potential pharmaceuticals.[147]

In 2019 Kitteringham *et al.* in collaboration with Montagner and Griffith[148] developed two steroidal platinum complexes. Both of the complexes contained a platinum (II) core and an estradiol modified triazole. (Figure 2.9)
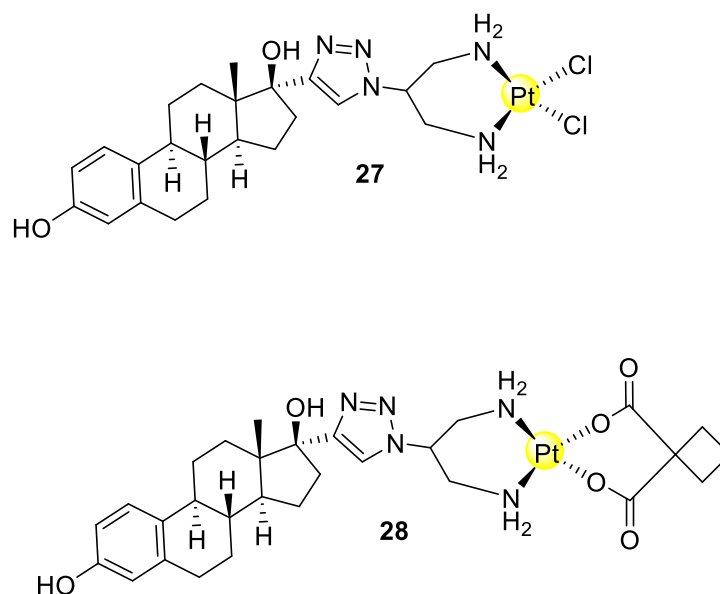
Figure 2.9: Complexes developed by Kitteringham *et al*.[148]

The two complexes were then screened against multiple cancer cell lines (A2780, 2008, A431, MCF-7 and HCT-15) andboth compounds exhibited far superior cytotoxicity *in vivo* than that of cisplatin against all five of the cancer cell lines they were screened against. IC$_{50}$ values as low as 0.01 µM were observed against A2780 and MCF-15 for compound **27** and values of 0.03, 0.09 and 0.4 µM for 2008, A431 and HCT-15 respectively.

Compound **28** did not perform as well but still had far lower IC$_{50}$ values than that of cisplatin or carboplatin. It preformed considerably well against A2780 and MCF-15 with IC50 values of 0.1 µM and 0.3 µM respectively. For comparison cisplatin displayed an IC$_{50}$ value of 2.6 µM and 7.2 µM for these cell lines. Carboplatin was not effective against MCF-15 or HCT-15

2.4   1,10 – phenanthroline as a scaffold

1,10-Phenanthroline (phen), (Figure 2.10) is one of the classic chelating bidentate ligands for transition metal ions and has played an important and extremely prominent role in the development of coordination chemistry.[149] [150] To date it continues to be of considerable

interest both as versatile starting material for organic synthesis and inorganic chemistry. Phen is a rigid and planar, hydrophobic, electron-poor heteroaromatic system containing two nitrogen atoms which are placed in the 1 and 10 positions to act very cooperatively in cation binding. These structural features determine its coordination ability and lead it to play a very dominant role in metal ion binding. 1, 10 – phenanthroline behaves as a weak base in aqueous solution, its basicity is far lower than other aliphatic diamines such as ethylenediamine. Phenanthroline displays incredible coordination properties for transition metal cations. It readily forms octahedral complexes in aqueous solution including $[M(phen)(H_2O)_4]^{2+}$, $[M(phen)_2(H_2O)_2]^{2+}$and $[M(phen)_3]^{2+}$ with all the first-row transition metal cations. The stability of the $[M(phen)]^{2+}$ complexes follow the Irving – William's series.[151] These range from 4.13 log units for $[Mn(phen)]^{2+}$ to 9.25 log units for $[Cu(phen)]^{2+}$.[152] [153] Despite the low σ-donor ability of the two heteroaromatic nitrogen atoms in the 1 and 10 positions, the stability of these phen complexes is somewhat higher than that found for the corresponding complexes with ethylenediamine. In fact, the complexes with phen exhibit a larger entropic contribution to complex stabilization than ethylenediamine, mainly due to the hydrophobic nature of phen and to the consequent larger desolvation of metal cations upon complex formation.[152] The increasing interest in the chemistry of phen derivatives has prompted the development of some very efficient synthetic procedures for the functionalization of the 1, 10 phenanthroline scaffold in various positions.

The symmetric synthetic manipulation at the 2,9-positions to prepare more elaborate phen-based structures represents the most preferred strategy. Symmetric substitution at the 3, 8, 4, 7 and 5,6 positions are less common, but have been done, famously of these is the oxidation in the 5, 6 position to yield 1,10 – phenanthroline – 5,6 – dione.[154] Even more rare are modifications to phen in a single position leading to unsymmetrical adducts of the molecule. Although these mono substitutions are rare, many have been carried out. One method regularly carried out in synthesis labs is the route proposed by Ji *et al*. (Figure 2.10) which allows the formation of a mono substituted nitro group and then amino in the 5 or 6 position.[155]
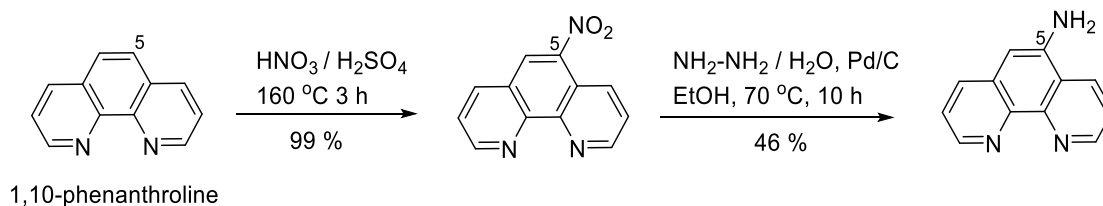
Figure 2.10: Synthesis of 5-amino-1,10-phenanthroline from 1,10-phenanthroline.[155]

2.5   Chapter Objective

This chapter deals with the synthesis, characterisation, and biological evaluation of steroid derived copper (II) compounds as potential antimicrobial and anticancer compounds. As discussed earlier in the introduction, there is currently a great need to develop drugs with less toxic side effect for cancer treatments. The compounds outlined in this chapter represent a promising alternative to overcome the toxicity cisplatin is famous for along with offering a potential more selective route to treatment.

The chapter will describe the synthesis of two novel steroid-based ligands which will become the targeting vectors for the drugs and then a series of 6 novel copper (II) compounds.

The coordination sphere of the copper complexes will be further functionalised with aromatic planar ligands such as phen, (1, 10 – phenanthroline), DPQ, (dipyridoquinoxaline), DPPZ, (dipyridophenazine) and DPPN (benzodipyridophenazine) that are DNA intercalators.

By taking this modular approach, the synthesis was broken down into manageable steps. Firstly, the steroids were coupled to a 1,10 – phenanthroline scaffold *via* Sonogashira coupling reaction, then the planar ligands were prepared using the Schiff base mechanism and later conjugated to the copper (II) core. In a final step the new targeting vector with the steroid derivative was attached to the copper (II) to yield six novel compounds. In this way, the final compounds will have three important features:

   i)   A less toxic and biocompatible metal centre such as Cu(II);

   ii)   An estrogen derivative that will act as a vector to target cancer cells;

   iii)   A planar aromatic ligand that will increase the DNA intercalation properties.
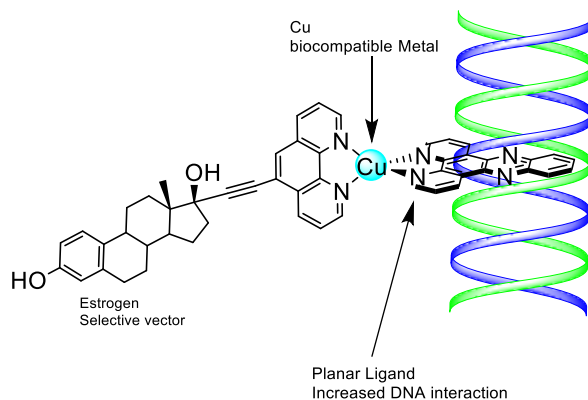
Figure 2.11: Illustration of one of the final compounds.

Two publications were produced from this chapter:

Evaluation of *in vitro* and *in vivo* antibacterial activity of novel Cu(II)-steroid complexes - S. Barrett, S. Delaney, K. Kavanagh, D. Montagner - *Inorg. Chim. Acta*, **2018**, 479, 261-265.

Anticancer Activity, DNA Binding and Cell Mechanistic Studies of Estrogen-Functionalised Cu(II) Complexes - S. Barrett, E. Negrelli, A. Kellett, E. Dempsey, A. Erxleben, V. Gandin, D. Montagner - *J. Biol. Inorg. Chem*, **2019**, 25, 49-60.

2.6   Synthesis & characterisation

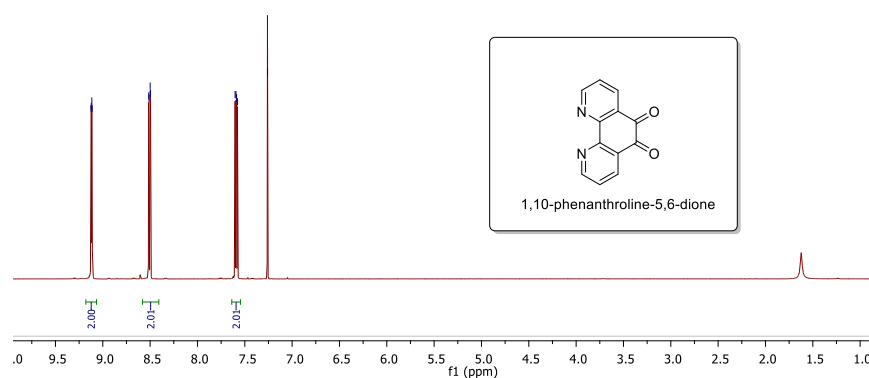## 2.7   Synthesis of planar ligands

All the planar ligands discussed in this chapter were synthesised from well-known synthetic routes. The phendione **2.10** was synthesised from the commercially available 1, 10 − phenanthroline.[154] The DPQ,[156] DPPZ,[157] and DPPN,[108] derivatives were made from the corresponding diamine precursors and **2.10**.
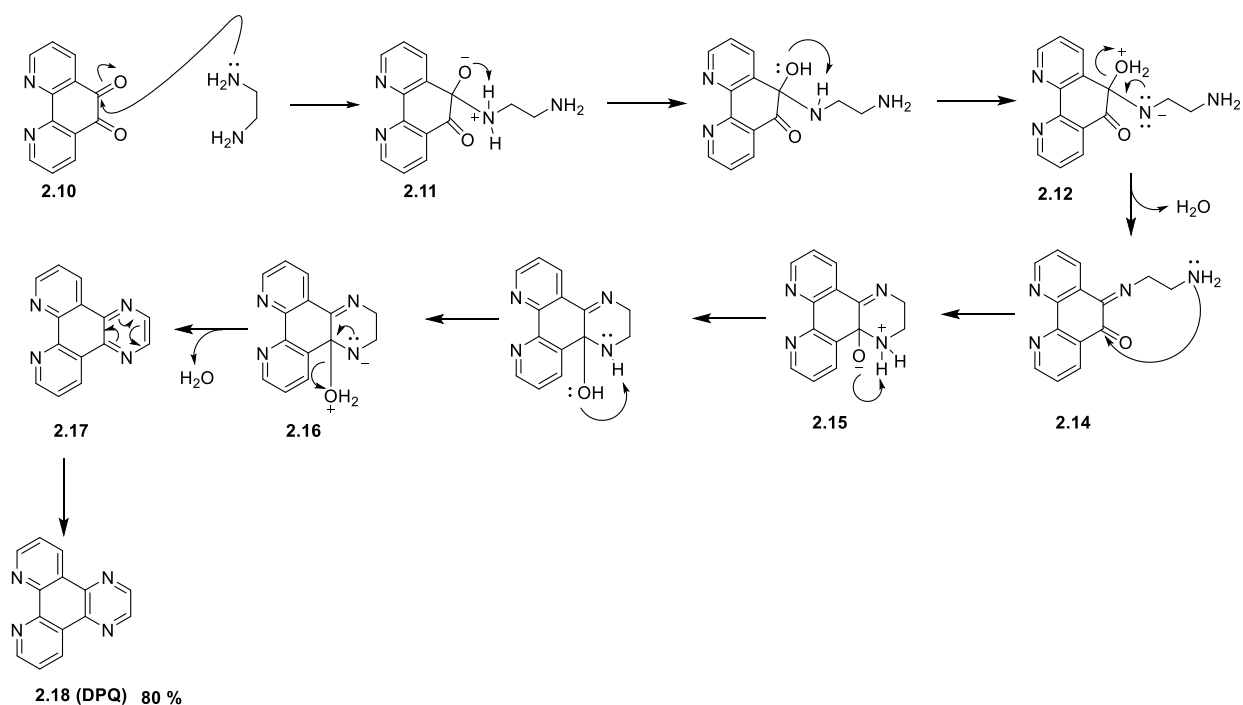
Scheme 2.1: Mechanism showing formation of (DPQ) via enamine formation under neutral conditions.

The phendione **2.10** undergoes nucleophilic attack from one of the nitrogen's on the ethylenediamine in the 5 or 6 position first, breaking the π bond on the carbonyl carbon - oxygen. This gives rise to the quaternary ammonium ion intermediate **2.11**, the negatively charged oxygen is able to deprotonate the amine as its in very close proximity. This forms the aqua leaving group seen in **2.12** and the lone pair of electrons on the Nitrogen donate back in towards the aromatic system forming a π bond and then leading to the ejection of the aqua group, therefore eliminating a molecule of water from the compound. The second amine now simultaneously carries out the process again as show in **2.14** and again the process is the same through **2.16** with the discharge of a second molecule of water. Finally,

the reaction terminates with a reshuffle of electrons **2.17** leading to the aromatic system in

the final product (DPQ) as seen in **2.18**. The mechanism for DPPZ and DPPN proceeds *via* the

same pathway to yield 70 % and 83 % respectively. The (DPQ) reaction was carried out in

H_2O with the product precipitating and the impurities remaining in the aqueous solution, for

the DPPZ and DPPN the reactions were done in EtOH with the same result. The precipitates

were washed with H_2O and then with Et_2O before recrystallising from MeOH. In the cases of

DPPZ and DPPN recrystallization was not required as the products were already pure upon

collection. The reactions can be easily followed *via* TLC (9:1 DCM: MeOH) and NMR. There is

a clear presence of the two new aromatic protons in the ^{1}H NMR at 8.97 ppm (Figure 2.12)

displaying as a singlet when compared with that of the phendione (Figure 2.11). This

spectrum also shows the absence of the aliphatic protons from the ethylenediamine, and the

amine protons associated with this reactant (Figure 2.12).

1,10-phenanthroline-5,6-dione
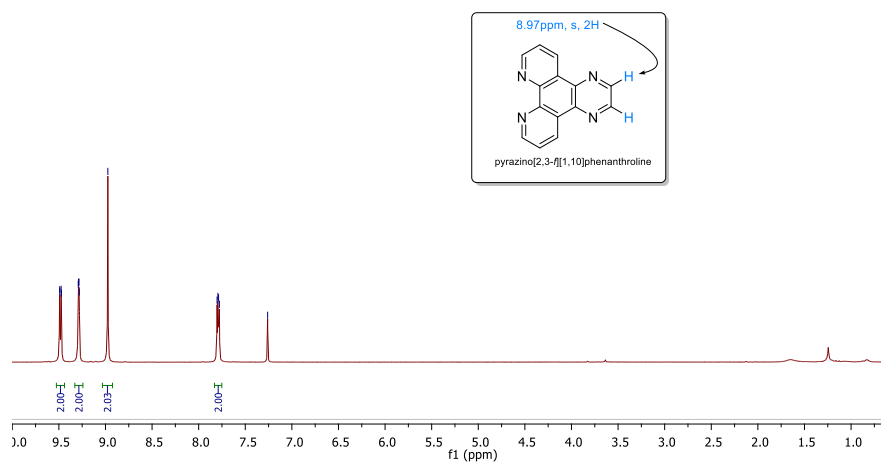
Figure 2.11: ^{1}H NMR ($CDCl_3$) of Phendione **2.10.**

Figure 2.12: ^{1}H NMR (CDCl$_3$) of DPQ, **2.18**.

2.8   Synthesis copper (II) complexes of DPQ, DPPZ and DPPN

The planar ligands discussed in the previous section were conjugated to the copper (II) centre to yield copper (II) monoadducts with increasing structural planarity These were prepared by reacting a slight excess of the copper nitrate salt with one equivalent of each of the ligands (Scheme 2.2). Ensuring there is an excess of the copper salt present promotes the formation of the mono substituted copper (II) complex as opposed to the bis compound. In each case, the reaction was done in MeOH as both starting materials were soluble in MeOH but the resulting products insoluble in MeOH. The resulting crude product was washed well with CHCl$_3$ to wash away any residual organic component and then with water to dispel the excess copper (II) nitrate salt. Finally, the compounds were wash with Et$_2$O and dried under vacuum.

The characterisation of the monoadducts were based on elemental analysis, IR, HR-MS and elemental analysis. Due to the paramagnetic properties displayed by the copper (II) core, NMR could not be used for characterisation. As these complexes were all previously synthesised by Molphy *et al*. the data and spectra collected were compared to this previously reported findings from this group.[158] It was concluded that the results achieved matched that of the reported data by Molphy *et al*.
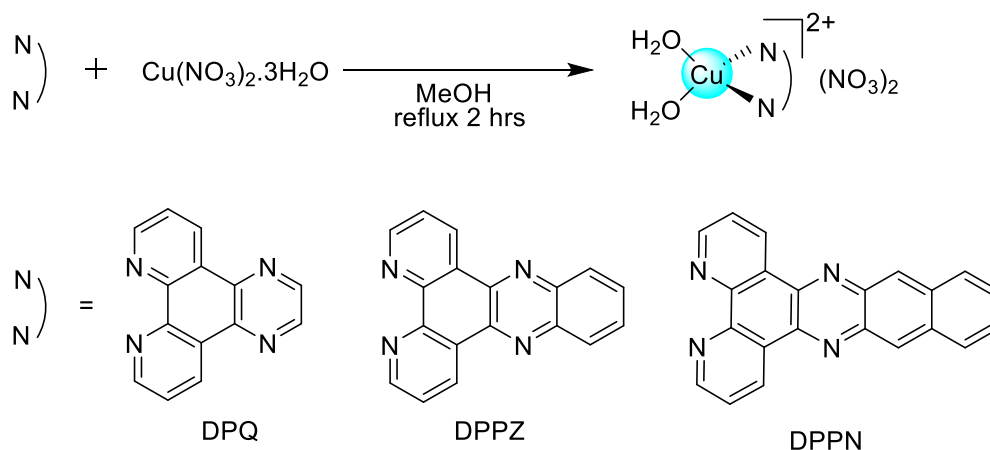
Scheme 2.2: Generic overview of the synthesis of [Cu(N∩N) (H$_2$O)$_2$].2NO$_3$.

2.9 Coupling of steroid to 1,10 – phenanthroline

The two novel phenanthroline - steroid derivatives of general formula ES or EE-5-phen (where ES-5-phen and EE-5-phen are the Estradiol and Testosterone derivatives, respectively) were obtained by a copper free Sonogashira coupling reaction between 5-Bromo-phenantroline and the corresponding commercially available alkyne derivative of the steroids. The two commercially sourced alkyne derivatives were Ethinylestradiol (EE) and Ethisterone (ES) (Figure 2.13).
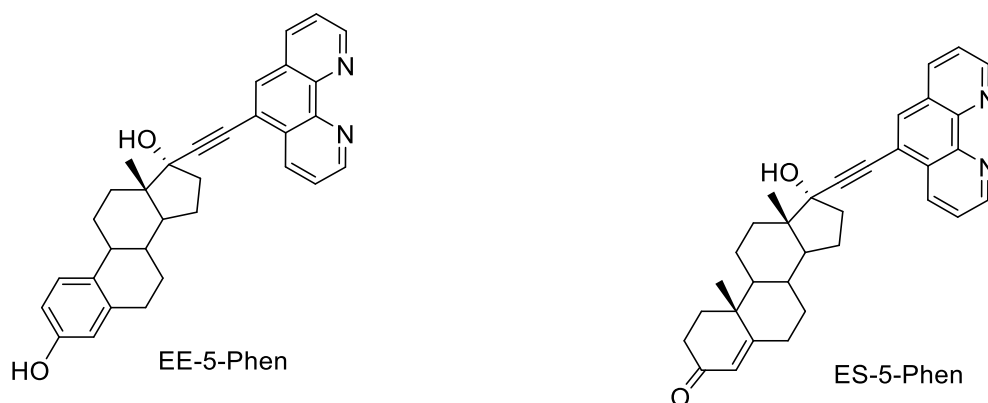
Figure 2.13: Structures of ligands EE-5-Phen and ES-5-Phen.

L = PPh$_3$
X = Halide
N = Base
R^1 = Aryl or Vinyl halide
R^2 = Terminal Alkyne
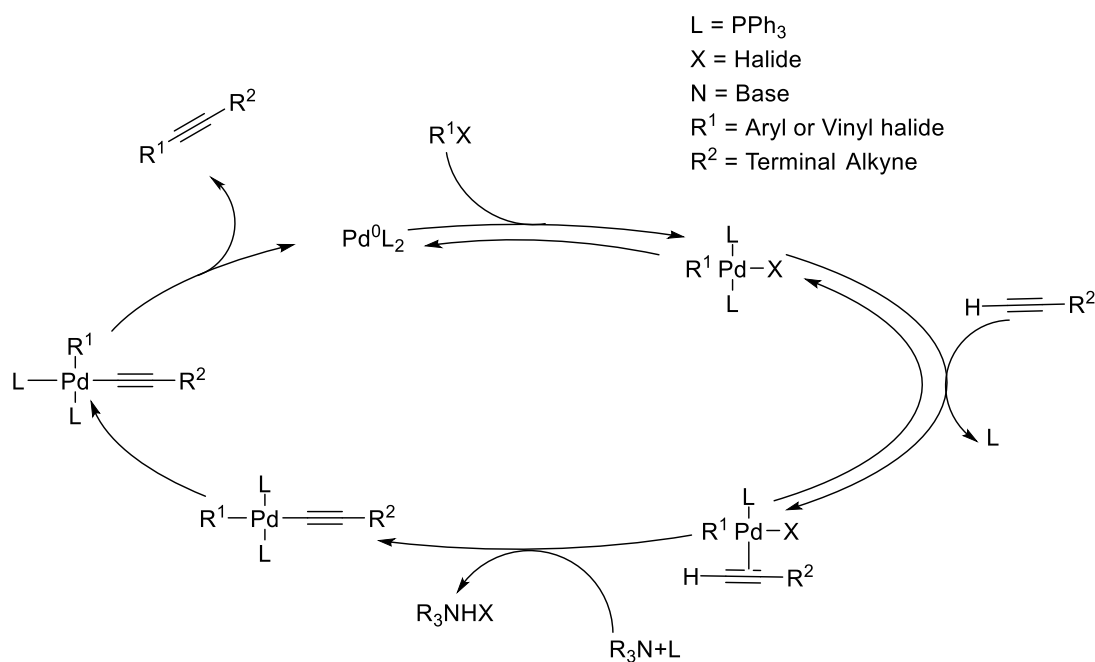
Scheme 2.3: Proposed copper free Sonogashira mechanism by Chinchilla *et al*.[159]

The copper-free Sonogashira reaction mechanism depicted in scheme 2.3 is explained by Chinchilla *et al*. The proposed catalytic cycle starts off under normal conditions *via* the oxidative addition of the vinyl or aryl halide to the catalytic [Pd(0)L$_2$]. The next step is a proposed reversible π - coordination of the alkyne, producing the familiar alkyne–Pd (II) complex seen in that of the traditional Songogashira reaction. The acetylenic proton is then acidified facilitating its removal by a base with coordination of the acetylene ligand to the metal. This [Pd(II)R^1 (C≡CR^{2}L$_2$] complex then releases the cross-coupled final compound by reductive elimination and thus re-forming the catalytic species [Pd(0)L$_2$]. The proposed catalytic cycle for attaching the steroid derivatives to the phenanthroline scaffold is displayed below in scheme 2.4.
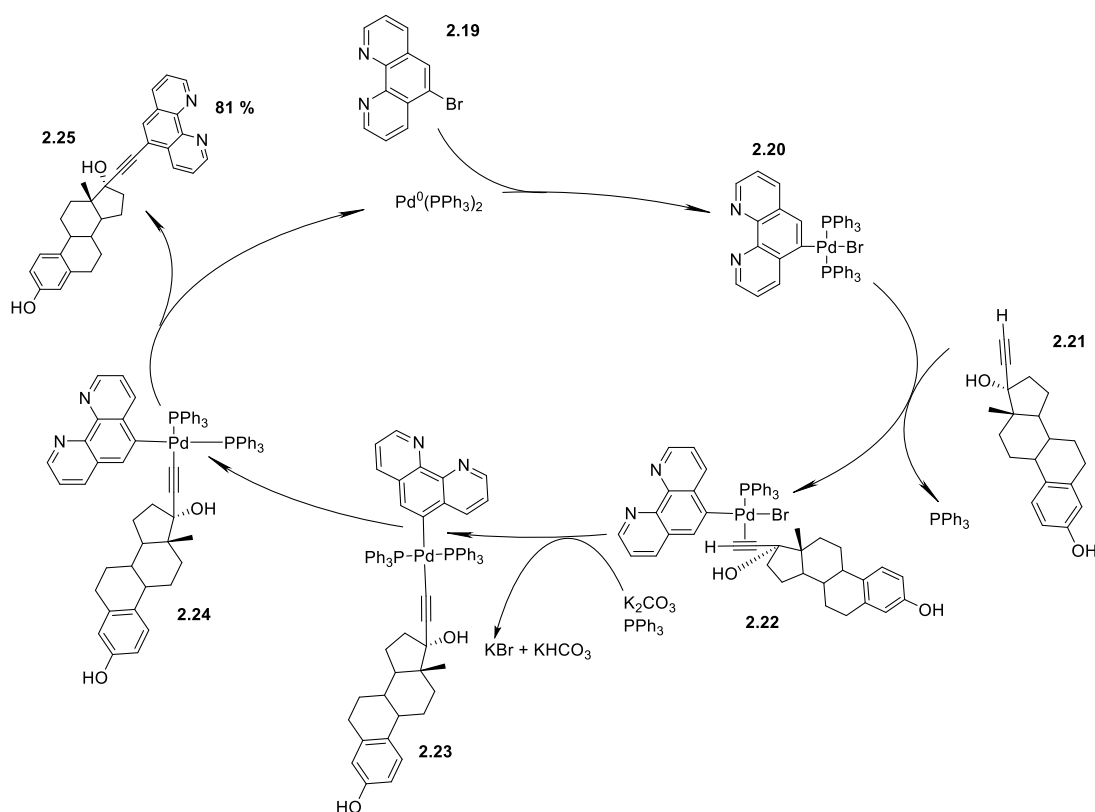
Scheme 2.3: Proposed catalytic cycle for copper free Sonogashira coupling.

Again, the cycle starts with the oxidative addition of the aryl halide 5-bromo-phenanthroline **2.19** across the palladium catalyst *via* oxidative addition, to give compound **2.20** with the palladium now after gaining two electrons. Compound **2.21**, the terminal alkyne (Ethinylestradiol) is now able to react with this new species formed *in situ* exchanging for one of the triphenylphosphine ligands and adding *via* π – coordination to the palladium core. The potassium carbonate is the base used to deprotonate the highly acidic alkyne proton followed by direct replacement of the bromine by the previously ejected triphenylphosphine giving rise to the *trans* conformation of compound **2.23**. This compound undergoes a reshuffle of electrons leading to cis – trans isomerization to yield the *cis* conformation of the palladium compound **2.24**. The final step in the cycle is reductive elimination of the newly coupled compound **2.25** (EE-5-phen) and therefore regenerating the original 14 electron catalyst [Pd^0(PPh$_3$)$_2$].

Several conditions were tried (Table 2.0) different solvents, different temperature, different base and the best way to obtain a high yield of the compounds were:

(i)   Use of extremely dried and degassed DMF (the degasification was performed using the known three cycles of vacuum/nitrogen);

(ii)   Reaction carried out under N$_2$;

57

(iii)   Dried K_2CO_3 as base;

(iv)   Freshly prepared tetrakis Palladium(0) catalyst.[160]

Table 2.0: List of solvents and bases tried while optimising the sonogashira reaction.

Solubility	
DCM	✓
MeOH	✗
EtOH	✗
DMF	✓
THF	✓
EtOAc	✗
DMSO	✓
Base Tried	
NET_3	✗
DIPEA	✓
$NaCO_3$	✓
K_2CO_3	✓
DIPA	✓
N-Methylmorphline	✗
K_2CO_3	✓

Moderate success was also achieved using THF and DIPA at room temp for 24 – 36 hours. Ultimately the best yield came from the use of dried and degassed DMF with K_2CO_3 and a freshly prepared catalyst.

Both (EE-5-phen) and (ES-5-phen) were prepared in this manner successfully in yield of 81 % and 89 % respectively. The reaction was followed by ^{1}H NMR as complete removal of the terminal alkyne proton at 2.60 ppm on the ethinylestradiol (EE), could be observed Upon successful coupling it was noted that there also was an up-field shift in the proton in the 6-position on the phenanthroline scaffold by 0.5 ppm with respect to that of the starting aryl halide (5-bromo-phenanthroline). The same trends were observed for the coupling of the Ethisterone (ES) to the 5-bromo-phenanthroline. With the alkyne proton [**B**] (Figure 2.14, completely disappearing and the proton in the 6-position [**A**] (Figure 2.14), shifting up field from 8.14 ppm to 7.98 ppm in this case. This full comparison is demonstrated in figure 2.14 below.
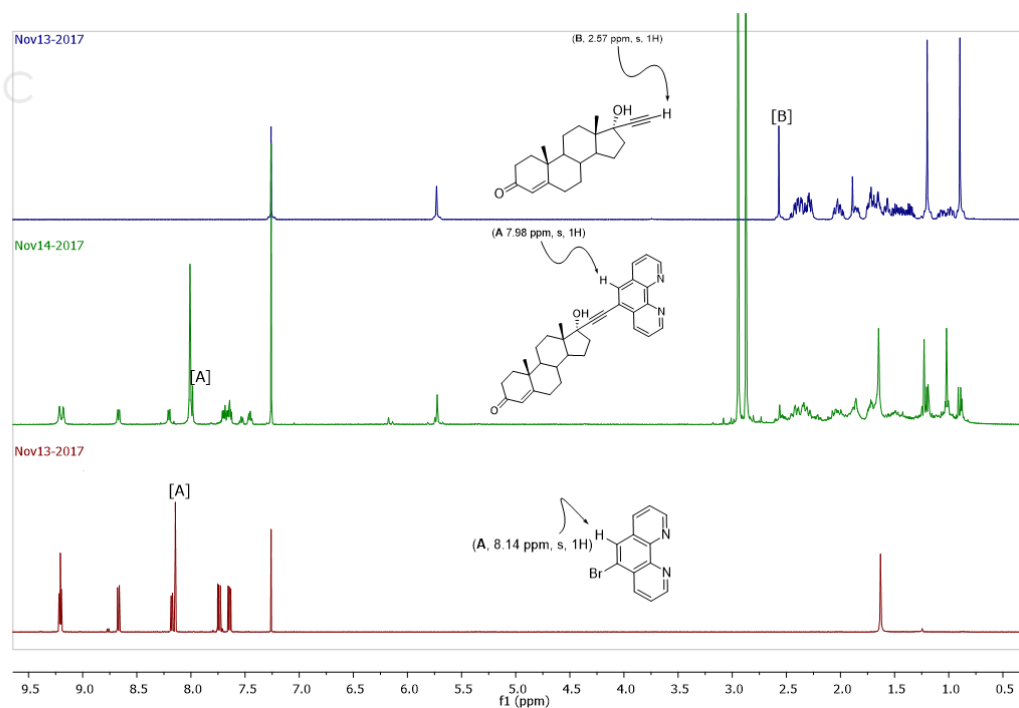
Figure 2.14: Stacked ^1H NMR ($CDCl_3$) spectra from top to bottom of free ethisterone (top), the newly coupled ligand ES-5-phen (middle) and free 5-bromo-phenanthroline (bottom). The alkyne proton labelled [**B**] and the phenanthroline proton in the 6 – position labelled [**A**].

2.10 Synthesis of steroid derived (II) compounds

The final steroid complexes with a generic formula [Cu(5-phen-steroid) (N⌒N)](NO_3)$_2$ (where N⌒N is Phen, DPQ, DPPZ and DPPN) were obtained by reacting the corresponding modified phenanthroline scaffold either (EE-5-phen or ES-5-phen) with the previously prepared [Cu(N⌒N)(H_2O)$_2$].(NO_3)$_2$ from section **2.8.** in a 1 to 1 ratio in DMF at 50 °C overnight. The crude product was precipitated into excess Et_2O and petroleum ethers (1: 1) followed by a wash with $CHCl_3$ to eliminate any unreacted steroid scaffold. It was found that carrying the reaction out at 50 °C encouraged formation of the final product much easier than at room temperature. The compounds have been characterised by Elemental Analyses, IR and HR-MS (Figure 2.15) as an example of HR-MS for compound **2.6.**
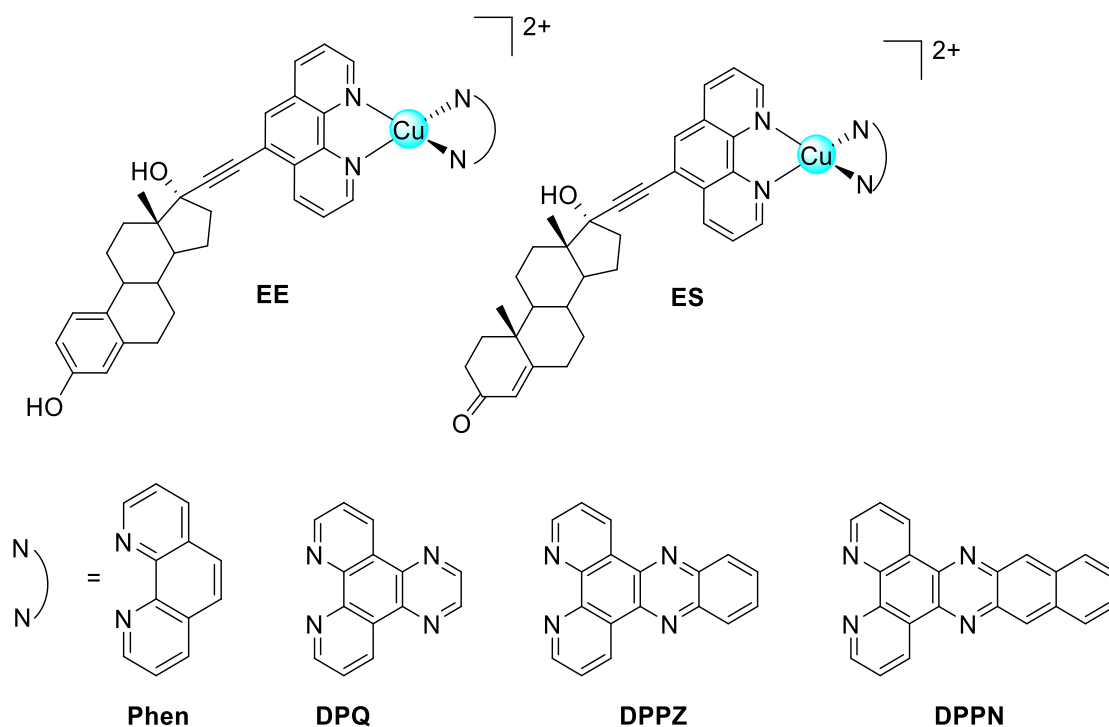
Figure 2.15: Structures of $[Cu(EE-5-phen)(Phen)]^{2+}$ **2.3**, $[Cu(EE-5-phen)(DPQ)]^{2+}$ **2.4**, $[Cu(ES-5-phen)(DPQ)]^{2+}$ **2.5**, $[Cu(EE-5-phen)(DPPZ)]^{2+}$ **2.6**, $[Cu(ES-5-phen)(DPPZ)]^{2+}$ **2.7**, $[Cu(EE-5-phen)(DPPN)]^{2+}$ **2.8**, $[Cu(ES-5-phen))(DPPN)]^{2+}$ **2.9**.

Table 2.1: Elemental analysis of the 7 final compounds.

Elemental analysis

Number	Formula	Calculated for %	Found %
2.3	$C_{44}H_{38}CuN_8O_8$	C 62.73 H 4.55 N 9.98	C 62.12 H 4.61 N 9.72
2.4	$C_{46}H_{38}CuN_8O_8$	C 61.77 H 4.28 N 12.53	C 61.43 H 3.98 N 12.92
2.5	$C_{47}H_{42}CuN_8O_8$	C 62.00 H 4.65 N 12.31	C 62.35 H 4.25 N 12.12
2.6	$C_{50}H_{40}CuN_8O_8$	C 63.59 H 4.27 N 11.86	C 63.37 H 4.48 N 12.21
2.7	$C_{51}H_{44}CuN_8O_8$	C 63.77 H 4.62 N 11.67	C 63.44 H 4.48 N 11.24
2.8	$C_{54}H_{42}CuN_8O_8$	C 65.22 H 4.26 N 11.27	C 65.06 H 3.98 N 11.53
2.9	$C_{55}H_{46}CuN_8O_8$	C 65.37 H 4.59 N 11.09	C 65.79 H 4.36 N 11.56

Elemental analysis displayed that all seven of the final compounds were observed without any hydrates and with both nitrates present (Table 2.1). Further characterisation was carried out by electron spray high resolution mass spectrometry. As seen below (Figure 2.16) the base peak for the compound **2.6** is seen as (M-2NO₃), however carrying a single positive

charge. This phenomenon is discussed in great detail in the following chapter (section **3.13**) (Figure **3.21**). The mass calculated for $C_{50}H_{40}CuN_6O_2$ is expected to return 819.2509, the found mass was 819.2498. which correlates to the loss of both nitrate ions in the outer sphere.
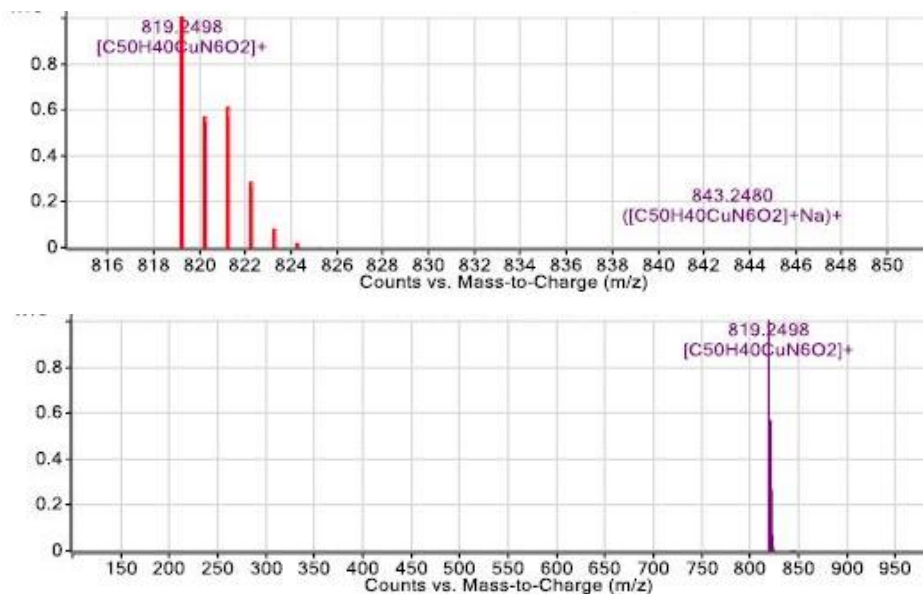
Figure 2.16: HRMS (ESI+): compound **2.6** m/z Calculated for $C_{50}H_{40}CuN_6O_2$ [M-2(NO$_3$)$^-$] 819.2509, Found 819.2498.

2.11   Biological Evaluation

2.11.1   In *vitro* antibacterial studies

The six Cu (II) complexes were evaluated as antibacterial agents in vitro against *S. aureus* and MRSA and *in vivo* using *Galleria mellonella* larvae. The immune system of insects displays many structural and functional similarities to the innate immune response of mammals[161] and consequently insects can be used to assess the virulence of microbial pathogens or the *in vivo* efficacy of antimicrobial drugs and give results similar to those obtained using mammals.[162] Larvae of *Galleria mellonella* are a popular choice for these types of tests and are inexpensive to purchase and give rapid results. *G. mellonella* larvae have previously been used to demonstrate the *in vivo* activity of novel metal-based drugs against pathogenic bacteria and fungi and show a strong correlation with results obtained in rats.[163]

2.11.2 Antibacterial activity assessment

The six complexes were dissolved in 1 mL DMSO to give a stock concentration of 5 mg/mL. Nutrient broth (100µL) was then added to each well of a 96 well plate. Each drug was serially diluted on the plate to give a concentration range 150 - 0.59 µM. The bacteria used were grown overnight and the OD_{600} was adjusted to 0.1 (equivalent to cell density of 4 x 10^7/ml). The bacterial cells (100 µL) were then added to each well and the growth was measured at 600nm after 24 hrs at 37°C using a spectrophotometer (BioPhotometer). The MIC_{50} values were calculated as the minimum concentration of drug that inhibited growth by 50% and are displayed in Table 2.2

Table 2.2: MIC_{50} values of the six copper (II) complexes examined.

Antimicrobial activity of copper (II) compounds. MIC_{50} [µM]		
Compound	**S. Aureus**	**MRSA**
2.4	4.7±0.9	219±10.4
2.5	1.5±0.2	125±9.5
2.6	2.1±0.1	102±8.9
2.7	2.0±0.2	32±3.2
2.8	2.5±0.4	17.5±1.5
2.9	2.0±0.3	88±7.8

The results displayed from this experiment indicate that all of the drugs were active against *S.* aureus with MIC_{50} values < 5 µM (Table 2.2) that are in line and even smaller with most of the Cu (II) complexes reported in literature. [6-12] The free estradiol and testosterone alkynes displayed no activity at all. Of the series, the testosterone derivatives (**2.5**, **2.7** and **2.9**) are more potent (average MIC_{50} of 1.83 µM) with respect the estradiol derivatives **2.4**, **2.6** and **2.8** (average MIC_{50} of 3.1 µM). The planar ligands seem to play an important role as the DPPZ derivatives **2.6** and **2.7** are the most active while DPQ (**2.4** and **2.5**) are the less potent with DPPN complexes (**2.8** and **2.9**) arriving in-between (average MIC_{50} of 2.05, 2.25 and 3.1 µM for DPPZ, DPPN and DPQ, respectively). There are two important considerations to be made at this point: lipophilicity and solubility. It is expected that the most lipophilic complexes would be more potent due to higher intracellular uptake; although DPPN derivatives **2.8** and **2.9** are more potent than the DPQ analogues (**2.4** and **2.5**) they are less active than the DPPZ (**2.6** and **2.7**) most likely because solubility issues arise. The large and steric encumbered DPPN complexes are less soluble than the smaller DPQ and DPPZ and this may be the reason

why the intermediate DPPZ complexes are the most potent. In the case of MRSA, the complexes showed far less activity (average MIC_{50} values of 97.4 μM) with one exception being that of compound **2.8** which has a MIC_{50} in the low micromolar region (Table 2.1). The complexes were also screened against the Gram-negative bacterium *Pseudomonas aeruginosa* and the yeast *Candida albicans* but were found to be inactive.

2.11.3   In *vitro* antibacterial studies

The promising results prompted an investigation into the *in vivo* antimicrobial properties of the Copper (II) complexes. MRSA was not studied *in vivo* due to the poor results obtained *in vitro*. *G. mellonella* larvae were used for the *in vivo* experiments as they are a useful medium in this type of study due to, their immune system displaying large similarities to that of mammals. They provide rapid and reliable results without ethical restrictions to their use. The larvae were inoculated by injecting the drug into the last left pro-leg and larval viability was determined by visualisation. Melanisation and lack of movement indicated the inoculation proved fatal.

The first study analysed the toxicity of the Cu (II) series in *G. mellonella* larvae. The larvae were injected with increasing concentrations of each compound and the viability was analysed after 24, 48 and 72 hours. Administration of   doses of 0.1mg/ml of each drug to larvae had little or no effect on viability over 72 hours. In the case of administration of the 0.25 mg/ml dose compounds **2.4** and **2.5** with DPQ ligand reduced viability by 60 and 20 %, respectively, by 72 hours. In the case of the DPPN derivatives **2.8** and **2.9** the reduced viability was of 20 % (72 h) while no significant decrease in viability at this dose over 72 hours was observed for the complexes **2.6** and **2.7** with DPPZ adduct. All drugs at a concentration of 0.5 or 1 mg/ml proved toxic to larvae and resulted in 80-100% death at 72 hours. The results from these viability assays are displayed below (Figures 2.17 – 2.19).
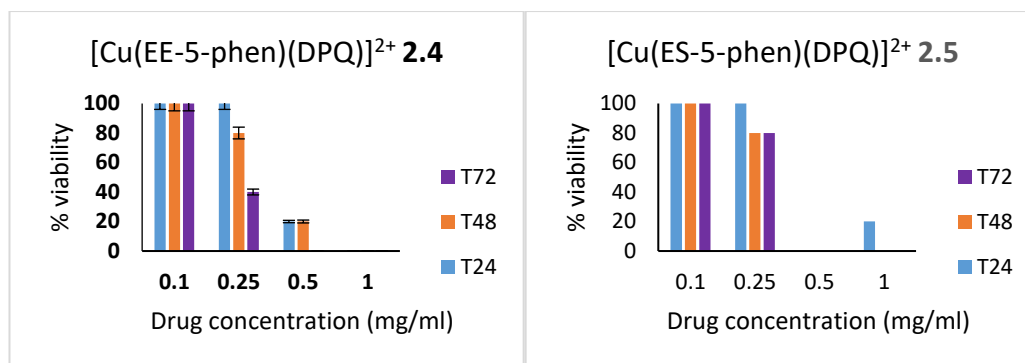
Figure 2.17: Viability of *Galleria mellonella larvae* upon treatment with different concentration of complex **2.4** & **2.5**.
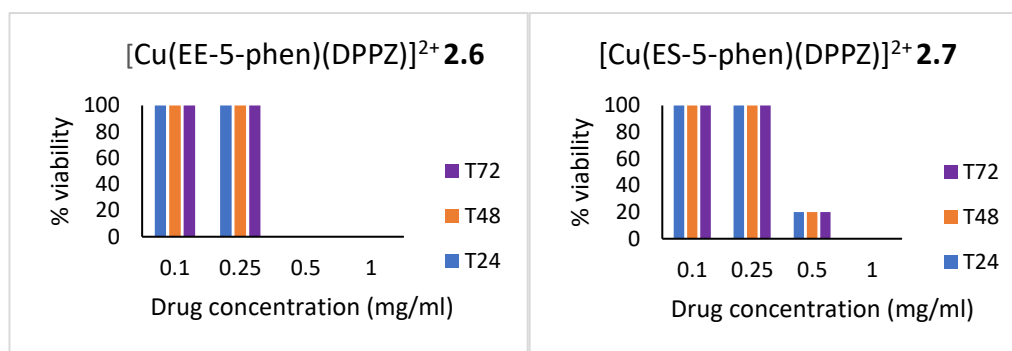
Figure 2.18: Viability of *Galleria mellonella larvae* upon treatment with different concentration of complex **2.6** & **2.7**.
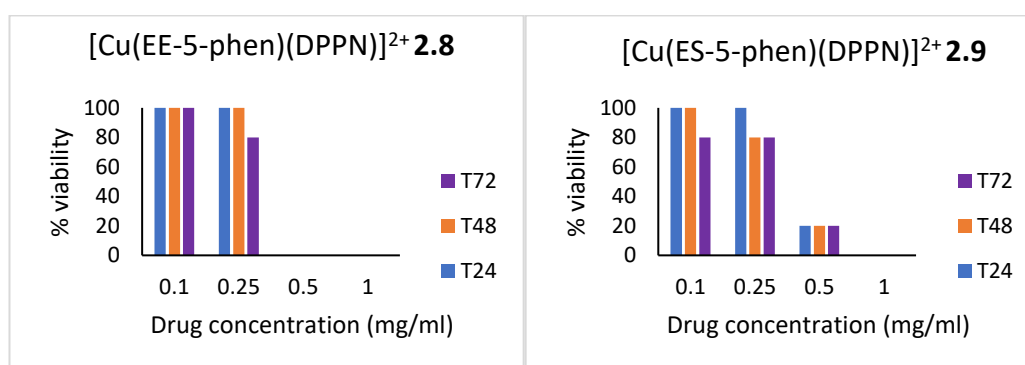
Figure 2.19: Viability of *Galleria mellonella larvae* upon treatment with different concentration of complex **2.8** & **2.9**.

2.11.4 In *vivo* antibacterial studies

To establish if the drugs had *in vivo* antibacterial activity, *G. mellonella* larvae were infected with a dose of *S. aureus* (1:2 dilution of OD_{600} 1.0) and one hour later followed up with a non-toxic dose of each drug at a concentration of 0.1 or 0.25 mg/mL. In the first series of experiments, in which a drug dose of 0.1 mg/mL was administered after the larvae were infected with the bacteria resulted in 60 % kill after 24 hours (Figure 2.20). In contrast those larvae which were administered with complexes **2.4** to **2.8** showed viability of 80 – 60 % at 24 hours and no significant change was noted after 48 h (Figure 2.20). In a second series of experiments the ability of the complexes to prevent *larvae* from infection was assessed at higher concentration, 0.25 mg/mL (Figure 2.21). In this experiment complexes **2.8** and **2.9** induced 100% survival of larvae at 24 hours and 80% at 48 hours.
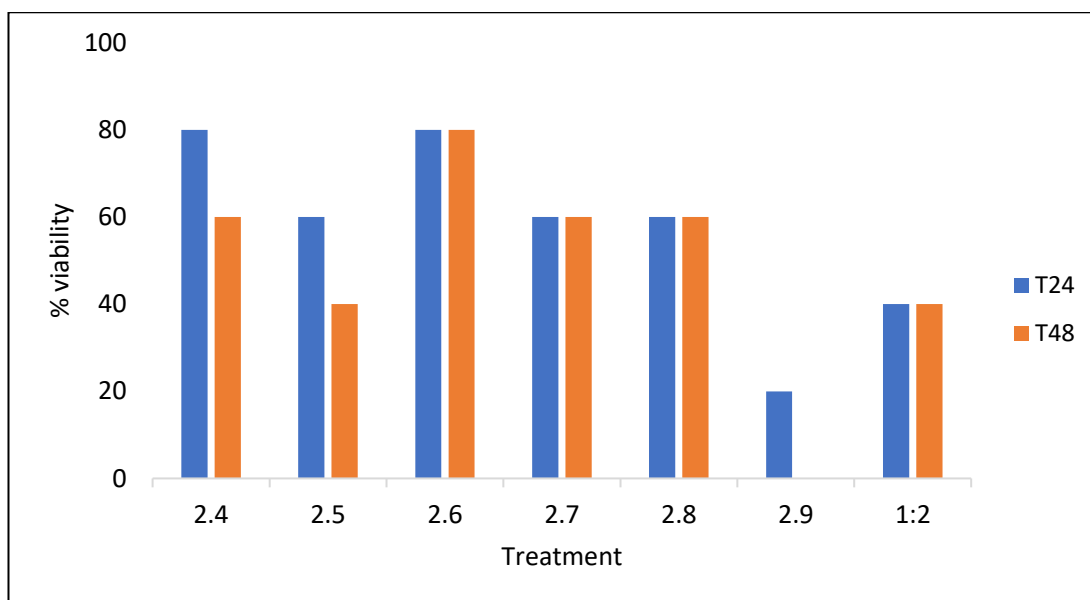
Figure 2.20: % Viability of larvae treated with 1:2 dilution of *S. aureus* and 0.1 mg/mL of the complexes 2.4-2.9. Standard error was less than ±10% of the mean in all cases.
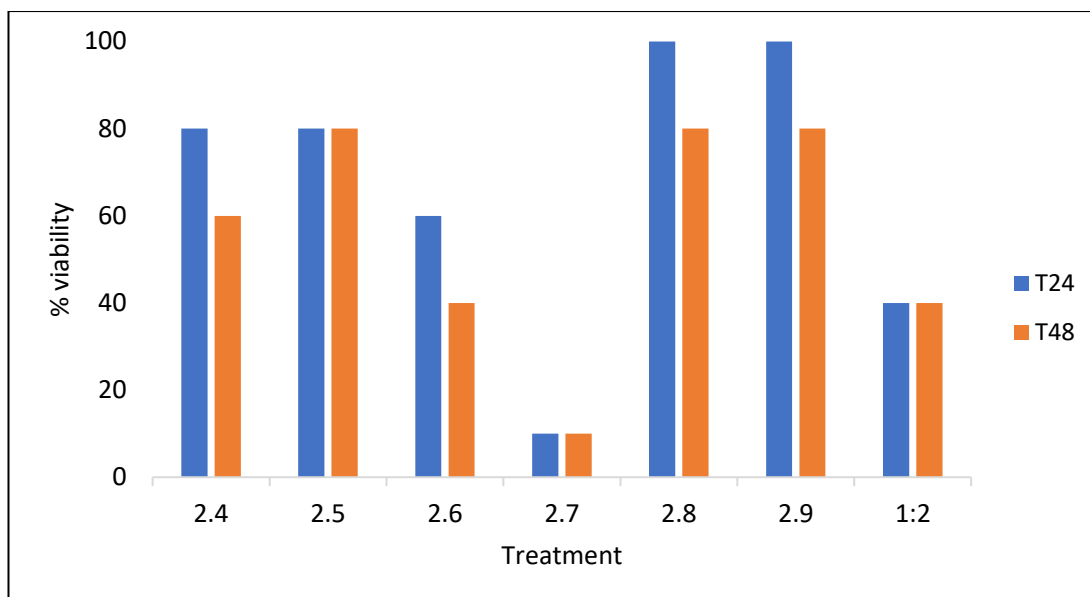
Figure 2.21: % Viability of larvae treated with 1:2 dilution of *S. aureus* and 0.25 mg/mL of the complexes **2.4**-**2.9**. Standard error was less than ±10% of the mean in all cases.

DPPN derivatives **2.8** and **2.9** displayed very high *in vivo* activity, but only at a higher concentration of 0.25 mg/mL. The DPPZ analogues **2.6** and **2.7** were more active at a lower concentration. The *in vivo* antimicrobial activity of the complexes does not strongly correlate with what was seen *in vitro*. Its largely possible due to the conditions *in vivo* being much different from those *in vitro*. The role of the steroids and of the planar ligands in the activity of this series of Cu (II) complexes is not completely clear; the enhanced lipophilicity due to presence of the steroids likely increases the bacterial uptake. This could in part explain the high antimicrobial activity, however other mechanisms most likely are involved. A deeper investigation would involve the use of proteomics to establish the exact mechanism of how the drug uptake is happening and what proteins if any are involved.

2.12   Anti-cancer activity of Estradiol derived compounds

For these studies four of the compounds were selected (**2.3**, **2.4**, **2.6** & **2.8**) which all contained the estradiol moiety. These were chosen as the rationale was the estradiol moiety will act as delivery vector to target estrogen-receptor positive (ER+) cancer cells. A fourth compound **2.3** (Figure 2.15) bearing the phen ligand was also synthesised via the route previous discussed in section 2.10. The complexes were subjected to a range of investigations which included electro-chemical studies, DNA binding and cleavage assays, ROS production, cellular uptake assays, viscosity assays. The results of these will be displayed and discussed below.

2.12.1 Electro-chemical studies.

The electrochemical behavior of complexes **2.4,2.6** & **2.8** was investigated (Figure 2.21), and Table 2.0 below summarises the electrochemical data generated. All compounds exhibited a quasi-reversible wave when examined over the potential range 1 to -1 V, being ascribed to the $Cu^{2+/1+}$ redox process (Figure 2.22). No clear trend was observed with respect to $Cu^{2+/1+}$ $E_{1/2}$ values for the series **2.3, 2.4** & **2.6** all of which fell within a similar interval (-0.29 to -0.27 V *vs.* Ag/Ag$^+$) that is within the biological range (-0.2—0.4 V) and they are likely to undergo reduction (Cu^{2+} + 1e$^-$ → Cu^{1+}) in physiological cell environment.[164] The relatively positive shift in all values for these complexes relative to that of the starting materials [Cu(N∩N)(OH$_2$)$_2$](NO$_3$)$_2$] with $E_{1/2}$ values -0.456 V *(phen),* -0.363 V *(DPQ)* and -0.311 V *(DPPZ),* may reflect the electron donating contribution of the estradiol moiety and geometric alterations upon reduction of the Cu^{2+} centres in **2.3, 2.4** & **2.6** to the Cu^+ forms. Thus, the processes may be influenced by steric effects of the ligands which overshadow electronic effects[165]. The ΔE_p values of the metal processes indicate a significant departure from a one electron reversible process, with the possibility of coupled chemical reactions and the geometric reorganisation which may accompany the $Cu^{2+/1+}$ redox system. All $I_{p(a)}/I_{p(c)}$ ratios are close to unity for the diffusion-controlled metal process. When the cathodic limit was extended to -2.0 V vs. Ag/Ag$^+$ the metal underwent further one electron reduction $Cu^{1+/0}$ with subsequent ligand dissociation and (in some cases) re-oxidation (stripping) of plated copper back to Cu^+ upon anodic switching.[165] The *quasi* reversibility of the $Cu^{2+/1+}$ metal processes (cathodic limit -1 V vs. Ag/Ag$^+$) indicates little structural change prior to this point, after which it is likely that the complexes undergo decomposition. In the case of compounds **2.3** and **2.4***,* a significant anodic shift in the $E_{p(c)}$ values for the phenanthroline and DPQ ligands was evident (-1.99 V to -1.3 V and -1.92 V to -1.37 V respectively). This may reflect a stabilisation of the LUMO state of the ligands, due in this case to the presence of the estradiol group, resulting in a more facile ligand reduction process. The electrochemical behaviour of natural and synthetic estrogens has been reported.[166] The ease of oxidation of the phenol group to the phenoxonium ion (a 2-electron process) being dependent on ring substitution and the solvent-electrolyte system. In these complexes, no estradiol anodic process is visible over the range examined, though clearly the presence of the steroid group influenced the phen, DPQ and DPPZ electrochemistry.

Table 2.3: Electrochemical data for complexes **2.3, 2.4 & 2.6**

Complex	Cathodic limit (V)	Cu(I/II)			Cu(0/I)	Ligand redox process			
		E ½ (V)	ΔE_p (V)	$I_{p(a)}/I_{p(c)}$	$E_{p(c)}$ (V)	$E_{p(a)}$ (V)	$E_{p(c)}$ (V)	$E_{1/2}$ (V)	ΔE_p (V)
2.3	-1	-0.2769	0.198	0.85	-	-	-	-	-
	-2	-	-	-	-	-	-1.30	-	-
2.4	-1	-0.272	0.296	1.00	-	-	-	-	-
	-2	-	-	-	-	-	-1.37	-	-
2.6	-1	-0.287	0.225	0.84	-	-	-	-	-
	-2				-1.17	-1.365	-1.475	-1.42	0.11
	-2						-1.845		

Figure 2.22: Cyclic voltammogram of 1 mM solution of complexes **2.3, 2.4 & 2.6** at a glassy carbon electrode (0.07 cm^2) in a three-electrode configuration with Pt wire counter and non-aqueous reference Ag/Ag$^+$ reference electrode in 0.1 M LiClO$_4$/DMF. Scan rate 100 mV s^{-1} over the potential range +1 to -1 V *vs.* Ag/Ag$^+$. Background electrolyte (●), **(2.3)** (●) **(2.4)** (●) **(2.6)** (●)

2.12.2 Binding affinity to calf thymus and salmon testes DNA

In this work carried out by the Kellet group *et al*. The DNA binding affinity of the series of estradiol complexes was determined with calf-thymus and salmon testes duplex DNA

polymers using a high throughput ethidium bromide and Hoechst 33258 fluorescence quenching assay, [167] competition assay, and viscosity analyses (Figure 2.23). The presence of modified phen ligands significantly enhanced the ctDNA binding affinity with K_{app} (apparent DNA binding constant) values rising from 7×10^6 M(bp)$^{-1}$ for complex **2.3** (phen) to $\sim 10^7$ M(bp)$^{-1}$ for complexes **2.4** and **2.6** (DPQ and DPPZ, respectively). Both phenazine complexes had a binding affinity comparable to a reference intercalating antibiotic, Actinomycin D (3×10^7 M(bp)$^{-1}$).[107] Complex **2.4,** containing the extended phenazine substituent DPPN, had a lower binding constant of $\sim 5 \times 10^6$ M(bp)$^{-1}$ (Table 2.4), this effect has been previously observed with copper(II) ternary complexes.[108] Fluorescence quenching (Q) of limited Hoechst 33258 (minor groove binder) and ethidium bromide (intercalator) bound ctDNA show the complex series were not selective in displacing these fluorophores, however, a similar trend was observed in the displacement of both reporters: **2.6 > 2.4 > 2.3 > 2.8** (Table 2.4). Viscosity analysis carried out with salmon testes duplex DNA confirmed complex **2.6**, containing the DPPZ ligand, as a strong intercalator and this hydrodynamic profile was followed by complex **2.4** (DPQ) and then **2.3** (phen, which presumably kinks DNA). Complex **2.8** with the larger DPPN ligand again displayed attenuated activity (Table 2.3). Moving from phen to DPQ and DPPZ the planarity and aromaticity of the ligands is optimized for DNA intercalation but the further modification to DPPN seems to lead to steric hindrance thereby preventing efficient DNA binding.
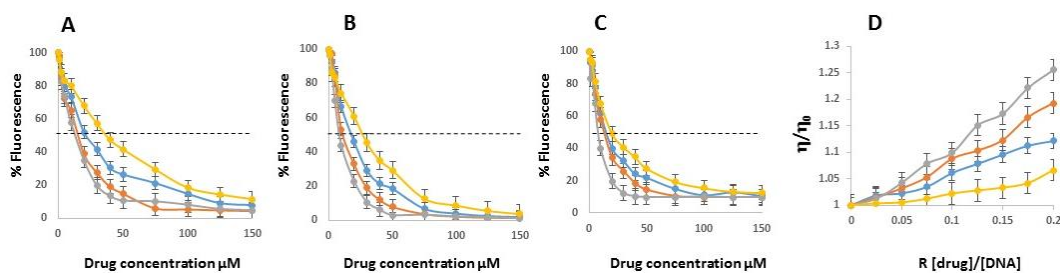
Figure 2.23: Binding of complexes **2.3** (●), **2.4** (●), **2.6** (●), and **2.8** (●) to A) Ethidium bromide saturated solution of dsDNA (ctDNA); B) and C) fluorescence quenching of limited ethidium bromide or Hoechst 33258 bound ds DNA (ctDNA) upon titration of complexes; D) viscosity properties of complex treated salmon testes dsDNA.

Table 2.4: DNA Binding properties of complexes **2.3, 2.4, 2.6 & 2.8**. ^{a}C$_{50}$ = concentration required to reduce fluorescence by 50 %; ^{b}K$_{app}$ = K$_e$ x 12.6/C$_{50}$ where K$_e$ = 9.5 x 10^6 M(bp^{-1}); ^{c}Reduction of 50 % initial fluorescence from DNA bound dye by tested compound (µM); ^{d}Relative viscosity value at r = 0.20.

Complex	C$_{50}$(μM)^a	K$_{app}$M(bp^{-1})^b	Q(EtBr,μM)^c	Q(Hoechst,μM)^c	n/n$_o$ (r=0.2)^a
2.3	16.13	7.21x10^6	21.5	16.4	1.12
2.4	12.70	9.43x10^6	15.1	12.9	1.19
2.6	8.32	1.44x10^6	12.5	9.29	1.25
2.8	21.50	5.57x10^6	37.6	2.1	1.06

2.12.3 Nuclease Activity

Kellet *et al.* carried out the DNA-cleavage ability of the four Cu (II) complexes was measured by monitoring the conversion of SC-DNA (form I) to the nicked-circular form (NC, form II) using agarose gel electrophoresis (Figure 2.24). SC pUC19 DNA (400 ng) was incubated with increasing complex concentrations (range 0.5–20 μM) in the presence of Na-*L*-ascorbate (1 mM) for 3 h. All complexes had the ability to convert SC-DNA into the nicked form at 1 μM but complex **2.6**, the DPPZ -containing complex, displayed the highest cleavage potency being able to cleave plasmid DNA already at 0.5 μM concentration. In absence of Na-*L*-Ascorbate no detectable cleavage was observed.
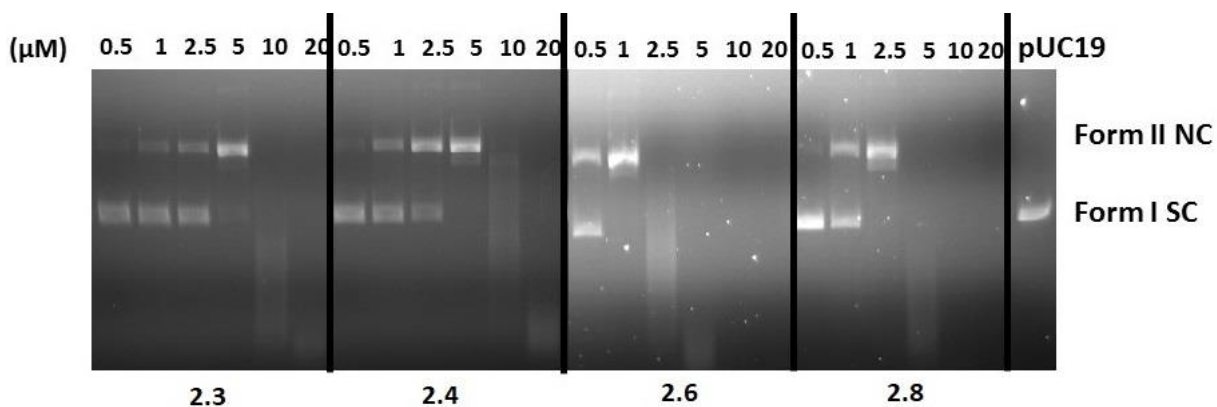
Figure 2.24: DNA cleavage. Agarose gel electrophoresis patterns of SC pUC19 DNA incubated with complexes **2.3, 2.4, 2.6** & **2.8** (0.5–20 μM)in HEPES buffer at 37 °C for 3 h.

2.12.4   2D & 3D *in vitro* cytotoxicity

Prof. Valentia Gandins lab evaluated the antitumor potential of the four newly developed Cu (II) estradiol derived complexes and in order to confirm if they were more effective in targeting ER+ cell lines with respect to ER- ones, their *in vitro* antitumor potential was assessed in a panel of ER+ human cancer cell lines, A431 (cervical), MCF-7 (breast), 2008 (ovarian) and A2780 (ovarian) cancer cells as well as against ER- HCT-15 colon cancer cells. Cells were exposed to the tested compounds for 72 h and the IC_{50} values, calculated from the dose–response curves, are reported in Table 2.5. The stability of complexes in phosphate buffer solution (37 °C, pH 7.4) was previously evaluated *via* HPLC in order to confirm that the estrogen moiety, which can be carcinogenic in its free state being a steroid, is not released from the coordination sphere of the metal centre. The chromatograms of **2.8** are displayed in the appendix as an example of this experiment. These were carried out immediately upon dissolution and after 72h where it is clearly visible that the complex is highly stable with negligible amount of steroid

released.

Table 2.5: In vitro cytotoxic activity of complexes **2.3, 2.4, 2.6** & **2.8**. Cells ($3–8 \times 10^3$ mL^{-1}) were treated for 72 h with increasing concentrations of the tested compounds. Cytotoxicity is assessed by MTT test. IC_{50} values (µM) were calculated by a four-parameter logistic model ($P < 0.05$). S.D. = standard deviation

			IC_{50} (µM) ± SD		
Compound	**A2780**	**2008**	**A431**	**MCF-7**	**HCT-15**
2.3	0.6 ± 0.1	1.5 ± 0.7	1.3 ± 0.3	1.0 ± 0.2	0.8 ± 0.3
2.4	0.3 ± 0.02	1.6 ± 0.4	2.0 ± 0.4	1.2 ± 0.3	0.8 ± 0.1
2.6	0.1 ± 0.04	0.2 ± 0.1	0.1 ± 0.1	0.7 ± 0.2	0.5 ± 0.2
2.8	0.04 ± 0.01	0.6 ± 0.03	0.3 ± 0.03	0.9 ± 0.2	0.5 ± 0.2
cisplatin	2.6 ± 0.8	2.2 ± 0.6	1.7 ± 0.3	7.6 ± 0.2	13.9 ± 1.7

.

It was found that all the complexes promoted a significant amount of cytotoxic activity, with IC_{50} values in the low-/sub-micromolar range against all cancer cell lines tested. In general, all derivatives were more effective in inducing cancer cell death with respect to the reference metallodrug cisplatin. Among the newly developed Cu(II) compounds, **2.6** and **2.8** were the most potent derivatives, with IC_{50} calculated towards all tested cancer cells in the sub-micromolar range. This data indicated that by increasing the lipophilicity of the diamine

ligand increases the cytotoxic activity of the related copper(II) complex. On the other hand, complexes **2.3, 2.4 & 2.6** displayed equally cytotoxic properties against ER+ and ER- cancer cells, thus suggesting the inability of these complexes to selectively target ER+ cancer cells. Conversely, **2.8** proved to be slightly more effective against ER+ A2780 ovarian cancer cells. The *in vitro* antitumor potential of the Cu(II) complexes was also examined in 3D cell culture models of ovarian (ER+) and colon (ER-) cancers. Actually, even if the 2D cell cultures is the most used in vitro method for screening of potential therapeutics due to its simplicity, reproducibility, and low cost, this method is unable to reproduce the properties of *in vivo* solid tumours. 3D cell cultures, possessing several features that more closely mimic the heterogeneity and complexity of in vivo tumours, are recognized to be more predictive for in vivo results than conventional 2D cell cultures.[168]The cancer spheroids were treated with copper (II) complexes or cisplatin for 72 h and cell viability was assessed by means of the acid phosphatase (APH) assay

Table 2.6: *In vitro* cytotoxicity against ovarian and colon cancer cell spheroids. Spheroids (1.5×10^3 cells/well) are treated for 72 h with increasing concentrations of test compounds. The growth inhibitory effect was evaluated by means of the APH test. IC_{50} values were calculated from the dose-survival curves by the four-parameter logistic model ($P < 0.05$). SD=standard deviation.

	IC_{50} (µM) ± SD	
	A2780	**HCT15**
2.3	10.6 ± 1.0	7.7 ± 1.6
2.4	7.7 ± 1.0	9.9 ± 1.0
2.6	4.1 ± 0.1	9.2 ± 0.6
2.8	3.0 ± 0.02	8.6 ± 0.5
cisplatin	91.3 ± 5.4	68.3 ± 2.1

These tested non-proliferative and very resistant tumour models, all complexes were extremely effective, being more active than cisplatin against both A2780 ovarian and HCT-15 colon cancer cell spheroids. In particular, **2.6** and **2.8** were confirmed as the most potent derivatives, being about 30 and 9 times more effective than cisplatin in A2780 and HCT-15 3D cell cultures, respectively.

Complexes **2.3, 2.4** & **2.6** showed a similar activity toward ER+ and ER- cancer cells, thus confirming the results obtained in the 2D system and supporting the hypothesis of their inability to selectively target ER+ cancer cells. On the contrary, in 3D systems, compound **2.8**

again showed a certain degree of selectivity towards A2780 cancer cells, being about 3 times more effective in ER+ human ovarian cancer cells with respect to ER- human colon cancer cells.

2.12.5 Cellular uptake assays

Gandin *et al*. carried out the cellular uptake assays and mechanistic studies below with the aim of identifying a possible correlation between cytotoxic activity and cellular accumulation, the cellular copper content was measured in ER+ A2780 and ER- HCT-15 cancer cells treated for 24 h with equimolar concentrations of the tested compounds. The cellular copper levels were quantified by means of GF-AAS analysis, and the results, expressed as ng Cu per 10^6 cells, are shown in Figure 2.25, panel A.
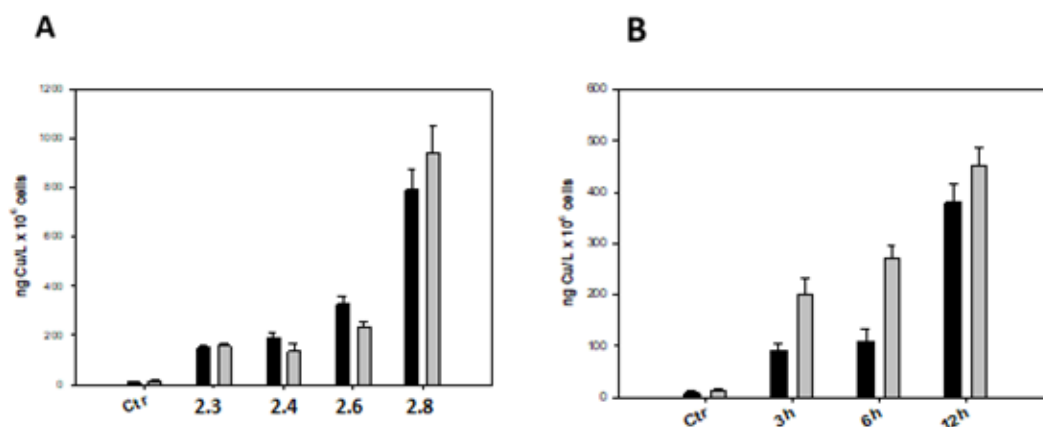

Figure 2.25: Cellular uptake in A2780 (grey bars) and HCT-15 (black bars) cancer cells. (**A**) Cancer cells were incubated with 0.5 µM of each of the copper complexes for 24 h, and cellular copper content was detected by GF-AAS analysis. (**B**) Cancer cells were incubated with 0.5 µM of copper complex **2.8** for 3, 6 or 12 h, and cellular copper content was detected by GF-AAS analysis. Error bars indicate the standard deviation.

Although to a different extent, all derivatives were able to cross the cancer cell membrane and enter cancer cells. Complexes **2.3, 2.4** and **2.6** were able to similarly accumulate into ovarian and colon cancer cells, whereas derivative **2.8** was sensibly more effective in entering ER+ A2780 cancer cells. Interestingly, **2.8** accumulated in a time-dependent manner, actually

both ovarian and colon cancer cells displayed a time-dependent increase in cellular copper content (Figure 2.25, panel B). By matching cytotoxic activity data with those arising from cellular uptake quantification, a linear and direct correlation which is shown below in figure 2.26 is very evident.
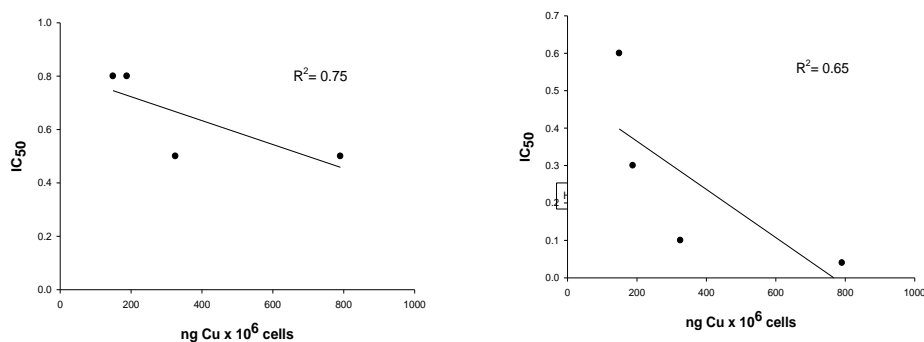
Figure 2.26: Correlation between cytotoxicity (IC_{50}) and cellular copper content in drug-treated HCT-15 (left) and A2780 (right) human cancer cells.

2.12.6   Mechanistic studies and ROS production

Copper species have long been identified as redox active compounds. It has been demonstrated that copper complexes may catalyze the reaction of hydrogen peroxide in the form of Fenton-like reactions inside the cell to produce ROS, thus altering cellular redox homeostasis and driving cells towards oxidative stress. On these bases, the cellular ROS levels were evaluated in A2780 cells treated with 10 µM of the most effective complex **2.8.** ROS production was monitored by using the peroxide-sensitive fluorescent probe CM-H$_2$DCFDA (5-(and-6)-chloromethyl-2',7'-dichlorodihydrofluorescein diacetate, acetyl ester). Antimycin, a classical inhibitor of the mitochondrial respiratory chain at the level of complex III, was used as a positive control.

A   **B**
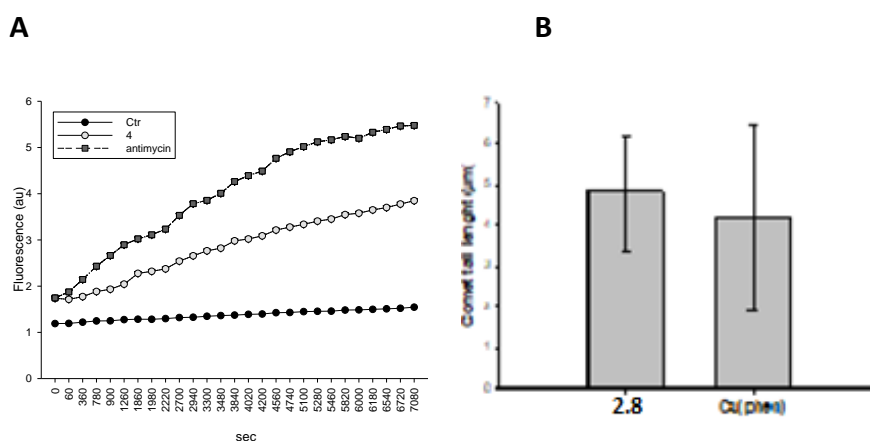
Figure 2.27: Mechanistic studies: ROS production (**A**) and DNA damage (**B**) in A2780 cancer cells. (**A**) Cells were preincubated in PBS/10 mM glucose medium for 20 min at 37 °C in the presence of 10 µM CM-DCFDA and then treated with derivative **4** (10 µM) or antimycin (3 µM). The fluorescence of DCF was measured as reported in the Experimental Section. (**B**) A2780 cells were treated for 3 h with 0.5 µM of compound **2.8** and then processed for the comet assay as reported in the Experimental Section. Comet tail length was calculated from the center of the cell and measured in micrometers with ImageJ software. The error bars indicate the standard deviation.

The results, expressed as arbitrary units of fluorescence as a function of time, are shown in Figure 2.27, panel A. Interestingly, **2.8** was able to substantially stimulate the production of hydrogen peroxide in a time-dependent manner, to a rather similar extent as the respiratory chain complex III inhibitor, antimycin.

In addition, it was confirmed the results obtained in cell-free experiments (DNA binding, cleavage, and viscosity studies). The ability of the newly synthesized copper (II) complexes to bind and to damage the DNA within intact cancer cells was then assessed. The DNA damage in A2780 cells was studied after treatment with **2.8** for 3 h, using alkaline single cell gel electrophoresis (Comet assay, Figure 2.27, panel B). The results were compared with those obtained after treatment of A2780 cells with equitoxic concentrations of dichloro(1,10-phenanthroline) copper(II), [Cu(phen)]. Similarly, to [Cu(phen)], the cells treated with **2.8** displayed a statistically significant increase in electrophoretic migration of the DNA fragments, evidenced by well-formed comets. To analyze the cellular DNA binding, cells A2780 were treated with complexes **2.3, 2.4, 2.6 & 2.8** for 24 h, as described in the experimental section, and the amount of copper covalently bound to the extracted DNA was determined via GF-AAS. All the complexes showed a very little capacity to bind to the DNA in a covalent mode comparison to the endogenous Cu control (Figure 2.27), confirming that the interaction between the complexes and DNA is purely electrostatic (intercalation).

These results confirmed the ability of these copper (II) complexes to target DNA in intact cancer cells.
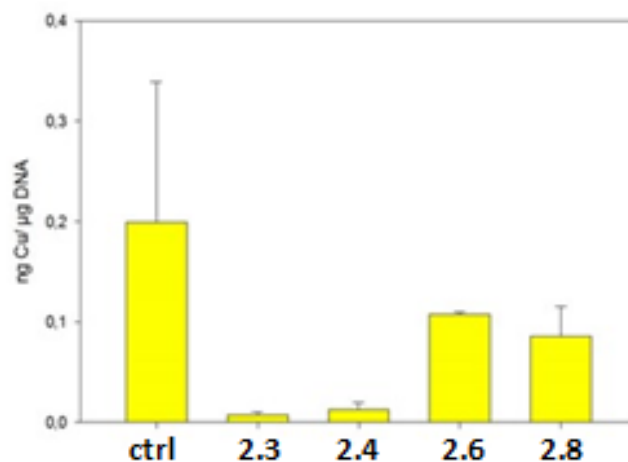
Figure 2.27: Determination of the amount of the covalent interaction between complexes **2.3, 2.4, 2.6 & 2.8** and the nuclear DNA in A2780 cells.

2.13   Chapter conclusions

In conclusion a small library of novel Cu (II)-steroid complexes were synthesised and characterised. The complexes showed high potency *in vitro* against *S. aureus* and MRSA and *in vivo* against *S. aureus*. When inoculated with the complexes larval viability noticeably increased in those larvae that were previously infected with *S. aureus.* The effect of the steroids on the antimicrobial activity of the metal complexes is still not completely clear and further studies using proteomics analyses to uncover the mechanism of action would be required. These complexes show great potential to become lead compounds which could eventually be developed into new treatments for *S. aureus* and possibly MRSA infections. Four of the copper (II) based complexes containing the female steroid estradiol, were then chosen with the aim to selectively target cancer cells overexpressing the estrogen receptors. The complexes proved to be very effective against all the cancer cell lines examined (low and sub µM IC_{50} values), much more with respect the reference drug cisplatin, complex **2.8** being the most effective one. Although a no selectivity was observed for ER+ with respect to ER- cells for complexes **2.3, 2.4** and **2.6**, for complex **2.8** a slight difference in anticancer potential towards ER+ cancer cells was underlined. Actually, a linear correlation was obtained in ER+ cancer cells between drug uptake and IC_{50} values. In general, the antiproliferative activity and cellular uptake increased with the lipophilic character of Cu(II) complexes, thus indicating that cellular internalisation is principally due to a passive diffusion mechanism with

a minimum role of the estrogen moiety. From a mechanistic point of view, cell-free fluorescent analyses evidenced for all copper complexes strong intercalation properties but a discrimination between major and minor groove was not observed. Cu(II) complexes were redox active at the physiological range and were able to cleave DNA at very low concentrations (0.5 µM) in the presence of a reducing agent. More interestingly, cell studies confirmed their ability to target DNA and to induce ROS production in ER+ human cancer cells.

2.14   Materials and methods

All reagents and reactants were purchased from commercial sources. The two sources used were Sigma Aldrich and Tokyo Chemical Industry. All solvents were used without further purification. The DMF used for the Sonogashira coupling reaction, was dried using 4 angstrom molecular sieves, it was then decanted into a round bottom flask and kept under high vacuum using a Schlenk line while immersed in liquid nitrogen. The DMF was then flushed with nitrogen gas. This step was repeated a minimum of three times for the Sonogashira coupling reaction. All NMR spectra were recorded on a Bruker Advance spectrometer with the probe at 293K, operating at 500MHz for the ^{1}H and at 125 MHz for ^{13}C nuclei. Spectra were recorded in CDCl$_3$ using Me$_4$Si as the internal standard. All chemical shifts are in ppm. Infrared (IR) spectra were recorded in the region 4000 - 400 cm^{-1} on a Perkin Elmer precisely spectrum 100 FT/IR spectrometer. The solid samples were run using ATR. Elemental analyses (carbon, hydrogen and nitrogen) were performed with a PerkinElmer 2400 series II analyser. ESI mass spectra were recorded in positive mode with an Agilent 6200 Series TOF LC/MS system.

Electrochemistry. Non-aqueous electrochemical analysis of 1 mM of the copper complexes **2.3, 2.4 and 2.6** was carried out at a glassy carbon electrode (0.07 cm^2) in a three-electrode configuration with Pt wire counter and non-aqueous reference Ag/Ag$^+$ reference electrode in 0.1 M LiClO$_4$/DMF (dimethylformamide). Glassy carbon electrodes were prepared by polishing with alumina suspension on a microcloth followed by sonication in deionised water. Voltammograms were generated over the range +1 to -1 or -2 V *vs.* Ag/Ag$^+$ in a deaerated solution (N$_2$ bubbling 10 min). Data analysis employed the third cycle of the voltammogram with cathodic scan direction at 100 mV s^{-1} in all cases.

Stability*.* Compound **2.8** was taken as reference being the most active. **2.8** was dissolved in DMF to obtain a 5 mM solution. 200 µL of this solution was diluted to 2.0 mL with phosphate buffer solution (pH = 7.4, [P] = 50 mM). The solution was kept at 37 °C and monitored by HPLC using a Phenomenex Luna C18 (5 µM, 100 Å, 250 mm × 4.60 mm i.d.) column at a flow rate of 1.0 mL/min with 280 nm UV detection at room temperature. The mobile phase was 80:20 acetonitrile (0.1% trifluoroacetic acid) : water (0.1% trifluoroacetic acid).

2.15   DNA Binding Experiments

2.15.1   Competitive ethidium displacement

A working solution of 20.0 μM UltraPure calf thymus DNA (CT-DNA, Invitrogen 15633-019, ε_{260} = 12,824 M (bp)$^{-1}$ cm^{-1}) along with 25.2 μM ethidium bromide (EtBr) in HEPES buffer (80 mM, pH = 7.2) and NaCl (40 mM) was prepared. Stock solutions of metal complexes, metal salts, and groove binding drugs were prepared at ~4.0 mM in DMSO (dimethylsulfoxide) and diluted further with ultra-pure water. 50 μL of DNA-Et working solution were placed each well of a 96 well microplate with the exception of the blanks which contained 100 μL HEPES buffer. Serial aliquots of the tested compound were added to the working solutions and the volume was adjusted to 100 μL in each well such that the final concentration of CT-DNA and EtBr were 10.0 μM and 12.6 μM, respectively. The plate was allowed to incubate at room temperature for 1 h before being analysed using a Bio-Tek synergy HT multi-mode microplate reader with excitation and emission wavelengths being set to 530 and 590 nm, respectively. Concentrations of the tested compounds were optimized such that fluorescence was 30-40% of the initial control (i.e., 50 µL working solution + 50 μL HEPES buffer) at their highest reading. Each drug concentration was measured in triplicate, on at least two separate occasions, and the apparent binding constants were calculated using K_{app} = K_e x 12.6/C50 where K_e = 9.5 x 10^{6}M(bp)$^{-1}$.

2.15.2   DNA–ethidium fluorescence quenching

A working solution of 50.0 μM UltraPure calf thymus DNA (CT-DNA, Invitrogen 15633 019, $\varepsilon 260$ = 12,824 M (bp)-1 cm-1) along with either 10.0μM ethidium bromide (EtBr) or Hoechst 33258 (Sigma) in HEPES buffer (80 mM, pH = 7.2) and NaCl (40 mM) was prepared. Stock solutions of metal complexes, metal salts, free ligands and groove binding drugs were prepared at ~4.0 mM in DMSO and diluted further with ultra-pure water. 50 μL of DNA-Et or DNA-Hoechst working solution were placed each well of a 96 well microplate with the exception of the blanks which contained 100 μL HEPES buffer and 5 μM of either Hoechst or EtBr. Serial aliquots of the tested compound were added to the working solutions and the volume was adjusted to 100 μLin each well such that the final concentration of CT-DNA and EtBr/Hoechst were 25.0 μM and 5 μM, respectively. The plate was allowed to incubate at room temperature for 5 min before being analysed using a Bio-Tek synergy HT multi-mode microplate reader with excitation and emission wavelengths being set to 530 and 590 nm for Et detection or 360 nm and 460 nm for Hoechst 33258 detection. Concentrations of the tested compounds were optimized such that fluorescence was 30-40% of the initial control at their highest reading. Each drug concentration was measured in triplicate, on at least two separate occasions. From a plot of fluorescence versus added drug concentration, the *Q* value is given by the concentration required to effect 50% removal of the initial fluorescence of bound dye.

2.15.3   Viscosity experiments

15 mL dsDNA (Deoxyribonucleic acid sodium salt from Salmon Testes, Sigma-Aldrich, D1626-1G) solution was prepared at 1 x 10^{-3} M in 80 mM HEPES buffer for each working sample. Stock solutions prepared in DMSO were added according to the gradual increasing [drug]/[DNA] (*r*) ratios of 0.025, 0.05, 0.075, 0.1, 0.125, 0.15, 0.175 and 0.2. Viscosity values, η, (unit: cP) were directly obtained by running 0# spindle in working samples at 60 rpm via DV-II-Programmable Digital Viscometer equipped with Enhanced Brookfield UL Adapter at room temperature. Data were presented as η/η_o versus [compound]/[DNA] ratio, in which η_o and η refers to viscosity of each DNA working sample in the absence and presence of complex.

2.15.4   Nuclease Activity

Reactions were carried according to the literature procedure.[108] Briefly, in a total volume of 20 μL using 80 mL of HEPES buffer (Fisher) at pH 7.2 with 25 mM NaCl, an aliquot of the stock complex (prepared in DMSO) was mixed with 400 ng of pUC19 (Roche) and 1 μL of 20 mM Na-L-ascorbate. Samples were incubated at 37°C for 3 h before being quenched with 6x loading dye (Fermentas), containing 10 mM Tris-HCl (pH 7.6), 0.03% bromophenol blue, 0.03% xylene cyanol, 60% glycerol and 60 mM EDTA, then loaded onto agarose gel 1% containing 2.0 μL of GelRedTM (10000X). Electrophoresis was completed at 80 V for 1.5 h using a wide mini-sub cell (BioRad) in 1XTAE buffer (Millipore).

2.15.5   2D and 3D spheroid studies

Copper complexes **2.3, 2.4, 2.6** and **2.8** were dissolved in the minimum DMSO amount prior to cell culture testing. A calculated amount of the stock drug DMSO solution was added to the cell culture media in order to reach a final maximum DMSO concentration of 0.5%, which had no effects on cell viability. Cisplatin was dissolved in 0.9% sodium chloride solution. MTT (3-(4,5-dimethylthiazol-2-yl)- 2,5-diphenyltetrazolium bromide), cisplatin and ImmunoPure p-nitrophenyl phosphate (APH) were obtained from Sigma Chemical Co, St. Louis, USA.

2.15.6   Cell cultures

Human colon (HCT-15) and breast (MCF-7) carcinoma cell lines were obtained from American Type Culture Collection (ATCC, Rockville, MD). Human ovarian 2008 cancer cells were kindly provided by Prof. G. Marverti (Dept. of Biomedical Science of Modena University, Italy). Human ovarian A2780 cancer cells were kindly provided by Prof. M.P.Rigobello (Dept. of Biomedical Science of Padova University, Italy). Human squamous cervical A431 carcinoma cells were kindly provided by Prof. F. Zunino (Division of Experimental Oncology B, Istituto Nazionale dei Tumori, Milan, Italy). Cell lines were maintained in the logarithmic phase at 37 °C in a 5% carbon dioxide atmosphere using RPMI-1640 medium (Euroclone) containing 10% foetal calf serum (Euroclone, Milan, Italy), antibiotics (50 units/mL penicillin and 50 μg/mL streptomycin), and 2 mM l-glutamine.

2.15.7 Spheroid cultures

Spheroids were initiated in liquid overlay by seeding 1.5×10^3 A2780 or HCT-15 cells/well in phenol red free RPMI-1640 medium (Sigma Chemical Co.), containing 10% FCS and supplemented with 20% methyl cellulose stock solution. A total of 150 µL of this cell suspension was transferred to each well of a round bottom non-tissue culture treated 96 well-plate (Greiner Bio-one, Kremsmünster, Austria) to allow spheroid formation within 72 h.

2.16 Cytotoxicity assays

2.16.1 MTT assay

The growth inhibitory effect towards adherent cancer cell lines was evaluated by means of MTT assay. Briefly, $3 - 8 \times 10^3$ cells/well, dependent upon the growth characteristics of the cell line, were seeded in 96-well microplates in growth medium (100 µL). After 24 h, the medium was removed and replaced with fresh media containing the compound to be studied at the appropriate concentration. Triplicate cultures were established for each treatment. After 72 h, each well was treated with 10 µL of a 5 mg/mL MTT saline solution, and after additional 5 h of incubation, 100 µL of a sodium dodecylsulfate (SDS) solution in HCl 0.01 M were added. Following an overnight incubation, cell growth inhibition was detected by measuring the absorbance of each well at 570 nm using a Bio-Rad 680 microplate reader. Mean absorbance for each drug dose was expressed as a percentage of the absorbance of the untreated control well and plotted vs drug concentration. IC_{50} values, the drug concentrations that reduce the mean absorbance at 570 nm to 50% of those in the untreated control wells, were calculated by four parameters logistic (4-PL) model. All the values are the means ± SD of not less than five measurements starting from three different cell cultures.

2.16.2 Acid phosphatase (APH) assay

An APH modified assay was used for determining cell viability in 3D spheroids. Briefly, the pre-seeded spheroids were treated with fresh medium containing the compound to be studied at the appropriate concentration. Triplicate cultures were established for each treatment. After 72 h, each well was treated with 100 µL of the assay buffer (0.1 M sodium acetate, 0.1% Triton-X-100, supplemented with ImmunoPure *p*-nitrophenyl phosphate) and, following 3 h of incubation, 10 µL of 1 M NaOH solution were added. The inhibition of the cell growth induced by the tested complexes was detected by measuring the absorbance of

each well at 405 nm, using a Bio-Rad 680 microplate reader. Mean absorbance for each drug dose was expressed as a percentage of the untreated control well absorbance (T/C) and plotted vs drug concentration. IC_{50} values, the drug concentrations that reduce the mean absorbance at 405 nm 50% of those in the untreated control wells, were calculated by four parameter logistic (4-PL) model. Evaluation was based on means from at least four independent experiments.

2.17 Cellular uptake and DNA binding

A2780 and HCT-15 cells ($3 \cdot 10^6$) were seeded in 75 cm^2 flasks in growth medium (20 mL). After overnight incubation, the medium was replaced and the cells were treated with tested compounds for 24 h. Cell monolayers were washed twice with cold PBS, harvested, and counted. Samples were than subjected to three freezing/thawing cycles at -80 °C, and then vigorously vortexed. The samples were treated with highly pure nitric acid (Cu: ≤0.5 µg·kg^{-1}, TraceSELECT® Ultra, Sigma Chemical Co.) and transferred into a microwave teflon vessel. Subsequently, samples were submitted to standard procedures using a speed wave MWS-3 Berghof instrument (Eningen, Germany). After cooling, each mineralized sample was analyzed for platinum by using a Varian AA Duo graphite furnace atomic absorption spectrometer (Varian, Palo Alto, CA; USA) at the wavelength of 324 nm. The calibration curve was obtained using known concentrations of standard solutions purchased from Sigma Chemical Co. purchased from Sigma Chemical Co.

For the DNA binding studies, DNA was extracted and purified by a commercial spin column quantification kit (Qiagen DNeasy Blood and Tissue Kit). Only highly purified samples (A260/A230 · 1.8 and A280/A260 · 2.0) were included for analysis to avoid any artefacts. The samples were completely dried and re-dissolved in 200 µL of Milli-Q water (18.2 MΩ) for at least 20 min at 65 °C in a shaking thermo-mixer, mineralized and analyzed for total Cu content by GF-AAS as described above.

2.18 Reactive oxygen species (ROS) production

The production of ROS was measured in A2780 cells (10^4 per well) grown for 24 h in a 96-well plate in RPMI medium without phenol red (Sigma Chemical Co.). Cells were then washed with PBS and loaded with 10 µM 5-(and-6)-chloromethyl-2',7'-dichlorodihydrofluorescein diacetate acetyl ester (CM–H$_2$DCFDA) (Molecular Probes-Invitrogen, Eugene, OR) for 25 min, in the dark. Afterwards, cells were washed with PBS and incubated with tested compounds. Fluorescence increase was estimated utilizing the wavelengths of 485 nm (excitation) and

527 nm (emission) in a Fluoroskan Ascent FL (Labsystem, Finland) plate reader. Antimycin (3 µM, Sigma Chemical Co), a potent inhibitor of Complex III in the electron transport chain, was used as positive control.

2.18.1 Comet assay

About 4x104 A2780 cells were seeded in 25 cm^2 flasks in growth medium (6 mL). After 24 h, cells were incubated for 3h with 2.5µM of tested compounds. Cells were washed twice with cold PBS, harvested, centrifuged, and DNA fragmentation was measured by the alkaline comet assay. Low melting point agarose, 300 µL (Trevigen Inc., Gaithersburg, MD, US) was heated to 37 °C and combined with 2×10^5 cells per mL cell suspension. Each well of a 20-well CometSlide was filled with 30 µL of the cell/agarose suspension. The slides were placed in a 4 °C refrigerator in the dark for 15 min to solidify. Slides were then immersed in 50 mL of pre-chilled lysis solution containing Trizma base, Triton X-100, DMSO and left at 4 °C for 30 min to facilitate cell membrane and histone removal. After draining excess liquid, the slides were transferred to 50 mL of freshly prepared (same day) alkaline DNA unwinding solution, (200 mmol/L NaOH, 1 mmol/L EDTA, pH > 13) and incubated at room temperature in the dark for 20 min. After the unwinding step, electrophoresis was performed at 21 V for 30 min. Slides were then rinsed with distilled water and fixed 5 min in 70% ethanol. Slides were dried and stained 5 min at 4 °C with SYBR Green I (Trevigen, Inc.,) diluted 1:10 000 in 10 mmol/L Tris pH 7.5, 1 mmol/L EDTA, drained to remove excess staining solution and thoroughly dried at room temperature in the dark.

2.19   Experimental Procedures for Chapter 2

2.10: Synthesis of 1,10 phenanthroline - 5,6-dione
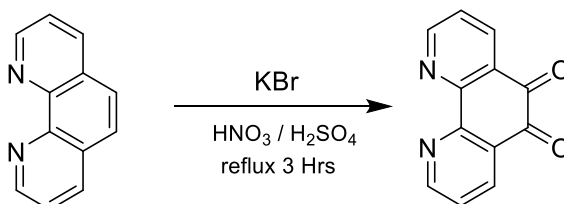
1,10 – Phenanthroline (2.0 g, 10 mmoles) and potassium bromide (2.0 g, 16.8 mmoles) were added to a round bottom flask containing an ice-cold mixture of H_2SO_4 (20 mL) and HNO_3 (10 mL). The solution was refluxed at 100 $^{\circ}$C for 3 hours, a dark orange colour was observed. The solution was allowed to cool to room temperature, then slowly poured into deionised iced H_2O (200 mL). To this was added slowly a solution of NaOH (200 mL, 5M) until a pH of ~ 6 was reached. The solution was then poured into a separation funnel and washed with $CHCl_3$ (2 x 50 mL). The organic phase was dried using anhydrous sodium sulphate. The solution was then filtered and reduced *in vacuo*. A yellow solid was recovered. The crude yellow solid was purified via recrystallization from MeOH to give yellow needles.

Yield: 1.62 g (77 %)

^{1}H NMR (500 MHz, $CDCl_3$) δ 9.11 (dd, 2H), 8.49 (dd, 2H), 7.58 (dd, *J* = 7.9, 4.7 Hz, 2H).
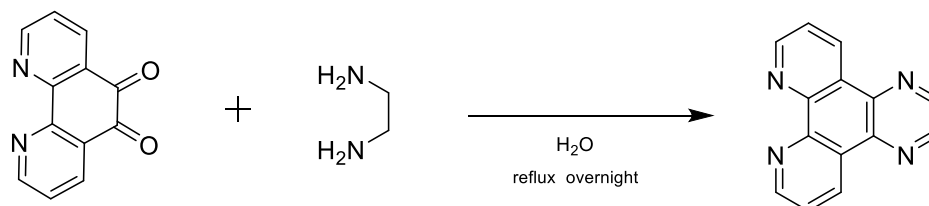
^{13}C NMR (126 MHz, $CDCl_3$) δ 178.8, 156.5, 153.0, 137.4, 128.2, 125.7.

IR (ATR) 3061, 1682, 1559, 1413, 1292, 1205, 1010, 806, 735 cm^{-1}

Elemental Analysis $C_{12}H_6N_2O$ % Calculated   C 68.57, H 2.88, N 13.51

                                    % Found: C 67.97, H 3.07, N 13.14

HRMS (ESI +): *m/z* Calculated for $C_{12}H_6N_2O$ + [H$^+$] 211.0508, Found 211.0507.

2.18: Synthesis of pyrazino [2,3-f] [1,10] phenanthroline (DPQ)

1,10-phenanthroline-5,6-dione (2.10) (0.25 g, 1.9 mmoles) was dissolved in deionised H_2O (17 mL) in a round bottom flask. To this was added ethelyne diamine (0.396 mL, 5.95 mmoles). The solution was then refluxed at 120 °C overnight, a grey / brown colour was observed. The solution was allowed to cool to room temperature. The precipitate was collected using vacuum filtration and washed with deionised H_2O (10 mL) and then Et_2O (10 mL). A grey / pale pink solid was recovered. The crude pink solid was Purified via recrystallization from MeOH to give orange needles.

Yield: 0.22 g (80 %)

^{1}H NMR (500 MHz, CDCl$_3$) δ 9.48 (dd, *J* = 8.1, 1.5 Hz, 2H), 9.29 (dd, *J* = 4.2, 1.5 Hz, 2H), 8.97 (s, 2H), 7.79 (dd, *J* = 8.1, 4.4 Hz, 2H).

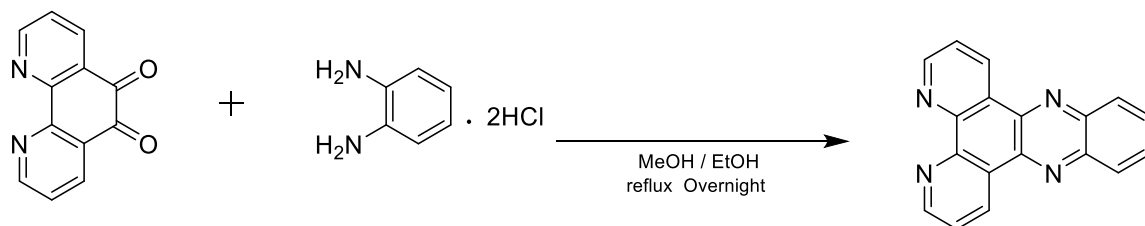**^{13}C NMR** (126 MHz, CDCl$_3$) δ 152.5, 147.6, 144.7, 140.7, 133.3, 127.1, 124.2.

IR (ATR) 1571, 1467, 1389, 1207, 1078, 804, 675 cm^{-1}

Elemental Analysis $C_{14}H_8N_4$ % Calculated: C 72.40, H 3.47, N 24.12

% Found: C 71.61, H 3.48, N 23.74

HRMS (ESI +): *m/z* Calculated for $C_{14}H_8N_4$+ [H$^+$] 233.0827, Found 233.0826.

2.19: Synthesis of dipyrido – phenazine (DPPZ)

1,2-phenylenediamine dihydrochloride (0.31 g, 1.7 mmoles) was dissolved in MeOH (16 mL) in a round bottom flask. In a separate flask 1,10-phenanthronline-5,6- dione (SB 1.0) (0.240 g, 1.14 mmoles) was dissolved in 50:50 warm EtOH / MeOH (40 mL, 50 °C). SB 1.0 was added dropwise with stirring to the solution of 1,2-phenylenediamine dihydrochloride. An orange colour was observed. The solution was allowed to reflux overnight at 90 °C. The solution was allowed to cool to room temperature and the precipitate was collected using vacuum filtration. The solid was washed using deionised H_2O (10 mL) and E_t2O (15 mL) and dried under high vacuum. A pale pink solid was recovered. No further purification was required.

Yield: 0.23 g, (70 %)

^{1}H NMR (500 MHz, DMSO) δ 9.56 (d, *J* = 7.9 Hz, 2H), 9.23 (d, *J* = 3.4 Hz, 2H), 8.33 (dd, *J* = 6.4, 3.4 Hz, 2H), 8.07 (dd, *J* = 6.2, 3.3 Hz, 4H).
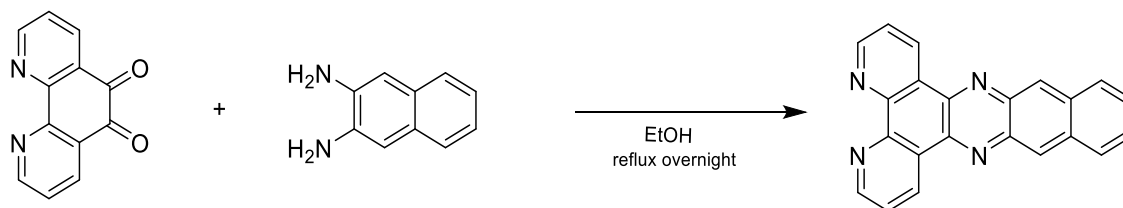
^{13}C NMR (126 MHz, DMSO) δ 151.2, 149.9, 142.0, 140.4, 135.1, 131.9, 129.4, 127.8, 125.7.

IR (ATR) 3385, 3014, 1610, 1488, 1411, 1246, 1137, 1076, 822 cm^{-1}

Elemental Analysis $C_{18}H_{10}N_4$ % Calculated: C 76.58, H 3.57, N 19.85

                                                            % Found: C 75.98, H 3.50, N 19.83

HRMS (ESI +): *m/z* Calculated for $C_{18}H_{10}N_4$ + [H$^+$] 283.0983, Found 283.0984.

2.20: Synthesis of benzo-dipyrido [3,2-2',3'] phenazine (DPPN)

1,10-phenanthroline-5,6-dione (**2.10**) (0.225 g, 1.07 mmoles) was dissolved in EtOH (35 mL) in a round bottom flask. To this was added slowly phenazine-2,3-diamine (0.254 g, 1.60 mmoles). A dark brown colour was observed as a precipitate formed. The solution was refluxed over night at 100 °C. The solution was allowed to cool to room temperature and the precipitate was collected via vacuum filtration. The solid was washed with EtOH (20 mL) and Et_2O (10 mL). The solid was dried under vacuum. An orange-coloured solid was recovered. No further purification was required.

Yield: 0.29 g, (83 %)

^{1}H NMR (500 MHz, CDCl$_3$) δ 9.57 (dd, *J* = 8.1, 1.8 Hz, 2H), 9.23 (dd, *J* = 4.4, 1.8 Hz, 2H), 8.87 (s, 2H), 8.16 (dd, *J* = 6.5, 3.2 Hz, 2H), 7.75 (dd, *J* = 8.1, 4.4 Hz, 2H), 7.60 (dd, *J* = 6.6, 3.1 Hz, 2H).
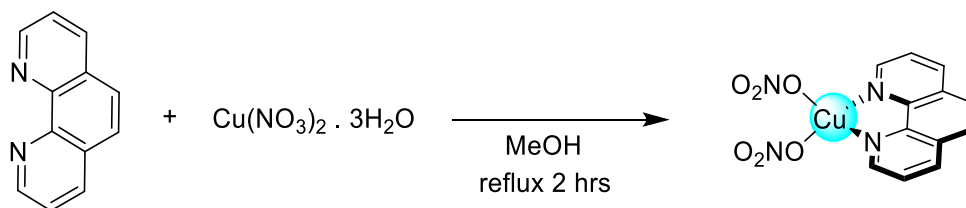
^{13}C NMR (126 MHz, CDCl$_3$) δ 153.2, 149.3, 142.7, 139.3, 134.9, 134.3, 129.0, 128.3, 127.5, 124.7.

IR (ATR) 3284, 1628, 1584, 1410, 1360, 1070, 872 cm^{-1}

Elemental Analysis $C_{22}H_{12}N_4$ % Calculated: C 79.50, H 3.64, N 16.86

                                        % Found: C 79.04, H 3.15, N 16.85

HRMS (ESI +): *m/z* Calculated for $C_{22}H_{12}N_4$ + [H$^+$] 333.1140, Found 333.1137.

2.21: Synthesis of [Cu(H₂O)₂(Phen)]. (NO₃)₂

1, 10 – Phenanthroline (0.25 g, 1.38 mmoles) was dissolved in methanol (30 mL). To this was added Copper (II) nitrate tri – hydrate (0.366 g, 1.51 mmoles) dissolved in MeOH (5 mL). The solution was refluxed for 2 hours at 80 °C. A bright blue colour was observed. The solution was allowed to cool to room temperature. Et₂O (20 mL) was added while stirring continued. A blue precipitate was observed. The precipitate was collected via vacuum filtration and washed with Et₂O (20 mL). The blue solid was purified via recrystallization from MeOH to give bright blue needles.
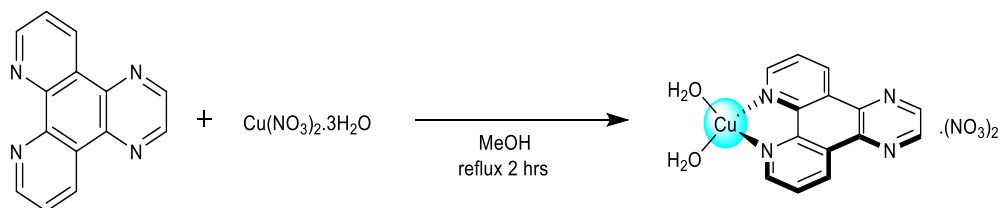
Yield: 0.25 g, (44 %)

IR (ATR) 3075, 2290, 1609, 1522, 1480, 1345, 1272, 1112, 1011, 807, 719 cm^{-1}

Elemental Analysis $C_{12}H_8CuN_4O_6 + H_2O$ % Calculated: C 37.36, H 2.61, N 14.52

                                                      % Found: C 37.61, H 2.96, N 14.71

HRMS (ESI +): *m/z* Calculated for $C_{12}H_8CuN_2$ [M – 2NO₃$^-$] 242.9983, Found 242.9993.

2.22: Synthesis of [Cu(DPQ) (H$_2$O)$_2$]. (NO$_3$)$_2$

DPQ (0.18 g, 0.775 mmoles) was dissolved in MeOH (20 mL). In a separate round bottom flask Copper (II) nitrate tri-hydrate (0.207 g, 0.860 mmoles) was dissolved in MeOH (26 mL). The copper (II) nitrate tri-hydrate solution was added slowly dropwise to the DPQ solution with stirring. A pale green / blue colour was observed. The solution was refluxed at 80 ^{o}C for 2 hours. The solution was allowed to cool to room temperature and Et$_2$O (25 mL) was added. The solution was allowed to stir for 15 minutes. The precipitate was collected using vacuum filtration and washed with CHCl$_3$ (20 mL), H$_2$O (10 mL) and finally, Et$_2$O (25 mL). Then dried under vacuum. A grey / blue solid was recovered.
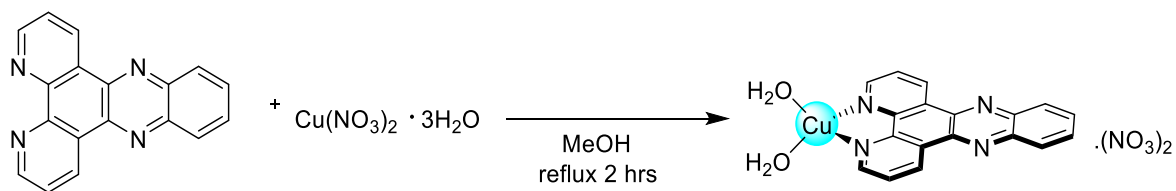
Yield: 0.25g (76 %)

IR (ATR) 1618, 1581, 1473, 1386, 1277, 1126, 1011, 817, 727 cm^{-1}

Elemental Analysis C$_{14}$H$_8$CuN$_6$O$_6$ + 2H$_2$O % Calculated: C 36.89, H 2.65, N 18.44

% Found: C 36.88, H 2.50, N 18.41

HRMS (ESI +): *m/z* Calculated for C$_{14}$H$_8$CuN$_4$ [M − 2NO$_3$$^-$] 346.8570, Found 346.8563.

2.23: Synthesis of [Cu(DPPZ) (H₂O)₂]. (NO₃)₂

DPPZ (0.189 g, 0.637 mmoles) was dissolved in methanol (33 mL). In a separate flask Copper(II) nitrate tri-hydrate (0.19 g, 0.708 mmoles) was dissolved in MeOH (20 mL). The copper (II) nitrate tri – hydrate was then added slowly with stirring to the DPPZ. The resulting solution was refluxed for 2 hours at 80 °C. A pale green colour was observed. The solution was allowed to cool to room temperature and Et₂O (20 mL) was added. The solution was allowed to stir for 15 minutes. A pale blue/ green precipitate was observed. The solid was collected using vacuum filtration and washed using Et₂O (30 mL). The solid was dried under high vacuum. A green / blue solid was recovered.
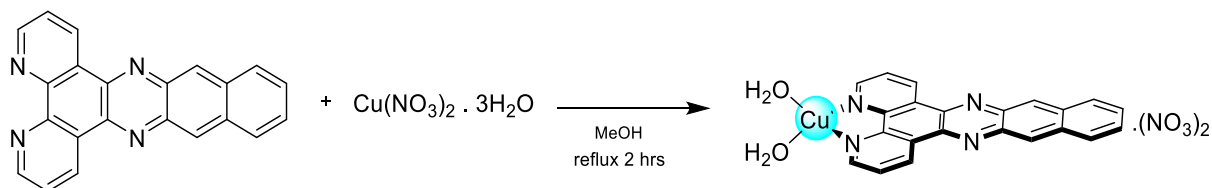
Yield: 0.18 g (57 %)

IR (ATR) 3082, 1979, 1605, 1583, 1494, 1495, 1280, 1139, 1076, 1004 816, 728 cm^{-1}

Elemental Analysis $C_{18}H_{10}CuN_6O_6$ + $2H_2O$ % Calculated: C 42.74, H 2.79, N 16.61

% Found: C 42.50, H 2.40, N 17.75

HRMS (ESI +): *m/z* Calculated for $C_{18}H_{14}CuN_6O_8$+ [Na$^+$] 528.0169, Found 528.0160.

2.24: Synthesis of [Cu(DPPN) (H₂O)₂]. (NO₃)₂

DPPN (0.25 g, 0.750 mmoles) was dissolved in MeOH (40 mL) in a round bottom flask. In a separate flask Copper (II) nitrate tri – hydrate (0.201 g, 0.830 mmoles) was dissolved in MeOH (20 mL). The copper (II) nitrate tri – hydrate solution was added slowly with stirring to the DPPN. An orange colour was observed. The solution was allowed to reflux for 2 hours at 80 °C. The solution was allowed to cool to room temperature and Et₂O (45 mL) was added. The solution was allowed to stir for 15 minutes, an orange / brown precipitate was observed. The solid was collected using vacuum filtration and washed with MeOH (30 mL) and dried under high vacuum. An orange coloured solid was recovered.
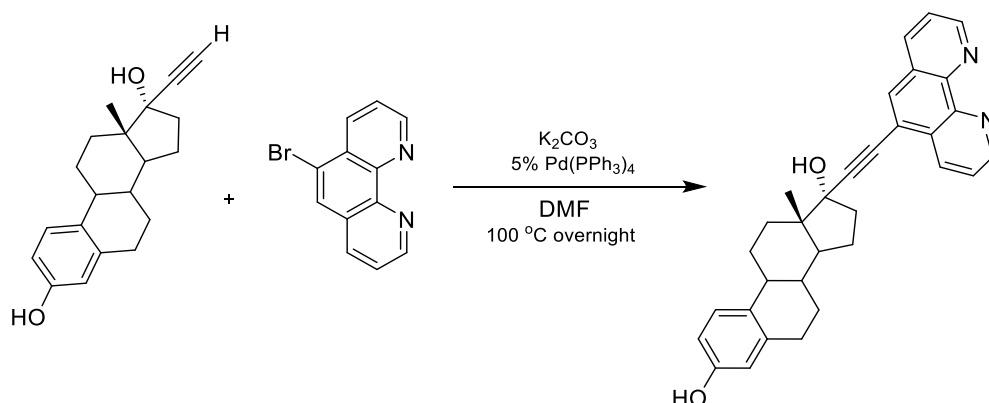
Yield: 0.3 g, (71 %)

IR (ATR) 3047, 2300, 1618, 1579, 1456, 1403, 1138, 1018, 815, 725 cm^{-1}

Elemental Analysis $C_{22}H_{12}CuN_6O_6$ + 2H₂O   **%** Calculated: C 47.53, H 2.90, N 15.12

% Found: C 46.99, H 2.85, N 15.10

HRMS (ESI +): *m/z* Calculated for $C_{22}H_{16}CuN_4O_2$ [M - 2 NO₃$^-$] 431.0323, Found 431.0331

2.25: Synthesis of Phenanthroline – 5 - Ethinyl Estradiol

Bromophenanthroline (0.150 g, 0.58 mmoles), Ethinyl Estradiol (0.171 g, 0.58 mmoles), potassium carbonate (0.400 g, 2.89 mmoles) and Tetrakis (triphenylphosphine) palladium (0.034 g, 0.0029 mmoles) were added to a round bottom flask sealed with a septum and kept under nitrogen gas. Dried and degassed DMF (5 mL) was added using a syringe. The solution was allowed to stir at 100 °C under N_2 atmosphere overnight. A dark brown colour was observed. The reaction was allowed to cool at room temp and deionised water (20 mL) was added. A pale brown precipitate was observed. The suspension was allowed to stir for 1 hour and the solid was collected using vacuum filtration. The solid was washed with copious amount of deionised H_2O and with 50:50 petroleum ether: Et_2O 3 x (10 mL) and then dried under high vacuum overnight. A light brown solid was recovered.

Yield: 0.222 g, (81 %)

1H NMR (500 MHz, CDCl₃) δ 9.20 (s, 1H,Ar-OH), 8.74 (m, 1H, Ar-H), 8.30 (dd, 1H. Ar-H), 8.20 (m, 1H, Ar-H), 8.02 (s, 1H, Ar-H), 7.72 (m, 1H, Ar-H), 7.65 (dd, 1H, Ar-H), 7.46 (d, 1H, Ar-H), 7.18 (d, 1H, Steroid Ar-H), 7.05 (d, 1H, steroid Ar-H), 6.65 (s, 1H, steroid Ar-H), 6.60 (s, 1H, Alkyne OH), 2.41 – 1.79 (m, 12H, steroid - 6xCH₂), 1.26 (s, 1H, steroid - *C*H), 1.01 (s, 1H, steroid *C*H), 0.83 (m, 3H, Steroid – *C*H₃).

13C NMR (126 MHz, CDCl₃) δ 151.0, 150.7, 146.2, 138.3, 135.8, 134.7, 132.4, 130.9, 128.5, 128.1, 126.7, 123.6, 123.5, 119.8, 115.4, 112.9, 99.2, 97.8, 83.6, 82.8, 80.9, 50.4, 48.0, 43.9, 39.6, 33.5, 31.7, 29.8, 27.5, 26.6, 23.2, 13.1.
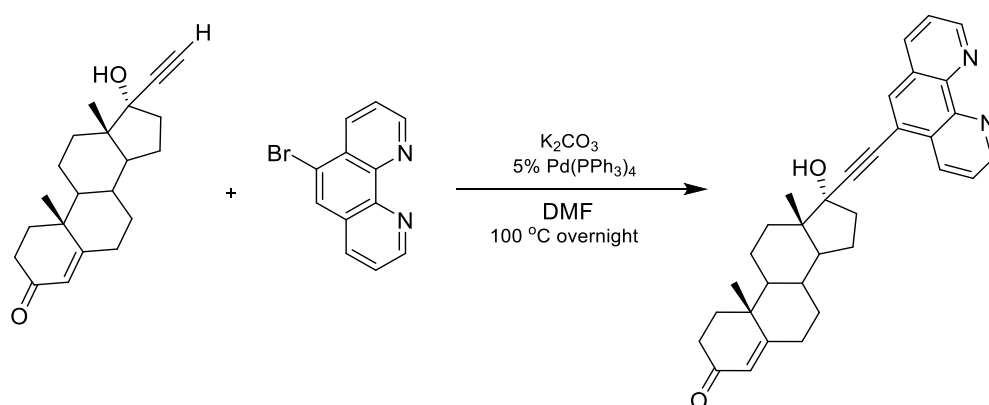
IR (ATR) 3302, 2862, 1656, 1401, 1090, 738 cm⁻¹

Elemental Analysis $C_{32}H_{30}N_2O_2$ **%** Calculated: C 80.98, H 6.37, N 5.90

                                                % Found: C 81.34, H 5.99, N 6.02

HRMS (ESI +): *m/z* Calculated for $C_{32}H_{30}N_2O_2 + [H^+]$ 475.2386, Found 475.2382.

2.26: Synthesis of Phenanthroline-5-Ethisterone

5-Bromo-1,10-phenanthroline (0.150 g, 0.58 mmoles), Ethisterone (0.180 g, 0.58 mmoles), K_2CO_3 (0.400 g, 2.90 mmoles) and Tetrakis(triphenylphosphine) palladium (0) (0.034 g, 0.0029 mmoles) were added to a round bottom flask sealed with a septum and kept under N_2 gas. Dried and degassed DMF (5 mL) was added using a syringe. The solution was allowed to stir at 100 °C under N_2 atmosphere overnight. A dark brown colour was observed. The reaction was allowed to cool at room temp and deionised H_2O (20 mL) was added. A pale brown precipitate was observed. The suspension was allowed to stir for 1 hour and the solid was collected using vacuum filtration. The solid was washed with copious amount of deionised H_2O and with 50:50 petroleum ether / Et_2O (3 x 10 mL) and then dried under high vacuum overnight. A dark brown solid was recovered.

Yield: 0.23 g, (89 %)

^{1}H NMR (500 MHz, $CDCl_3$) δ 9.20 (dd, 1H,Ar-H), 9.16 (dd, 1H, Ar-H), 8.65 (dd, 1H, Ar-H), 8.19 (dd, 1H, Ar-H), 7.97 (s, 1H,Ar-H), 7.69 (dd, 1H, Ar-H), 7.58 (dd, 1H, Ar-H), 5.71 (s, 1H-Steroid-H), 2.52 – 0.79 (m, 20H, Steroid aliphatic H, 8xCH_2 & 2 x CH), 1.21 (m, 3H, Alkeyne-OH- CH_3), 1.01 (s, 3H, CH_3).

¹³C NMR (126 MHz, CDCl₃) δ 190.7, 171.3, 151.0, 150.8, 146.8, 145.8, 136.1, 135.2, 129.8, 128.9, 128.0, 124.1, 124.0, 123.8, 120.9, 87.4, 79.8, 74.3, 53.5, 50.0, 46.8, 39.0, 38.7, 36.3, 35.8, 34.1, 32.9, 32.5, 31.6, 23.2, 20.8, 17.5, 12.8.
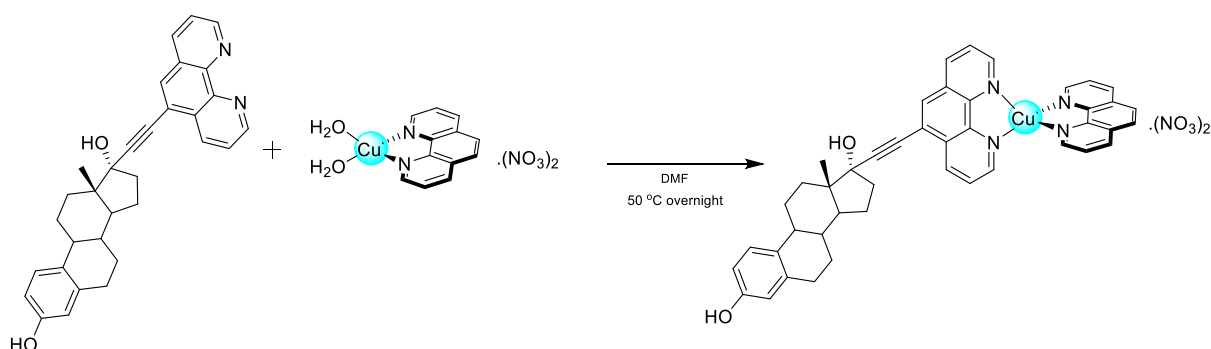
IR (ATR) 2942, 2871, 1661, 1421, 1069, 741 cm⁻¹

Elemental Analysis   C₃₃H₃₄N₂O₂   % Calculated: C 80.78, H 6.99, N 5.71

                          % Found: C 81.12, H 7.08, N 5.98

HRMS (ESI +): *m/z* Calculated for C₃₃H₃₄N₂O₂ + [H⁺] 491.2699, Found 491.2693.

2.3: Synthesis of [Cu (EE-5 - Phen) (Phen)]. (NO₃)₂

Phenanthroline – 5 – Estradiol (**2.25**) (0.055 g, 1.58 mmoles) was dissolved in DMF (5 mL). in a separate round bottom flask [Cu(phen)(H₂O)₂]. (NO₃)₂ (**2.21**) (0.29 g, 1.58 mmoles) was dissolved in DMF (5 mL). The solution of **2.21** was then added slowly with stirring to the solution of **2.25**. A pale green / brown colour was observed, the solution was allowed to stir overnight at 50 °C. The solution was allowed to cool to room temp and Et₂O (50 mL) was added. A pale brown precipitate was observed. The solution was allowed to stir for 3 hours at room temp. The pale brown solid was collected using vacuum filtration and then washed with CHCl₃ (10 mL) and then with H₂O (5 mL). Finally, it was washed with Et₂O (50 mL). No further purification was required. The pale brown solid was dried under vacuum.
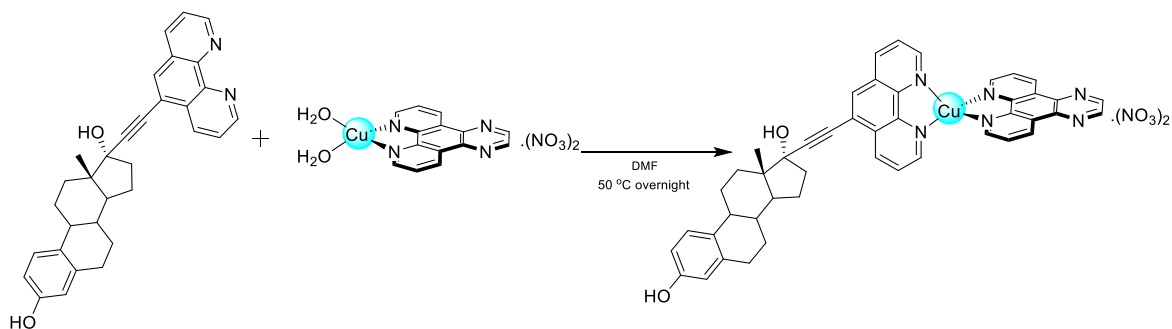
Yield: 0.072 g, (71 %)

IR (ATR): 3356, 2928, 1660, 1519, 1428, 1326, 1286, 1007, 848, 723 cm⁻¹.

Elemental Analysis: $C_{44}H_{38}CuN_8O_6$ **% Calculated:**   C 62.74, H 4.55, N 9.98

% Found: C 62.12, H 4.61, N 9.72

HRMS (ESI +): *m/z* Calculated for $C_{44}H_{38}CuN_4O_2$ [M − 2NO$_3$⁻] 717.2291, Found 717.2298.

2.4: Synthesis of [Cu(DPQ)(ES-5-phen)] .(NO₃)₂

EE-5-phen (**2.25**) (0.055 g, 0.1158 mmoles) and [Cu(DPQ)(H₂O)₂].(NO₃)₂ (**2.22**) (0.053 g, 0.1158 mmoles) were dissolved separately in dried and degassed DMF (5 mL). The [Cu(DPQ)(H₂O)₂].(NO₃)₂ was then added slowly with stirring to the solution of EE-5-phen. A light brown colour was observed. The solution was allowed to stir overnight at 50 °C. The solution was allowed to cool to room temperature and Et₂O (50 mL) was added. A pale brown / green precipitate was observed. The solution was allowed to stir for 3 hours at room temperature. The pale green was collected using vacuum filtration and washed using Et₂O (50 mL). The solid was dried under high vacuum for 3 hours. The solid was washed with CHCl₃ (10 mL) and then with MeOH (5 mL). Finally, it was washed with Et₂O (50 mL). No further purification was required. A pale green solid was recovered.
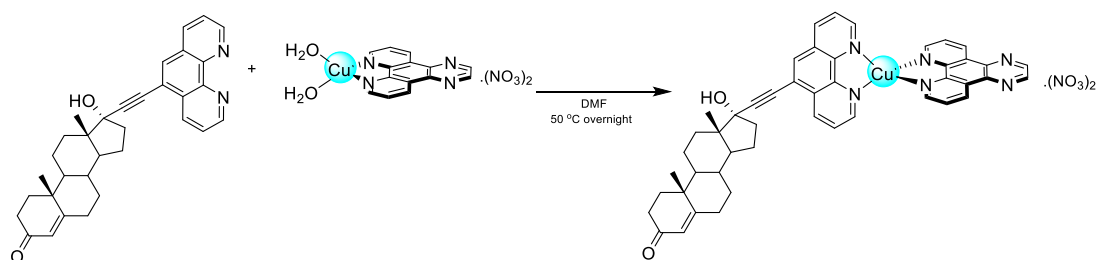
Yield: 0.079 g, (77 %)

IR (ATR): 3062.28, 2928, 1655, 1375, 1288, 1083, 814, 730 cm⁻¹

Elemental Analysis: $C_{46}H_{38}CuN_8O_8$ % Calculated C 61.77, H 4.28, N 12.53

% Found: C 61.43, H 3.98, N 12.92

HRMS (ESI +): *m/z* Calculated for $C_{46}H_{38}CuN_6O_2$ [M - 2NO$_3$⁻] 769.2346, Found 769.2342.

2.5: Synthesis of [Cu(DPQ)(ES–5-Phen)](NO₃)₂

ES-5-phen (**2.26**) (0.050 g, 0.101 mmoles) and [Cu(DPQ)(H₂O)₂].(NO₃)₂ (**2.22**) (0.046 g, 0.1 mmoles) were dissolved separately in dried and degassed DMF (5 mL) The [Cu(DPQ)(H₂O)₂].(NO₃)₂ was then added slowly dropwise and with stirring to the solution of EE-5-Phen. A dark green colour was observed. The solution was allowed to stir overnight at 50 °C. The resulting solution was reduced *in vacuo* to half volume and Et₂O (50 mL) was added. A dark green precipitate was observed that was recovered *via* centrifuge. The solid was washed with CHCl₃ (10 mL) and then with MeOH (5 mL). Finally, it was washed with Et₂O (50 mL). No further purification was required. The pale green solid was dried under high vacuum.

Yield: 0.014 g, (15 %)

IR (ATR): 3061, 2938, 2869, 1657, 1358, 1286, 1016, 814, 730 cm⁻¹.

Elemental Analysis: $C_{47}H_{42}CuN_8O_8 + H_2O$ % Calculated C 62.00, H 4.65, N 12.31

% Found: C 62.35, H 4.25, N 12.12

HRMS (ESI +): *m/z* Calculated for $C_{47}H_{42}CuN_6O_2$ [M − 2NO₃⁻] 785.2665, Found 785.2665.

2.6: Synthesis of [Cu(DPPZ)(EE-5-phen)](NO$_3$)$_2$
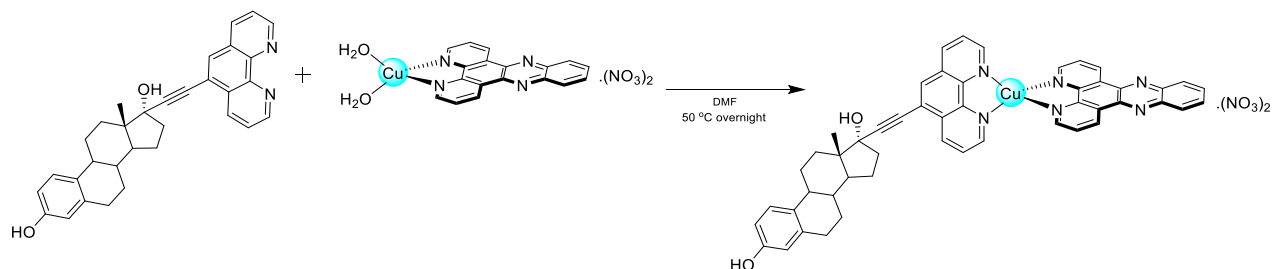
EE-5-phen (**2.25**) (0.055 g, 0.115 mmoles) and [Cu(DPPZ)(H$_2$O)$_2$].(NO$_3$)$_2$ (**2.23**) (0.058 g, 0.158 mmoles) were dissolved separately in dried and degassed DMF (5 mL). The [Cu(DPPZ)(H$_2$O)$_2$].(NO$_3$)$_2$ was then added slowly with stirring to the solution of ES-5-phen. A light brown colour was observed. The solution was allowed to stir overnight at 50 ^{O}C. The solution was allowed to cool to room temperature and Et$_2$O (50 mL) was added. A pale brown / green precipitate was observed. The solution was allowed to stir for 3 hours at room temperature. The pale green / brown solid was collected using vacuum filtration. The solid was washed with CHCl$_3$ (10 mL) and then MeOH (5 mL). Finally, it was washed with Et$_2$O (50 mL). A pale green solid was recovered. No further purification was required.

Yield: 0.089 g, (81 %)

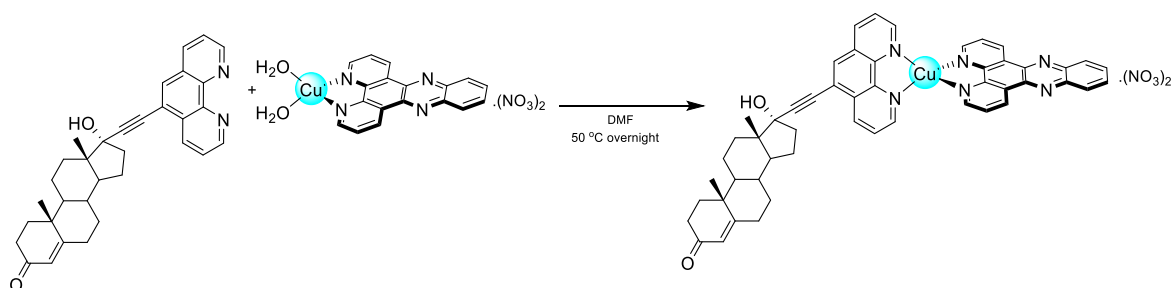**IR (ATR):** 3064, 2929, 1657, 1497, 1421, 1359, 1332, 1289, 1077, 823, 729 cm^{-1}.

Elemental Analysis: C$_{50}$H$_{40}$CuN$_8$O$_8$ % Calculated C 63.59, H 4.27, N 11.86

                                                                          % Found: C 63.37, H 4.48, N 12.21

HRMS (ESI +): Calculated for C$_{50}$H$_{40}$CuN$_6$O$_2$ [M - 2NO$_3^-$] 819.2504, Found 819.2498.

2.7: Synthesis of [Cu(DPPZ)(ES–5-Phen)](NO₃)₂

ES-5-phen (**2.26**) (0.05 g, 0.101 mmoles) and [Cu(DPPZ)(H₂O)₂].(NO₃)₂ (**2.24**) (0.051 g, 0.10 mmoles) were dissolved in dried and degassed DMF (5 mL). The [Cu(DPPZ)(H₂O)₂].(NO₃)₂ was then added slowly dropwise and with stirring to the solution of ES-5-Phen. A dark green colour was observed. The solution was allowed to stir overnight at 50 °C. The solution was allowed to cool to room temperature and Et₂O (50 mL) was added. A pale green precipitate was observed and was collected *via* centrifuge and the solid was washed with CHCl₃ (10 mL) and then MeOH (5 mL). A final washing with Et₂O (10 mL) was carried out. The dark green solid was dried under high vacuum for 3 hours. No further purification was required.

Yield: 0.024 g, (27 %)

IR (ATR): 2940, 1656, 1582, 1486, 1331, 1077, 822, 730 cm⁻¹.

Elemental Analysis: C₅₁H₄₄CuN₈O₈   % Calculated C 63.77, H 4.62, N 11.67

                                                                   % Found: C 63.44, H 4.48, N 11.24

HRMS (ESI +): *m/z* Calculated for C₅₁H₄₄CuN₆O₂ [M − 2 NO₃⁻] 835.2822, Found 835.2814.

2.8: Synthesis of [Cu(DPPN)(EE-5-phen)](NO₃)₂
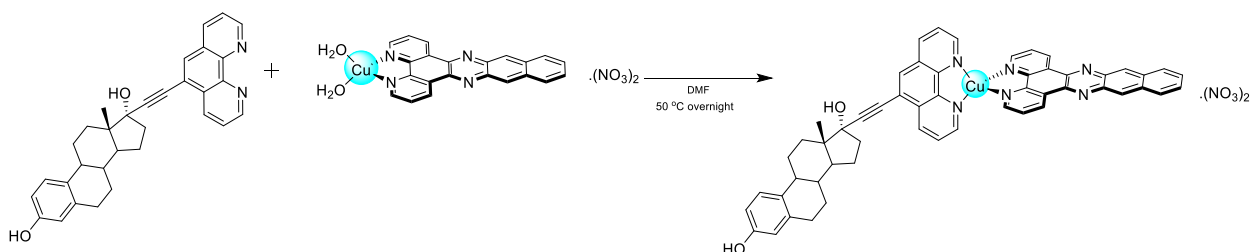
EE-5-phen (0.055 g, 0.1158 mmoles) (**2.25**) and [Cu(DPPN)(H₂O)₂].(NO₃)₂ (0.064 g, 0.1156 mmoles) (**2.24**) were dissolved separately in dried and degassed DMF (5 mL). The [Cu(DPPN)(H₂O)₂].(NO₃)₂ was then added slowly with stirring to the solution of EE-5-phen. A

light brown colour was observed. The solution was allowed to stir overnight at 50 °C. The solution was allowed to cool to room temperature and Et₂O (50 mL) was added. An orange / brown precipitate was observed. The orange / brown solid was collected using vacuum filtration and washed using Et₂O (50 mL). the solid was washed with CHCl₃ (10 mL) and MeOH (5 mL). The solid was dried under high vacuum for 3 hours. An orange / brown solid was recovered. No further purification was required.
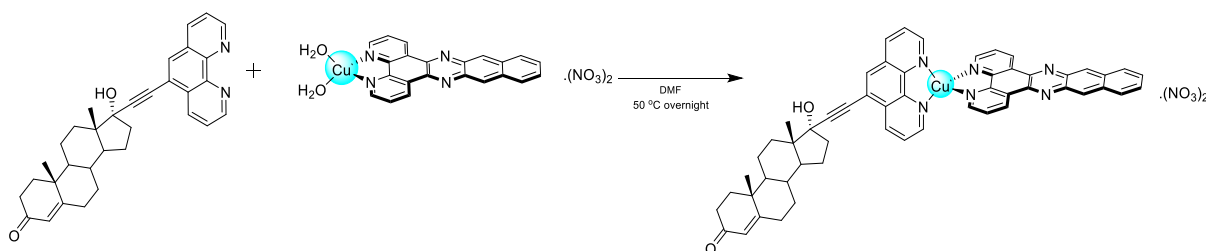
Yield: 0.097 g, (81 %)

IR (ATR): 3063, 2929, 1660, 1420, 1288, 1047, 821, 730 cm⁻¹.

Elemental Analysis: $C_{54}H_{42}CuN_8O_8$ % Calculated C 65.22, H 4.26, N 11.27

                                   % Found: C 65.06, H 3.98, N 11.53

MS (ESI +): Calculated for $C_{54}H_{42}CuN_7O_5$ 931.25 [M - NO₃⁻]; Found 931.29

2.9: Synthesis of [Cu(DPPN)(EE–5-Phen)](NO₃)₂

ES-5-phen (0.05 g, 0.101 mmoles) (**2.26**) and [Cu(DPPN)(H₂O)₂].(NO₃)₂ (0.056 g, 0.1 mmoles) (**2.24**) were dissolved separately in dried and degassed DMF (5 mL). The [Cu(DPPN)(H₂O)₂].(NO₃)₂ was then added slowly dropwise and with stirring to the solution of ES-5-Phen. A dark orange colour was observed. The solution was allowed to stir overnight at 50 °C. The solution was allowed to cool and Et₂O (50 mL) was added. An orange / brown precipitate was observed. The solution was allowed to stir for 3 hours. The orange / brown solid was collected using *vacuum* filtration and washed with CHCl₃ (10 mL) and then MeOH (5 mL) following a further washing using Et₂O (50 mL). No further purification was required. The solid was dried under high vacuum for 3 hours. An orange / brown solid was recovered.

Yield: 0.075 g, (74 %)

IR (ATR): 3402, 3086, 2941, 1655, 1418, 1328, 1073, 1046, 868, 729 cm⁻¹.

Elemental Analysis: $C_{55}H_{46}CuN_8O_8 + 2H_2O$ % Calculated: C 65.37, H 4.59, N 11.09

                                       % Found: C 65.79, H 4.35, N 11.56

HRMS (ESI +): *m/z* Calculated for $C_{55}H_{46}CuN_6O_2$ [M – 2 NO₃⁻] 885.2978, Found 885.2971

3   Chapter 3: Biotinylated copper (II) compounds

3.1   Introduction

3.2   Biotin and its role in the human body

Biotin (Figure3.0) is one of the vitamins from the family of B vitamins, more specifically it is known as vitamin B_7 or vitamin H. The molecule is involved in a huge array of metabolic processes in humans but also in many other organisms also. Mostly it is used for the regulation of carbohydrates and amino acids. Biotin is responsible for mediating gene regulation as it is covalently bound to the lysine residues in histones which in turn affects the chromatin structure.[169] This *biotinylation* of the histone proteins within the nuclear chromatin lends favour to chromatin stability and in turn the expression of certain genes.[170]
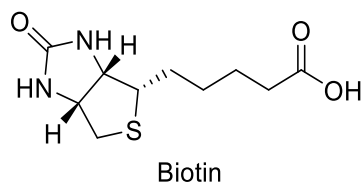
Biotin

Figure 3.0: Molecular structure of Biotin.

Biotin is a coenzyme for five carboxylase enzymes, which are involved in the synthesis of fatty acids, digestion of carbohydrates and gluconeogenesis. Biotin is a fundamental molecule for humans; however, it is not synthesised within the body. The biotin found in humans arrives *via* diet where it is bound to several proteins. Biotin is found in a relatively large amounts in a wide variety of foods, as shown in Table 3.0.

Table 3.0: Table displaying some sources of biotin and the amounts in µg /100g[171]

SOURCE	AMOUNT
	(µg / 100 g)
CHICKEN LIVER	187
BEEF LIVER	42
EGGS	21
EGG WHITE	5.8
EGG YOLK	27
SALMON, CANNED IN WATER	5.9
PORK CHOP	4.5
TURKEY BREAST	0.7
TUNA, WHITE, CANNED	0.7

Biotinidase is an intestine enzyme, which is able to displace biotin from the proteins and it favours the absorption by the intestine.

Biotin also plays an important role in delivering bicarbonate to acetyl-CoA, which is responsible for converting it to malonyl-CoA which is in turn used for the synthesis of fatty acids within the body.[172] Other applications of biotin include the maintaining of healthy skin, nails and hair in which many people seek out dietary supplements in order to strengthen their nails or encourage hair growth.[173]

3.3   Biotin as a molecular target

Biotin is a water-soluble heterocycle molecule formed of two condensed five member rings (a tetrahydrothiophene ring fused to an ureido ring) and a carboxylic acid at the end of a 4-carbon chain (Figure 3.0).

As the biotin synthetic pathway is absent in the mammalian system, mammals need to obtain biotin as a nutrient from plants or bacterial systems. This is accomplished via two transport systems, a high-affinity biotin transporter and a sodium-dependent multivitamin transporter (SMVT). Both the transporter systems have what is known as saturation behaviour for biotin uptake; the biotin transporter holds a very high affinity for biotin at concentrations less than 10 nM, while the SMVT is a low-affinity transporter at concentrations of greater than 10 mM.[174] The human SMVT gene was cloned from HeLa cells; its transcript levels are abundant in the intestinal mucosa, kidney and placenta, which are also the point of absorption for biotin.[175] [176] A significant amount of SMVT is expressed in the liver, brain, lung, heart, and skeletal muscle with active metabolism. SMVT is responsible for biotin uptake into the cells and cancer cells have elevated SMVT expression and therefore increased biotin uptake capacity.

Recent reports have shown that the biotin-specific uptake systems are enhanced in many cancer cells including leukemia (L1210FR), ovarian (Ov2008, ID8), colon (Colo-26), mastocytoma (P815), lung (M109), renal (RENCA, RD0995), and breast (4T1, JC, MMT06056) cancer cell lines.[177] In this chapter the use of biotin as a vector to target biotin receptors (BRs) in cancer cells will be discussed.

3.4   Avidin and streptavidin

Avidin is located in all vertebrates which produce eggs, including various birds, reptiles, and amphibians, however no analogous protein has been detected as of yet in any mammalian

species. Chicken avidin, which is isolated from egg white of hens, and streptavidin, secreted by numerous species of the Streptomyces family of bacteria, are functionally [178] and structurally [179] analogous proteins. The main biological function of avidin is to bind biotin, the fundamental enzymatic cofactor also known as vitamin H. Both proteins share a somewhat similar secondary, tertiary and quaternary structure forming tetrameric complexes of around 60 kDa in which each subunit can bind a single molecule of biotin with incredibly high affinity as demonstrated by Livnag *et al.* (1013 – 1015 Kd M^{-1}).[179] This interaction is primarily thought to be a natural defence mechanism against biotin requiring microbes, [180] however other roles have been suggested for avidin. [181] In addition to their exceptional ligand binding ability, avidin and streptavidin are incredibly stable against high concentrations of denaturing agents, proteases, and a in wide range of pH and temperature.[178]`

### 3.4.1   Avidin and biotin in targeting

The specific traits of avidin have been demonstrated to be of immense advantage in drug targeting: the large positive charge of avidin compliments the efficiency of cellular uptake of biotinylated particles. [182] Zeng *et al*. found that incubation of bioconjugates avidin with biotinylated cell lines resulted in in very rapid surface binding and endocytosis, with efficiencies of almost 100%. [183] Moreover, it is known that (strept)avidin has been confirmed to accumulate within specific tissues,[184] particularly in tumours *in vivo.*[185] This powerful biotin – avidin interaction can be exploited to develop targeted therapies by the biotinylation of ligands or tissues *in vivo.* [186] Numerous studies have been carried out displaying promising results using monoclonal antibodies in the targeting of biotinylated therapeutic or diagnostic compounds using the avidin approach in experimental animals. [187] [188] The body can be shielded from the drug by incorporating it inside the carriers, essentially hiding it and then targeting the complex to desired location. The classic example of this, paclitaxel was incorporated into biotinylated PLA-PEG nanoparticles and targeted to tumour cell *in vitro* by means of the transferrin ligand. The liberation of drug from the nanoparticles was incredibly swift at 24 hours or less and results indicated that the nanoparticle displayed increased antitumoral activity.[189]

The biotin - avidin system has also been utilized very successfully in drug pre - targeting applications. These involve the separation of the targeting antibody from the subsequent delivery of a therapeutic agent, which is then able to find its way to the tumour localized

antibody. This approach dramatically reduces the level of free radiolabelled agent and therefore improves the exposure ratio between tumour and healthy tissue.

## 3.5   Biotin labelled metallodrugs

As stated in the previous section, Biotin has been demonstrated to be very rapidly taken up into tumorous cells which over express the receptors unique to biotin on their cell surface. Therefore, based on this knowledge, biotin can be exploited as a very effective and selective drug transporter. Studies have already shown that tagging classical chemotherapy drugs with a biotin moiety lead to very positive effects, especially with doxorubicin and gemcitabine (**1** and **2**, Figure 3.1).[190]
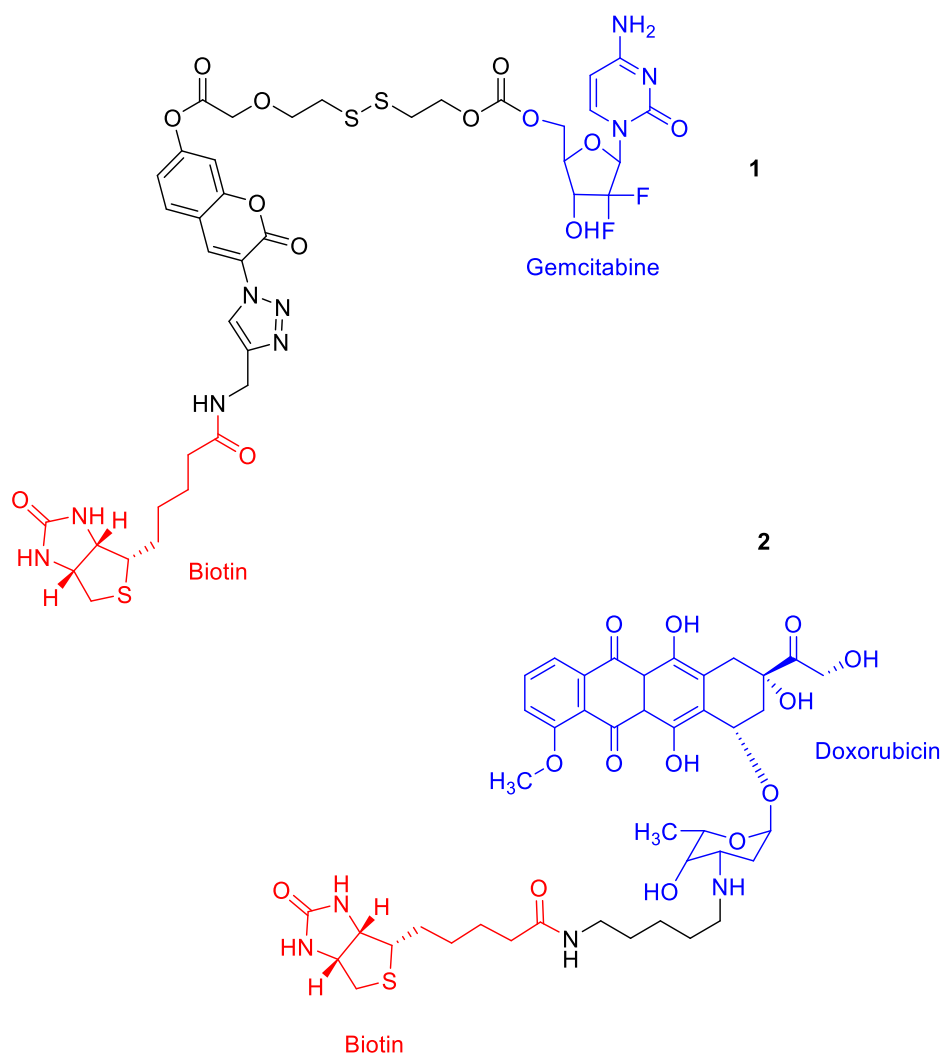
Figure 3.1: Biotin labelled chemotherapy drugs (**1**) Gemcitabine and (**2**) Doxorubicin.

More recently, in 2017, Wang, Gou, *et al.*[191] set about investigating a concept to establish if biotin could be used to selectively deliver platinum (IV) drugs into tumour cells. A biotin was

attached to a cisplatin scaffold generating two new compounds. A complex with one biotin on the axial position (**3**) and another with a bis addition of two biotins, one in each axial position (**4**), (Figure 3.2.).
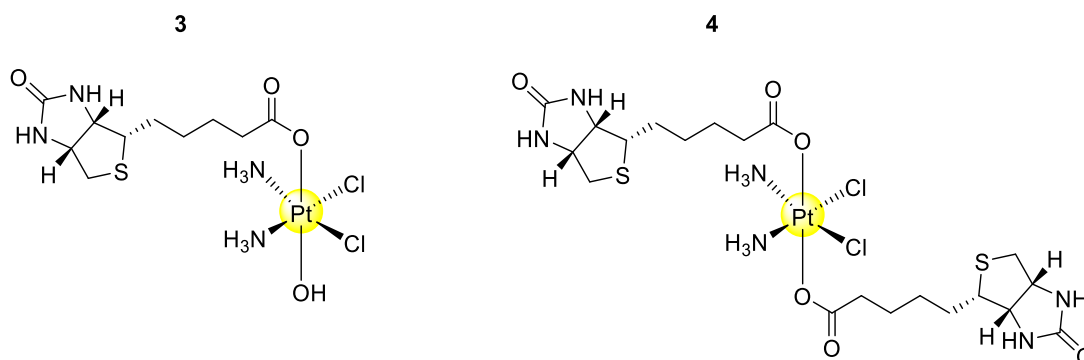

Figure 3.2: Structures of the first two platinum (IV) drugs developed by Wang *et al*.

Upon attaching the biotin moieties to the platinum (IV) centre, they discovered there was a significant enhancement in the uptake of the compounds into breast cancer cells, while also lowering the accumulation of the complexes in breast epithelial cells. The mono biotinylated complex showed superior cytotoxic properties in comparison to its bis-biotinylated analogue against the breast cancer cell lines (MDA-MB-231 and MCF-7). This may potentially be attributed to the presence of the hydroxido ligand in (**3**), which would impact on the overall reduction rate of the complex or in turn on its accumulation within the tumour cells. This phenomenon has previously been reported by Gibson *et al* .[192] Compound (**3**) had very similar cytotoxicity to cisplatin against MCF-7 cells at 72 h (10 vs 9 µM for cisplatin) but dramatically improved cytotoxicity against the cisplatin resistant MDA-MB-231 cells at both 48 and 72 h (18 and 12 vs 45 µM and 40 µM for cisplatin). The cell cycle arrest studies carried out on both complexes in MCF7 cells suggested that the active form and DNA damage mechanism of the complexes were similar to cisplatin, and this would compare desirably with the similar cytotoxicity profiles of both complexes and cisplatin against this cell line.[191]

The group sought to develop the work further after these studies by substituting the hydroxido ligand for a chloride and also introducing biotin in a single axial position to a carboplatin and oxaliplatin scaffold. (Figure 3.3 (**5** - **7**)). The chlorido ligands, like hydroxido ligands, are thought to facilitate enhanced reduction of the platinum(IV) to platinum(II) by forming bridges between the reducing agent and platinum centre, therefore facilitating electron transfer. [192]
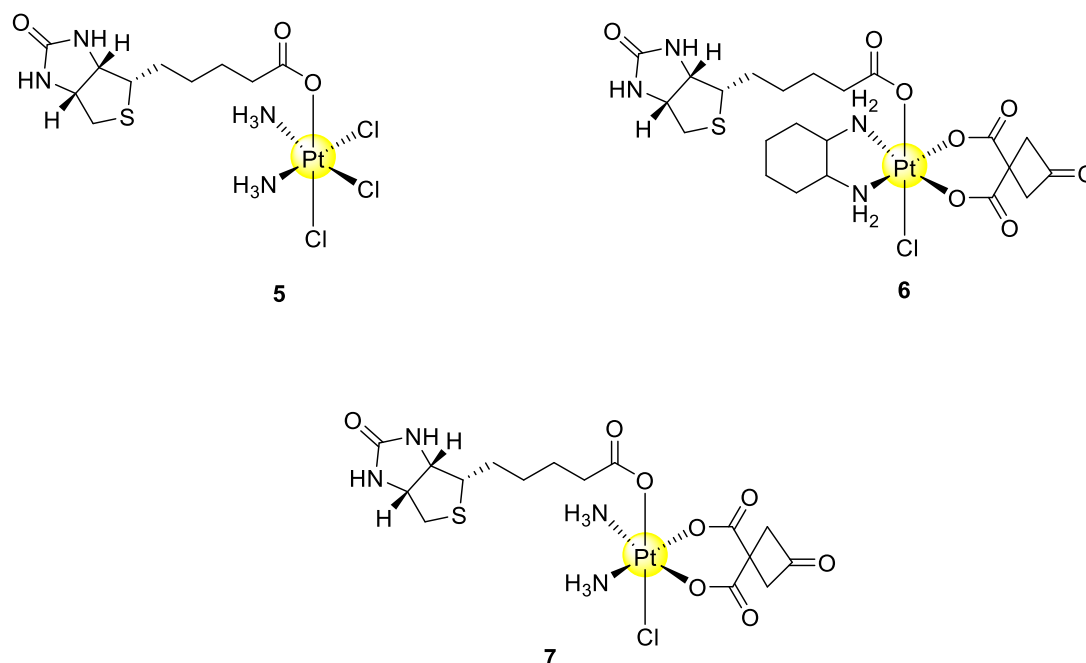
Figure 3.3: Wang *et al*. further compounds as platinum (IV) pro drugs for biotin receptor targeting.

The cytotoxicity of the complexes was tested against HepG2a, MCF7b, SGC7901c (cisplatin sensitive), and SGC-7901/Cisd (cisplatin resistant) cell lines. Complex (**5**), with the cisplatin base, was found to be more cytotoxic than cisplatin alone across all cell lines, between 2 and 3 times more so for the non-resistant cell lines, and a nearly a 10-fold increase in potency against the cisplatin resistant cell line. The cellular accumulation studies of Finnin *et al.* revealed it did not have substantial cellular uptake against the non-resistant cell lines, but uptake was amplified by 4.5 times in the resistant cell line.[193] This offered insight into its ability to overcome cisplatin resistance through significantly higher cellular accumulation. Reduction studies with ascorbic acid showed that the prodrug was reduced to its platinum (II) form with the loss of its biotin axial ligand, which was then shown to be able to bind to streptavidin, the bacteria protein with an extremely high affinity for biotin. These encouraging results highlight how biotin can be exploited as a tumour cell targeting ligand for platinum (IV) prodrugs, with the added evident benefit of being able to overcome cisplatin resistance. The team noted that further studies would be needed in order to probe and understand how the nonreduced complexes interacted with the cell-surface biotin receptors.

3.6   Ruthenium (II) and Osmium (II) complexes of biotin modified scaffolds

Very recently, in May of 2021, Berger *et al.* developed a number of ruthenium and osmium complexes with the goal of selective targeted therapy in mind.[194] Two of these compounds (Figure 3.4) contained a 1,10 – phenanthroline scaffold tethered to a biotin moiety (**8 – 9**). The compounds were screened by MTT assay on five cancer cell lines: the non-small cell lung cancer cell line A549 (human lung carcinoma), MCF-7 (human breast adenocarcinoma), SKMEL28 (human melanoma), U373 (human glioblastoma) and B16F10 (murine melanoma). Berger *et al*. compared the cytotoxic profile against those of the parent 1,10 – phenanthroline complexes of ruthenium and osmium which did not bear the biotin. Although the IC$_{50}$ values for these compounds were attractive, they showed no improvement on the values for the non-substituted metal complexes of phenanthroline. With values of 118 μM and 77μM for the biotinylated ruthenium and osmium respectively, versus 75μM and 73μM for the non-substituted ruthenium and osmium complexes in MCF-7 human breast cancer cells. This trend was observed for all the cell lines examined.[194]

However, in the cellular accumulation assays an almost identical uptake of biotin modified complexes was observed over both cell cells examined A549 (which over expressed the biotin receptor) and B16F10 (which has a very low level of expression of this receptor). Berger *et al*. found that in this case the addition of the biotin group did not increase the cellular uptake or the cellular activity when compared to the RuPhen and OsPhen compounds.[194]

8

9
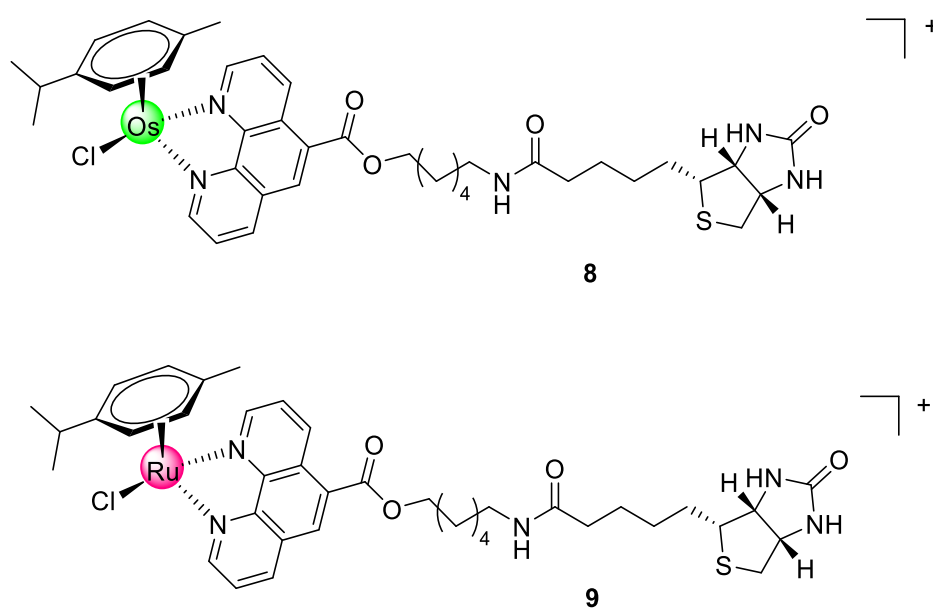
**Figure 3.4:** Compounds developed by Berger and Marloye *et al.* 2021.

3.7   Iridium (III) and Rhodium (III) with biotin as a targeting vector

Lo *et al.* synthesized a series of luminescent iridium (III) **11** or rhodium (III) **10** anti-cancer complexes bearing biotin-derived moieties connected *via* a long hydrocarbon chain. (Figure 3.5) Both the mono tagged iridium (III) and rhodium (III) complexes exhibited higher cytotoxicity's compared to cisplatin toward HeLa cells, while on the other hand, the hydrophobic di and tri-substituted biotin metal complex conjugates **12a-d** (Figure 3.6) were inactive against HeLa cells.[195] However, the exact mode of action of these complexes has yet to be elucidated and may involve protein–binding interactions imparted by the biotin unit.
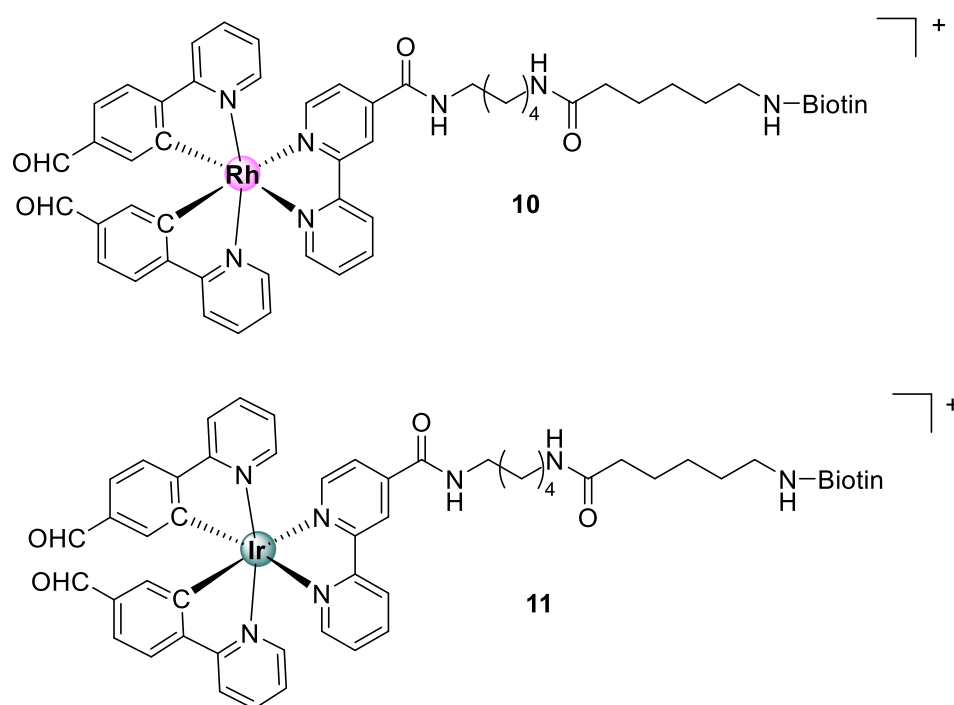
Figure 3.5: Mono tagged Iridium and rhodium complexes (**10 & 11**) synthesised and examined by Lo *et al.*[195]

The di and tri valent biotin substituted compounds **12a-d** are displayed in (Figure 3.6). No increased activity was observed on any of these compounds which brought Lo *et al.* to the conclusion that most likely a single biotin moiety brings about more potent uptake than a di or tri valent approach while targeting.[196]
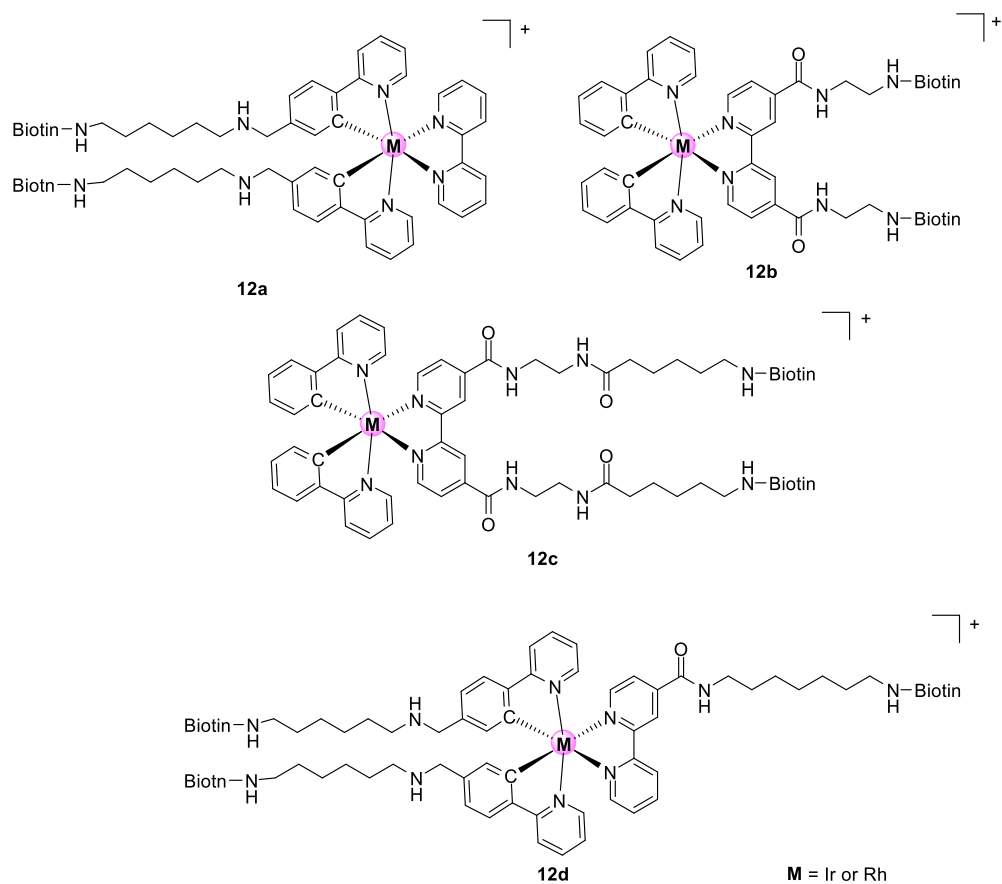
Figure 3.6: Di and tri valent analogues of Lo's *et al.* compounds bearing either an iridium or rhodium centre.[196]

Recently in 2019 Kallus *et al.*[197] developed two transition metal complexes of copper and iron (Figure 3.7), both of which were tagged with biotin.
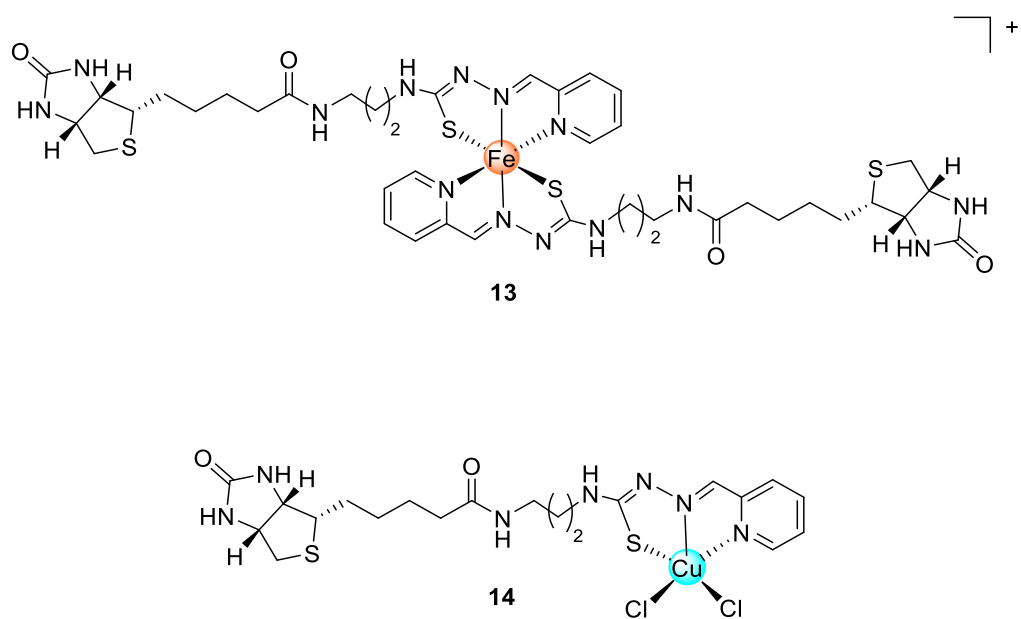
Figure 3.7: Iron (**13**) and Copper (**14**) biotin derived triapine complexes developed by Kallus *et al.*[197]

Each of the compounds were screened against multiple cancerous cell lines and the cellular uptake and also IC$_{50}$ was measured. In the case of the iron complex **13** (Figure 3.7) it was established that it was largely ineffective against every cell line it was tested on. The group did report problems with the complex precipitating out of solution also making measuring anything meaningful very difficult. However, with the copper (II) complex **14** (Figure 3.7) values of 19. 3 µM, 18.3 µM and 19.1 µM were observed for HCT116, MDA-MB-231 and SKBR-3 cell lines respectively. This did point towards the copper centre playing an active role in therapeutic role of the compounds. Nonetheless in each case the free ligand triapine performed up to 20 times better than the compound **14** displaying values as low as 0.8 µM , 1.5 µM and 8.8 µM for the three respective cell lines mentioned above. In the case of the experiments on the cell line MCF-7 the free ligand performed almost 37 times better than complex **14** and 100 time better than complex **13.** The free ligand displayed values of 1.0 µM whereas the copper complex **14** displayed a value of 37.5 µM and the iron complex **13** showing a value in excess of 100 µM. The group did note that upon complexing the biotin modified triapine to the iron core it resulted in almost 100 % deactivation of the molecule in comparison to both the free ligand and the non-biotin modified iron complex.

Organic ligands have also been modified with biotin in order to create bifunctional chelators for bio imaging agents. In 2010 Orvig *et al*.[135] developed two biotinylated conjugates and proceeded to complex them to various metals including their isotopes. The ligands (Figure 3.8) were complexed to Cu^{2+}, ^{64}Cu^{2+}, and Co^{2+} along with examples of [M(CO)$_3$]$^+$ where M = ^{99m}Tc or Re.
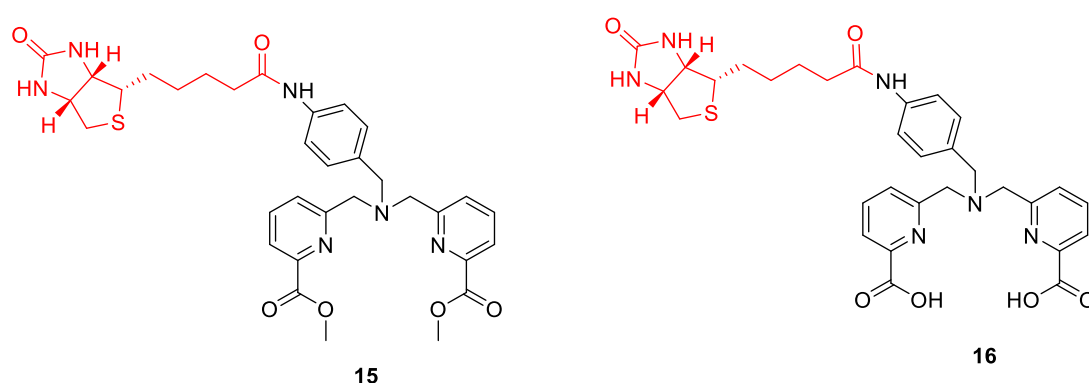
Figure 3.8: Biotin conjugates **15** & **16** synthesised by Orvig *et al.*

The group found that the radiolabelling was both fast and efficient with ^{64}Cu using ligand **16**. However it was found that the copper complexes where not as stable as those of ^{99m}Tc(CO)$_3$ and were not carried forward for further development for *in vivo* applications. The ^{64}Cu

complex of **16** displayed a labelling yield of 95 % but as mentioned its stability was very poor at 22 % leaving it only stable for 1 hour. In comparison the ^{99m}Tc complexes of **15** and **16** displayed labelling yields of 72 % and 85 % but had stabilities of 99 % in both cases and were stable for 24 hours. The group is currently investigating other options for multidentate ligands for the purpose of labelling radionuclides.

3.8   Chapter Objective

This chapter will outline the synthesis, characterisation, and biological evaluation of a family of biotin derived copper (II) compounds as selective anti-cancer agents. By using biotin as a selective vector, it is speculated that the uptake of the drug into cells which over express this receptor will give a targeted approach. Secondly, with the addition of the biotin to the planar scaffold leading to water soluble compounds, leaves a very attractive target product for biological testing and again aims to overcome a real-world barrier in a lot of metal-based compounds.

This chapter will describe the synthesis of two novel biotin-substituted ligands followed by a series of four final copper (II) complexes (Figure 3.9). Two with a 1,10 – phenanthroline moiety (**3.3** and **3.5**) and the second two with two chlorido ligands in a similar set up to that of cisplatin. The approach, similar to what was described with the estrogens in chapter 2, is to synthesise a multifunctional molecule containing simultaneously a targeting vector, an endogenous copper (II) centre and a DNA intercalator or chlorines. The final structure of the complexes is displayed below (Figure 3.9)
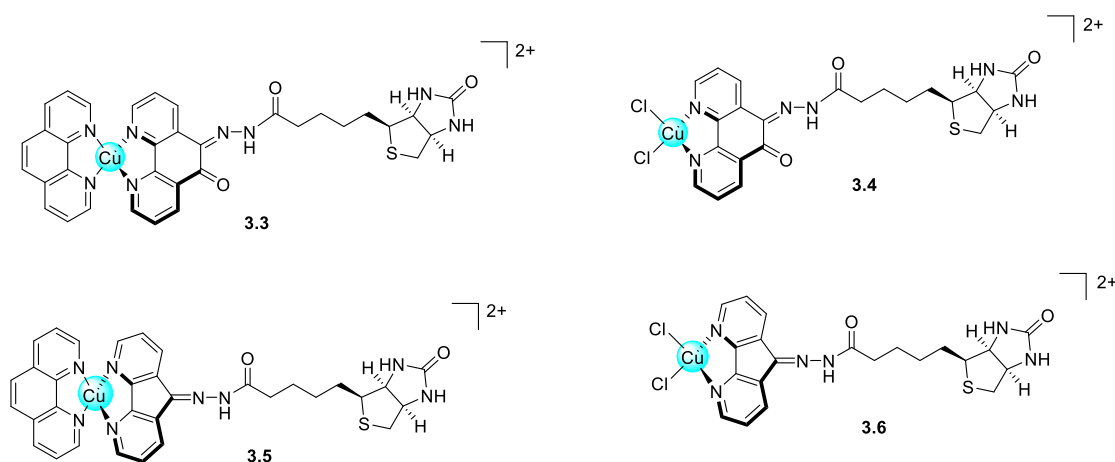
Figure 3.9: Final structures of the four compounds outlines in this chapter.

A building block approach was used to successfully complete the synthesis of the final Cu(II) complexes.

Initially it was decided that the biotin would be conjugated to a 5 – carboxylic acid dipyridophenazine (DPPZ) scaffold. The rational was that one of the carboxylic acids could be converted into an amine and then coupled to the other using peptide chemistry. This would give rise to a biotin modified DPPZ scaffold which still held the two nitrogen atoms in the desired 1 and 10 positions which would facilitate an optimum binding to the copper (II) core. Some of these reactions will be shown and discussed later in the chapter as examples.

After trying unsuccessfully many peptide coupling reactions, it was decided to couple the biotin moiety to the phendione or dafone scaffold, using hydrazone chemistry. For this reason, biotin is functionalised with a hydrazine groupm(-NH**2**) that will allow the conjugation to the ketone groups of phendione or dafone. The newly formed ligands were then attached to the copper (II) core and the phenanthroline was finally attached in the opposite side to yield the target compounds (Figure 3.9).

3.9   Synthesis & characterisation

3.10   Biotin methyl ester

The commercially available biotin (**3.0)** was firstly converted to its acyl chloride **3.14** using an excess of thionyl chloride and then reacted in MeOH to form its methyl ester analogue **3.15** (Scheme 3.0). This was optimised to become a one pot synthesis to give a quantitative yield of the biotin methyl ester. The methyl ester **3.15** would then be reacted in excess hydrazine to yield the biotin Hydrazide.
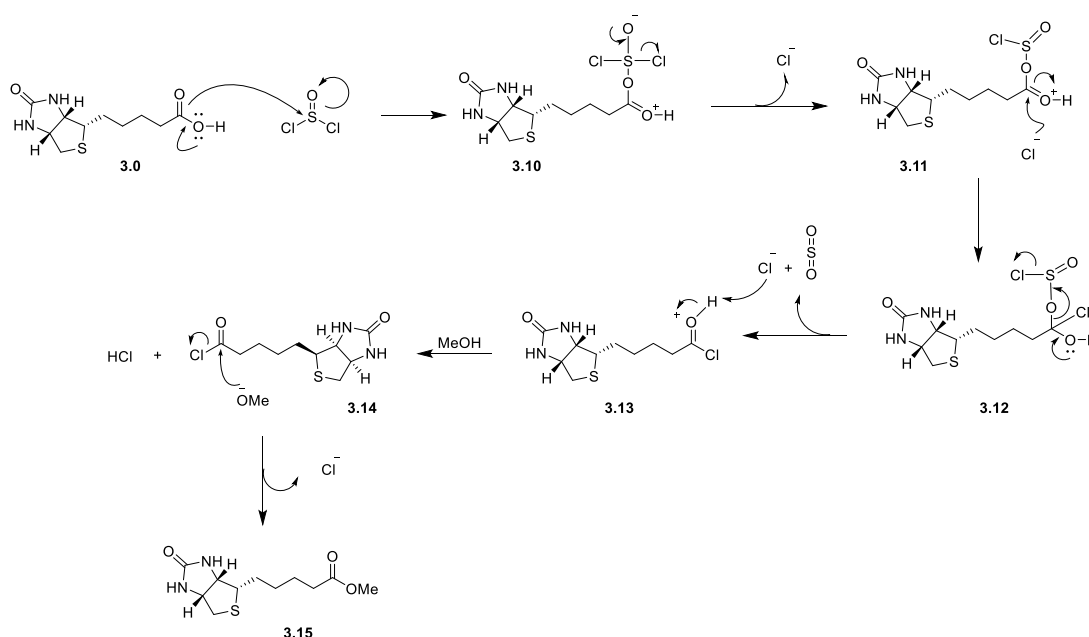

Scheme 3.0: Reaction mechanism showing the conversion of **3.0** (Biotin) to (**3.15**) Biotin methyl ester.

The reaction is initiated *via* nucleophilic attack from the biotin **3.0** on the sulphur of the thionyl chloride to give the short lived intermediate **3.10**. and the liberation of a chloride ion. Following the reformation of the π bond the corresponding chlorosulphite is formed **3.11.** Nucleophilic attack then proceeds *via* the liberated chloride ion ejecting a sulphite and a chloride from the molecule **3.12** to give **3.13**. Deprotonation of the hydroxy group *via* the liberated chloride ion or by the methoxy from the methanol yields the biotin acyl chloride **3.14**. The reaction terminates with nucleophilic attack from a methoxy leading to the discharge of the chloride ion and the formation of the target compound **3.15**. The biotin methyl ester **3.15** was recovered as a crude oil. The oil was washed with sodium hydrogen carbonate and brine and the organic layer dried over sodium sulphate to yield the pure

product **3.15** in a quantitative yield. The reaction was monitored on TLC (DCM: MeOH 90:10) using vanillin as a stain and via ^{1}H NMR which will be discussed below.
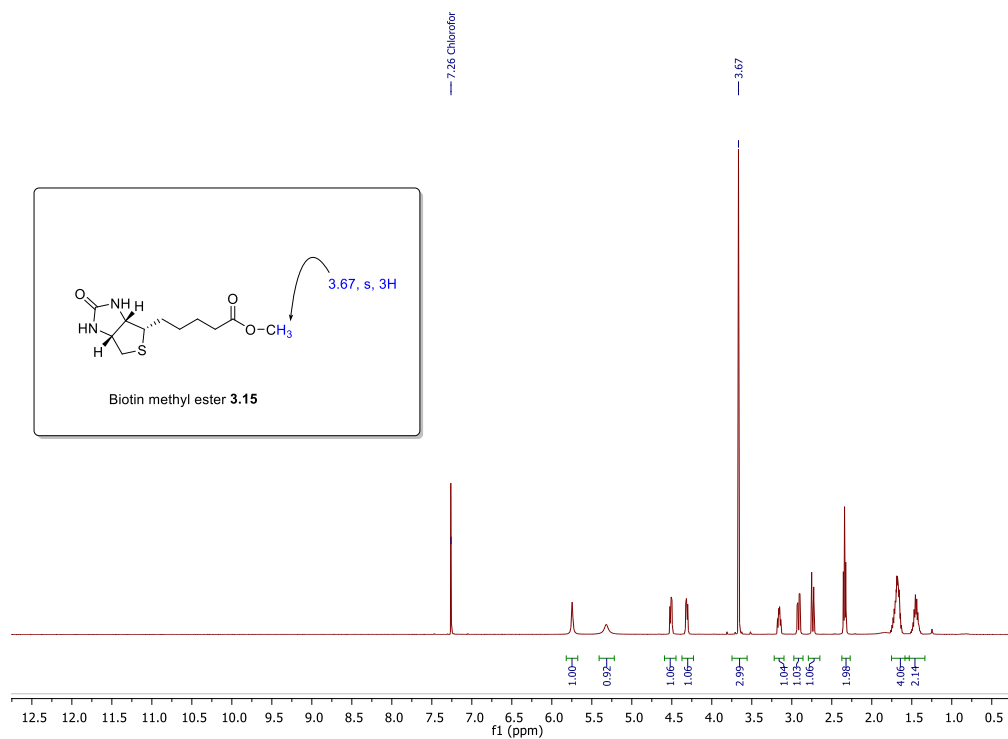
Figure: 3.10: ^{1}H NMR spectra of **3.15** (biotin methyl ester) in CDCl$_3$.

A very large distinctive peak which is characteristic of the 3 protons belonging to the methyl ester can been seen at 3.67 ppm (Figure 3.10). There is also a very visible elimination of the broad singlet O-**H** from the biotin carboxylic acid which can be seen below in (Figure 3.11) at 11.95 ppm. The spectrum of biotin is displayed below in DMSO for clarity (Figure 3.11). Furthermore, biotin itself is water soluble and not soluble in organic solvents while the methyl ester of biotin is highly soluble in chlorinated solvents (Figure 3.10).
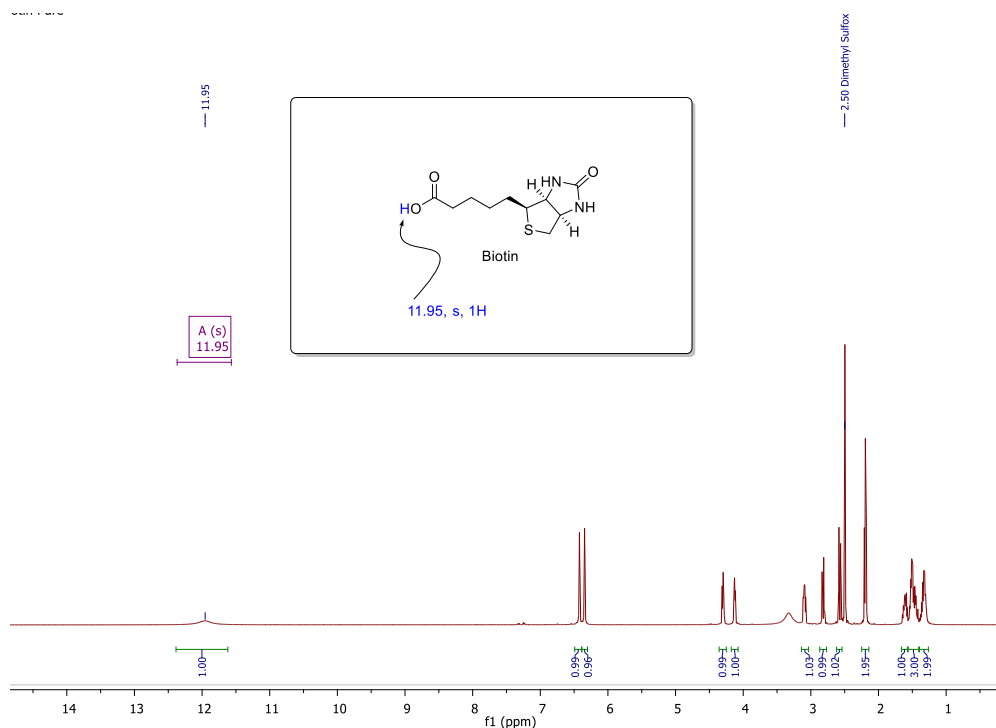
Figure 3.11: ^{1}H NMR spectra of (**3.0**) biotin in DMSO displaying the carboxylic acid proton at 11.95 ppm.

3.11   Biotin hydrazide

The freshly prepared **3.15** was then reacted in excess hydrazine hydrate under nitrogen to yield its corresponding hydrazide **3.18** shown below (Scheme 3.1)
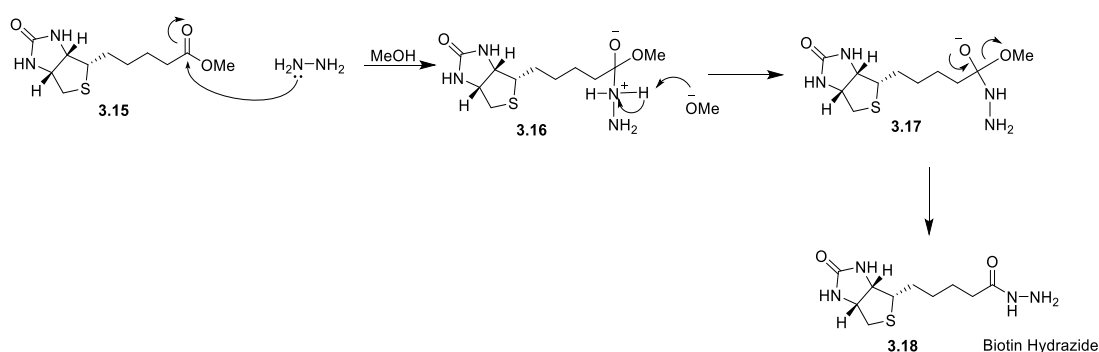

Scheme 3.1: Reaction mechanism showing the formation of biotin hydrazide **3.18** from biotin methyl ester.

Once more, the reaction kicks off with nucleophilic attack on the carbonyl carbon of **3.15** from the hydrazine molecule leading to the intermediate **3.16**. The positive charge on the nitrogen is then relieved *via* either a methoxy or another hydrazine molecule to yield

115

compound **3.17** stabilising the molecule and making the methoxy the most likely leaving group. A quick reformation of the π bond on the carbonyl carbon then leads to the ejection of the methoxy group from the system to yield the target compound **3.18** biotin – hydrazide.

The reaction is done in dry methanol and the system purged with nitrogen continuously to reduce the risk of reforming the carboxylic acid **3.0**. However, the methyl ester **3.15** is incredibly stable. The product **3.18** precipitated out of solution leaving any dimer formed in the methanol. It was then taken up in water and washed with chloroform to remove any unreacted methyl ester. The solubility of the reactant **3.15** and that of **3.18** differed and the newly formed hydrazide was now water soluble. This reaction was followed by ^{1}H NMR. The details will be displayed and discussed below.
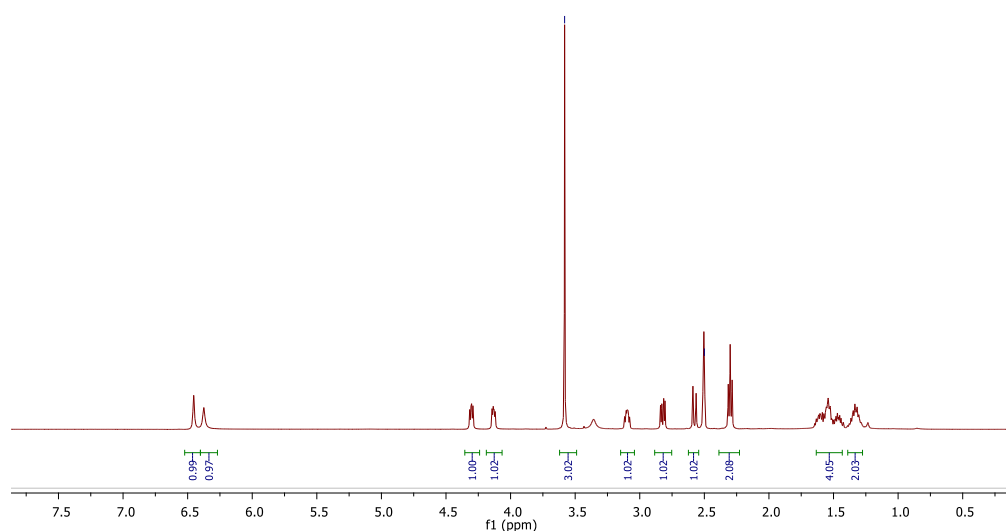

Figure 3.13: ^{1}H NMR of **3.15** (Biotin methyl ester) in DMSO-*d*6.

The characteristic methoxy group at 3.58 ppm (Figure 3.13) disappears upon the conversion to the hydrazide (Figure 3.14) with the formation of two new broad NH signals at 4.22 ppm at 8.93 ppm (Figure 3.14)

116
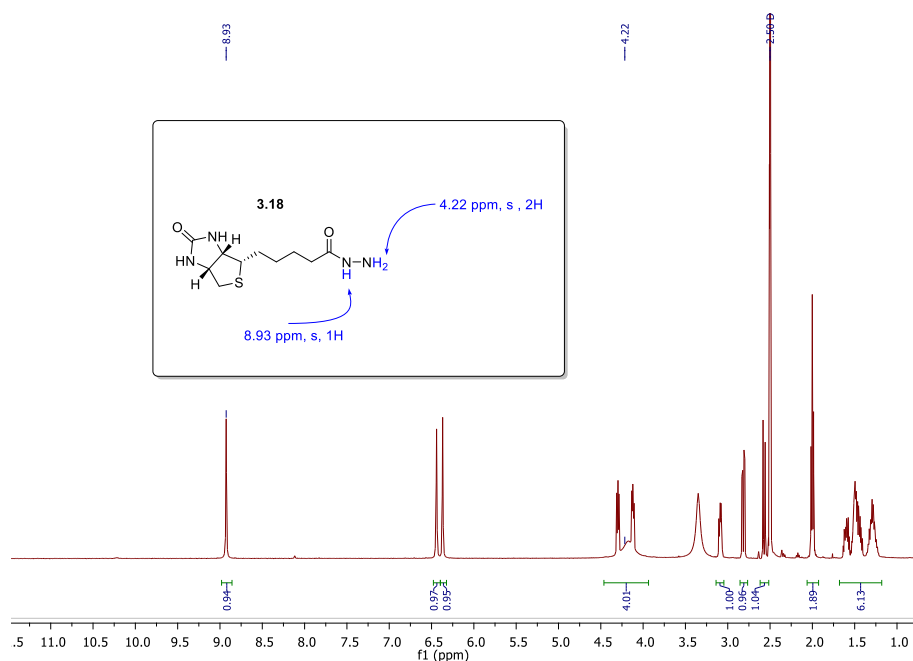
Figure 3.14: ^{1}H NMR spectrum of **3.18** biotin hydrazide in DMSO-*d*6

The assignment of these peaks is confirmed by 2D NMR experiments and by a D_2O shake as the protons are exchangeable. The D_2O shake for **3.18** is displayed below in figure 3.15.
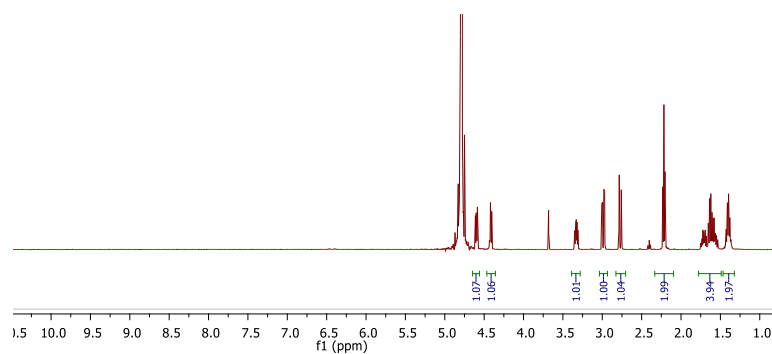
Figure 3.15: ^{1}H NMR D_2O shake of **3.18**.

As seen above in figure 3.15 the proton count is reduced to 13H from that of 18H in figure 3.14 confirming the presence of the three new N-**H** & N-**H$_2$** exchangeable protons along with the already existing two exchangeable N-**H** in the biotin ring itself. Further conformation (Figure 3.16) would come from the presence of the IR band at 3319 for the primary amine and the bend at 1688 (N-H).[198]
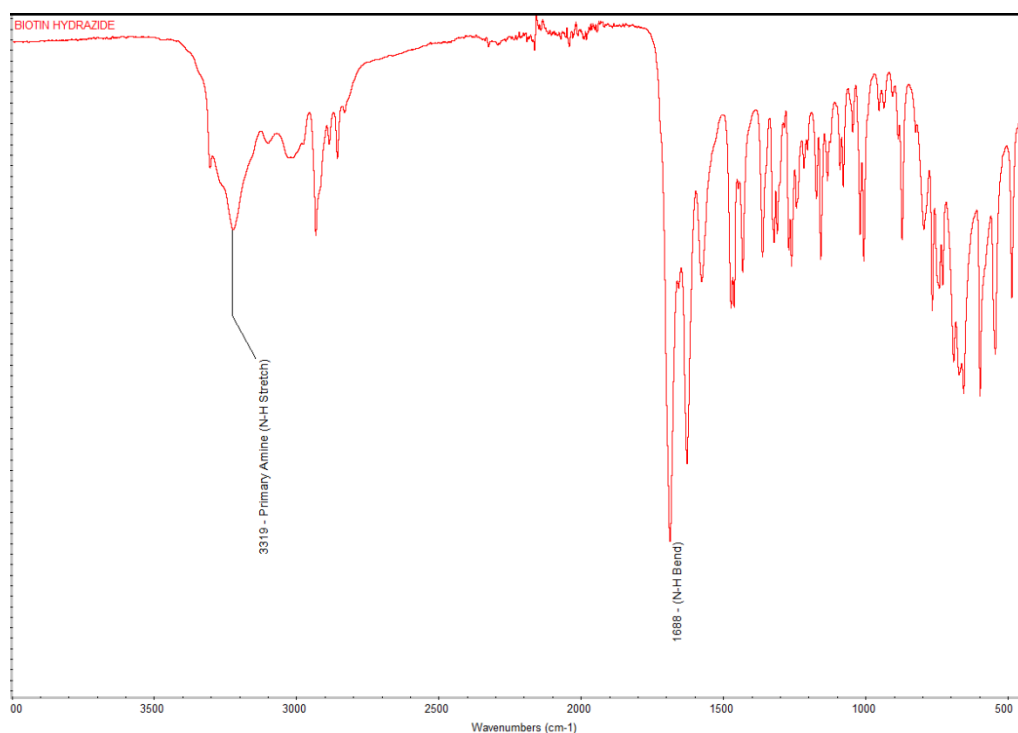
Figure 3.16: IR spectra displaying the band for the primary amine at 3319 cm^{-1} and the N-H bend at 1688 cm^{-1} for compound **3.18**.

3.12   Coupling biotin hydrazide to a 1,10 – phenanthroline scaffold

After isolating the pure biotin hydrazine **3.18,** it was decided that conjugating it to an aromatic scaffold such as phenanthroline with the nitrogen's placed in the 1 and 10 positions again would be the most desirable approach in order to achieve successful binding to the copper (II) centre.

As mentioned previously, initially this started with peptide coupling *via* an aromatic scaffold like 1,10- phenanthroline of DPPZ with a carboxylic acid substituted in the 11 or 12 position, but it proved to be very difficult (Figure 3.17). The synthesis was laden with issues like solubility and further problems with yield along with trying to isolate a pure product in any sort of meaningful amount could not be achieved. Most likely the carbonyl carbon was not electrophilic enough due to the aromatic scaffold pulling electron density away from it.
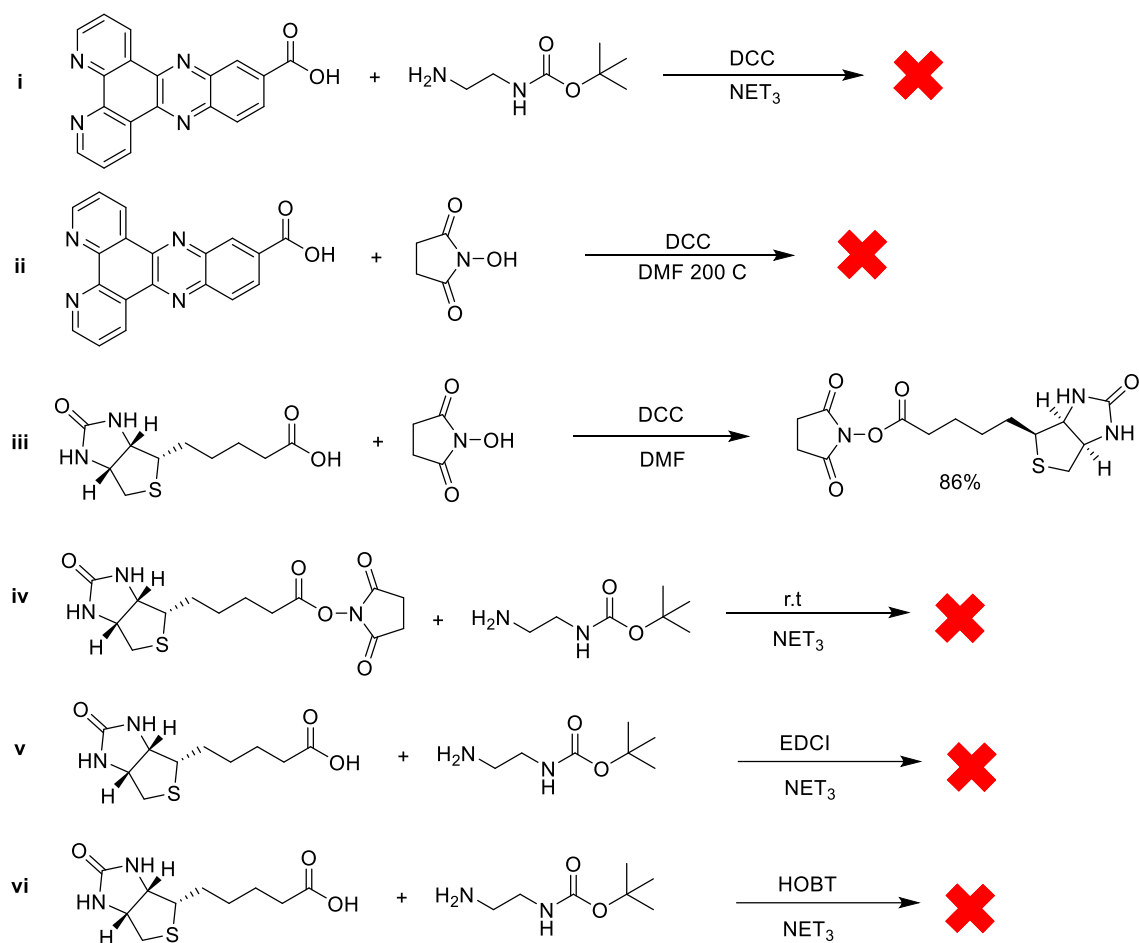
Figure 3.17: Failed coupling reactions using NHS and mono boc protected ethylene diamine.

i. Returned starting materials

ii. Returned starting materials

**iii.** Isolated the NHS – DPPZ at 86 %

iv. Pure product could not be isolated

v. Very little product formation (< 10%)

vi. Returned starting materials

A suggestion after carrying out all these reactions would be to proceed with uranium-based coupling agents such as HATU or TBTU.

It was finally decided that the biotin hydrazide (**3.18**) could be attached to 1,10-phenthroline -5,6-dione (**2.10**) via a hydrazone bond.
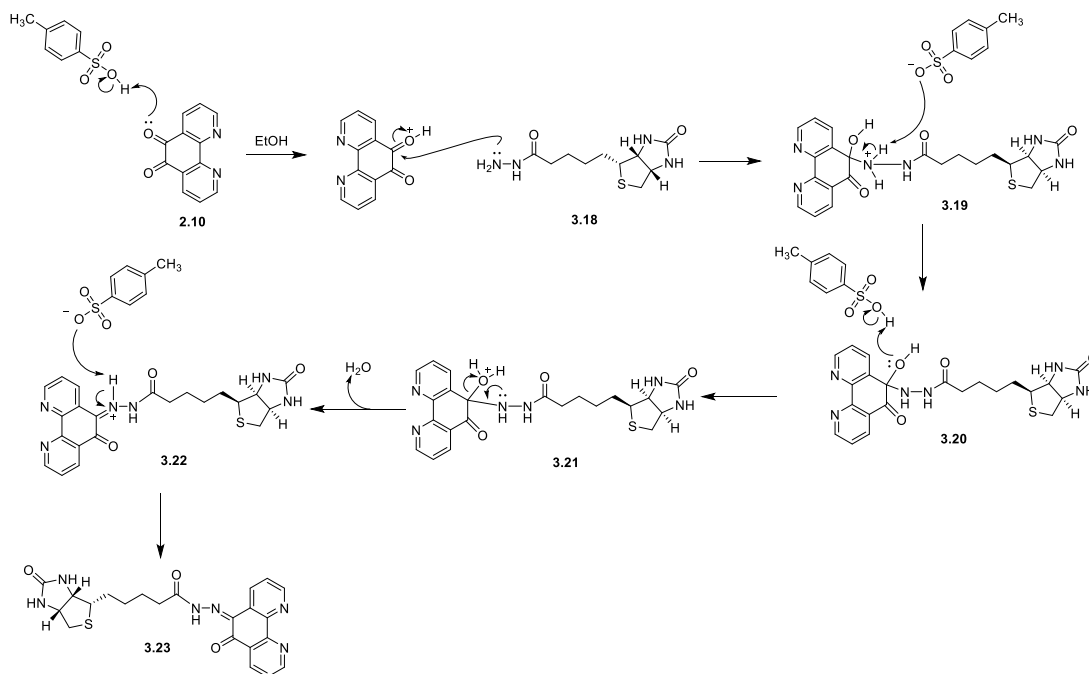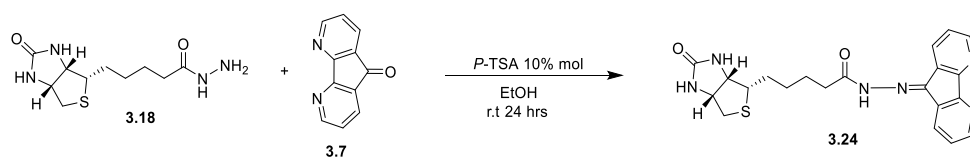

Scheme 3.2: Reaction mechanism showing the formation of the final hydrazone product via the Iminium ion.

As this reaction was carried out in the presence *p*- TSA, the first step is protonation of the ketone **2.10**. After protonation occurs, the carbonyl carbon is more susceptible to nucleophilic attack from the primary amine **3.18**. that gives rise to the carbinolamine ion **3.19**. This intermediate is deprotonated via *p*-TSA to give **3.20**. Donation of the lone pair on the nitrogen atom in **3.21** leads to the ejection of the water molecule from the system to yield the iminium ion **3.22**. This swiftly deprotonated to yield the target product **2.33**.

The reaction was carried out on a 1:1 ratio with **2.10** and **3.18** in ethanol with a catalytic amount of *p* – TSA. The reaction was monitored on TLC (DCM: MeOH, 90: 10) and upon completion the solvent weas reduced by 50% and the crude product was precipitated into the mother liquor overnight at 4 °C. It was taken back up in chloroform and the organic layer washed with brine and then dried over sodium sulphate. The crude product was then purified by silica chromatography (DCM: MeOH, 98: 2) to yield the pure final compound **3.23** at 85 %.

A very similar procedure was then carried out to yield a second novel ligand **3.24** the scheme for this synthesis is displayed below (Figure 3.17).

Figure 3.18: Reaction scheme for the formation of compound **3.24**.

The compound **3.24** is formed *via* the same mechanism shown above in figure 3.18. The compound **3.7** was synthesised in accordance with literature, [199] containing only a single ketone this time on a five-member ring but the nitrogens in the 1 and 10 positions remained. **3.24** did not require a precipitation in the fridge as the pure compound fell out of solution upon formation. It was washed with chloroform firstly and then with water to dispel any residual biotin hydrazide. The rationale here was the nitrogens would still be relatively in the same positions to achieve a stable bond to the copper (II) without much bond strain and being only one ketone now available the likely hood of a second biotin hydrazide reacting was now eliminated. However, in the case of **3.23** attachment of a second biotin was not observed. This is most likely due to steric hindrance on the scaffold after the attachment of one biotin hydrazide. It was also observed that the N-*H* hydrazone proton on **3.23** was thrown downfield to 13.98 ppm which would indicate some strong hydrogen bonding to the ketone on the scaffold which is in close proximity. The ^{1}H NMR for **3.23** is displayed below.
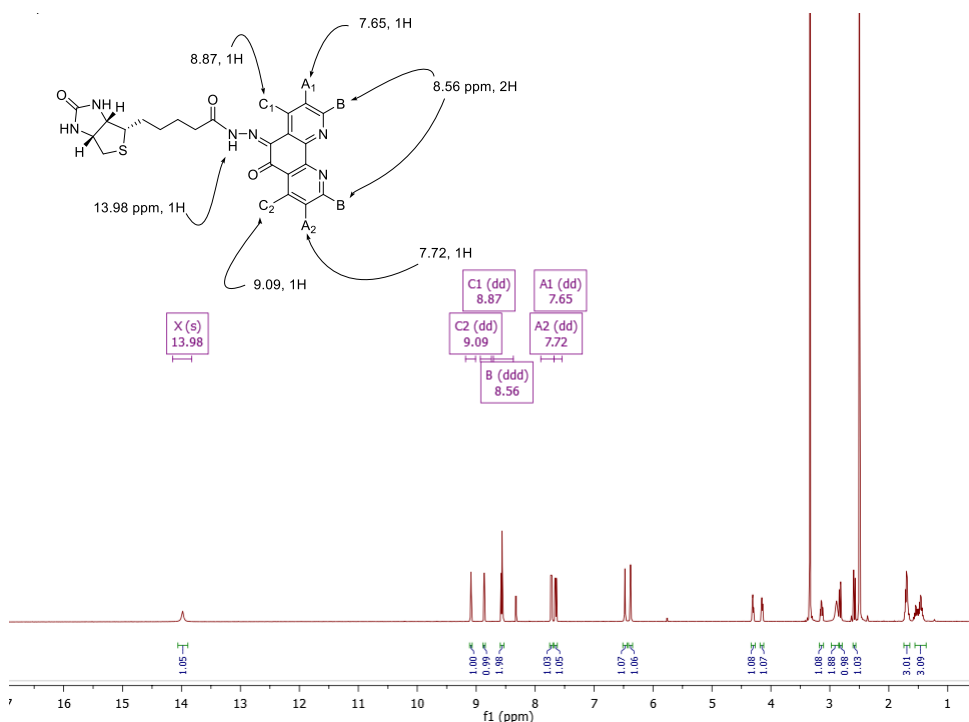

Figure 3.19: ^{1}H NMR spectra of **3.23** in DMSO-*d*6.

As can be seen in figure 3.19, the characteristic symmetry of the six protons on the phendione molecule is now broken displaying 5 separate signals in the aromatic region. This is representative of the molecule being substituted in a single position either at the 5 or 6 position. The singlet appearing at 13.98 ppm is that of the hydrazone N-*H*. As stated above it is most likely experiencing some H-bonding interaction with the ketone oxygen giving rise to this signal appearing so far downfield. The two new ligands **3.23** and **3.24** were then conjugated to a copper (II) phenanthroline scaffold, previously prepared by the group in chapter two (**2.21**)

3.13   Synthesis of biotinylated copper (II) compounds

A family of four final complexes were synthesised bearing the two biotin-modified aromatic scaffolds (Figure 3.20). The newly synthesised ligands **3.23** and **3.24** were reacted in a 1:1 ration with the mono copper phenanthroline complex nitrate from chapter two, **2.21,** in DMF overnight at 40 °C and then precipitated into excess Et$_2$O to yield a green solid (compounds **3.3** and **3.5)**. As the final copper (II) compounds were water soluble they were then purified on preparative HPLC using (45:55 ACN: H$_2$O) to yield 67 and 49 % respectively for **3.3** and **3.5**.
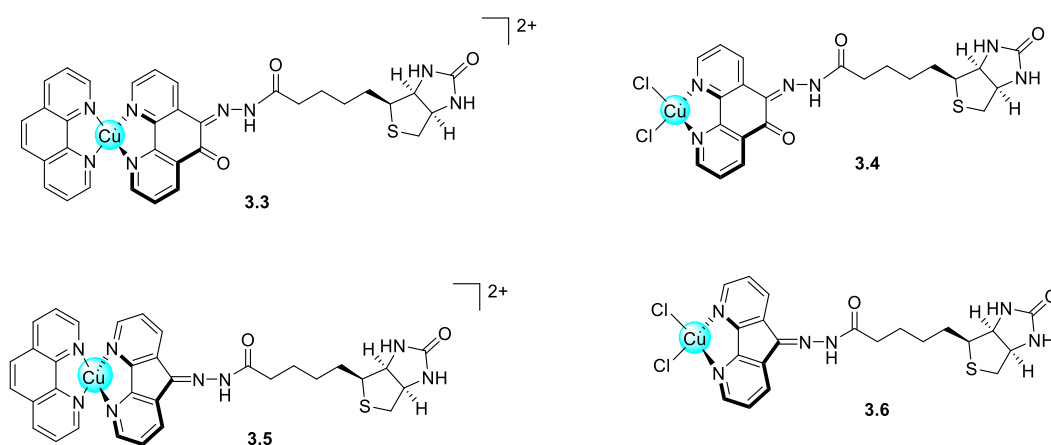
Figure 3.20: Structures of four biotin tagged copper (II) complexes.

In the case of the two complexes bearing the chlorido atoms (**3.4** and **3.6**) the ligands **3.23** and **3.24** were reacted with a slight excess of copper chloride and the resulting pure compounds **3.4** and **3.6** precipitated out of solution. They were washed very gently with a minimum amount of cold water to dispel any unreacted copper (II) salt. The purity of all four compounds was examined by elemental analysis (Table 3.3) and also on analytical HPLC (ACN: H$_2$O, 80: 20) (see appendix).

Table 3.3: Elemental analysis of final compounds.

Elemental analysis

Number	Formula	Calculated for %	Found %
3.3	$C_{34}H_{30}CuN_8O_9S$	C 49.91 H 3.70 N 17.12	C 49.42 H 3.56 N 16.92
3.4	$C_{22}H_{22}Cl_2CuN_6O_3S$	C 45.17 H 3.79 N 14.37	C 46.38 H 3.91 N 14.24
3.5	$C_{33}H_{30}CuN_{10}O_8S$	C 50.16 H 3.83 N 17.72	C 49.90 H 3.79 N 17.78
3.6	$C_{21}H_{22}Cl_2CuN_6O_2S$	C 43. 87 H 4.21 N 14.62	C 43.68 H 3.98 N 14.30

3.24 - Dafone-biotin free ligand

3.6 - [Cu(dafone-biotin)].Cl2
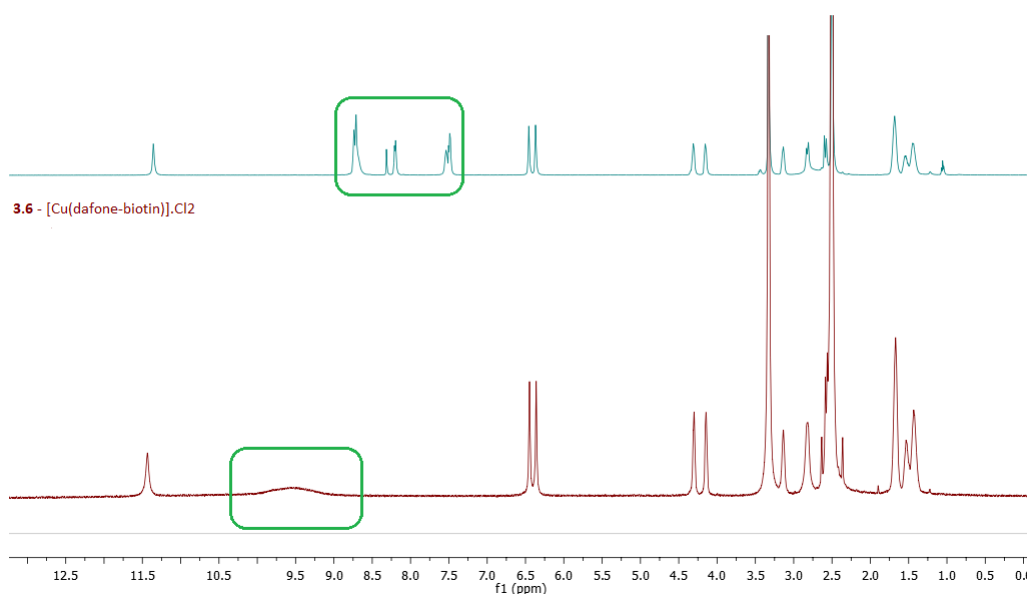
**Figure 3.21:** ^{1}H NMR of compound **3.6** in DMSO-*d6* displaying the extreme broadening of the aromatic region.

Due to the paramagnetism of copper (II), a complete characterisation *via* NMR was not possible, however figure 3.21 above displays a ^{1}H NMR comparison of the copper (II) compound **3.6** and the free ligand **3.24**. Clear peak broadening of the aromatic protons can be observed in the case of the copper (II) complex **3.6** this is most likely caused by shortening of the relaxation times from the paramagnetism of the copper (II) nucleus leading to broadening of the protons in close proximity to the copper (II) centre and loss of resolution. This method was used as quick verification to see if conjugation of the ligand to the copper (II) centre had occurred.

The nature of the complexes was confirmed by high resolution mass spectrometry and an example of the isotopic distribution of copper is shown below in figure 3.22. for the complex **3.3**. The remaining spectra can be viewed in the appendix.
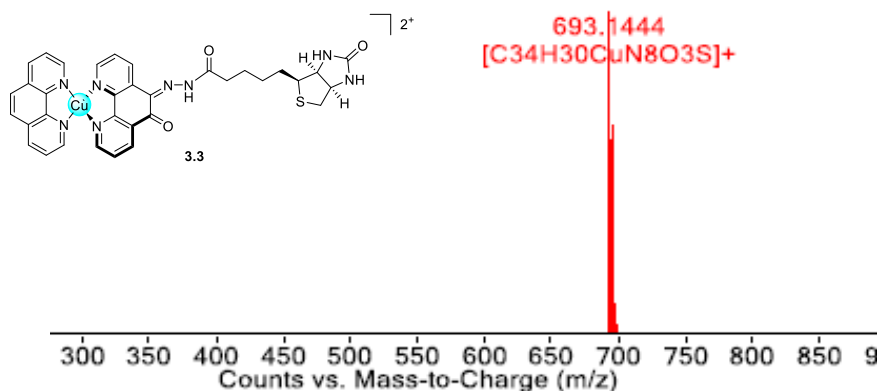
Figure 3.22: HRMS (ESI+): compound **3.3** m/z Calculated for $C_{34}H_{30}CuN_6O_3S$ [M-2(NO₃)⁻] 693.1442, Found 693.1444.

In the mass spectra (+) of **3.3** and **3.5,** the species observed corresponds to the mono-cationic metal scaffold with the two ligands (loss of both nitrates), as if Cu(II) is reduced to Cu(I). For example, the peak observed in complex **3.3** (Figure 3.) corresponds to the species [Cu(phen)(phendione-biotin)]⁺. This behaviour of Cu(II) complexes in the mass spectrometer conditions has already been observed by Gianelli *et al*. group.[200] Gianelli found that during the transfer of ions from solution to the gas phase, can then induce ion structure transformation. For example, multiply charged ions, in which the charges are localized on one atom or a small group of atoms, specifically multiply charged metal ions, M^{z+} because of their high columbic repulsion, are difficult to observe in the gas phase, and can frequently undergo gas-phase charge reduction.[200] The mass of **3.4** and **3.6** was also observed as described above with the loss of the chlorine ligands.

3.14   pH dependency assay

The four compounds were then further examined for stability over a range of pH (pH 4 – 10) and evaluated by UV-Vis.
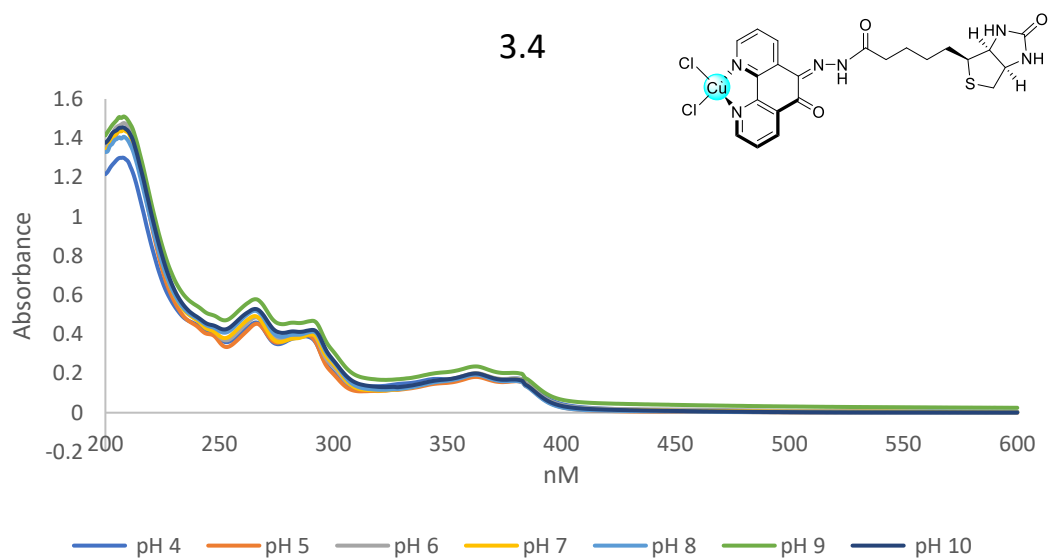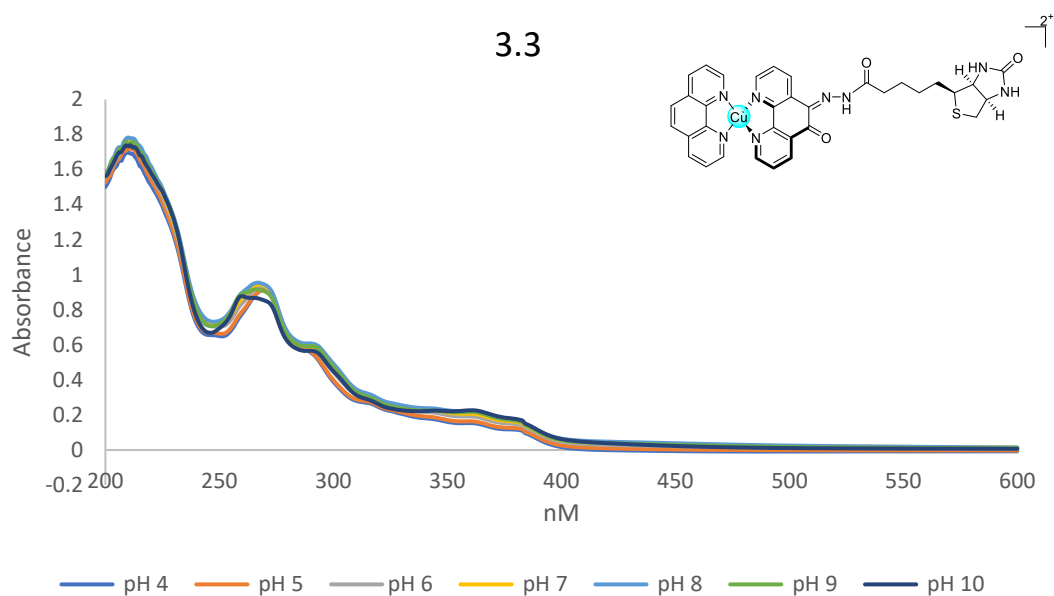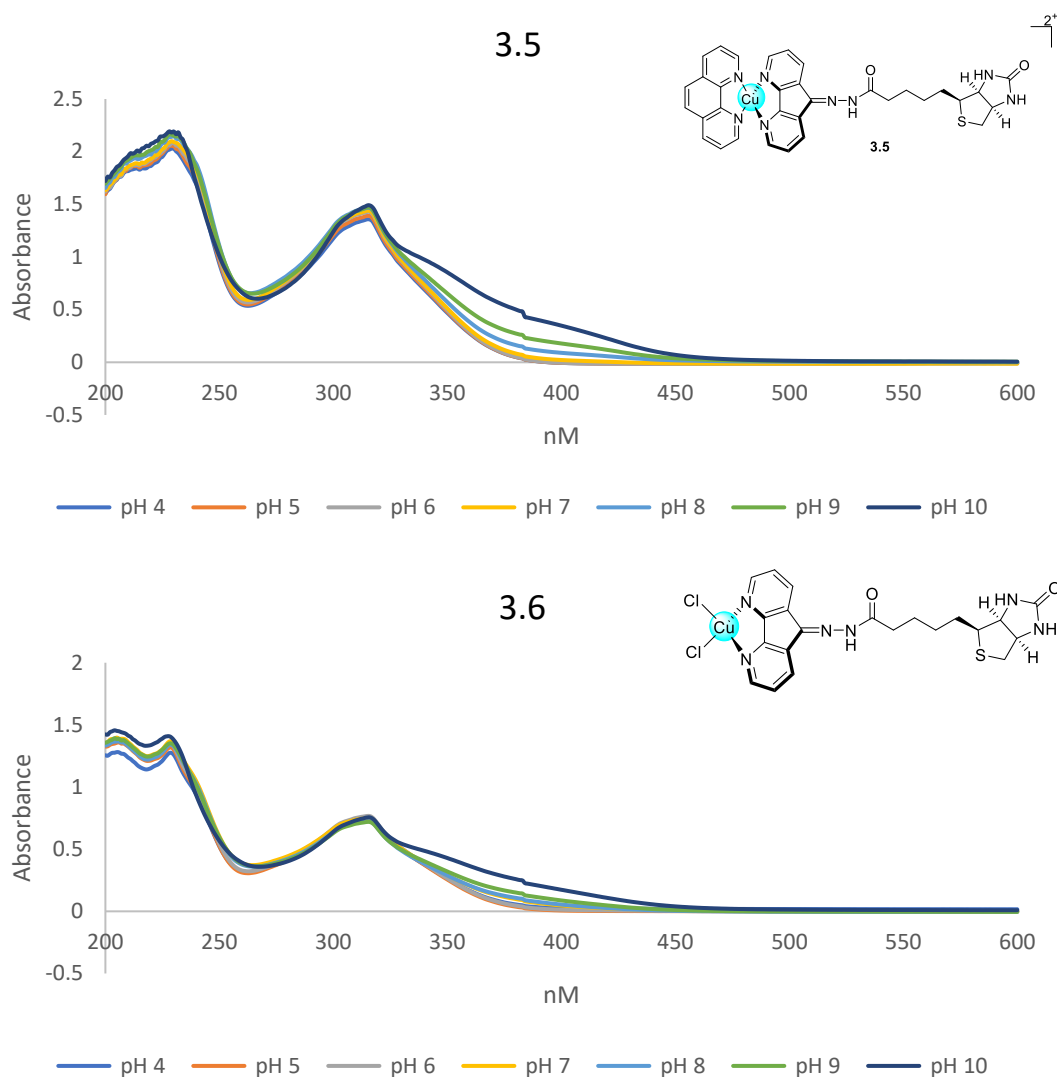
Figure 3.23: Uv-Vis spectra of all four compounds run over a pH range of 4 – 10.

Figure 3.23 shows the UV- Vis spectra of all four compounds over a range of pH 4 – 10 at a concentration of 10 µM in H_2O. Each compound was stable over the range of pH values and no release of the ligand is observed over the range of pH examined, however it was noted that at pH 10 for compound **3.6** something was starting to occur. Most likely deprotonation is occurring but also its largely possible the chloride ligands are exchanging for the hydroxy in this case where the pH is at 10. Further studies would need to be carried out to evaluate what exactly is happening in solution.

3.15   Ethidium bromide displacement assays

In order to establish if the compounds were capable of interacting with the DNA, ethidium bromide displacement assays were carried out in a 1:1.6 ratio (DNA: EtBr) in order to completely saturate the DNA helix with EtBr. EtBr, a heterocyclic aromatic compound, is a known intercalating agent which is very often used as a fluorescent tag (Figure 3.24). When the molecule is intercalated into the double helix of the DNA and is exposed to ultraviolet light, it will fluoresce with an intense orange colour. The absorption maxima of EtBr are 210 and 285 nm which correspond to the UV range, as a result it emits orange light in the region of 605 nm.
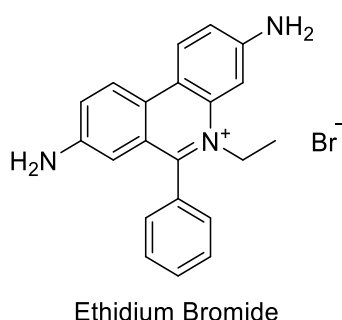
Ethidium Bromide

Figure 3.24: Molecular structure of Ethidium Bromide salt.

Because of its intense fluorescence, after binding to DNA, it is very often used to detect nucleic acids or double stranded DNA. This can be exploited to determine if a drug or molecule is a strong or weak intercalator by measuring the fluorescence as the drug is added to the cuvette. Ideally a decrease in fluorescence would be seen if the drug or compound added was displacing the EtBr in the helix and thus leading to a quenching of the fluorescence. Stock solutions of the metal complexes were then made up to 1.3 mM and added in very small aliquots in order to not change the volume and concentration in the cuvette. The aliquots started at 4 µL and increased to 20 µL over the course of the experiment. To allow a final ratio of ~ 3 equivalents of drug to that of a single EtBr. The results of these assays are displayed and discussed below.
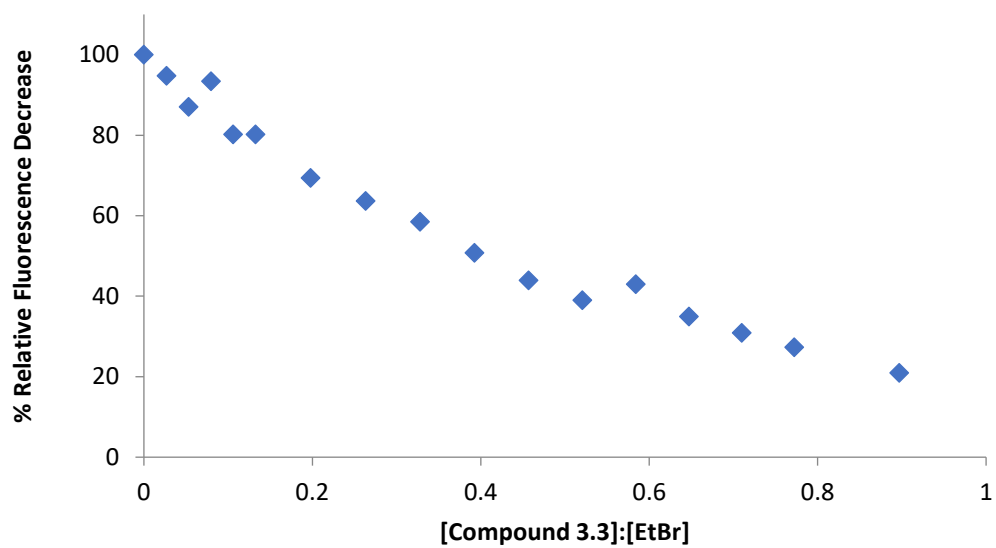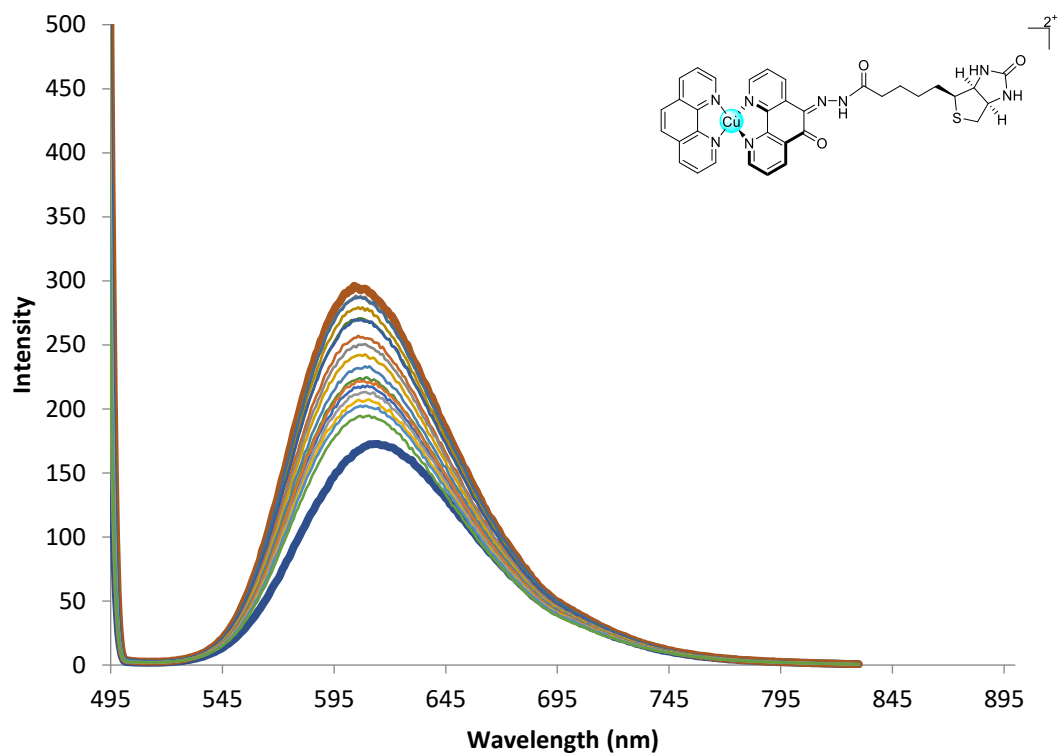
Figure 3.25: Graphs displaying fluorescence quenching (top) and relative displacement of EtBr by compound **3.3** (bottom).
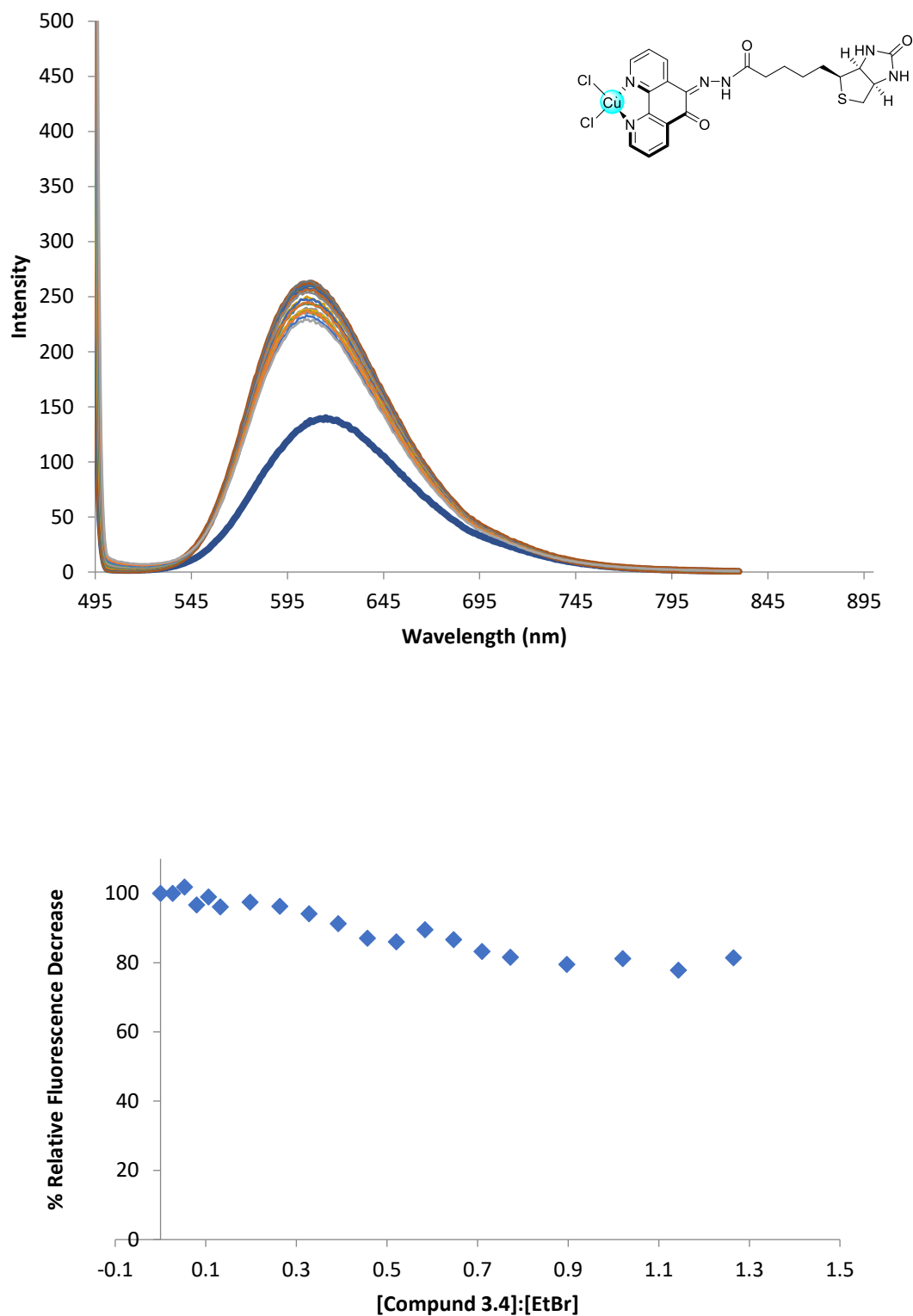
Figure 3.26: Graphs displaying fluorescence quenching (top) and relative displacement of EtBr by compound **3.4** (bottom).
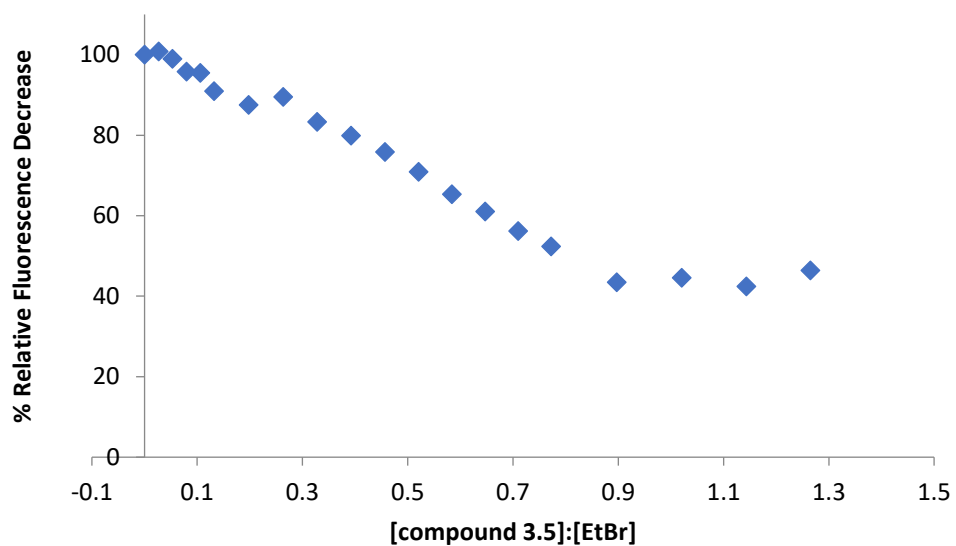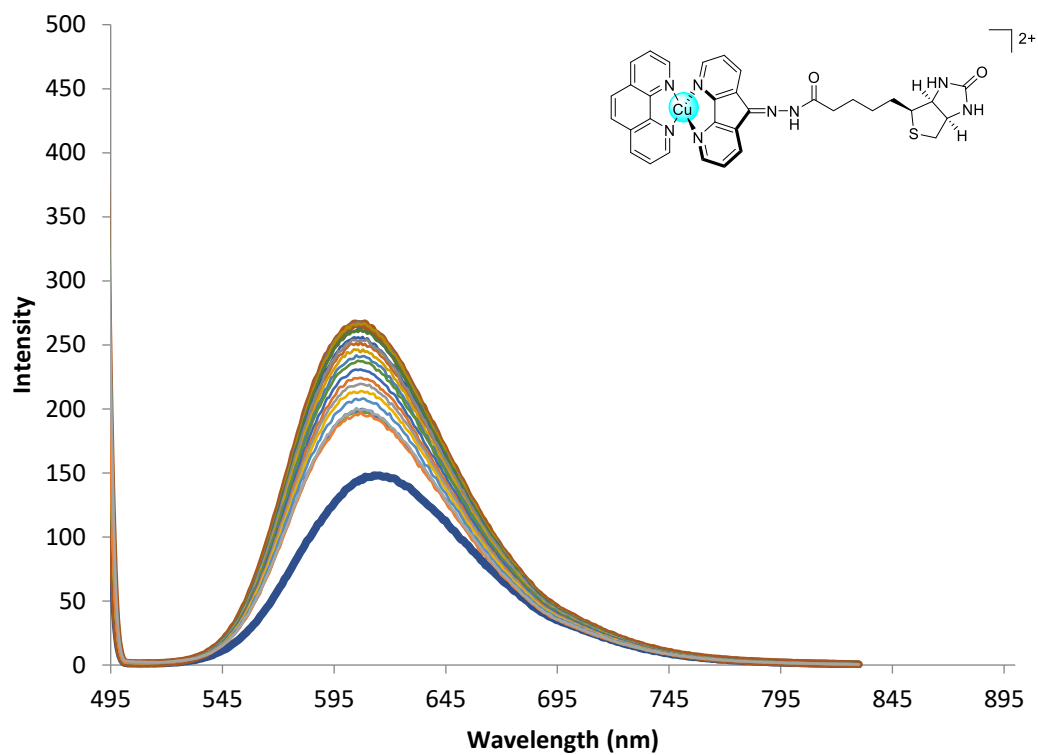
Figure 3.27: Graphs displaying fluorescence quenching (top) and relative displacement of EtBr by compound **3.5** (bottom).
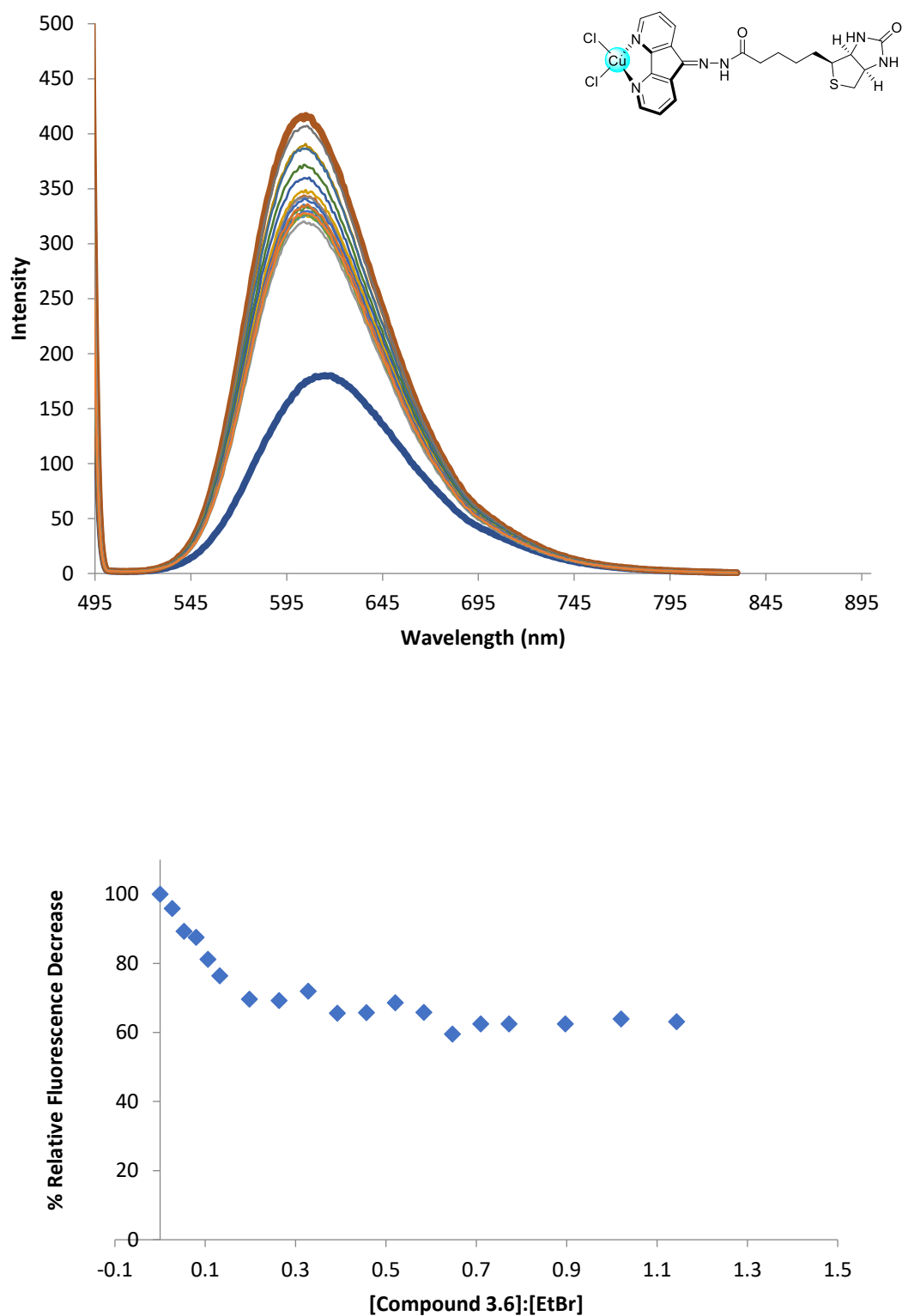
Figure 3.28: Graphs displaying fluorescence quenching (top) and relative displacement of EtBr by compound **3.6** (bottom).

Compounds **3.3** and **3.5** displayed the highest quenching values and as the relative fluorescence decrease was greater than 50% and the binding constants were able to be

established. These were calculated to be 2.53×10^7 M(bp^{-1}) for **3.3** and 1.28×10^7 M(bp^{-1}) for compound **3.5**. These values were very much in line with what was previously seen in the group [201] and also very close to reported literature values of 2.60×10^7 M(bp) and 3.04×10^7 M(bp) for the bis complexes of CuPhen and CuDPQ reported by Molphy *et al.* in 2019.[202] The binding values were calculated using the % relative decrease of fluorescence at 50% and the equation below.

$$E_{EB=} \frac{[EtBr]}{[compound]50\%_{FI}}$$

Compounds **3.4** and **3.6** showed some quenching but were unable to displace 50 % of the EtBr after adding up to 3.2 equivalents of the drug in respect to EtBr. This can be seen in Figures 3.25 and 3.27. It is possible that in this case the presence of the 1,10-phenanthroline scaffold on compounds **3.3** and **3.5** is contributing to the increased displacement of the EtBr (maybe by intercalation) and leading to a more noticeable decrease in the fluorescence. These data show that the complexes interact somehow with the DNA but to confirm intercalation, other studies (i.e. viscosity) should be carried out.

3.16   Biological evaluation

In collaboration with Prof. Valentina Gandin of the Department of Pharmaceutical Science at the University of Padua (Italy), the complexes were tested against a panel of four different cancer cell lines with different degrees of biotin receptors expression.

The cell lines examined are PSN-1 (pancreatic) and HCT15 (colorectal) with ++ of biotin expression) and A431 (epidermoid) and 2008 (ovarian) with no expression of biotin receptors. The IC_{50} values after 72 h incubation period are reported (**Table 3.4**)

Complexes (**3.3, 3.4, 3.5** and **3.6**) were dissolved in water while the ligands (**3.23** and **3.24**) in DMSO.

Table 3.4: IC_{50} values (μM) of complexes **3.3-3.6** and of the ligands **3.23** and **3.24**. In vitro antitumor activity of tested in 2D cell cultures. Cells (3–8×10³ mL⁻¹) were treated for 72 h with increasing concentrations of the tested compounds. The cytotoxicity was assessed by the MTT test. IC_{50} values were calculated by a four-parameter logistic model 4-PL (P<0.05).

	PSN-1 (pancreatic) ++	A431 (epidermoid)	2008 (ovarian)	HCT-15 (colorectal) ++
3.3	0.9 ± 0,5	0.3 ± 0,1	0.6 ± 0,2	0.4 ± 0,1
3.4	0.4 ± 0,1	1.2 ± 0,5	1.1 ± 0,3	0.4 ± 0,1
3.5	0.7 ± 0,2	0.9 ± 0,2	3.3 ± 0,1	1.8 ± 0,2
3.6	0.7 ± 0,1	7.2 ± 0,6	4.5 ± 0,7	0.4 ± 0,1
3.23	1.7 ± 0,2	3.7 ± 0,8	10.5 ± 1,9	3.6 ± 0,1
3.24	1.4 ± 0,3	>50	>50	>50
cisplatin	12.1 ± 2,9	1.3 ± 0,2	2.2± 1,4	16.5 ± 2.2

All the four tested compounds are much more active that cisplatin in all the four cancer cell lines with average IC_{50} values of 0.55, 0.78, 1.68, 3.2 and 8.02 μM for complex **3.3, 3.4, 3.5, 3.6** and cisplatin, respectively. The two complexes with the biotin conjugated with a phendione scaffold (**3.3** and **3.4,** IC_{50} average of 0.55 and 0.77 μM, respectively) are more potent with respect those two with the dafone scaffold (**3.5** and **3.6** average of 1.67 and 3.2 μM, respectively). If we compared the complexes with the same biotin-scaffold, it is evident that the presence of the phenanthroline as ancillary ligand (**3.3** and **3.5**) is of benefit with

respect the two chlorides (**3.4** and **3.6**). In fact, the average IC_{50} for **3.3** is 0.55 while for **3.4** is 0.77 μM and for **3.5** is 1.67 while for **3.6** is 3.2 μM). This change in potency could be linked with the DNA intercalation properties; **3.3** and **3.5** showed stronger DNA intercalation with the EtBr displacement essays with respect **3.4** and **3.6** (Section 3.15). The results are still at a preliminary phase, but it seems that the strategy of using biotin as a receptor is promising because the four compounds have an average IC_{50} values of 0.67 and of 0.75 μM toward the two cell lines that overexpress the biotin receptor (PSN-1 and HCT-15) and of 2.4 and 2.38 μM against the other two. Quite interesting to observe that cisplatin is more active in the two lines that do not overexpress the biotin receptors. Of the two ligands, only **3.23** (derivative of phendione) show some activity against the examined cancer cell line with average IC_{50} value of 4.88 μM while **3.24** (the dafone derivative) is almost inactive. Due to note that the two ligands were dissolved in DMSO while the complexes in water. The water solubility (and stability) is a huge advantage for metal-based complexes as the use of organic solvents in the biological system are almost always toxic at larger concentrations. With the aim of identifying a possible correlation between cytotoxic activity and cellular accumulation, the cellular copper content was measured in all the four cancer cells lines which were treated for 24 h with equimolar concentrations of the compounds. The cellular copper levels were quantified by means of GF-AAS analysis, and the results, expressed as ng Cu per 10^6 cells, are shown in Figure 3.29. The cellular uptake correlates with the cytotoxic activity, confirming that there is a strict relationship between drug internalisation and the anticancer activity. Interesting to note, that the complexes are internalised better in the two cancer cell lines that overexpress the biotin receptors (PSN-1 pancreatic and HCT-15 colorectal), supporting the hypothesis of the role of the biotin as a selective vector.
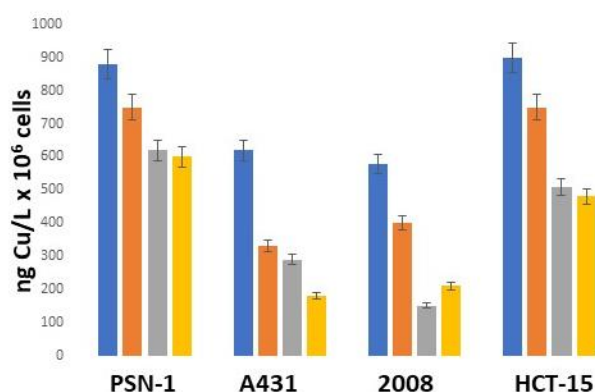
Figure 3.29: Cellular uptake of the complexes **3.3** (blue bars), **3.4** (orange bars), **3.5** (grey bars) and **3.6** (yellow bars) on the four tested cancer cells. Cancer cells were incubated with 0.5 μM of each of the copper complexes for 24 h, and cellular copper content was detected by GF-AAS analysis.

3.17   Chapter Conclusion

In this chapter, four novel copper (II) complexes tethering biotin as selective vector have been synthesised, characterised, and screened as DNA binding and cytotoxic agents. After several attempts, biotin was successfully conjugated, *via* Schiff base chemistry, to two phenanthroline scaffolds, in particular phendione (**3.23**) and dafone (**3.24**). The two ligands have been fully characterised *via* LC/HR-MS, multinuclear NMR techniques, IR and Elemental Analyses. The two ligands were then conjugated to a Cu(II) centre forming four novel complexes, two with another phenanthroline as ancillary ligand (**3.3** and **3.4**) and two with two chlorides (**3.5** and **3.6**). The complexes, that very soluble in water, are stable in physiological condition and have been characterised with El. Analyses, IR, HR-MS and UV-VIS. The stability of the complexes have been investigated *via* UV-VIS spectroscopy over a range of pH (4-10) and they are pretty stables from the acidic to the basic conditions.

 The complexes have been also investigated as DNA intercalator/binder with the EtBr displacement assay and the two compounds with a phenanthroline as ancillary ligands showed the highest DNA affinity (**3.3** and **3.4**). Preliminary cytotoxicity data revealed that the complexes, dissolved in water, are very active against a panel of cancer cells (sub-micromolar IC_{50} values) and that they seem to show selectivity for the cancer lines which overexpress the biotin receptors (PSN-1 and HCT-15) with respect to the ones that do not (A431 and 2008). This very promising data is in line with the cellular drug uptake, but the role of biotin must be further analysed and confirmed in detail. For example, the cell will be incubated with some inhibitors of the biotin receptor like phosphonoacetic acid (Figure 3.30) in order to verify the role of the biotin vector. ROS production and mechanism of cell death will be also studied.
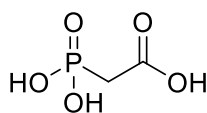
Figure **3.30:** Structure of Phosphonoacetic acid.

3.18   Experimental Procedures for Chapter 3

3.15: Synthesis of Biotin methyl ester
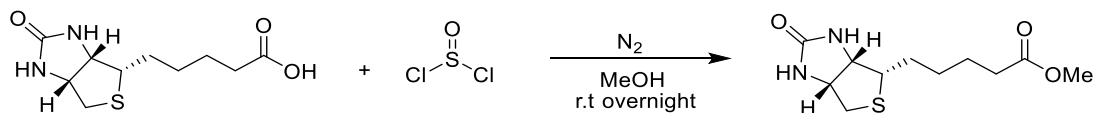
This compound was synthesised as reported in literature with slight modification.[32] Biotin (0.3 g, 1.23 mmoles) was suspended in dry MeOH (3 mL) and placed under N_2. The system was flushed entirely with N_2. $SOCl_2$ (0.3 mL, 4 mmoles) was then added dropwise via cannula. The solution was allowed to stir over night at room temperature. A clear golden solution was observed. The excess $SOCl_2$ and MeOH were removed under reduced pressure. The flask was cooled on ice bath for an hour and a crystalline solid was obtained. The white solid was taken up in $CHCl_3$ (25 mL) and washed with $NaHCO_3$ (2x30 mL) and then with brine (25 mL). The organic layer was dried over Na_2SO_4 (anhydrous) and the solvent removed under reduced pressure to yield a white solid.

Yield: 0.2686 g (85 %)

^{1}H NMR (500 MHz, DMSO) δ 6.46 (s, 1H), 6.38 (s, 1H), 4.30 (dd, *J*=7.5, 5.3, 1H), 4.13 (m, 1H), 3.57 (s, 3H, O-C*H₃*), 3.09 (m, 1H), 2.81 (dd, *J*=12.4, 5.1, 1H), 2.56 (t, *J*=13.4, 1H), 2.29 (m, 2H), 1.53 (m, 4H), 1.27 (m, 2H).

^{13}C NMR (126 MHz, DMSO) δ 173.3,162.7, 61.1, 59.3, 55.4, 51.2, 48.6, 33.1, 28.1, 28.0, 24.5

IR (ATR) 3271, 3193, 2923, 2850, 1741, 1700 (*C=O*-OMe) 1463, 1237 cm^{-1}

Elemental Analysis: $C_{11}H_{18}N_2O_3S$ % Calculated: C 51.14, H 7.02, N 10.84

                                            % Found: C 50.86, H 6.77, N 10.56

R$_f$ 0.72 (DCM: MeOH 90:10) (stains yellow in vanillin)

3.18: Synthesis of biotin hydrazide

This compound was synthesised as reported in literature with slight modification.[33] Biotin methyl ester (0.2 g, 0.77mmoles) was suspended in dry MeOH (10 mL) and placed under N_2. Hydrazin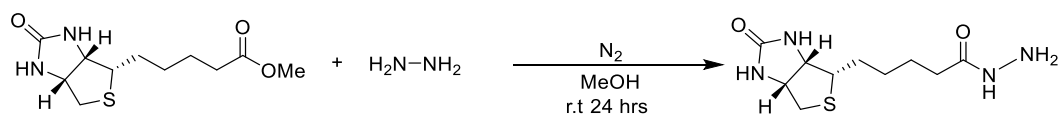e hydrate (0.21 g, 6.77mmoles) was added dropwise via a cannula to the suspension of biotin methyl ester. The solution was warmed to 50 °C until a clear solution was observed (10 – 12 mins). The solution was allowed to stir for 24 hours at room temperature and a white precipitate was observed. The MeOH was removed under reduced pressure to yield a white solid. The crude product was taken up in warm H_2O (40 mL) and the aqueous layer was washed with $CHCl_3$ (3x30 mL). The aqueous layers were combined, and the H_2O was removed under reduced pressure to yield a white solid.

Yield: 0.184 g (92 %)

¹H NMR (500 MHz, DMSO) δ = 8.93 (s, 1H, *N-H*), 6.44 (s, 1H), 6.37 (s, 1H), 4.30 (dd, 1H), 4.19 (s, 2H, N-*H₂*), 4.12 (m, 1H), 3.09 (m, 1H), 2.82 (dd, *J*=12.4, 5.1, 1H), 2.61 (m, 1H), 2.00 (m, 2H), 1.43 (m, 6H). Matches literature.[203]

¹H NMR (500 MHz, D_2O) δ = 4.55 (d, *J*=4.2, 1H), 4.37 (m, 1H), 3.29 (d, *J*=4.2, 1H), 2.94 (m, 1H), 2.73 (d, *J*=12.9, 1H), 2.18 (t, *J*=6.9, 2H), 1.59 (m, 4H), 1.35 (m, 2H). Matches literature.[203]

¹³C NMR (126 MHz, D_2O) δ = 175.6, 165.3, 62.0, 60.2, 55.2, 39.6, 33.3, 27.7, 27.5, 24.8.

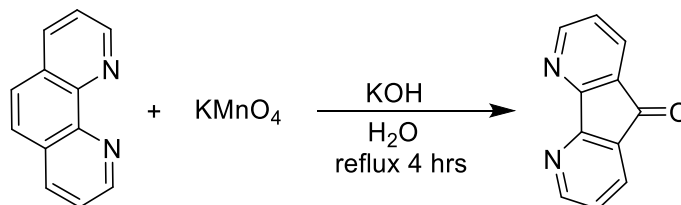**IR (ATR)** 3319 (N-*H* stretch primary amine), 3011, 2929, 1688 (N-*H* bend), 1603 (C=O stretch), 1471, 1004, 869 cm^{-1}

Elemental Analysis: $C_{10}H_{18}N_4O_2S$ % Calculated: C 59.70, H 5.25, N 19.89

                                                      % Found: C 58.59, H 5.16, N 19.46

HRMS (ESI +): m/z Calculated for $C_{10}H_{18}N_4O_2S$ + [Na$^+$] 281.1047, Found 281.1049.

3.7: Synthesis of 5H-cyclopenta[2,1-b:3,4-b'] dipyridin-5-one (Dafone)

This compound was synthesised as reported in literature with slight modification. [30] 1,10-phenanthroline (1.0 g, 5.54 mmoles) and KOH (1.01 g, 18.1 mmoles) were refluxed into H_2O (60 mL). In a separate flask $KMnO_4$ (2.54 g, 16.01 mmoles) was dissolved in warm H_2O (35 mL, 85 °C). The $KMnO_4$ was then added dropwise with stirring over the course of 3.5 hours. It was kept at 85 °C for the duration of the addition. After the final addition, the stirring was allowed to continue for 1 hour. The brown solution was gravity filtered while hot and the brown solid was washed extensively with H_2O. The orange filtrate was allowed to cool to room temperature and then extracted with $CHCl_3$ (3x150 mL). The organic layers were combined and washed with brine (100 mL), then dried over Na_2SO_4 anhydrous. The solvent was removed under reduced pressure to yield the crude yellow / orange solid. The crude product was purified via recrystallization from acetone to give needles.

Yield: 0.45 g (45 %)

^{1}H NMR (500 MHz, $CDCl_3$) δ 8.80 (ddd, *J*=5.0, 1.5, 1.0, 2H), 7.99 (ddd, *J*=7.5, 1.5, 1.1, 2H), 7.35 (ddd, *J*=7.5, 5.0, 0.8, 2H).

**^{13}C NMR** (126 MHz, $CDCl_3$) δ 189.7, 163.5, 155.3, 131.6, 129.4, 124.8

Matches literature.[199]

IR (ATR) 3218, 3011, 2929, 1684, 1625, 1471, 1004, 869 cm^{-1}

Elemental Analysis: $C_{11}H_6N_2O$ % Calculated: C 72.52, H 3.32, N 15.38

                                     % Found: C 73.06, H 3.83, N 15.94

HRMS (ESI +): m/z Calculated for $C_{11}H_6N_2O$ + [H$^+$] 183.0482, Found 183.0561.

3.23: Synthesis of N'-((Z)-6-oxo-1,10-phenanthrolin-5(6H)-ylidene)-5-((3aS,4S,6aR)-2-oxohexahydro-1H-thieno[3,4-d]imidazol-4-yl)pentanehydrazide (Phendione- Biotin)
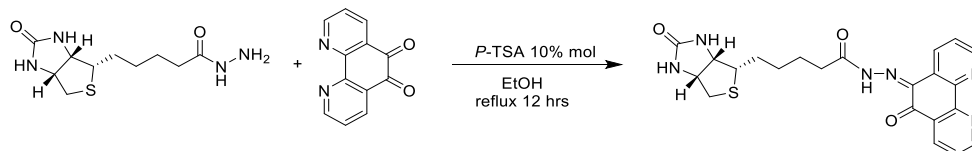
Biotin hydrazide (0.245 g, 0.948 mmol) was suspended in warm EtOH (20 mL, 50 °C). In a separate flask phendione **2.10** (0.2 g, 0.948 mmol) was dissolved in warm EtOH (20 mL, 50 °C). The phendione **2.10** was then added dropwise with stirring to the biotin hydrazine over the course of 45 mins. A yellow mixture was observed. *P*-TSA (10 % mol) was added and after 20 mins the solution turned a clear yellow colour. The solution was allowed to reflux for 12 hours and then allowed to cool to room temperature. The EtOH was reduced under vacuum to 25% volume and the flask placed in the fridge overnight. A bright yellow precipitate was observed. The yellow solid was taken up in CHCl$_3$ (20 mL), washed with brine (2 x 30 mL) and dried over Na$_2$SO$_4$. The excess CHCl$_3$ was removed under reduced pressure to yield a bright yellow solid. The crude product was purified via flash chromatography (95:5) DCM/MeOH. The bright yellow solid was dried under high vacuum.

Yield: 0.36 g, (85 %)

^{1}H NMR (500 MHz, DMSO) δ = 13.97 (s, 1H, N-*H*), 9.08 (dd, J=4.5, 1.8, 1H, Ar-H), 8.86 (dd, *J*=4.5, 1.7, 1H, Ar-H), 8.55 (m, *J*=8.0, 1.7, 2H, Ar-H), 7.73 (dd, 1H, Ar-H), 7.64 (dd, *J*=8.1, 4.5, 1H, Ar-H). 6.48 (s, 1H, CN-*H*), 6.37 (s, 1H, CN-*H*), 4.31 (dd, *J*=7.6, 5.2, 1H, C*H*), 4.15 (m, 1H, C*H*), 3.14 (m, 2H, SC*H$_2$*), 2.83 (m, 2H, amide C*H$_2$*), 2.60 (m, 1H, SC-*H*), 1.71 - 1.52 (m, 6H, 3x C*H$_2$*).

^{13}C NMR (126 MHz, DMSO) δ = 180.8, 162.7, 155.5, 152.2, 150.6, 146.2, 135.7, 131.5, 131.4, 130.8, 128.4, 127.4, 125.0, 124.0, 79.2, 61.0, 59.2, 55.4, 54.9, 40.1 (under DMSO dept – 135), 28.1, 24.1.

IR (ATR) 3221, 2919, 2852, 1705, 1628, 1402, 1063, 727 cm^{-1}

Elemental Analysis: C$_{22}$H$_{22}$N$_6$O$_3$S   % Calculated: C 58.65, H 4.92, N 18.65

% Found: C 58.90, H 5.11, N 18.22

HRMS (ESI +): *m/z* Calculated for C$_{22}$H$_{22}$N$_6$O$_3$S + [Na$^+$] 473.1372, Found 473.1366.

R$_f$ 0.88 (DCM: MeOH 95:5)

3.24: Synthesis of N'-(5H-cyclopenta[2,1-b:3,4-b'] dipyridin-5-ylidene)-5-((3aS,4S,6aR)-2-oxohexahydro-1H-thieno[3,4-d] imidazol-4-yl) pentanehydrazide. (Dafone – biotin)
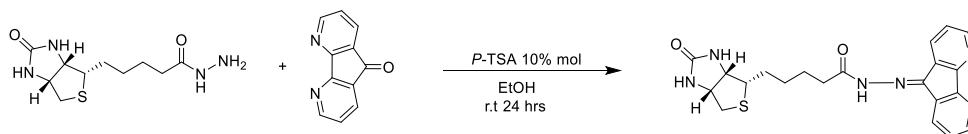
Biotin hydrazine **3.18** (0.138 g, 0.537 mmoles), **3.7** (0.098 g, 0.537 mmoles) and *p*-TSA (10% mol) were suspended in EtOH (20 mL). The solution was refluxed until a clear solution was observed (1-1.5 hours). The solution was allowed to stir for 24 hours at room temperature. A white precipitate was observed. The white solid was collected via Buchner filtration, washed with $CHCl_3$ (2x30 mL) and dried under high vacuum. No further purification was required.

Yield: 0.112 g (54%)

^{1}H NMR (500 MHz, DMSO) δ 11.38 (s, 1H,*H*-N-N), 8.73 (dd, *J*=11.9, 7.0, 3H, Ar-H), 8.22 (s, 1H, Ar-H), 7.51 (m, 2H, Ar-H), 6.47 (d, *J*=4.7, 1H, C=O-N-*H*), 6.38 (d, *J*=5.2, 1H, C=O-N-*H*), 4.32 (d, *J*=4.4, 1H, NC*H*), 4.12 (m, 2H, S-C*H₂*), 3.17 (m, 2H, SC*H* & NC*H*), 2.83 (d, broad, *J*=5.0, 2H, C=O-C*H₂*), 1.78 – 1.28 (m, 6H, 3x C*H₂*).

^{13}C NMR (126 MHz, DMSO) δ 162.7, 158.4, 156.7, 151.3, 140.4, 134.5, 132.4, 129.0, 124.3, 123.5, 89.8, 87.7, 61.1, 59.2, 55.4, 48.6, 40.4 (under DMSO, DEPT - 135), 28.3, 28.1, 24.5, 16.9

IR (ATR) 3208, 2867, 1687, 1665, 1400, 1367, 1067, 747. cm^{-1}

Elemental Analysis: $C_{21}H_{22}N_6O_2S$ % Calculated: C 59.70, H 5.25, N 19.89

                                                      % Found: C 58.96, H 5.16, N 19.46

HRMS (ESI +): *m/z* Calculated for $C_{21}H_{22}N_6O_2S$ + [Na$^+$] 445.1423, Found 445.1390.

3.3: Synthesis of [Cu(phen)(phendione-biotin)](NO₃)₂
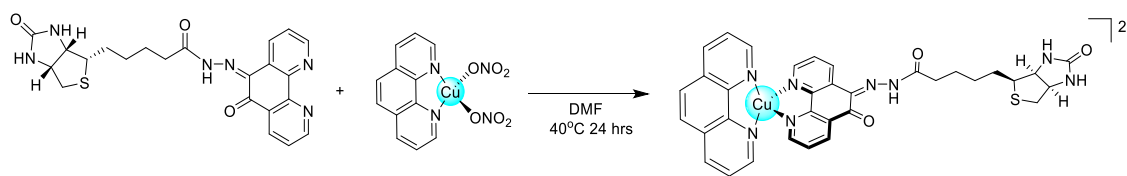
3.23 (0.073 g, 0.162 mmol) was dissolved in DMF (15 mL); in a separate flask **2.21** (0.0654 g, 0.162 mmol) was dissolved in DMF (5 mL). The solution of **2.21** was then added dropwise with stirring to the solution of **3.23**. A green colour was observed. The solution was allowed to stir for 24 hours at 40 °C after which a brown colour was observed. The solution was allowed to cool to room temperature and diethyl – ether (30 mL) was added. A pale precipitate was observed. The brown solid was filtered off and the filtrate concentrated *in vacuo*. The remaining green concentrate was precipitated into excess Et$_2$O and the pale green solid was collected. The solution was spun in the centrifuge for 10 mins at 4000 rpm and a dark green pellet was recovered. The pellet was washed gently with CHCl$_3$. The powder was dried under high vacuum.

Yield: 0.082 g (67 %)

Elemental Analysis: C$_{34}$H$_{30}$CuN$_8$O$_9$S   % Calculated: C 49.91, H 3.70, N 17.12

                                                        % Found: C 49.42, H 3.46, N 16.82

IR (ATR): 3058, 1647,1518, 1361, 1298, 1033, 846, 718. cm^{-1}

HPLC (RP): CH$_3$CN: H$_2$O (80:20) RT, 3.23 mins, 100 %.

HRMS (ESI +): m/z Calculated for C$_{34}$H$_{30}$CuN$_6$O$_3$S [M-2(NO$_3$)$^-$] 693.1442, Found 693.1444.

3.4: Synthesis of [Cu(phendione-biotin)Cl₂]
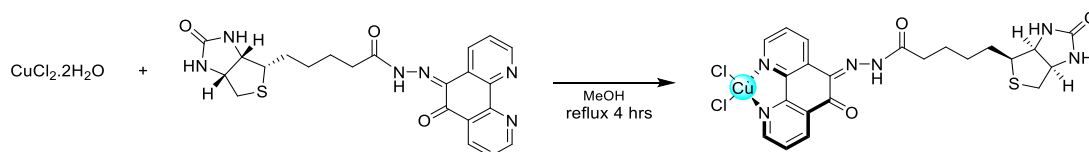
3.23 (0.246 g, 0.546 mmol) was suspended in MeOH (30 mL) and warmed to 50 °C and a solution of CuCl₂.2H₂O (0.111 g, 0.655 mmol) in MeOH was added dropwise. The solution was refluxed. After 10 – 15 mins a clear green solution was observed for a brief few moments before a green precipitate began to form. The reflux was allowed to continue for a further 4 hours before allowing the solution to cool to room temperature. The fine green precipitate was collected *via* Buchner filtration and washed very gently with CHCl₃ (10 mL) to dispel any unreacted ligand. No further purification was required.

Yield: 0.1483g (47 %)

Elemental Analysis: $C_{22}H_{22}Cl_2CuN_6O_3S$ % Calculated: C 45.17, H 3.79, N 14.37

% Found: C 45.78, H 3.91, N 14.76

IR (ATR): 3341, 2907, 1650, 1608, 1480, 1078, 741. cm^{-1}

HPLC (RP): CH₃CN: H₂O (80:20) RT 2.2 mins 100 %

HRMS (ESI +): m/z Calculated for $C_{22}H_{22}CuN_6O_2S$ [M⁺] 583.0147, Found 584.0004.

3.5: Synthesis of [Cu(phen)(dafone-biotin)](NO₃)₂
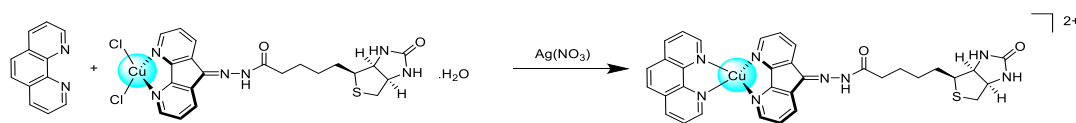
3.6 (0.104 g, 0.180 mmol) was dissolved in anhydrous DMF (20 mL). AgNO₃ (0.0614g, 0.36mmol) dissolved in anhydrous DMF (3 mL) was added to the solution containing 3.6 and the solution was allowed to stir at r.t and in darkness for 4 hours. An extremely fine white precipitate was observed. The white precipitate was filtered off and 2 drops of HCl (1M) were added to the filtrate to examine for excess Ag. The filtrate was filtered a second time and the clear green filtrate was placed back into a round bottom and protected from light. To this was added solid 1,10 – phenanthroline (0.035g, 0.0180mmol). Immediately a deep green solution was observed. The solution allowed to stir overnight at r.t.; the DMF was reduced *in vacuo* and the resulting solution precipitated into excess Et₂O. A light green solid was observed. This solid was filtered and washed with CHCl₃ (20 mL) and dried under high vacuum.

Yield: 0.108g (74%)

HPLC (RP): CH₃CN: H₂O (80:20) RT 1.97 mins 97% 2.36 min 3%

HRMS (ESI +): m/z Calculated for $C_{33}H_{30}CuN_8O_2S$ [M-2(NO₃)⁻] 665.1508, Found 665.1505.

Elemental Analysis: $C_{33}H_{30}CuN_{10}O_8S$ % Calculated: C 50.16, H 3.83, N 17.72.

% Found: C 49.72, H 3.50, N 17.28

3.6: Synthesis of [Cu(dafone-biotin)Cl₂]
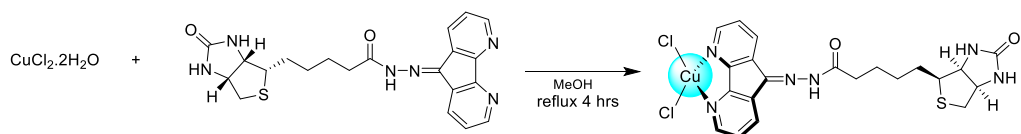
3.24 (0.153 g, 0.363 mmol) was suspended in refluxing MeOH (40 mL). CuCl$_2$.2H$_2$O (0.068 g, 0.398 mmol) was added dropwise while stirring . A green suspension was observed and after 5 -6 minutes a clear solution was observed. The solution was allowed to reflux for another 4 hours at which stage a fine green precipitate was formed. The solution was allowed to stir for a further 3 hours and then was cooled at r.t. and the green solid was collected via Buchner filtration and washed with cold MeOH.

Yield: 0.098 g (49 %)

Elemental Analysis: C$_{21}$H$_{22}$Cl$_2$CuN$_6$O$_2$S   % Calculated: C 43.87, H 4.21, N 14.62

% Found: C 43.38, H 3.88, N 14.20

IR (ATR): 3335, 2922, 1655, 1610, 1481, 1086, 741. cm^{-1}

HPLC (RP): CH$_3$CN: H2O (80:20) RT 2.6 mins 100 %

HRMS (ESI +): m/z Calculated for C$_{21}$H$_{22}$CuN$_6$O$_2$S [M-2Cl$^-$] 485.0830, Found 485.0821.

4   Chapter 4: *Bis*-(dipyridophenazine) copper (II) complexes

4.1   Introduction

4.2   Dipyridophenazine (DPPZ)

DPPZ is a planar hetero-pentacyclic system of five six membered rings fused together with molecular formula $C_{18}H_{10}N_4$. This molecule has two nitrogen atoms in the 1 and 10 positions resembling the phenanthroline scaffold (Figure 4.0). Due to its very planar structure and its rigidness, it has sprung huge interest as a ligand, particularly with transition metals. The DPPZ-transition metal complexes showed interesting biological properties, in particular anticancer and antimicrobial.[204] Furthermore, DNA intercalation,[205] molecular light switches [206] and recently anti – fungal activity are other important biological applications.[207]

dipyridophenazine
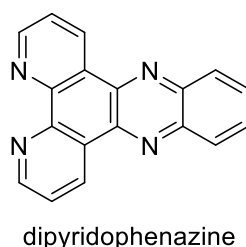
Figure 4.0: Structure of dipyridophenazine (DPPZ).

DPPZ can be readily synthesised using Schiff base chemistry from phendione **2.10** and 1,2-phenylenediamine dihydrochloride (Scheme 4.0). This can be achieved under mild conditions and at high yield, making it a very attractive molecule.
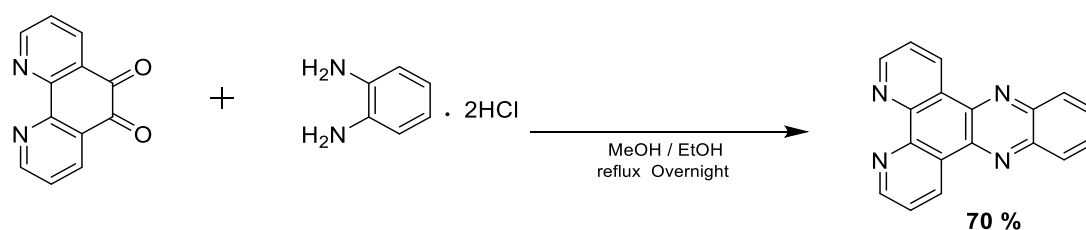
Scheme 4.0. Reaction pathway for the synthesis of DPPZ.

DPPZ lends itself very nicely to purification *via* recrystallization from alcohols like methanol or ethanol due to its natural ability to form $\pi - \pi$ stacking.[157] The above route displays a yield of 70 % but it is worth noting that Swaminathan et *al.* in 2020 optimised the synthesis using titanium oxysulfate as a catalyst achieving yields in excess of 95 %.[157]

4.3   Fungicidal properties of DPPZ metal complexes

In 2019 Ude *et al.* prepared a number of copper (II) compounds containing derivatives of ciprofloxacin antibiotic agent (CipA) with planar ancillary ligands including DPPZ (Figure 4.1).[207] The complexes were tested against various fungi. While Cu-phen-CipA and Cu-DPQ-CipA complexes showed little anti-fungal activity towards the panel tested, Cu-DPPZ-CipA (compound **1**) was very potent with MIC_{80} of 15.62 µM toward the *Candida krusei* ATCC 6258 (CK1) and *Candida krusei* E28 (CK2) strains and an MIC_{80} of 31.25 µM toward the *Candida lusitaniae* 2446/I (CL) strain.
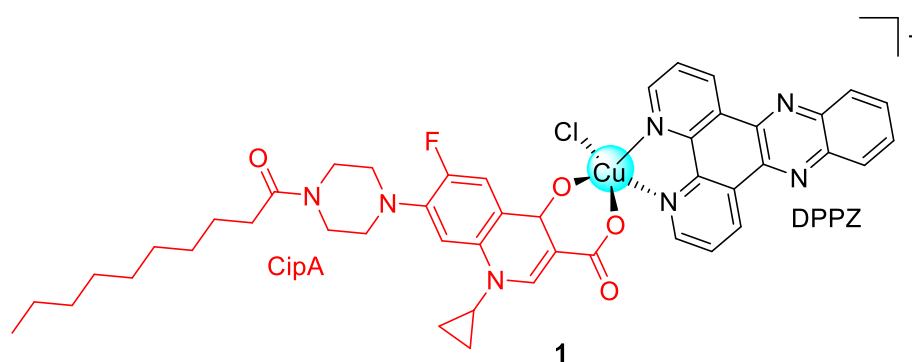
Figure 4.1: Molecular structure of compound 1 prepared by Ude *et al.*

Studies carried out in 2015 by Pathak et *al.* also involved two copper (II) based DPPZ compounds and two novel Schiff base ligands (Figure 4.2).[208] The compounds were screened against *C. albicans* and *P. chrysogenum* and the zone of inhibition was measured in mm and recorded as a percent. **2a** displayed the second largest zone of inhibition % of the nine compounds tested in the experiment with a value of 10% for *C. albicans* and 8% *P. chrysogenum*. Compound **2b** did not perform as well with a value of 8 % and 6 % for *C. albicans* and *P. chrysogenum* respectively. What was interesting was that compound **2a** did perform better than both the free DPPZ and the ligands **a** and **b,** separately. Pathak *et al.* surmised the enhanced growth inhibition activity of the metal complexes when compared to their ligands might be due to their chelating ability. The redox behaviour of the copper ion in the complexes might also add to the higher antifungal activity observed. [208]
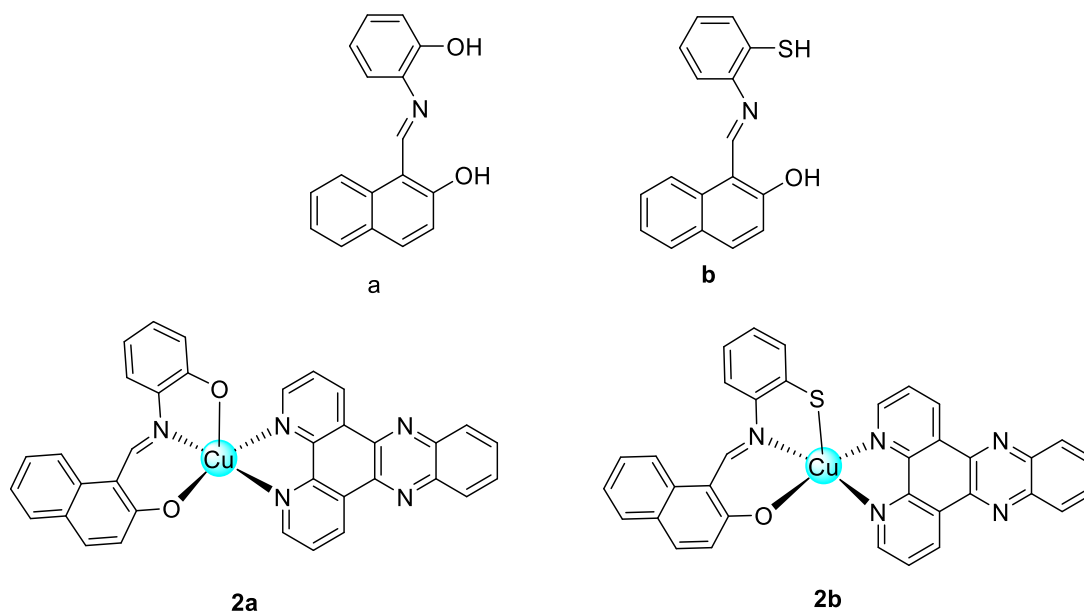
Figure 4.2. Ligands **a** and **b** and compounds **2a** and **2b** developed by Pathak *et al.*

Further studies were carried out by Śliwińska *et al.* in 2013 against AD1-9 and FY yeast strains with a number of iridium and rhodium complexes containing 1,5-cyclooctadiene and a number of planar ligands.[209] Of the nine compounds synthesised, only that one with DPPZ ligand (complex **3**) displayed activity against the two yeast strains (Figure 4.3) with MIC values of 30 and 50 µM for AD1-9 and FY yeast strains, respectively.[209] The research group did note that the iridium complex of the same ligands showed no activity against the two yeasts.
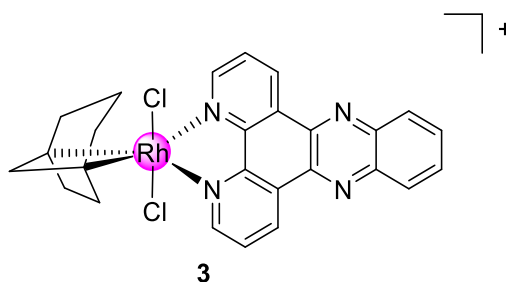
Figure 4.3: Rhodium complex of DPPZ developed by Śliwińska *et al.*

4.3.1 Anti-microbial activity of DPPZ metal complexes

The most recent anti-microbial study of DPPZ metal complexes have come from Kumar *et al.* where a number of *bis*- DPPZ metal complexes were prepared.[210] These included metal centres of Cobalt, Nickel and Copper (Figure 4.4). Each of the compounds contained two DPPZ ligands and single *o*-sulfobenzimide in the axial position.
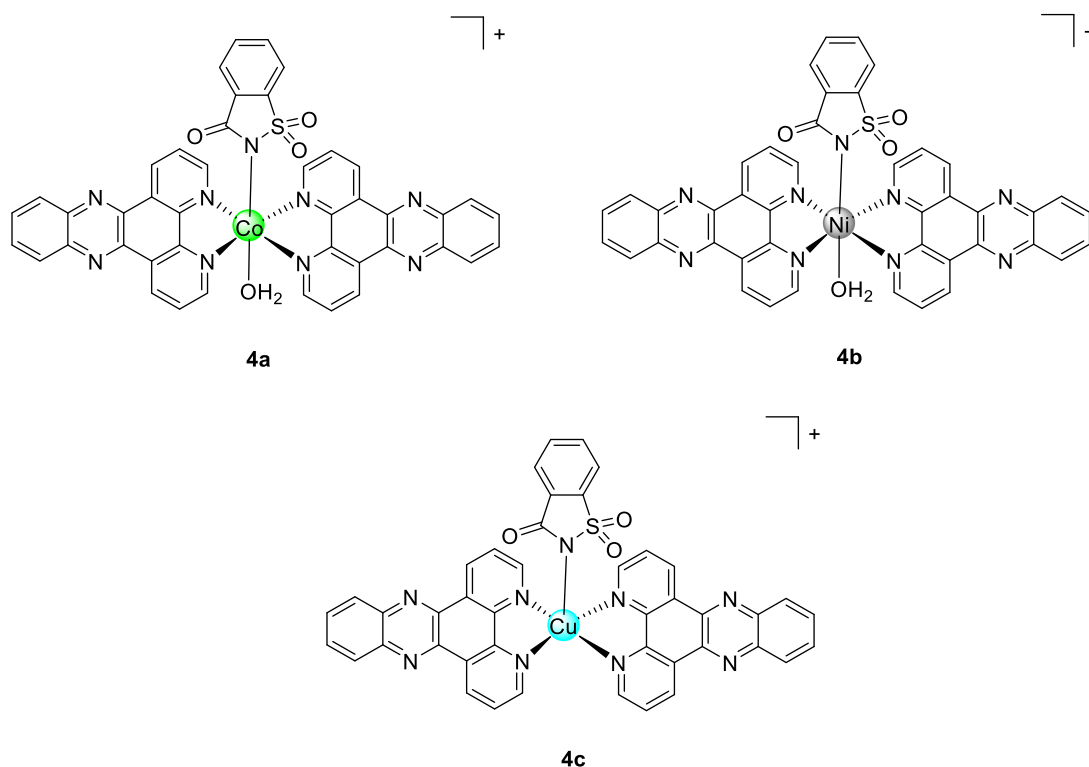
Figure 4.4: Structures of the three *bis-* DPPZ-metal complexes by Kumar *et al.*

Kumar et al. reported that all three of the complexes showed remarkable anti-microbial activity for Gram-positive *S. aureus* bacteria of 1-2 µg /mL, which has been known to express resistance towards clinical used antibiotics methicillin (MRSA) and vancomycin (VRSA). The *o*-sulfobenzimide ligand does not have anti-bacterial properties on its own, but the complexes all showed a higher activity. The Nickel complex **4b** displayed very high activity against the Gram-negative strain *A. baumanni.* With a n MIC value of 8-16 µg /mL.[210]

In 2011 Bolhuis *et al.* tested the anti-microbial activity of three Ruthenium complexes, one of which contained the DPPZ ligand.[211]   Of the three compounds screened, the DPPZ conjugate **5** performed the best by a large margin (Figure 4.5)with MIC Values of 2 and 4 mg/L against MRSA252 and MRSA41, respectively.
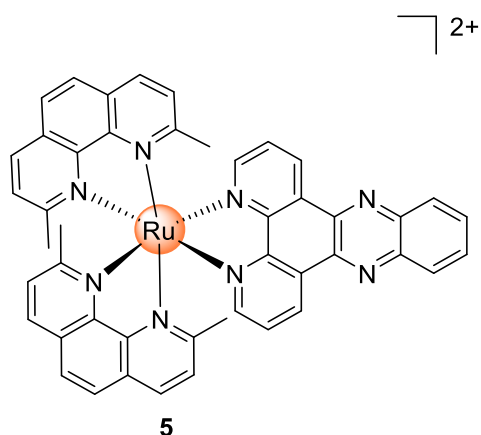
Figure 4.5: DPPZ complex of ruthenium tested by Bolhuis *et al.*

Compound **5** also displayed the highest activity of the three complexes against *B.subtilis* and MSSA160 with MIC values of 4 and 8 mg/L.[211] Compound **5** was then carried forward into *in vivo* studies in nematodes infected with *S. aureus*. Bolhuis *et al.* demonstrated that **5** is active *in vivo* as it prevented death of *C.elegans* nematodes infected with *S. aureus.* Importantly, the compound was also not toxic to *C. elegans,* which is a good indicator that they are also not toxic in higher eukaryotes.[212]

In 2018 Liu *et al.* also synthesised two analogues of compound 5**, 6a** and **6b** (Figure 4.6) with two methyl - BIPY conjugates bridged with an alkyl chain.[213] The compounds were screened against both Gram positive and Gram negative bacteria.
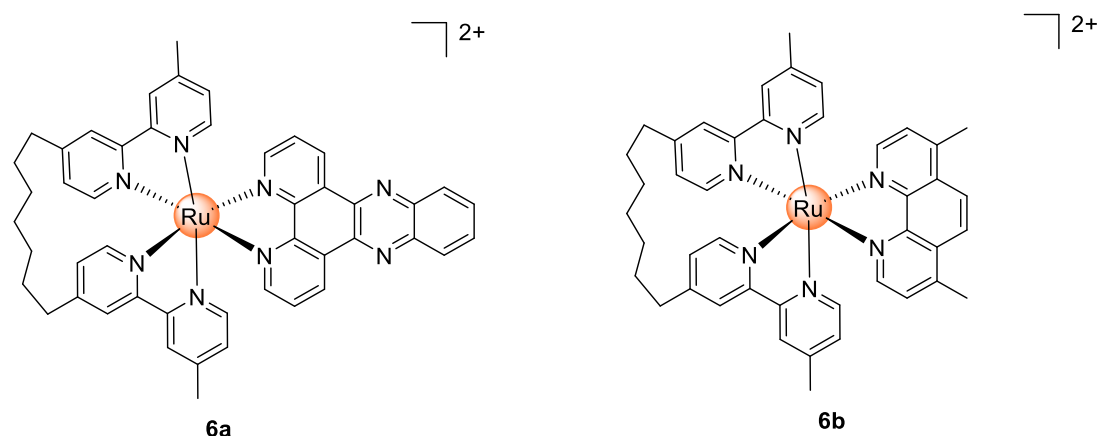
Figure 4.6: Ruthenium compound developed by Liu *et al.*

When tested against *S. aureus* and MRSA compound **6a** showed MIC values of 4 μg/mL for both bacteria in comparison to values of values of 64 and 16 μg/mL for **6b**. In the Gram negative testing compound **6b** showed instead activity far greater than compound **6a** for the cell lines MG1655, APEC and UPEC with values of 8, 16 and 16 μg/mL respectively, whereas

compound **6a** displayed values in excess of 64 μg/mL for all three cell lines.[213] In the cellular accumulation assays it was demonstrated compound **6b** was accumulating in the cells at 4 to 5 times the amount of compound **6a** and up to nine time that of the antibiotic ampicillin. Particularly in the Gram negative strain P. aeruginosa which is known to be resistant to many anti microbials due to the low permeability of its outer layer.[214]

4.3.2   DPPZ metal complexes as DNA intercalators

One of the most important application for DPPZ derivatives is the ability to act as a DNA intercalator or DNA groove binder.[205] DPPZ itself has shown binding values of $K_b > 10^5$ M^{-1} [202] where as some of its metal complexes have displayed values at $K_b > 10^6$ m^{-1}. [205] In 2004 Philips *et al.* carried out DNA binding studies on a ruthenium metal complex of DPPZ **7** (Figure 4.7).
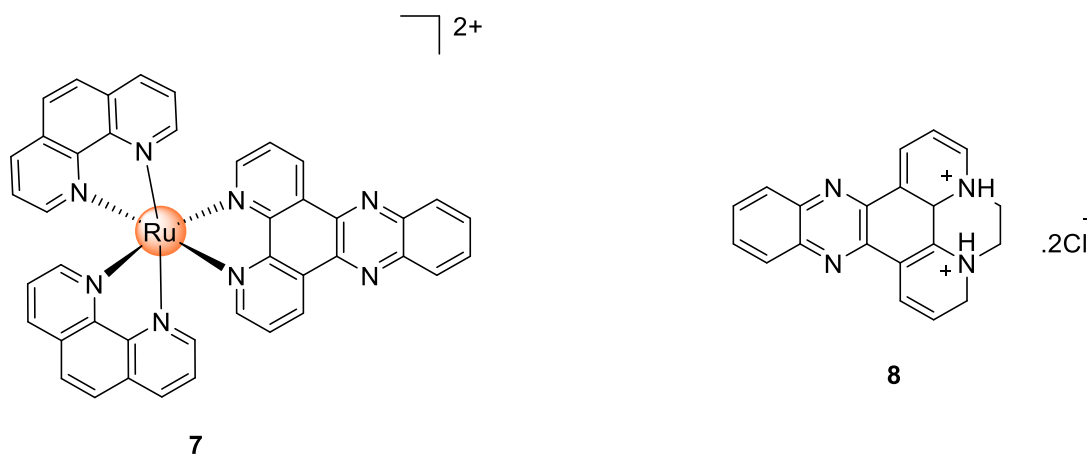
Figure 4.7: Metal complex of DPPZ and DPPZ analogue tested by Philips *et al.*

Philips *et al.* reported values of 3.2×10^6 for the Δ isomer of compound **7** and 1.7×10^6 K_b (M^{-1} bp) for that of the Λ isomer of the same compound. Also compared in the experiment was an analogue of the DPPZ ligand, compound **8**. It was found that **8** displayed a binding value of 5.4×10^4 K_b (M^{-1} bp). Philips *et al.* reported that more detailed biophysical and photophysical studies on the nature of the interaction of **8** with DNA, including an investigation of photoinduced redox processes are ongoing.

In 2006 Cusumano *et al.* synthesised and tested the DNA binding ability of a number platinum (II) complexes. These complexes contained a platinum (II) core with two pyridine moieties along with a Phen (**9a**), DPQ (**9b**), DPPZ (**9c**) or DPPN (**9d**).[215] Binding values for the DPQ and Phen derivatives were established to be 2.3×10^5 K_b (M^{-1} bp) and 2.2×10^5 K_b (M^{-1} bp) and were

established via the McGhee-von Hippel equation. Self-aggregation of compound **9c** (Figure 4.8) prevented even a rough rating of the KB values for the complexes **9c** and the **9d** complex.
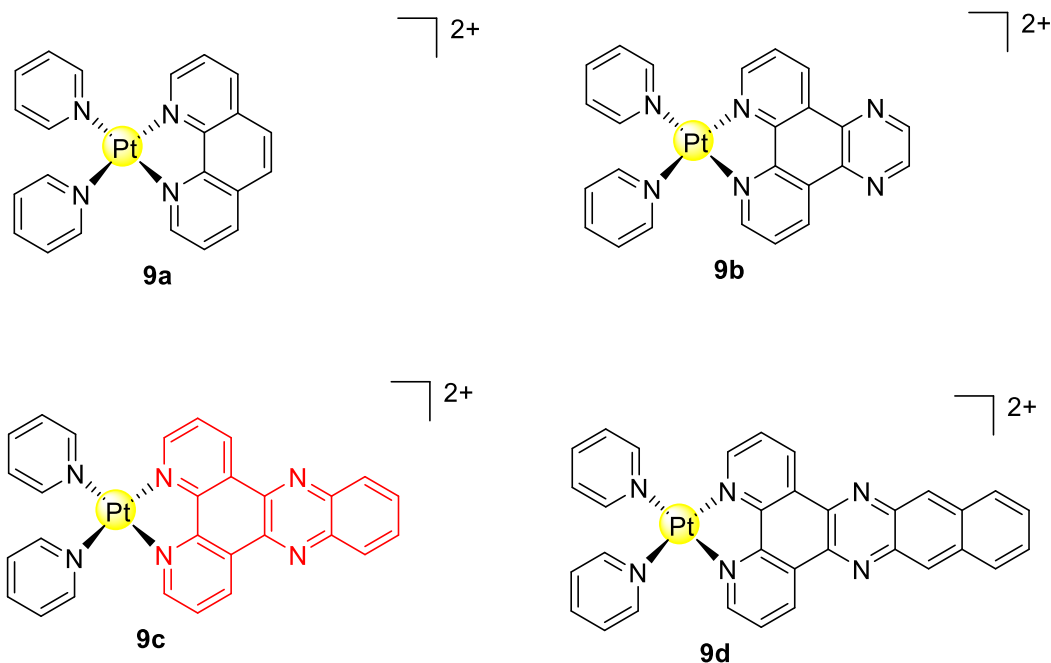
Figure 4.8: Platinum derived compounds developed by Cusumano *et al.*

The group also carried out further studies by subjecting the compounds to aggregation studies with the DNA. The dimerization constants could be obtained and used to speculate on how the compounds were interacting with the DNA. Cusumano *et al.* discovered that at low [DNA]/[complex] ratio, when few intercalation binding sites are available, the complexes bind externally aggregating along the helix while when the [DNA]/[complex] ratio increases the aggregates break up and the complexes intercalate within the base pairs. It was found that for compound **8** the two binding modes seem to coexist almost at any DNA concentration. For [Pt(DPQ)(py)$_2$] $^{2+}$ and [Pt(Phen)(py)$_2$]$^{2+}$, where the tendency to stack is much lower, aggregation along the helix is not significant and the binding equilibrium occurs essentially between free and intercalated form. [215]

Studies carried out by the Montagner group in collaboration with Kellet *et al.* also displayed large binding values for a copper compound containing the DPPZ ligand. The group determined a value of 1.44×10^7 K$_{app}$ (M^{-1} bp) for the DPPZ derived copper (II) complex (Figure 4.9) in comparison to values $\sim 10^6$ for the other three compounds tested.[216] All four of the estrogen derived compounds (**2.3**, **2.4** , **2.6** & **2.8**) which had increasing structural planarity like the Cusumano *et al.* compounds (Figure 4.8) can be viewed in chapter 2 (Figure 2.15) of this thesis.
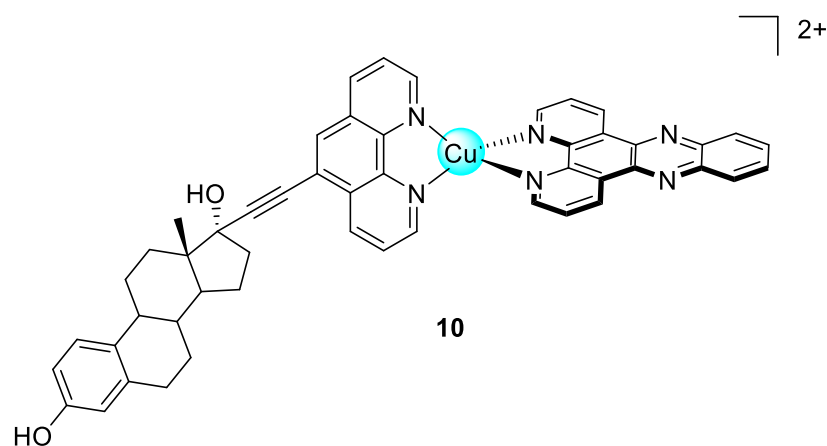
Figure 4.9: Steroid derived copper (II) complex containing the DPPZ ligand previously developed in the group.

Viscosity studies were also carried out and they revealed that compound **10** was the strongest intercalator. More on these studies can be found in Chapter two of this thesis in section **2.6.5.2**.

In 2003 Navarro *et al.* synthesised a *Bis*-[Cu(dppz)$_2$](NO$_3$)$_2$ (**11**) and a *Bis*-[Cu(DPQ)$_2$](NO$_3$)$_2$ (**12**) (Figure 4.10).[217] Navarro *et al.* reported binding values of 8.1x10^4 K$_b$ (M^{-1} bp) for compound **11** and 3.8x10^3 K$_b$ (M^{-1} bp) for compound **12,** once again demonstrating the potency of DPPZ to intercalate in comparison to its lesser extended sister molecules like DPQ and Phen.
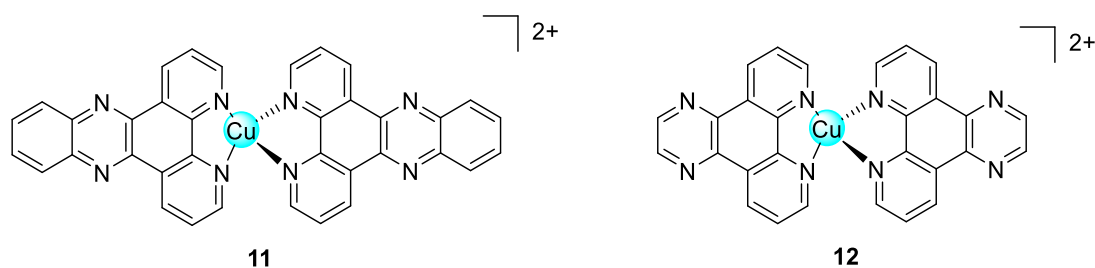
Figure 4.10: Bis- copper (II) complexes developed and tested by Navarro *et al.*

Navarro *et al.* also reported that the compounds displayed activity against the parasitic Leishman's disease with compound **12** displaying the higher activity. The group suggested that the nucleus DNA may be the associated with the cellular target for the complexes.

Gupta *et al.* also carried out substantial studies on compounds **13** and **14** in 2004, using calf thymus DNA.[218] This time the copper core had attached a chlorine in the fifth coordination position (Figure 4.11). The DNA binding studies showed values of the same magnitude of that discovered by *Navarro et al*. in 2003. Gupta et al. reported a value of 2.8x10^4 K$_b$ (M^{-1} bp) for

compound **13** but reported a much higher value for that of compound **14** of 4.5x104 K_b (M^{-1} bp). Gupta *et al.* noted the angular orientation of the DPPZ ligands in the five-coordinate structure of **11** could reduce its ability for efficient binding to DNA now that the chlorine moiety was attached.
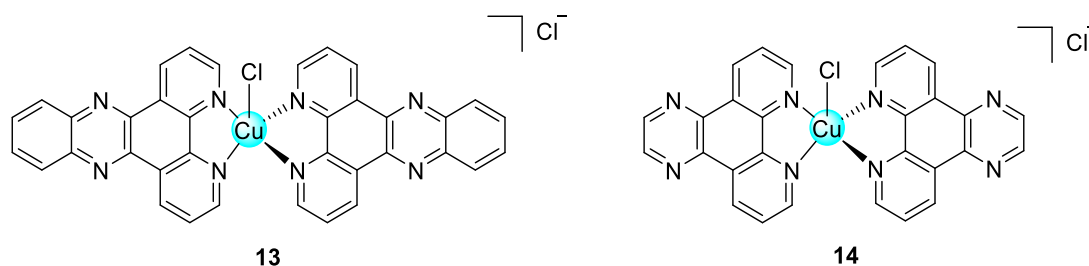
Figure 4.11: Figure 4.10. Bis- copper (II) complexes developed and tested by Gupta *et al.*

In 2013 Hall *et al.* and co synthesised a chloro substituted DPPZ ligand (in the position 11) and proceeded to attached it to a ruthenium centre (Figure 4.12).[219]

As discussed previously in this section there is an enormous interest in these [Ru(Phen)$_2$(DPPZ)]$^{2+}$ compounds, both as molecular light switches and also as DNA intercalators. However, much less is known about the precise DNA binding modes of this family of complexes. The group were able to grow crystals and report the atomic resolution of structure of Λ-[Ru(TAP)$_2$(11-Cl-DPPZ]$^{2+}$ crystallized with the d(TCGGCGCCGA) DNA duplex, which adopts the overall conformation shown (Figure 4.13) in the crystal lattice.
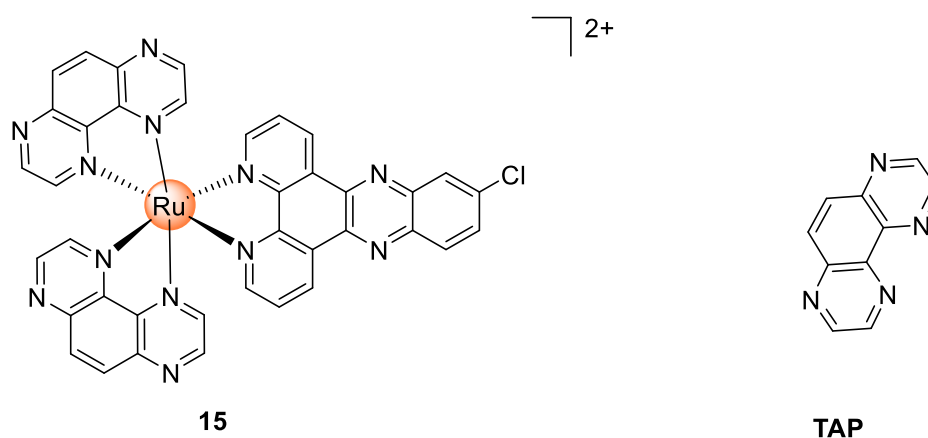
Figure 4.12: Complex synthesised by Hall *et al*. containing two TAP ligands and the mono substituted DPPZ.

Although the group were able to isolate very detailed images of the co – crystal (Figure 4.13), they did investigate on the effect of the chloro substitution on the DPPZ group in relation to

its DNA binding properties.[219] Complex **15** has been the subject of a biophysical studies, and it was found that the binding to DNA *via* intercalation is proposed as the major binding mode for the complex. This would suggest that the effect of the chloro substitution is to lower the binding constant, but further studies using a range of substituents will be necessary to judge the balance between steric and electronic effects.
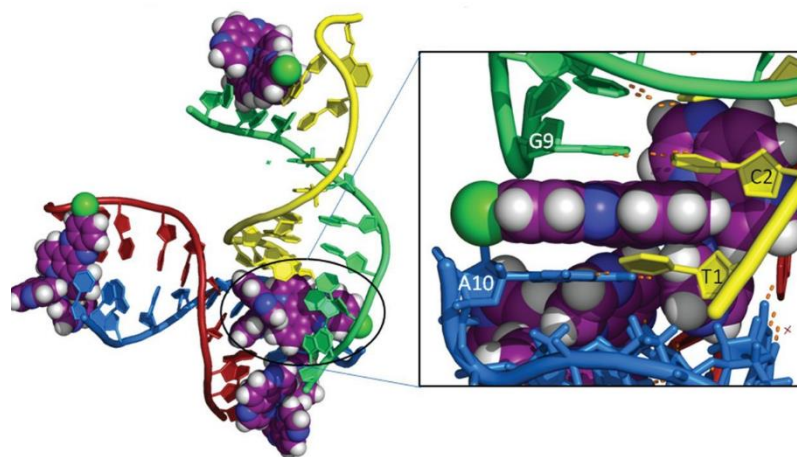
Figure 4.13: The interactions of compound **13** and DNA helix. [219]

4.4   Chapter Objective

This chapter will outline the synthesis, characterisation, biological evaluation and computational studies of a series of *bis-* (11-R-dipyridophenazine) copper (II) complexes.

This chapter will describe the synthesis of four DPPZ ligands substituted in the 11 position with varying groups to provide a range of electron donating and electron withdrawing activities. This structure activity relationship will be studied using a variety of spectroscopic techniques in a bid to understand the role of the substituent on the biological properties of the new complexes and compared to that of DPPZ which is a known very strong intercalator. The final structure of this series of complexes is shown below (Figure 4.14)
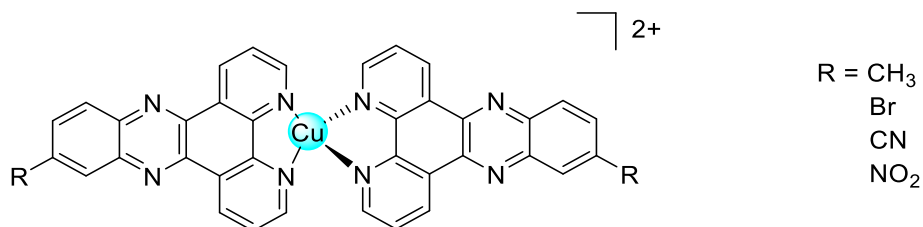
Figure 4.14: Final structure of the compounds outlined in this chapter.

The organic component was synthesised using a similar method to that in Chapter 2, using Schiff base chemistry *via* a diamine and phendione. This again would allow the nitrogens to

be seated in the desirable 1 and 10 positions to facilitate smooth binding to the copper (II) core. After completing the synthesis and characterisation of the substituted ligands, they would be reacted with the copper (II) salt to yield the target compounds shown above (Figure 4.14).

4.5   Synthesis & characterisation

4.6   Synthesis of planar ligands

The planar ligands discussed in this chapter were synthesised *via* the same route proposed in chapter 2 of this thesis. Phendione **2.10** was synthesised using commercially available 1,10-phenanthroline.[154] The substituted 11-DPPZ adducts were made from the corresponding diamine precursor and phendione.
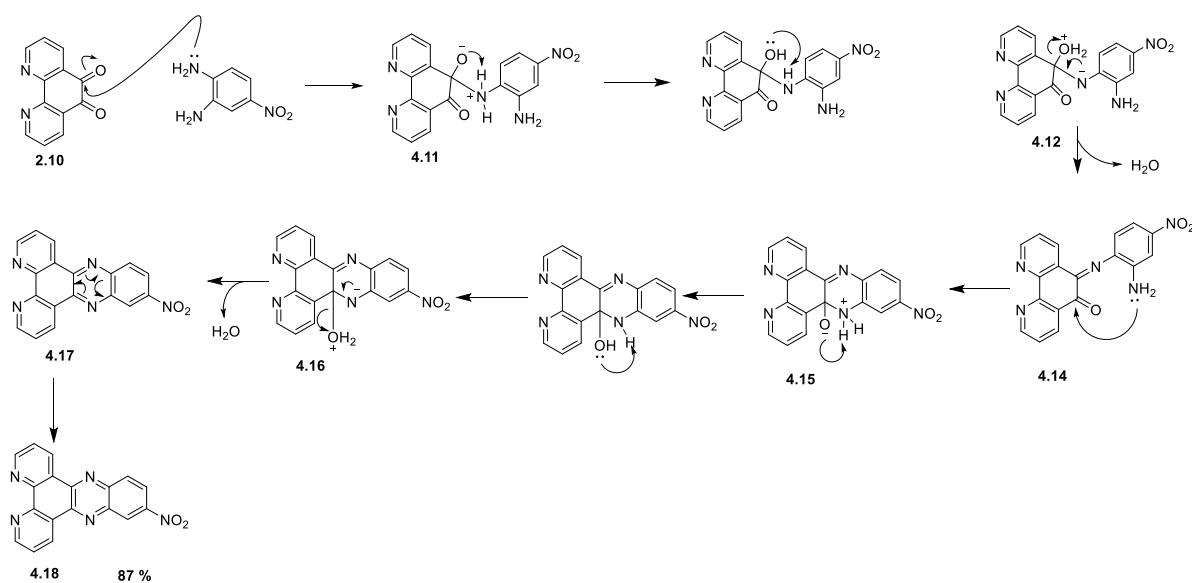
Scheme 4.0: Mechanism describing the formation of 11-nitro-dipyridophenazine under neutral conditions.

Phendione **2.10** undergoes nucleophilic attack from one of the nitrogen on the 2-amino-5-nitrobenzenaminium in the 5 or 6 position first, breaking the π bond on the carbonyl carbon - oxygen. This gives rise to the quaternary ammonium ion intermediate **4.11**, the negatively charged oxygen is able to deprotonate the amine as its in very close proximity. This forms the hydroxyl leaving group seen in **4.12** and the lone pair of electrons on the Nitrogen donate back in towards the aromatic system forming a π bond and then leading to the ejection of the aqua group, leading to the elimination of a water molecule from the reaction. The second amine now simultaneously carries out the process again as show in **4.14** and again the

process is the same through **4.16** with the discharge of a second molecule of water. Finally, the reaction terminates with a reshuffle of electrons **4.17** leading to the aromatic system in the final product (11-nitro-dipyridophenazine) as seen in **4.18**. The mechanism for all four of the DPPZ derivatives in this chapter proceeds via the same pathway providing yields of 48 %, 61 % and 70 % respectively for three remaining R substituted (Scheme 4.1) Br, CH^3 and CN derivatives of the DPPZ.

The reactions were carried out in a 90:10 mixture of ethanol / methanol with the exception of 11-methyl-DPPZ **4.21** which was carried out in 100 % ethanol. On the rare occasion where the pure product did not precipitate from the solution, recrystallization from methanol was preformed to yield the final product. The reaction progress can be followed *via* TLC (70:30 EtOAc: EtOH, 0.1 % NEt₃) and by ^{1}H NMR. Figure 4.15 shows the ^{1}H NMR of **4.18**. It is very clear there is a complete splitting of the symmetry of the starting molecule **2.10**, along with the absence of the four amine protons from the amine starting material.
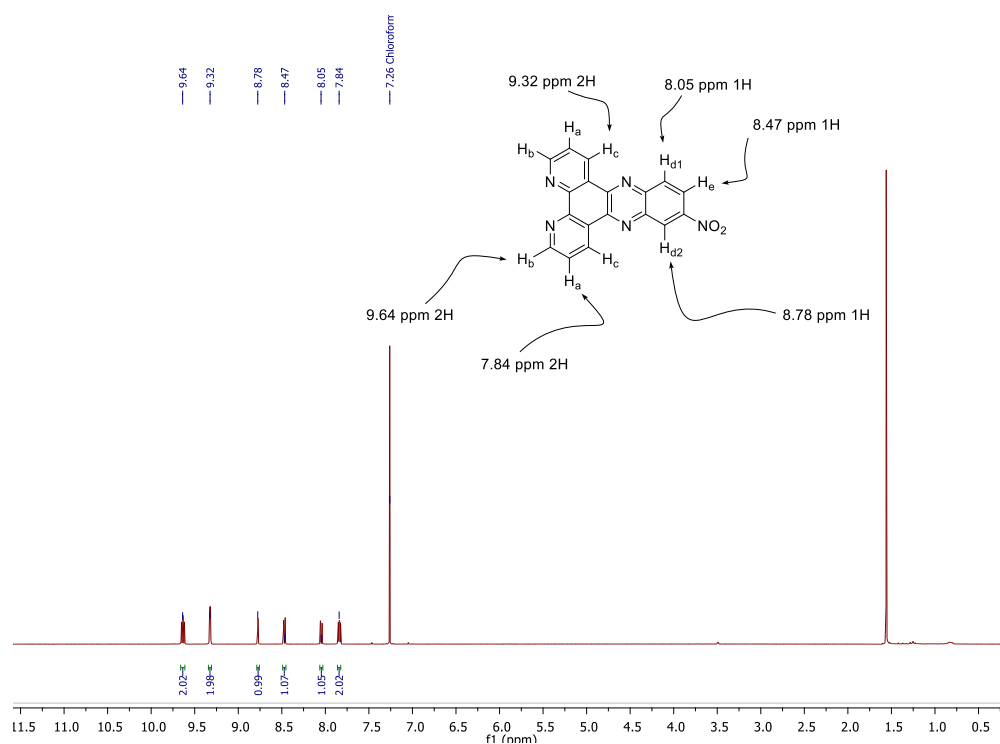
Figure 4.15: ^{1}H NMR (CDCl₃) of 11-nitro-DDPPZ **4.18**.

The characterisations of the four planar ligands was very similar with the only difference being that the 11-methyl-DPPZ **4.21** displayed a large singlet at 2.71 ppm representative of the methyl protons in the 11 position. In all cases the protons in the a, b and c positions (Figure 4.15, did not lose the symmetry and the ring closest to the 11 position would appear

as expected in individual signals. The assignment has been done *via* 2D-COSY and TOCSY NMR.

4.7   Synthesis of *Bis-* (11R-dipyridophenazine) copper (II) complexes

The planar dipyridophenazine ligands were complexed to the copper (II) core to yield the final *bis* – $[Cu(11\text{-R-DPPZ})_2]^{2+}$ complexes. These were prepared by reacting the 11-substituted DPPZ planar ligands (Scheme 4.1) in a 2.1 : 1 ration to the copper (II) chloride salt. The reactions were carried in MeOH as the copper salt was highly soluble in MeOH and the ligands partially. Almost immediately the final crude product would begin to precipitate out of solution. These resulting crude products were than washed with $CHCl_3$ in order to dispel any unreacted ligand and then finally with MeOH to remove any unreacted copper (II) salt.
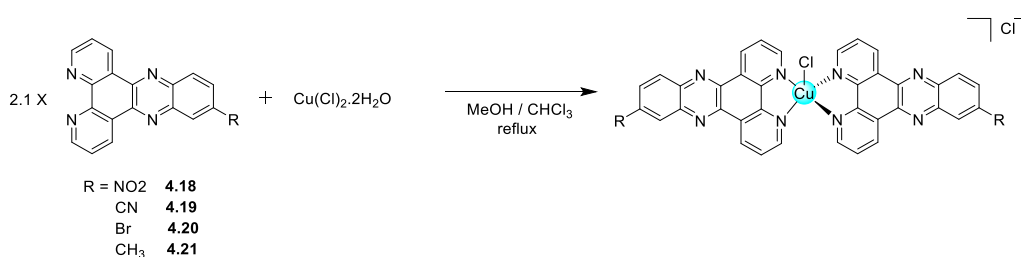
Scheme 4.1: Generic outline of the synthesis of Bis – (11-R-dipyridophenazine) copper (II) complexes.

The characterisation of these compounds was based on elemental analysis (Table 4.0), IR, HR-MS (Figure 4.16) and UV-Vis. Due to the paramagnetic properties displayed by the copper (II) core, NMR could not be used for characterisation.

Table 4.0: Elemental analysis of final compounds.

Elemental analysis

Number	Formula	Calculated for %	Found %
4.3 - NO₂	$C_{36}H_{18}Cl_2CuN_{10}O_4$	C 54.80, H 2.30, N 17.75	C 54.37, H 2.03, N 17.44
4.4 - CN	$C_{36}H_{18}Cl_2CuN_{10}$	C 60.93, H 2.42, N 18.70	C 61.24, H 2.98, N 18.19
4.5 - Br	$C_{36}H_{24}Br_2Cl_2CuN_8$	C 50.46, H 2.12, N 13.08	C 50.87, H 2.60, N 13.59
4.6 – CH₃	$C_{38}H_{24}Cl_2CuN_8$	C 62.77, H 3.33, N 15.41	C 62.28, H 3.10, N 15.78
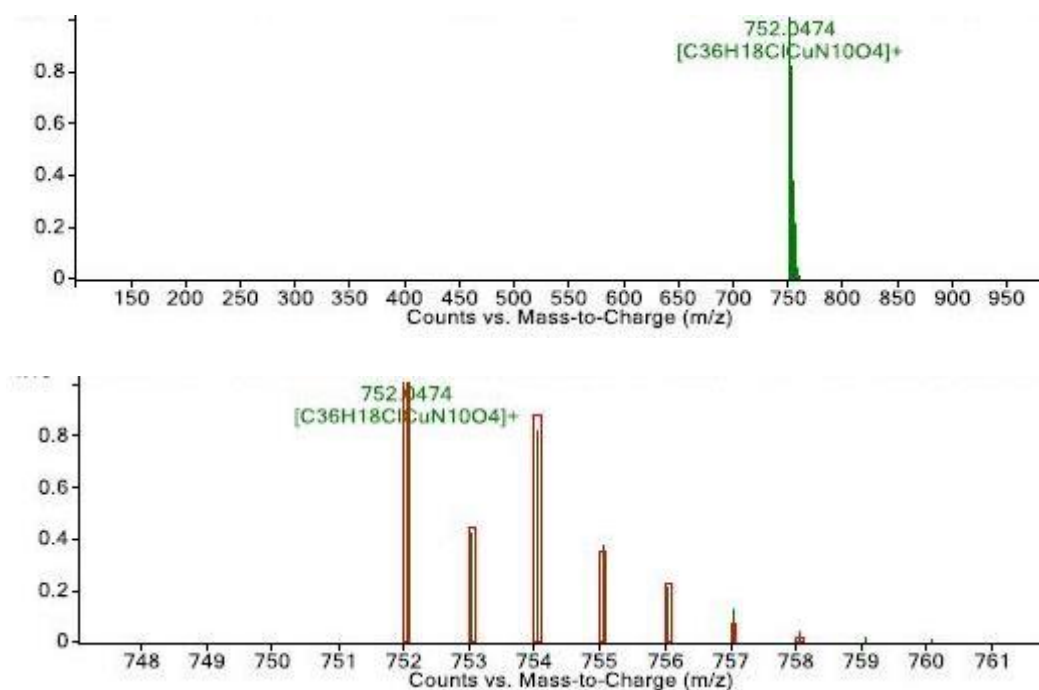
Figure 4.16. HR-MS (ESI +) of compound **4.3** *m/z* Calculated for $C_{36}H_{18}ClCuN_{10}O_4$ [M – Cl⁻] 752.0497, Found 752.0474.

The mass spectra for the species corresponds to the mono-cationic metal scaffold with the loss of a single chloride (most likely from the outer sphere). With the removal of a single chloride the molecule now presents itself as an overall positive charge of 1. For example, the peak observed in complex **4.3** (Figure 4.16) corresponds to the species *Bis* - [Cu(11-nitro-DPPZ)₂(Cl)] ⁺ with a 99.56 % isotope match score. The same was observed for complex **4.4.** However complex complexes **4.5** and **4.6** were ionised with a sodium with **4.5** showing the loss of a single chloride plus a sodium in which case this would indicate the Cu(II) being reduced to Cu(I).The HR-MS spectra for these compounds can be viewed in the appendix in full.

4.8   Uv-Vis studies of *Bis*- (11R-dipyridophenazine) copper (II) complexes

UV-Vis studies were conducted and in are shown the spectra in the range 290-900 nm (Figure 4.17). The first set of experiments were run over 290 nm to 800 nm at a concentration of 5 μM. For the 560 – 900 nm experiment a concentration of 180 μM was required as the bands are weaker for the d-d transitions.

Uv-Vis trace of all four compounds 4.3 - 4.6
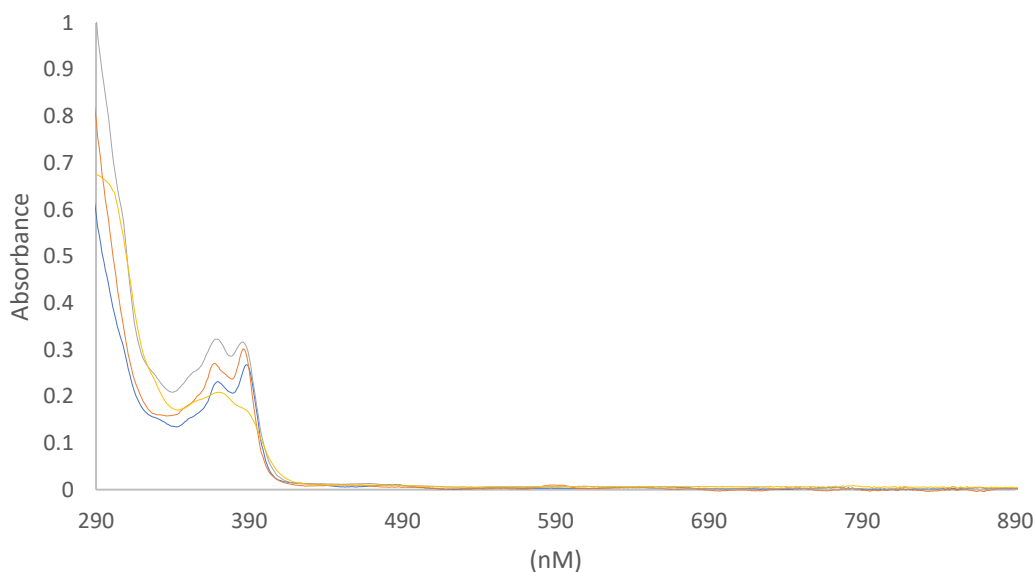
Figure 4.17. Uv-Vis spectra of compounds **4.3 – 4.6** (• NO$_2$), (• CN), (• Br), (• CH$_3$).

The UV-Vis spectra of the compounds in (DMSO) show the intra ligand transitions π-π*, n-π* between 372 and 389 nm as strong peaks. The LMCT and MLCT are quite strong and overlap with the π-π*, n-π* transitions. These values are very close to those reported experimentally for the unsubstituted copper (II) bis complex of DPPZ of 355 nm.[208] These values were confirmed theoretically by TDDFT calculations, discussed later. The weaker d-d transitions were observed 560 – 900 nm (Figure 4.18). This very broad peak which is due to the weak transitions in d* - d is displayed at 710 -760 nm.
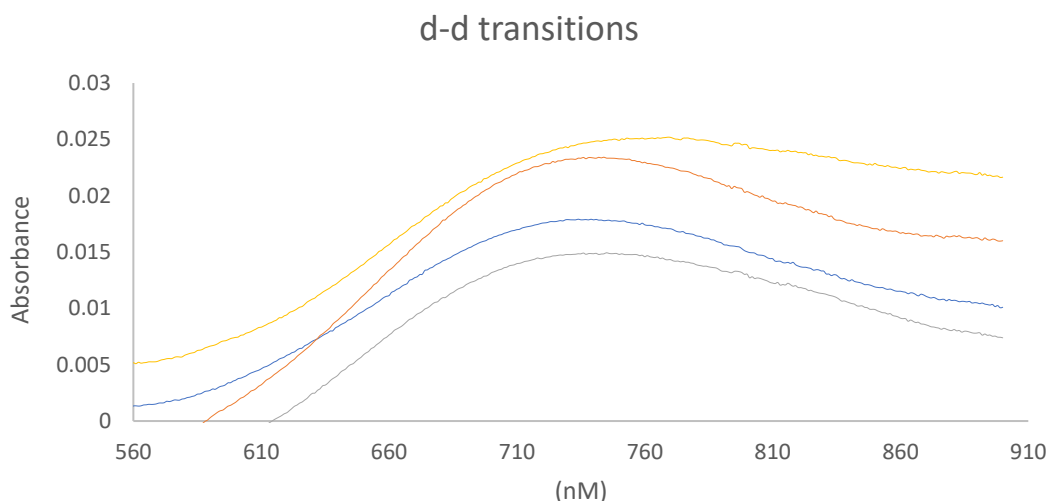
Figure 4.18: UV-Vis 560 – 900 nm displaying the d-d transitions of the four compounds **4.3 – 4.6** (• NO$_2$), (• CN), (• Br), (• CH$_3$).

The stability of the compounds was evaluated through UV-Vis at 5 µM (Figure 4.19) in (DMSO) over a period of 7 days. Compound **4.3** proved to be the most stable over the 7 days with minor changes observed in compounds **4.4 – 4.6**. In order to probe fully what is happening to these compounds' extinction coefficients would need to be computed and further studies carried out from there.
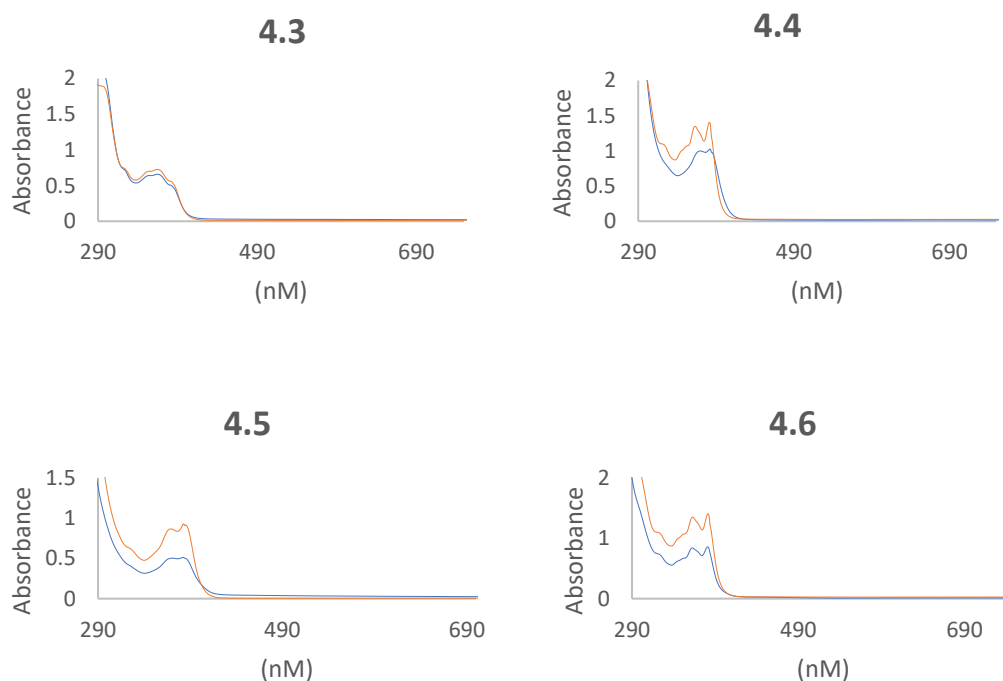
Figure 4.19: UV-Vis spectra of the four compounds 4.3 **– 4.6.** Day 1 (•) and day 7 (•)

4.9   Ethidium bromide displacement assays

In order to establish if the compounds were capable of interacting with the DNA, ethidium bromide displacement assays were carried out in a 1:1.6 ratio (DNA:EtBr) in order to completely saturate the DNA helix with EtBr. EtBr is a known intercalating agent which is very often used as a fluorescent tag. If the molecule, intercalated between the DNA nucleobases, is exposed to ultraviolet light, it will fluoresce with an intense orange colour. As with most similar compounds it is a heterocyclic aromatic compound. The absorption maxima of EtBr are 210 and 285 nm and emits orange light at 605 nm. When EtBr is not intercalating in the DNA, is less fluorescence and this important feature can be exploited to study the drug-DNA interaction. In fact, if a molecule is able to interact with the DNA, it will displace the EtBr and a decrease of the fluorescence intensity is observed. By measuring the fluorescence intensity decrease, is possible to determine if a drug or molecule is a strong or weak intercalator. Ideally a decrease in fluorescence would be seen if the drug or compound added was displacing the EtBr in the helix and thus leading to a quenching of the fluorescence. Stock solutions of the metal complexes were then made up to 1.3 mM and added in very small aliquots in order to not change the volume and concentration in the cuvette. The aliquots started at 4 µL and increased to 20 µL over the course of the experiment. The results of these assays are displayed and discussed below. The solutions were prepared as described in chapter 3 section 3.5.6 with the only difference being the stock solutions were made up to 1.3 mM in DMSO before being titrated into the cuvette which contained the DNA and EtBr in water. Both the ligands and final complexes were evaluated.
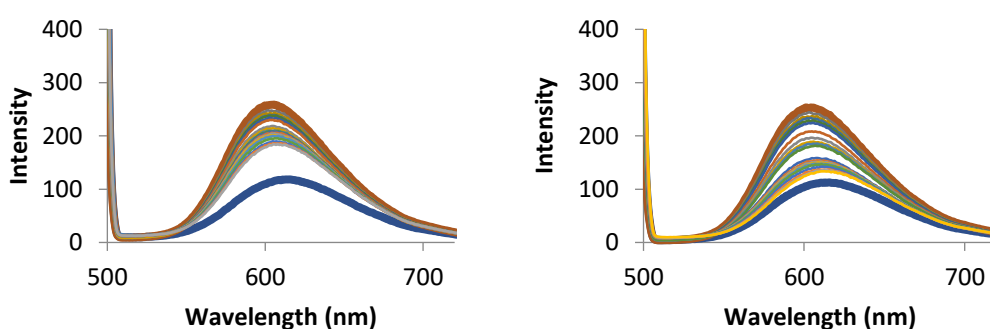
Figure 4.20: Fluorescence quenching of the free 11-nitro-DPPZ **4.18** (left) and its corresponding *bis-*copper (II) complex **4.3** (right).
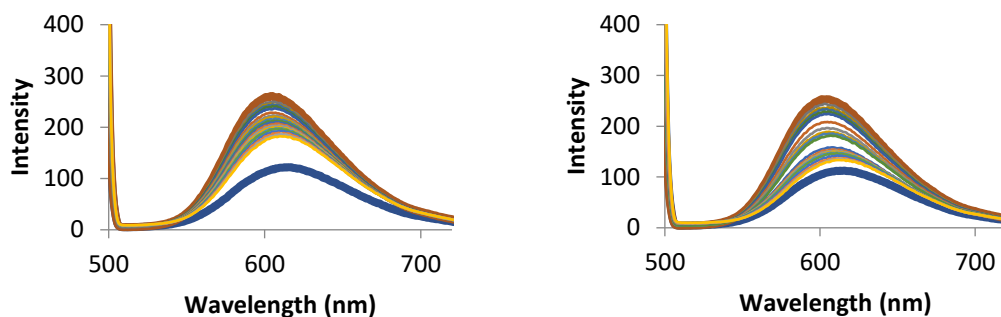
Figure 4.21: Fluorescence quenching of the free 11-cyano-DPPZ **4.19** (left) and its corresponding *bis-* copper (II) complex **4.4** (right).
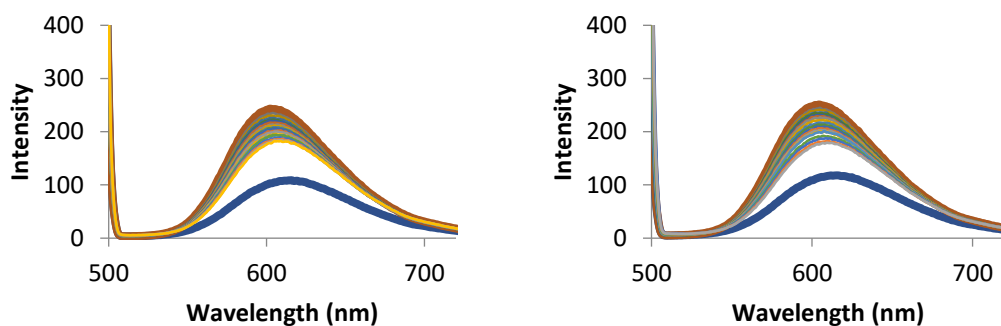
Figure 4.22: Fluorescence quenching of the free 11-bromo-DPPZ **4.20** (left) and its corresponding *bis-* copper (II) complex **4.5** (right).
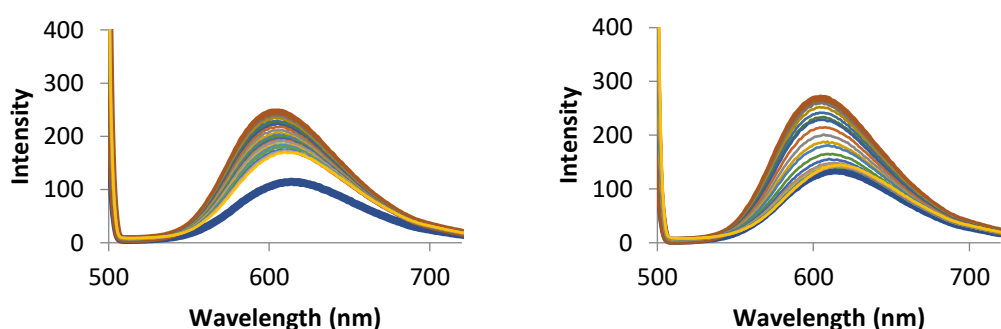
Figure 4.23: Fluorescence quenching of the free 11-methyl-DPPZ **4.21** (left) and its corresponding *bis-* copper (II) complex **4.6** (right).

The copper (II) complexes performed far better than their corresponding free ligands, with the exception of the Bromo complex **4.5**. However, in all cases more than 50% relative quenching was observed and binding constants were able to be established (Table 4.1). The

binding values were calculated using the % relative decrease of fluorescence at 50% and the equation below.

$$E_{EB=} \frac{[EtBr]}{[compound]50\%_{FI}}$$

Table 4.1: Binding constants of ligands (**4.18 - 4.21**) and final copper (II) complexes (**4.3 – 4.6**)

Compound	M(bp)$^{-1}$
4.18	**7.21 x 10^6**
4.19	**8.09 x 10^6**
4.20	**8.08 x 10^6**
4.21	**9.21 x 10^6**
4.3	**8.08 x 10^6**
4.4	**1.82 x 10^7**
4.5	**7.21 x 10^6**
4.6	**3.17 x 10^7**

The free ligands and the final metal complexes displayed binding constants in the region of x10^6 with two of the final complexes showing values in the x10^7 range. These values are very consistent with the values Molphy *et al.* established for [Cu(phen)(DPPZ)](NO$_3$)$_2$ in 2015.[220] Molphy established values of ~ 3x10^7 M(bp)$^{-1}$ for a number of DPPZ derived copper (II) complexes.

Although all eight of the compounds are effective intercalators, the strongest were found to be the copper (II) complexes of cyano **4.4** and the methyl **4.6**. with values of 1.82x10^7 and 3.17x10^7 M(bp)$^{-1}$ respectively. The free 11-methyl-DPPZ ligand **4.21** also displayed a very strong binding constant at a value of 9.21x10^6 M(bp)$^{-1}$. The compounds with weaker interaction with the DNA are the NO$_2$ and Br derivatives, possibly due to the size of the bromine and nitro group atom that can prevent a tight intercalation.

4.10   Biological evaluation of compounds

The final compounds and the free ligands were screened as antibacterial agents against *S. aureus, E. Coli* and MRSA and then against *C. Albicans* for anti – fungal activity. The four final

complexes and four free ligands were dissolved in 1 mL DMSO to give a stock concentration of 5 mg/mL. Nutrient broth (100μL) was then added to each well of a 96 well plate. Each drug was serially diluted on the plate to give a concentration range 150 - 0.59 μM. The bacteria used were grown overnight and the OD_{600} was adjusted to 0.1 (equivalent to cell density of 4×10^7/ml). The bacterial cells (100 μL) were then added to each well and the growth was measured at 600nm after 24 hrs at 37°C using a spectrophotometer (BioPhotometer). The MIC_{50} values were calculated as the minimum concentration of drug that inhibited growth by 50% and the MIC_{80} for that which inhibits growth by 80 % were calculated from the graphs and are displayed in the tables below (Table 4.2 and 4.3).

Table 4.2: MIC values for free ligands and complexes against *C. Albicans.*

Anti – fungal activity against *C. Albicans*		
Compound:	MIC_{50} [μM]	MIC_{80} [μM]
4.18	476	955
4.19	1010	-
4.20	433	868
4.21	327	1055
4.3	6.09	24.1
4.4	6.42	25.4
4.5	182	-
4.6	210	-

The above data (Table 4.2) indicated that all four of the metal complexes were far more effective at inhibiting the growth than that of each of their respective free ligands. Particularly compounds **4.3** and **4.4** (Nitro and Cyano) were the most potent displaying values < 10 μM for their MIC_{50}. Compounds **4.5** and **4.6** did display activity and both were deemed to be almost twice as active as their respective free ligands. However, MIC_{80} values could not be established as the compounds began to precipitate out of solution at these high concentrations. It was also observed that among the free ligands the methyl substituted DPPZ (**4.21**) displayed the most activity, but its corresponding copper (II) complex performed the worst of all the copper (II) complexes. Bearing this in mind it still did perform over twice as good as the free ligand itself. It seems to be that having the ligands chelated to the copper (II) is certainly increasing the activity in all four cases as the free copper (II) chloride salt displays no activity as all against *C. Albicans*.

Table 4.3: MIC values for free ligands and complexes against MRSA.

Anti – bacterial activity against MRSA		
Compound:	MIC_{50} [µM]	MIC_{80} [µM]
4.18	1016	106
4.19	992	102
4.20	1073	54
4.21	1710	134
4.3	198	6.2
4.4	100	6.5
4.5	91	5.7
4.6	107	6.7

The above table (Table 4.3) displays the MIC_{50} and MIC_{80} values for all four of the ligands **4.18** – **4.21** and their corresponding copper (II) complexes **4.3** – **4.6** against the Methicillin-resistant Staphylococcus aureus bacteria (MRSA). All four of the metal copper (II) complexes were extremely potent at very low concentrations < 7 µM. In fact, it was discovered that they were all much more effective at low concentration than at higher concentrations as can be seen from the table (Table 4.3). The compounds were able to inhibit the growth of MRSA by 80 % at a concentration of roughly 20 times less than that which was required to inhibit it by 50 %. The most active compound was found to be **4.3** (Nitro) with an MIC_{80} of 6.2 µM. Once again, all the copper (II) complexes showed superior activity to that of their free ligands displaying MIC_{80} values of 15-20 times less than their corresponding free ligand. The compounds were also screened against *S. aureus* and *E. Coli* but displayed no activity against these bacteria.

4.11   Computational studies

4.11.1   Geometry Optimisation

In order to gain insight into the electronic structures of the [Cu(DPPZ-R)2]2+ (R = NO_2, CN, CH_3, Br, H) complexes, computational models of these compounds in both their cuprous and cupric state were examined via numerous quantum chemical methods. Geometry optimisations of all structures were performed, and their electronic properties probed via single-point calculations. All calculations presented in this study were carried out using Gaussian 09 (revision E.01).[221] The geometries of all bis(dipyridophenazine)copper(II) complexes were fully optimised without imposing symmetry constraints at the B3LYP-D3/6-

31G(d,p) level of theory.[222], [223], [224],[225]. Subsequent frequency calculations on the optimised geometries were performed to confirm the presence of a true minimum on the potential energy surface by absence of any imaginary vibrational modes. Optimised geometries of complexes A – D in presence of water as a fifth ligand along with the parent complex [Cu(DPPZ)$_2$(H2O)]$^{2+}$ are depicted in Figure 4.24.
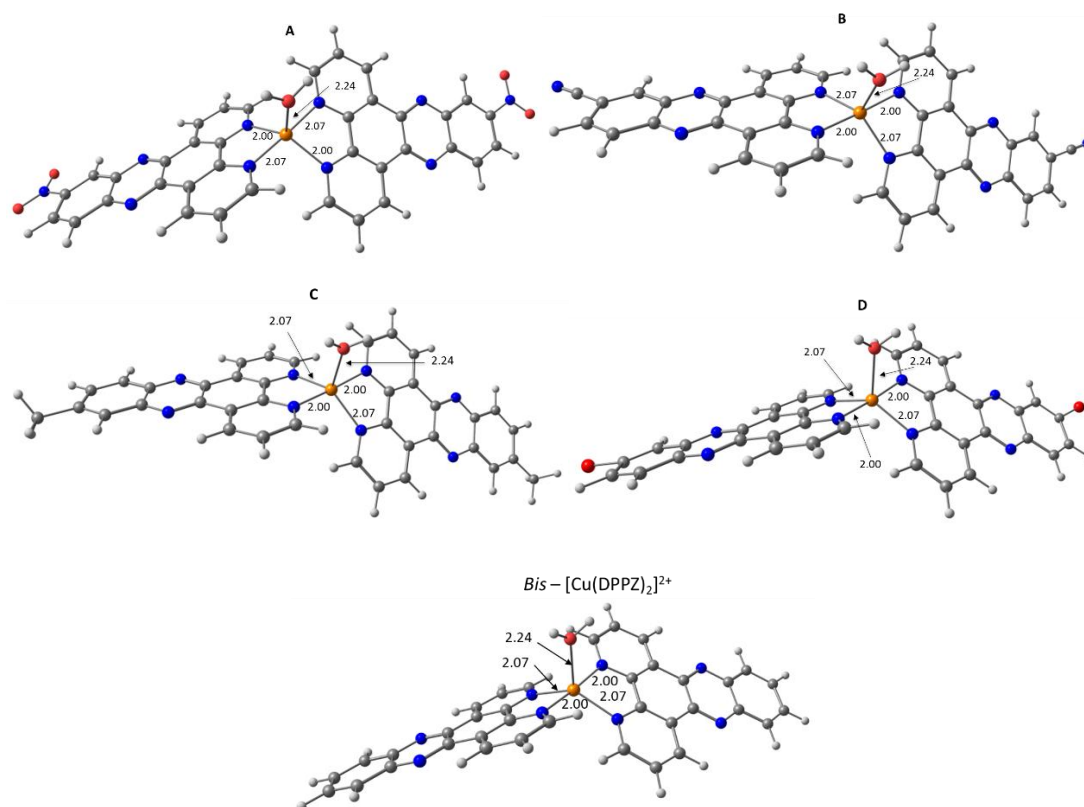
Figure 4.24: Optimised geometries of compounds **A – D** and also the unsubstituted bis – DPPZ compound for reference. (**A** – NO$_2$), (**B** – CN), (**C** – Br), (**D** – CH$_3$).

After carrying out the geometry optimisations for each of the cupric complexes **A – D** it was discovered that there was no notable difference in the bond angles between the five donor atoms on the reference compound [Cu (DPPZ)$_2$(H$_2$O)]$^{2+}$ and that of the four compounds **A – D**. All five of the models examined displayed a distorted trigonal-bipyramidal geometry which is in alignment with similar studies carried out by Madureira *et al*.[226] and Reedijk *et al.* [227] The presence of the aquo ligand renders the four Cu–N bond lengths not equivalent, with two shorter (*trans* Cu–N = 2.00 Å) and two longer (Cu–N = 2.07 Å) distances observed for the axial and equatorial positions, respectively. The Cu–O distance of 2.24 Å for the equatorial aqua ligand is longest in all cases. In all five of the molecular models these distances are virtually indistinguishable, indicating that any substitution in the 11 position leads to no change in the bond length or angle at the copper centre.

The compounds **A** – **D** were then subjected to geometry optimisation with the copper core in oxidation state of +1 and the water ligand removed. These geometries are displayed below **A$_1$ – D$_1$** (Figure 4. 25).
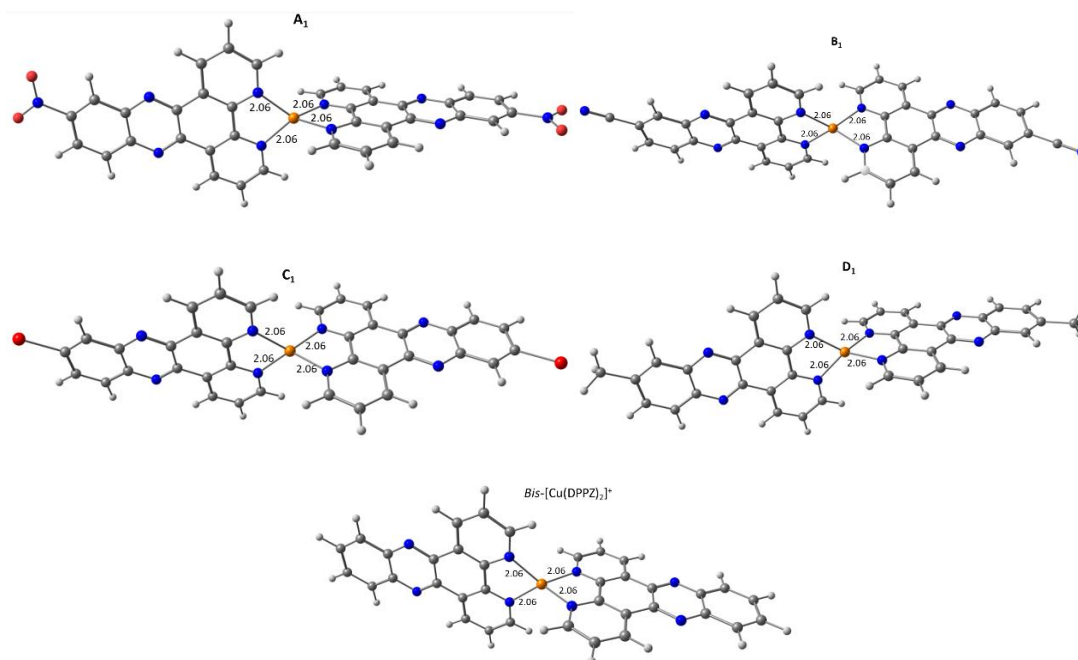
Figure 4.25: Optimised geometries of copper (I) compounds A$_1$ – D$_1$ and also the unsubstituted *Bis* – DPPZ compound for reference. (**A$_1$** – NO$_2$), (**B$_1$** – CN), (**C$_1$** – Br), (**D$_1$** – CH$_3$).

After geometry optimisation of the closed-shell copper(I) complexes it was again established that the substitution in the 11 position had no impact on the bond length from the donor nitrogen's to the copper(I) core. All complexes display approximate D_{2d} symmetry, with all four donor Cu–N distances having equal length of 2.06 Å. These observed distances were very close to the Cu–N = 1.99 Å distances that Huang *et al*. observed for similar compounds with 4 coordinated nitrogen atoms. In summary, the DPPZ complexes discussed above reveal typical geometries as expected for reduced and oxidised copper complexes coordinated by bidentate ligand architectures. [130]

4.11.2   Time-Dependent Density Functional Theory Studies

The copper (II) complexes **4.3** – **4.6** were subjected to Time-Dependent Density Functional Theory (TD-DFT) calculations (B3LYP/SDDALL/6-31G(d,p)) in order to predict their absorption spectra in the UV-visible region of the electromagnetic spectrum. This process enables the

prediction of the theoretical absorption maximum (λmax) and further examine the states involved in the transitions, i.e. characterise the dominant orbital contributions and overlaps within the molecules by means of Natural Transition Orbitals. The computed λmax and experimental λmax are displayed below (Table 4.4) for comparison along with the individual calculated TD-DFT absorption spectra (Figures 4.26 – 4.29).
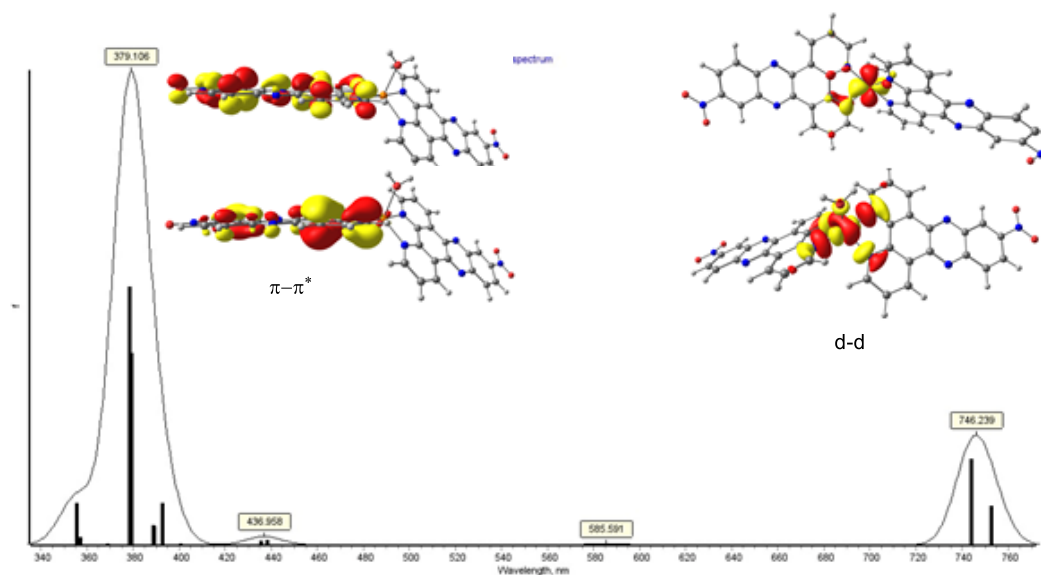
Figure 4.26: TD spectra of compound **4.3** (R = NO$_2$) displaying λ max and ligand based and d-d transitions.
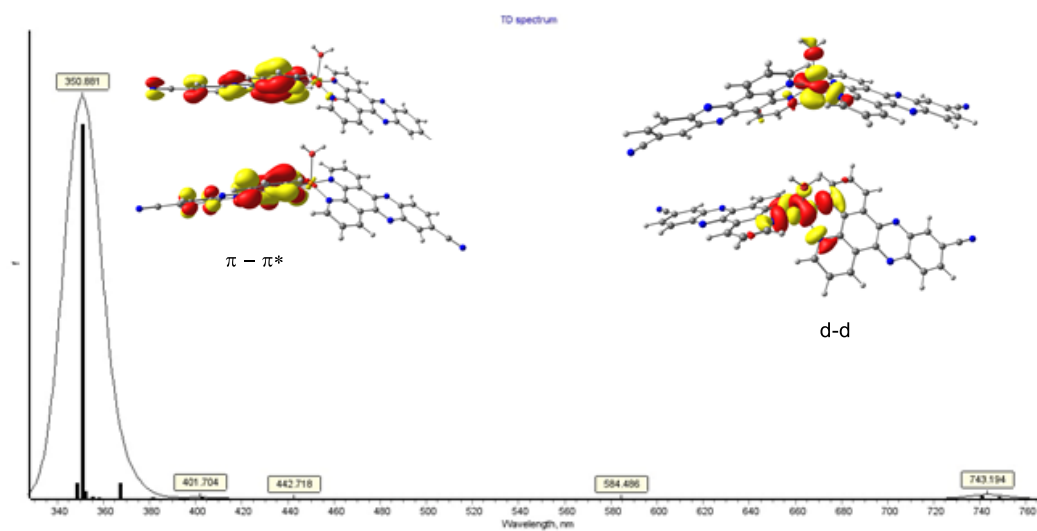
Figure 4.27: TD spectra of compound **4.4** (R = CN) displaying λ max and ligand based and d-d transitions.
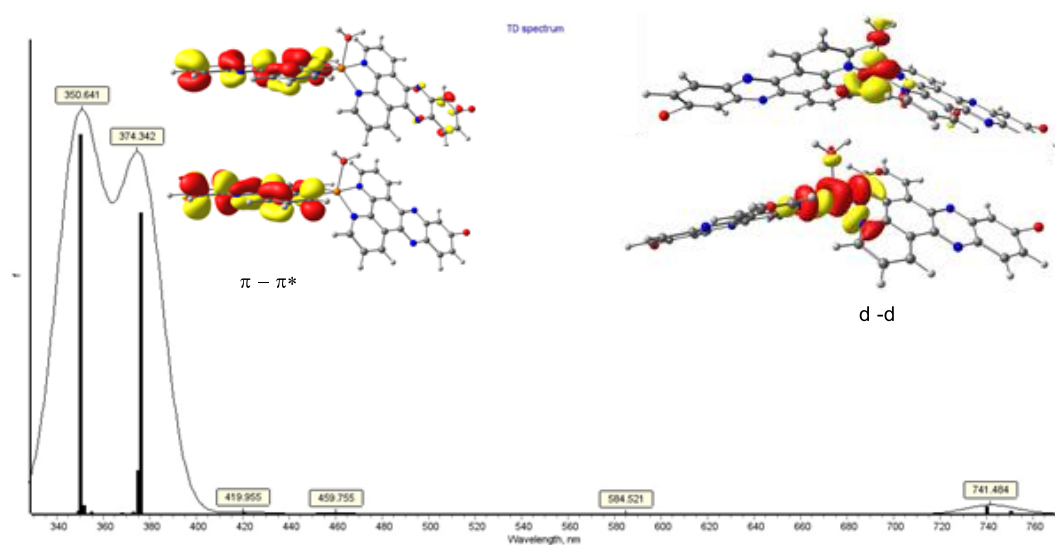
Figure 4.28: TD spectra of compound **4.5** (R = Br) displaying λ max and ligand based and d-d transitions.
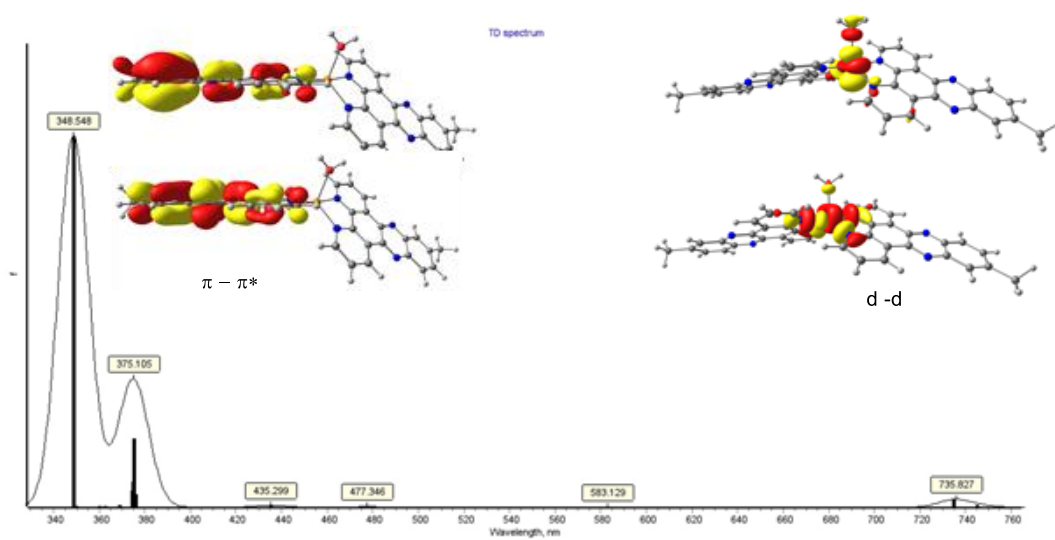
Figure 4.29: TD spectra of compound **4.6** (R = CH_3) displaying λ max and ligand based and d-d transitions.

The above data was compared with that of the experimental data gathered in section 4.4.3 of this chapter and the results are compared below (Table 4.4).

Table 4.4: Comparison of TDDFT λ max and experimental λ max from section 4.4.3

λ max (nM)		
Compound:	TDDFT	Experimental
4.3	379.10	372.00
4.4	350.88	349.63
4.5	350.61	351.02
4.6	348.54	350.14

The calculated values for the $\pi - \pi^*$ interactions were found to be very close to the experimental values. In the case of compound **4.3** a noticeable shift in the band was observed in both the TDDFT and experimental value. The d-d transitions were also examined and compared with those found in section 4.4.3 (Figure 4.18) these results are displayed below (Table 4.5).

Table 4.5: TDDFT and experimental values of d-d transitions.

d – d transitions (nM)		
Compound:	TDDFT	Experimental
4.3	746.23	741.02
4.4	743.19	747.40
4.5	741.48	744.16
4.6	735.82	738.79

Once again excellent agreement between TD-DFT and the experimental values was found. Although the UV-vis experiment generally establishes a single value for the maximum of the absorption band λ_{ma}, it is clear that several absorptions in the 290–350 nm region corresponding to n-π^* and π–π^* excitations cause broadening of the bands observed. The most prominent band in this region is certainly that of the π–π^* transitions, however some transitions also involve metal-to-ligand and ligand-to-metal character. The d-d transitions although weak were still able to be observed and did match those from the experimental values very closely.

In order to get further insight into the electronic structure of the Cu(II) complexes Molecular Orbital (MO) diagrams were constructed for $[Cu(DPPZ)_2]^+$ and $[Cu(DPPZ)_2(H_2O)]^{2+}$. Due to the open shell nature of the copper (II) complexes, two spin-orbital manifolds are obtained, corresponding to α- and β-spin electrons. These diagrams are displayed below (Figure 4.30) for the copper(I) and (Figure 4.31) for the copper(II).

From the orbital diagram of the Cu(I) complex five orbitals with dominant copper character can be readily identified, forming a set of orbitals near the HOMO-LUMO gap. In the chosen cartesian coordinate system, the d_{yz} orbital is the highest-lying orbital. These five d-orbitals accommodate the 10 electrons associated with the Cu(I) metal centre. Despite the fact that some π-symmetric ligand-centred orbitals are interwoven into this metal manifold, the observed diagram corresponds to a normal ordering of orbitals.
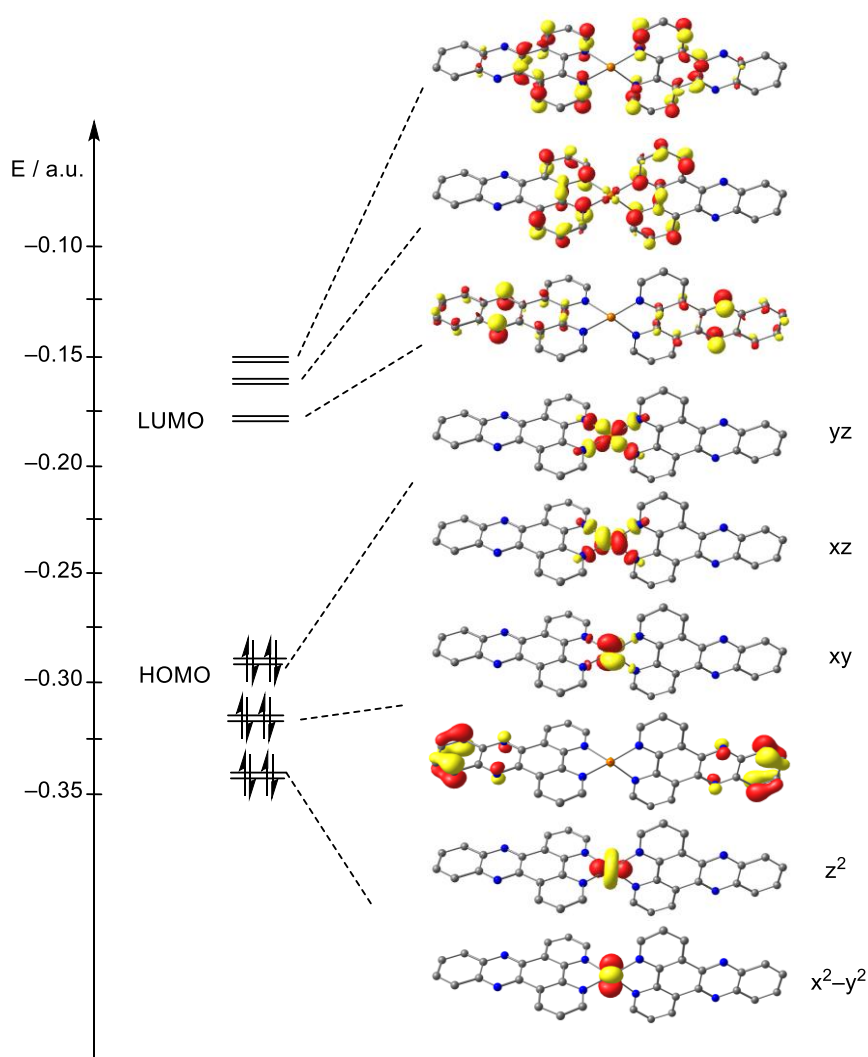
Figure 4.30: Molecular orbital diagram displaying the frontier orbitals and relative energies for exemplary complex $[Cu(DPPZ)_2]^+$.
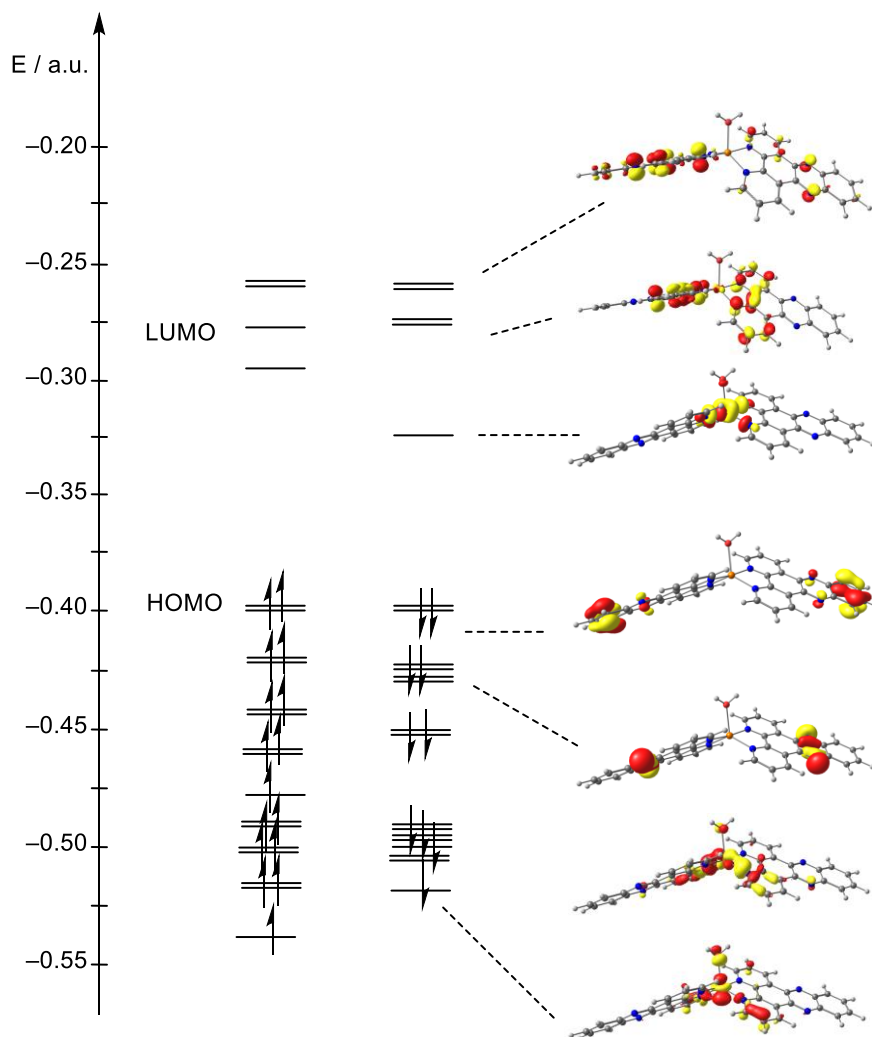
Figure 4.31: Molecular orbital diagram displaying the frontier orbitals and relative energies for exemplary complex [Cu(DPPZ)$_2$(H$_2$O)]$^{2+}$.

The MO diagram for the Cu(II) complex is unambiguous and typical for a d^9 system with the electron hole in the d$_{x^2-y^2}$ orbital. Removal of the single electron slightly stabilises the **α**-spin manifold relative to their **β**-spin counterparts. As stated above due to the open-shell nature of the copper(II) system, promotion of a single **β**-electron from energetically lower-lying occupied d orbitals can occur into the d$_{x^2-y^2}$ acceptor orbital. Additionally, a range of higher-energy vacant π* orbitals are available for transitions. Here the MO diagrams for the *Bis* – [Cu(DPPZ)$_2$]$^{2+}$ complex are only a visualisation tool to aid the description of the assignment of these electrons.

4.11.3 Redox studies

A DFT approach for the calculation of redox potential was employed for both the copper (I) and copper (II) *Bis* – [Cu (DDPZ)$_2$] $^{2+/+}$ complexes in order to establish potential redox values. The redox potentials were calculated in terms of Gibbs free energy change of the redox reaction at the theory level of CAM-B3LYP/6-31+G(d,p). With the overall Gibbs free energy change being partitioned into the Gibbs free energy change of the gas phase reaction and the Gibbs free energy change of solvation. In addition, the calculated Gibbs free energy change of solvation is corrected by a unified correction factor of - 0.258 eV as the second-layer Gibbs free energy change of solvation and other interactions for each redox reaction. The equations used are displayed below along with the redox potentials for reduction of the 5-coordinate copper (II) complex with an aqua in the 5th to the 4 – coordinate copper (I) complex and then for the oxidation back to copper (II). Using an adapted procedure from Li *et al.* [228] the below values were established (Table 4.6).

Due to copper (I) and copper (II) forming compounds that display different coordination numbers and structures, and the reduction of Cu(II) may involve an inner – sphere mechanism particularly in aqueous media.

$$[CuL(H_2O)_n]^{2+}(aq) + e^-\ (g) \longrightarrow (n\text{ - }m)\ H_2O\ (aq) + [CuL(H_2O)_m]^+\ (aq) \quad \textbf{(1)}$$
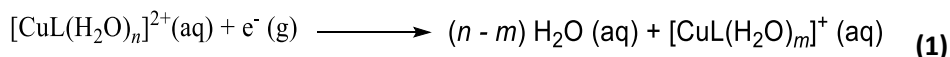
where the oxidised species is abbreviated as *O* below, the reduced species abbreviated as *R* and the multidentate ligand as *L* the standard Gibbs free energy change is given by the equation **(2)** below.

$$\Delta G^o_{O|R} = \Delta G^o(R(aq)) + (n\text{ - }m)\Delta G^o(H_2O(aq))\text{ - }\Delta G^o(O(aq)) \quad \textbf{(2)}$$

In order to evaluate the standard Gibbs free energy change from gas phase calculations and solvation theory calculations a Born – Haber cycle was adopted from Li *et al*. (Figure 4.32).
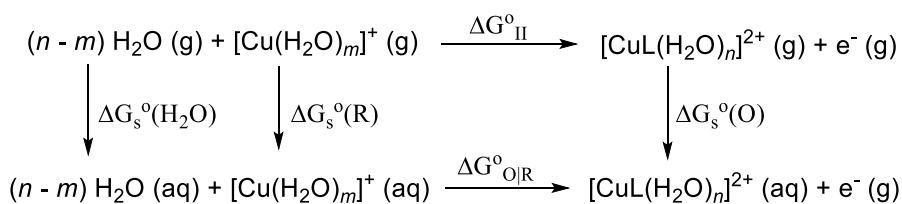
Figure 4.32: Born – Haber cycle for the calculation of redox potentials of copper complexes. [228]

The Born–Haber cycle was designed (Figure 4.32), and the Gibbs free energy change is

$$- \Delta G^{o}_{O|R} = \Delta G_{II} + \Delta\Delta G_{s}^{o} \qquad \textbf{(3)}$$

Where the Gibbs free energy for the change in solvation is

$$\Delta\Delta G = \Delta G_{s}^{o}(O) - \Delta G_{s}^{o}(R) - (n - m)\Delta G_{s}^{o}\ (H_{2}O) \qquad \textbf{(4)}$$

And the Gibbs free energy for the gas phase oxidation reaction is

$$\Delta G_{II}^{o} = \Delta G^{o}(O(g)) - \Delta G_{s}^{o}(R(g)) - (n - m)\Delta G_{s}^{o}\ (H_{2}O(g)) \qquad \textbf{(5)}$$

The redox potential relative to the standard hydrogen electrode (SHE) is evaluated as the standard Gibbs free energy change subtracting the Gibbs free energy change for the standard hydrogen electrode ΔG^{o}_{SHE} [229]

$$E^{o}_{O|R} = \frac{1}{F}\ (\Delta G^{o}_{O|R} - \Delta G^{o}_{SHE}) \qquad \textbf{(6)}$$

where F is the Faraday constant, and the widely accepted value of ΔG^{o}_{SHE} is -4.28 eV.[230] The Gibbs free energy of a gas molecule at temperature *T* is evaluated as

$$G_{T} = \varepsilon_{DFT} + \varepsilon_{ZPE} + G_{th} \qquad \textbf{(7)}$$

where ε_{DFT}, ε_{ZPE}, and G_{th} are the total energy, zero-point energy, and thermal corrections made to the Gibbs free energy at temperature *T*.

Table 4.6: Redox potentials of the five Bis compounds without an aqua (top) and with an aqua molecule (bottom)

Compound:	ΔG_{solv}	$E_{O|R}$ (eV)
Bis – [Cu(dppz)$_2$]$^{2+}$	-143.06	- 0.154
Bis – [Cu(11-methyl-dppz)$_2$]$^{2+}$	-139.14	- 0.140
Bis – [Cu(11-cyano-dppz)$_2$]$^{2+}$	-160.91	- 0.182
Bis – [Cu(11-nitro-dppz)$_2$]$^{2+}$	-160.69	- 0.217
Bis – [Cu(11-bromido-dppz)$_2$]$^{2+}$	-146.98	- 0.184
Bis – [Cu(dppz)$_{2(}$H$_2$O)]$^{2+}$	-140.19	- 0.871
Bis – [Cu(11-methyl-dppz)$_2$H$_2$O)]$^{2+}$	-136.54	-0.859
Bis – [Cu(11-cyano-dppz)$_2$(H$_2$O)]$^{2+}$	-157.75	- 0.895
Bis – [Cu(11-nitro-dppz)$_2$(H$_2$O)]$^{2+}$	-157.73	- 0.912
Bis – [Cu(11-bromido-dppz)$_2$(H$_2$O)]$^{2+}$	-14.37	- 0.889

4.12   Theoretical DNA intercalation and binding studies of Bis – [Cu (DPPZ)$_2$]$^{2+}$

As a final part to the computational studies a set of all 10 DNA base pair dimers were optimised at B3LYP/6-31G(d,p) level of theory. A graphic representing some of these combinations is displayed below (Figure 4.32). The binding energies were determined by optimising each DNA step intercalated by the unsubstituted parent complex [Cu(DPPZ)^2]$^{2+}$ and subsequently computing a single point energy of the DNA step in the absence of the copper complex. The binding energy was obtained as the energy difference shown in the following equation

$$E_{bind} = E_{intercalated}(opt) - E_{complex}(opt) - E_{step}(fixed)$$

The energy required to distort the DNA step from its relaxed and closed geometry to the open form that is able to accept the copper complex intercalator is obtained from

$$E_{distort} = E_{step}(fixed) - E_{step}(opt)$$

Where fixed indicated that the geometry was held constant at the atomic positions of the intercalated DNA step and opt indicates that the DNA step was allowed to relax to the nearest minimum-energy geometry on the potential energy surface. The various dimer base pair steps were then probed using optimised structure of $[Cu(DPPZ)_2]^{2+}$ in order to establish binding energies (Table 4.7) and identify and preferential site or step for the molecule to dock in. The graph below (Figure 4.32) displays the E_{bind} and $E_{distort}$ energies for each DNA dimer base pair in kcal mol^{-1}.
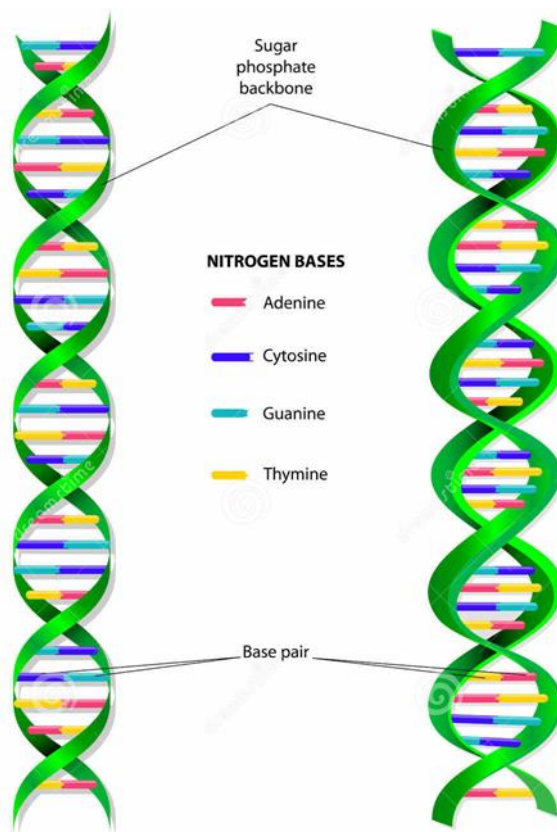
Figure 4.32: Graphic displaying multiple combinations of the dimers examined in a DNA helix.
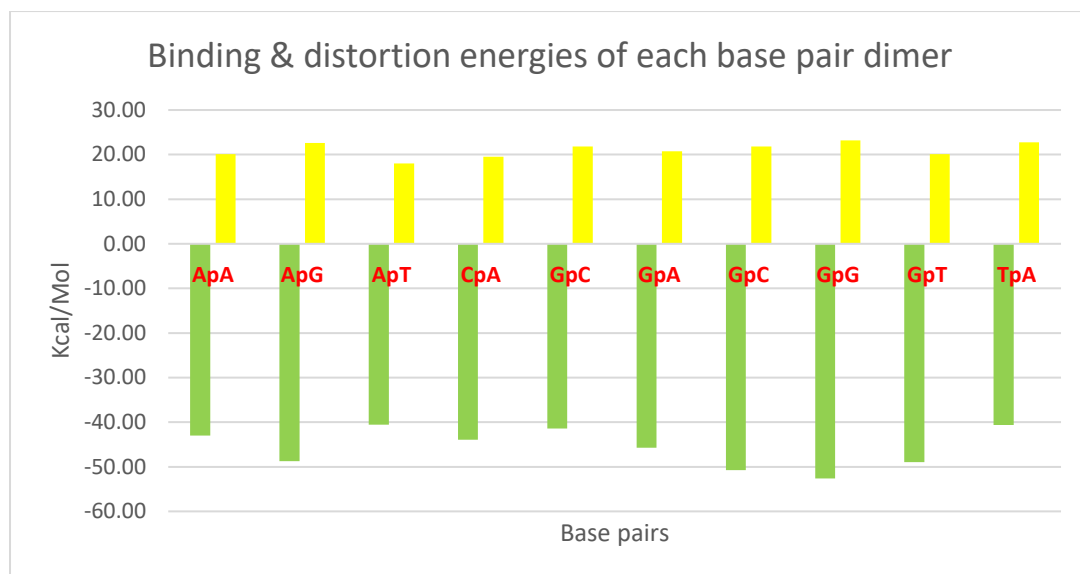
Figure 4.33: Binding (•) and distortion (•) values for each dimer base pair set.

Whilst this only serves as a first approximation, the data clearly shows a slight preference for the GG–CC the GC-CG steps with the largest absolute binding energies (> 50 kcal mol^{-1}). This may indicate that there is a preference for binding to the major grove in the helix with this type of molecule which is in line with experimental studies carried out by Molophy *et al*. in 2018. [231] Figures showing the optimised geometries of these two base pair steps in a frontal and side view for clarity (Figure 4.34 & 4.35), with [Cu(dppz)$_2$)]$^{2+}$ intercalated into the base pair with a distance of 3.53 Å from the ligand to the ceiling of the step and 4.32 Å to the bottom of the cavity showing the step was more prone to breathing open to facilitate the insertion of the compound.
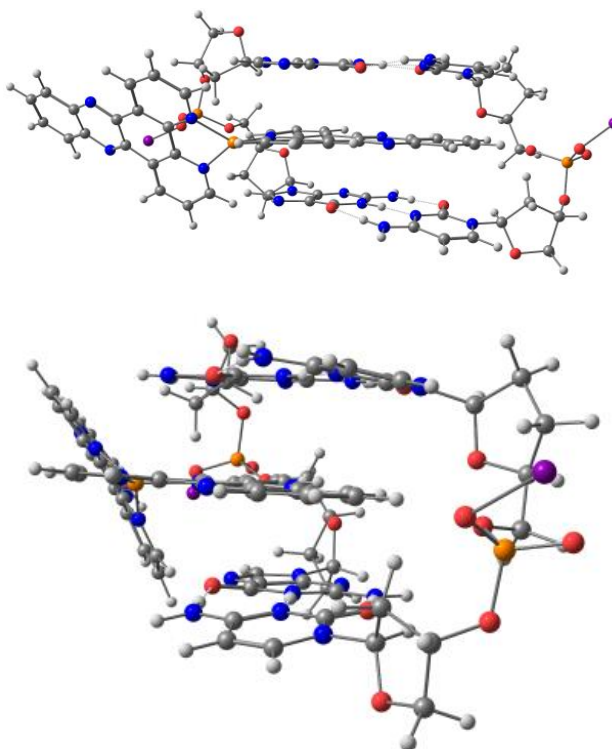
Figure 4.34: GG-CC step frontal view (top) and side view (Bottom).

As can be seen in figure 4.34 the compound sits relatively flat into this base pair causing minimal distortion to the step. Below is shown (Figure 4.35) the base pair set of GC-CG.
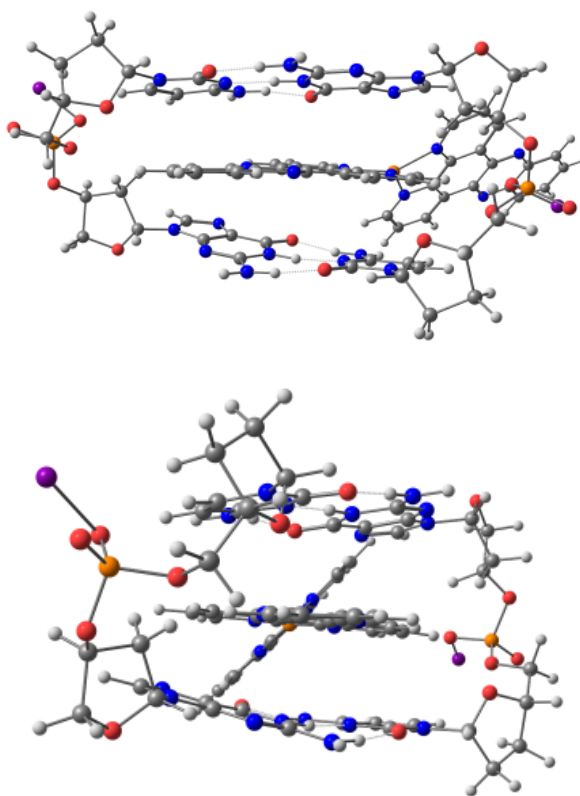
Figure 4.35: GC-CG step frontal view (top) and side view (Bottom).

Once more very little distortion is shown, and the molecule seems to slip nicely into this base pair dimer with a distance of 3.60 Å from the planar ligand to the ceiling of the dimer and 4.1 Å to the floor of the dimer set. In the case of the base pairs from the minor groove side of the helix severe distortion was observed when intercalating the molecule into these base pairs. Specifically with the sets TA-AT and AT-TA. However almost every set displayed binding energies far greater than those observed for the sets GG-GG and GC-CG. An example of this distortion is displayed below (Figure 4.36).
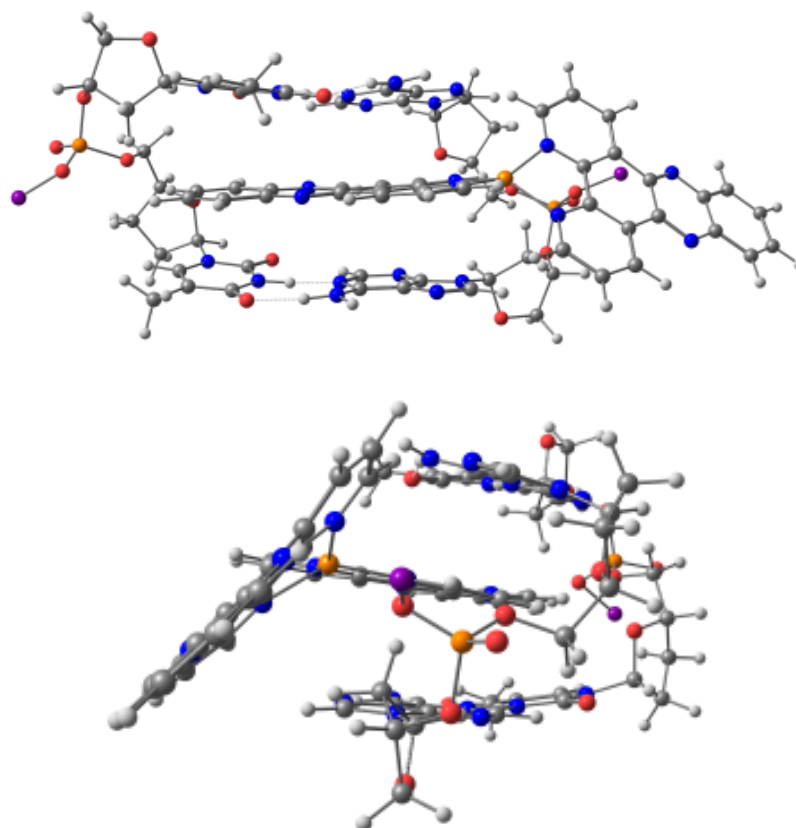
Figure 4.36: AA-TT step frontal view (top) and side view (Bottom).

A clear bending of the molecule around the dimer step is observed but also the phosphate backbone appears to be under duress and has lost its structural rigidity leading to distortion of the step and a larger binding energy along with a value of 3.31 Å from the compound to the ceiling of the dimer and 3.33 Å to the bottom of the dimer cavity. It appeared to me much more difficult for this dimer to breathe open to allow the insertion of the compound. The energies computed are displayed in full below (Table 4.7)

Table 4.7: Binding energies computed for Bis – [Cu(Dppz)$_2$]$^{2+}$ in each base pair dimer step of a full twist in DNA helix.

	E bind Kcal/mol	E distort Kcal/mol
AA-TT	-43.03	20.11
AG-TC	-48.73	22.65
AT-TA	-40.57	17.98
CA-GT	-43.91	19.53
CG-GC	-41.40	21.86
GA-CT	-45.70	20.76
GC-CG	-50.72	21.82
GG-CC	-52.64	23.19
GT-CA	-48.92	20.09
TA-AT	-40.62	22.78

4.13 Chapter Conclusions

In this chapter, four novel *Bis* – [Cu(11-R-Dppz)$_2$]$^{2+}$ were synthesised, characterised, and screened for anti-microbial properties and as DNA intercalators. The ligands were prepared by Schiff base chemistry and then attached to the copper (II) core. The compounds were evaluated for stability via Uv- Vis spectroscopy at a 7-day interval and it was revealed that all four novel compounds were stable in DMSO. The compounds were then examined as DNA intercalators *via* Ethidium Bromide displacement assays, all four compounds were found to have greater binding affinities than the free ligands but particularly compounds **4.4** and **4.6** displaced values in the x10^7 M(bp)$^{-1}$ range which were in line with previously reported values for the unsubstituted *Bis* – [Cu (Dppz)$_2$]$^{2+}$. The final compounds and the ligands were then screened for their antibacterial properties against *S. aureus, E. Coli* and MRSA and for anti-fungal properties against *C. Albicans*. It was established that most active compound against MRSA was compound **4.3** (nitro) with a MIC$_{80}$ of 6.2 µM but all of the copper (II) complexes displayed greater activity than the corresponding ligands. After screening against the *C. Albicans* it was discovered that compounds **4.3** and **4.4** were the most active with MIC$_{50}$ values of 6.09 and 6.42 µM respectively. No significant activity was recorded against *S. aureus* or *E. Coli.* In the final part of this chapter the four complexes were optimised using a

density functional theory approach. In each case it found that the bond distance from the donor atom to the copper (II) core was not affected in any way by the substitution in the 11 position. Time dependant density functional theory experiments were carried out and the Uv trace was compared to that of the experimental trace confirming very close values for both the MTLCT and LTMCT bands and also the d-d transitions. The final study involved the optimisation of 10 dimers of the base pairs found within the DNA helix followed by the insertion of a molecule of *Bis* – [Cu (Dppz)$_2$]$^{2+}$ and these energies were extrapolated and evaluated. A preference was shown for the GG-CC and GC-CG dimers, which would confirm the preference for the major groove in the DNA helix.

4.14   Materials and methods

All reagents and reactants were purchased from commercial sources. The sources used were Sigma Aldrich, FluoroChem and Tokyo Chemical Industry. All solvents were used without further purification. All NMR spectra were recorded on a Bruker Advance spectrometer with the probe at 293K, operating at 500MHz for the ^{1}H and at 125 MHz for ^{13}C nuclei. Spectra were recorded in CDCl$_3$ or DMSO using Me4Si as the internal standard. All chemical shifts are in ppm. Infrared (IR) spectra were recorded in the region 4000 - 400 cm-1 on a Perkin Elmer precisely spectrum 100 FT/IR spectrometer. The solid samples were run using ATR. Elemental analyses (carbon, hydrogen, and nitrogen) were performed with a PerkinElmer 2400 series II analyser. ESI mass spectra were recorded in positive mode with an Agilent 6200 Series TOF LC/MS system. UV-Vis spectra were recorded in a Perkin Elmer precisely Lambda 35 UV/Vis spectrometer.

4.14.1   Anti – Candida susceptibility testing

The metal-free ligands (**4.18 – 4.21**) and their Cu (II) complexes(**4.3 – 4.6**) were tested for their antifungal activity against a clinical isolate of the fungal strain C. albicans (ATCC 10231) The screening was carried out according to the broth microdilution susceptibility protocol method (NCCLS). Isolates were grown for 24 h on SDA plates at 37°C. Cells were suspended in sterile PBS (phosphate buffered saline) to a concentration equal to a 1.0 McFarland standard (1x10^6) and further diluted (1:100) with minimal media (MM). All compounds were prepared as 1% (v/v) solutions in DMSO, and each compound was tested in the range of 1–50lgmL^{-1}. Plates were incubated in an Anthos plate reader for 24 h at 37°C with continuous shaking. Each compound was screened in triplicate and three independent experiments were

performed. The stock solution of the compounds which were prepared initially at lower concentration (0.001 g mL^{-1}) yielded a clear solution.

4.14.2 MRSA susceptibility assay

All workspaces were washed down with 70% (v/v) ethanol prior to use. Bacterial strains were taken from nutrient agar plates and cultures were grown in nutrient broth overnight in an orbital shaker at 37 °C and 200 rpm, in a fully aerated conical flask. The cells were diluted to give an OD_{600} = 0.1. Fresh solutions (200 µg/mL) of the compounds were prepared using distilled water and DMSO, less than 1% DMSO, and made up immediately prior to testing. Compounds with low solubility were tested as fine suspensions. Nutrient broth (100 µl) was added to each well of a 96-well flat-bottomed microtitre plate. An additional 100 µl was added to columns 1 and 2 of the plate. Serial dilutions (1:1) of the test complex were made from columns 12-4 giving a test concentration range of 100–0.39 µg/mL. Bacteria suspensions (100 µl of OD_{540} = 0.1) were added to each well and the plate was incubated for 24 hours at 37 °C. The optical density was read at λ_{max} 540 nm and growth were then quantified as a percentage of control. All assays were run in triplicate. The results were analysed using Excel. The MIC_{50} (Minimum Inhibitory Concentration) and MIC_{80} were taken to signify the concentration of compound that would inhibit the growth of the microorganism in question by 50% and 80%, respectively.

4.14.3 Ethidium Bromide displacement assay

10 mg of DNA sodium salt from salmon testes (Sigma Aldrich) was suspended in 20 ml of deionised water in a beaker. The mixture was allowed stir for 4 hours at room temperature. The DNA solution was divided in 500 µL aliquots. From this was taken 100 µL and placed into 2.9 mL of PBS buffer. Stock solutions of metal complexes and organic ligands were prepared (5 mg compound per 1 mL of solvent) in DMSO and appropriately diluted further with DMSO to obtain 1 mL of a 10 mM solution. A solution of 4.3 µM ethidium bromide in 1 M PBS buffer was prepared. The UV-Vis spectrum was obtained (600 to 200 nm) and the absorbance maximum (ε260) was used to obtain the DNA base pair concentration: 1.4316×10^{-3} M. 3 mL of PBS buffer was added to 3 fresh cuvettes (labelled "blank", "EtBr", "DNA & EtBr"). From the "EtBr" & "DNA & EtBr" cuvettes, 2.1 µL of PBS was removed and replaced with EtBr stock solution. From the "DNA & EtBr" cuvette, 21 µL was removed and replaced with DNA. The fluorescence spectra of each cuvette were recorded (Excitation = 450 nm: 455 - 900nm). To the cuvette was then added 5 µL of compound and the fluorescence spectrum was recorded.

This was repeated with a further 4 x 5 µL, 10 x 10 µL and 5 x 20 µL in order. The concentrations of compound used were optimized, to unsure fluorescence had quenched by at least 50% for each compound by the final addition. Each assay was conducted in triplicate, on three separate occasions. The binding constants were calculated using K = K_{EtBr} x [EtBr]/[compound]50%FI where, K_{EtBr} = 10 x 10^6M(bp)$^{-1}$ and [compound]50%FI is the concentration of compound added when relative fluorescence intensity had decreased by 50%.

4.15 Experimental Procedures for Chapter 4

4.18: Synthesis of 11-nitrodipyrido[3,2-a:2',3'-c] phenazine (11-nitro-DPPZ)
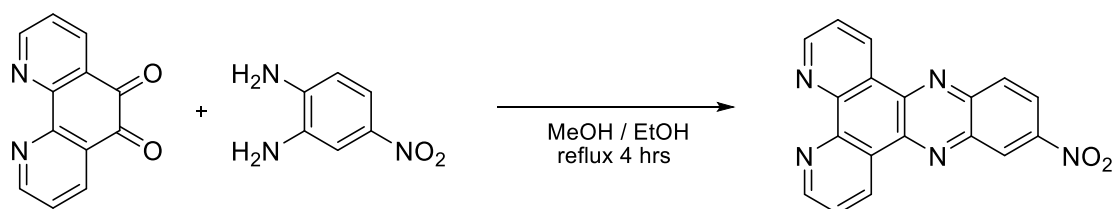
Phendione (0.2 g, 0.95 mmoles) was dissolved into warm EtOH (20 mL, 50 ^{o}C). In a separate flask 2-amino-5-nitrobenzenaminium (0.145 g, 0.95 mmoles) was dissolved into EtOH (20 mL). The solution of phendione was then added dropwise to the 2-amino-5-nitrobenzenaminium. An orange colour was observed. The solution was refluxed at 80 ^{o}C for 4 hours. The solvent was removed under reduced pressure and the yellow / green solid taken back up in CHCl$_3$ (20 mL). The organic phase was washed with brine (2x20 mL). the organic layers were combined and dried over Na$_2$SO$_4$ anhydrous and the CHCl$_3$ removed under reduced pressure. A pale green solid was obtained. Further purification was not required.

Yield: 0.27 g (87 %)

^{1}H NMR (500 MHz, CDCl$_3$) δ 9.66 (dd, J = 9.8, 1.7, 0.8 Hz, 2H), 9.33 (d, 2H), 9.30 (d, J = 2.4 Hz, 1H), 8.69 (d, 1H), 8.53 (d, J = 9.3 Hz, 1H), 7.86 (m J = 8.1, 4.4 Hz, 2H).

^{13}C NMR (126 MHz, CDCl$_3$) δ 153.8, 153.6, 149.2, 148.8, 148.3, 148.2, 144.3, 143.6, 143.2, 141.0, 134.4, 134.2, 131.3, 126.9, 126.92, 126.1, 124.6, 124.6, 123.8.

IR (ATR) 3098, 1979, 1618, 1577, 1480, 1030, 811, 723 cm^{-1}

Elemental Analysis: C$_{18}$H$_9$N$_5$O   % Calculated: C 66.05, H 2.77, N 21.40

                                          % Found: C 66.24, H 2.61, N 21.98

HR-MS (ESI +): *m/z* Calculated for C$_{18}$H$_9$N$_5$O$_2$ + [Na$^+$] 350.0654, Found 350.0650.

4.19: Synthesis of dipyrido[3,2-a:2',3'-c] phenazine-11-carbonitrile (11-cyano-DPPZ)
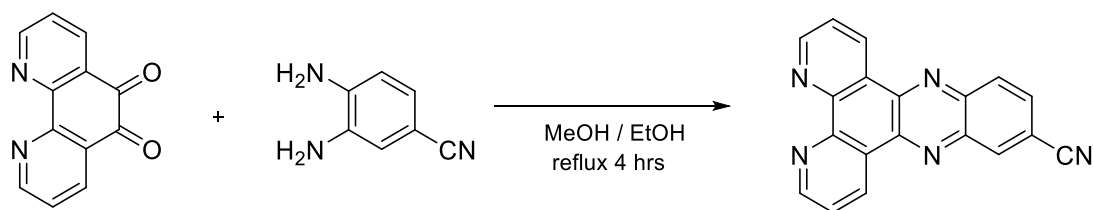
1, 10 – phenanthroline, 5,6 – dione (0.2 g, 0.95 mmoles) was dissolved in warm EtOH (20 mL, 50 °C) and MeOH (30 mL). In a separate flask 3,4 - diaminobenzonitrile (0.139 g, 1.045 mmoles) was dissolved into MeOH (20 mL). The phendione solution was then added slowly and dropwise with stirring to the solution of 3,4 – diaminobenzonitrile. A light orange / brown colour was observed. The reaction was allowed to reflux for 4 hours at 80 °C. A pale yellow precipitate was observed. The solvent was removed under reduced pressure and the pale solid taken back up in CHCl$_3$ (20 mL). The organic phase was washed with brine (2x20 mL). the organic layers were combined and dried over Na$_2$SO$_4$ anhydrous and the CHCl$_3$ removed under reduced pressure. A pale-yellow solid was obtained. Further purification was not required.

Yield: 0.21 g (70 %)

^{1}H NMR (500 MHz, CDCl$_3$) δ 9.59 (ddd, J=13.0, 8.1, 1.7, 2H), 9.31 (ddd, J=4.8, 3.1, 1.8, 2H), 8.74 (d, J=0.6, 1H), 8.44 (d, J=8.7, 1H), 8.03 (dd, J=8.7, 1.7, 1H), 7.82 (dd, J=8.1, 4.4, 2H).

^{13}C NMR (126 MHz, CDCl$_3$) δ 153.6, 153.5, 149.0, 148.8, 143.3, 143.2, 142.8, 141.1, 135.8, 134.1, 131.2, 130.8, 126.9, 124.5, 118.1, 114.0, 77.4 (C-N).

IR (ATR) 3001, 2227, 1576, 1441, 1359, 1217, 1071, 855 cm^{-1}

Elemental Analysis: C$_{19}$H$_9$N$_5$ % Calculated: C 74.26, H 2.95, N 22.79

                                                % Found: C 74.06, H 2.96, N 23.21

HR-MS (ESI +): *m/z* Calculated for C$_{19}$H$_9$N$_5$ + [Na$^+$] 330.0753, Found 330.0756

4.20: Synthesis of 11-bromodipyrido[3,2-a:2',3'-c] phenazine. (11-Bromo-DPPZ)
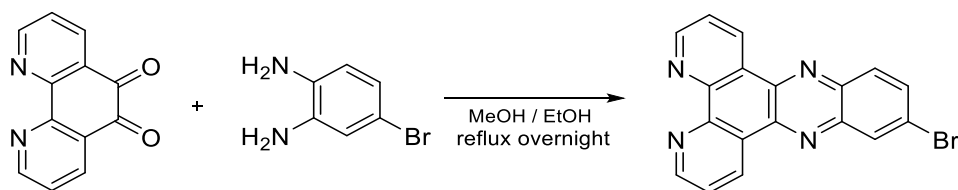
4 – bromobenzene – 1,2 – diamine (0.316 g, 1.69 mmoles) was dissolved in EtOH (12 mL). In a separate flask 1,10 – phenanthroline – 5,6 – dione (0.240 g, 1.41 mmoles) was dissolved in warm EtOH (20 mL, 50 °C). The phendione solution was then added dropwise with stirring to the solution of 4 – bromobenzene – 1,2 – diamine. A pale orange / brown colour was observed. The reaction mixture was refluxed overnight at 90 °C. The solvent was removed under vacuum to yield an orange / brown solid and the pale solid taken back up in $CHCl_3$ (20 mL). The organic phase was washed with brine (2x20 mL). the organic layers were combined and dried over Na_2SO_4 anhydrous and the $CHCl_3$ removed under reduced pressure. A pale-yellow solid was obtained. The Crude yellow solid was recrystallized from MeOH to give orange needles.

Yield: 0.25 g (61 %)

^{1}H NMR (500 MHz, $CDCl_3$) δ 9.50 (td, J = 8.1, 1.8 Hz, 2H), 9.26 (dd, J = 4.4, 1.8 Hz, 2H), 8.51 – 8.43 (m, 1H), 8.18 – 8.10 (m, 1H), 7.95 (td, J = 8.7, 2.9 Hz, 1H), 7.81 – 7.70 (m, 2H).

^{13}C NMR (126 MHz, $CDCl_3$) δ 153.0, 152.9, 148.7, 148.6, 142.9, 141.8, 141.4, 141.2, 134.4, 133.9, 133.9, 131.8, 130.9, 127.4, 127.3, 125.1, 124.3.

IR (ATR) 3227, 1574, 1476, 1403, 1357, 1071, 822, 739 cm^{-1}

Elemental Analysis: $C_{18}H_9N_4Br$ % Calculated: C 59.86, H 2.51, N 15.51

% Found: C 59.78, H 2.46, N 15. 46

HR-MS (ESI +): *m/z* Calculated for $C_{18}H_9N_4Br$ + [H$^+$] 361.0089, Found 361.0085.

4.21: Synthesis of 12-methyldipyrido[3,2-a:3',4'-c] phenazine (11-methyl-DPPZ)
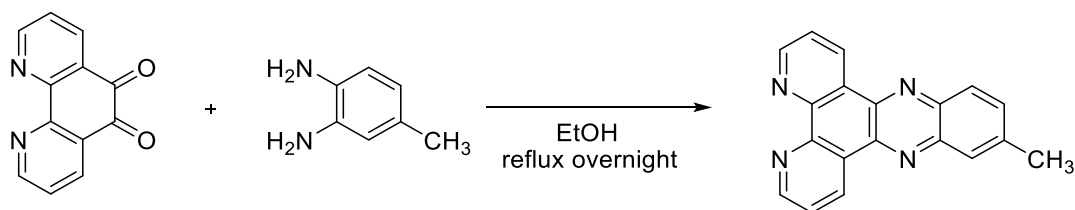
4 – methylbenzene – 1,2 – diamine (0.1392 g, 1.14 mmoles) was dissolved in EtOH (20 mL). In a separate flask 1, 10 – phenanthroline - 5,6, dione (0.24 g, 1.14 mmoles) was dissolved into warm EtOH (20 mL, 50 °C). The phendione solution was then added dropwise with stirring to the solution of 4 – methylbenzene – 1,2 – diamine. The reaction mixture was allowed to reflux over night at 90 °C. The reaction as allowed to cool to room temperature and the solvent removed under vacuum to yield a pale brown coloured solid. The solvent was removed under reduced pressure and the pale solid taken back up in $CHCl_3$ (20 mL). The organic phase was washed with brine (2x20 mL). The organic layers were combined and dried over Na_2SO_4 anhydrous and the $CHCl_3$ removed under reduced pressure. A pale brown solid was obtained. Further purification was not required.

Yield: 0.13 g (48 %)

^{1}H NMR (500 MHz, $CDCl_3$) δ 9.62 (dd, J=8.0, 2H), 9.25 (dd, 2H), 8.23 (d, J=8.6, 1H), 8.11 (s, 1H), 7.80 (dd, J=7.2, 4.2, 2H), 7.79 (dd, J=8.7, 1.6, 1H), 2.71 (s, 3H).

^{13}C NMR (126 MHz, $CDCl_3$) δ 152.6 148.5, 148.4, 142.8, 141.6, 141.3, 141.2, 140.5, 133.8, 133.7, 133.5, 129.6, 129.2, 128.2, 127.9, 127.4, 126.9, 124.2, 22.3.

IR (ATR) 3355, 1623, 1574, 1494, 1358, 1071, 810, 697 cm^{-1}

Elemental Analysis: $C_{19}H_{12}N_4$ % Calculated: C 77.01, H 4.08, N 18.91

                              % Found: C 77.43, H 4.13, N 18.89

HR-MS (ESI +): *m/z* Calculated for $C_{19}H_{12}N_4$ + [H$^+$] 297.1140, Found 297.1139.

4.3: Synthesis of *Bis* - [Cu(11-nitro-DPPZ)₂(Cl)]Cl
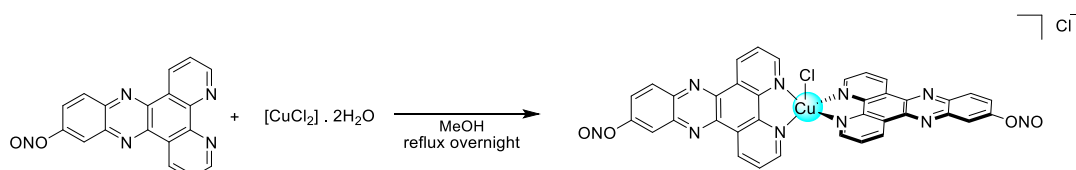
11-nitro-DPPZ (0.180 g, 0.549 mmoles) was dispersed in MeOH (15 mL). To this was added dropwise with stirring copper (II) chloride dihydrate (0.0444 g, 0.261 mmoles) in MeOH (5 mL). A green colour was observed. The solution was allowed to reflux overnight. A light green / blue precipitate was observed. The solution was allowed to cool to room temperature and the solid was collected via Buchner filtration. The precipitated isolated was washed with MeOH (5mL) and CHCl₃ (5 mL) and dried under high vacuum.

Yield: 0.200g (74%)

IR (ATR): 3054, 1978, 1609, 1579, 1415, 1223, 1067, 725 cm^{-1}

Elemental Analysis: $C_{36}H_{18}Cl_2CuN_{10}O_4$ % Calculated: C 54.80, H 2.30, N 17.75

                                          % Found: C 54.37, H 2.03, N 17.44

HRMS (ESI +): *m/z* Calculated for $C_{36}H_{18}ClCuN_{10}O_4$ [M – Cl⁻] 752.0497, Found 752.0474

4.4: Synthesis of *Bis* - [Cu(11-nitrile-DPPZ)₂(Cl)] Cl
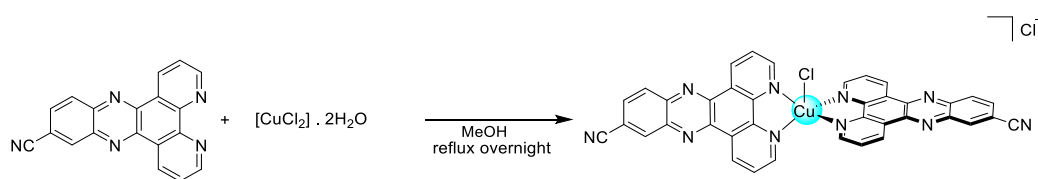
11-nitrile-DPPZ (0.180 g, 0.585 mmoles) was suspended in MeOH (15 mL). To this was added dropwise with stirring copper (II) chloride dihydrate (0.0386 g, 0.277 mmoles) in MeOH (5 mL). A green colour was observed. The solution was allowed to reflux overnight. A light green / blue precipitate was observed. . The solution was allowed to cool to room temperature and the solid was collected via Buchner filtration. The precipitated isolated was washed with MeOH (5mL) and CHCl₃ (5 mL) and dried under high vacuum.

Yield: 0.195g (73 %)

IR (ATR) 3448, 3067, 2229, 1608, 1578, 1356, 1076, 732 cm^{-1}

Elemental Analysis: $C_{36}H_{18}Cl_2CuN_{10}$ % Calculated: C 60.93, H 2.42, N 18.70

% Found: C 61.24, H 2.98, N 18.19

HR-MS (ESI +): *m/z* Calculated for $C_{36}H_{18}ClCuN_{10}$ [M – Cl$^-$] 712.0700, Found 712.0693

4.5: Synthesis of *Bis* - [Cu(11-bromo-DPPZ)₂(Cl)]Cl
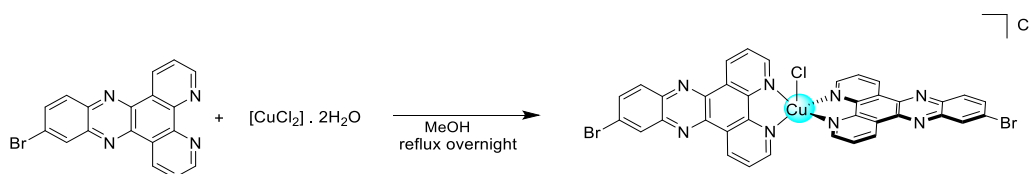
11-bromo-DPPZ (0.168 g, 0.456 mmoles) was suspended in MeOH (15 mL). To this was added dropwise with stirring copper (II) chloride dihydrate (0.0376 g, 0.221 mmoles) in MeOH (5 mL). A green / blue colour was observed. The solution was allowed to reflux overnight. A light green precipitate was observed. The precipitate was collected via Buchner filtration and washed with cold MeOH (5 mL) and CHCl₃ (5 mL) and dried under high vacuum.

Yield: 0.12 g (63 %)

IR (ATR): 3064, 1979, 1594, 1490, 1352, 1210, 1075, 917, 821 cm^{-1}

Elemental Analysis: $C_{36}H_{24}Br_2Cl_2CuN_8$ % Calculated: C 50.46, H 2.12, N 13.08

% Found: C 50.87, H 2.60, N 13.59

HR-MS (ESI +): *m/z* Calculated for $C_{36}H_{24}Br_2ClCuN_8$ [M-Cl$^-$ + Na$^+$] 842.8883, Found 842.8864

4.6: Synthesis of *Bis* - [Cu(11-methyl-DPPZ$_2$)(Cl)]Cl
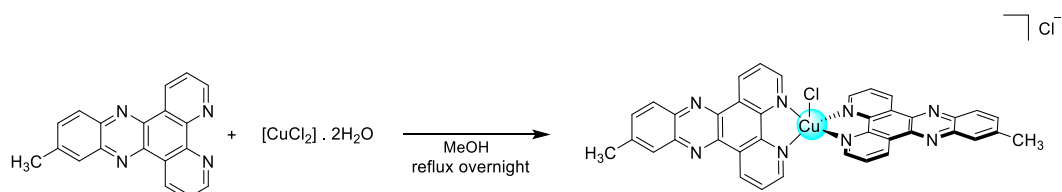
Scheme: Reaction scheme for the synthesis of *Bis*-[Cu(12-methyl-DPPZ)$_2$]. 2(NO$_3$).

11-methyl-DPPZ (0.179 g, 0.604 mmoles) was disolved in MeOH (15 mL). To this was added dropwise with stirring copper (II) chloride dihydrate (0.0489 g, 0.287 mmoles) in MeOH (5 mL). A green / brown colour was observed. The solution was allowed to reflux overnight. The solution was allowed to cool to room temperature and diethyl – ether (30 mL) was added. The stirring was continued for 2 hours. A light green precipitate was observed. The precipitate was collected *via* Buchner filtration and washed with cold MeOH (5 mL) and then CHCl$_3$ (5 mL). The solid was then dried under high vacuum.

Yield: 0.135 g (64 %)

IR (ATR) 3064, 2161, 1625, 1577, 1496, 1409, 1076, 822, 713 cm^{-1}

Elemental Analysis: C$_{38}$H$_{24}$Cl$_2$CuN$_8$ % Calculated: C 62.77, H 3.33, N 15.41

                                        % Found: C 62.28, H 3.10, N 15.78

HRMS (ESI +): *m/z* Calculated for C$_{38}$H$_{24}$Cl$_2$CuN$_8$ [M + Na$^+$] 750.1018, Found 750.0659

5   Chapter 5: Final Conclusions

In this thesis, a series of Copper (II) complexes with the ability to target cancer tissues were synthesised, characterised and screened with different biological assays. Copper was chosen due to its lower toxicity compared with most of the other transition elements and in particular platinum, whose success in medicinal chemistry is dominated by cisplatin. Copper is an endogenous metal that plays crucial roles in many enzymes (i.e. superoxo dismutase, cytochrome c oxidases…). Its role as anticancer drug is related to redox properties of copper, with two available oxidation states in physiological conditions (+1 and +2) that are able to interfere with the cellular redox stress. To selective target cancer cells, two families of vectors were chosen, estrogens (Chapter 2) and Biotin (Chapter 3), whose receptors are over expressed in the tumoral cells. The coordination sphere of these novel copper based metallodrugs have been completed with planar aromatic ligands that improve the DNA interaction. The novel complexes have been synthesised and characterised with a plethora of spectroscopic techniques and their stability in physiological conditions was studied. In collaboration with other research groups (Prof. Kavanagh, Biology Department, Maynooth University; Prof. Gandin, Depart. Pharmaceutical Science, University of Padua) the complexes have been tested as both anticancer agents and antimicrobial agents with very promising results. In particular, it was shown that most of the complexes with estrogens and biotin in the coordination sphere, are more active in the cancer cell that overexpress that specific receptor. Drug uptake confirmed that the internalisation is higher in those cells that overexpress the receptors, confirming that this strategy is producing positive outcomes. For the estrogen derivatives, ROS production studies and mechanistic evaluation was proposed. All the complexes show strong ability to interact with the DNA that is one target of these novel copper-based compounds. Very interesting to note is that the biotin derivatives are soluble and stable in water, that is a very important aspect in medicinal inorganic chemistry. In chapter four a series of Cu (II) complexes with dipyridophenazines (DPPZ) ligand was synthetised where DPPZ is a planar aromatic ligand with strong affinity for DNA intercalation. The ligands used in chapter four have different substituents at the 11 position, electron withdrawing and electron donating groups (Br, CH_3, CN and NO_2). These complexes have been characterised (Mass, IR, Elemental Analyses, Electrochemistry) and analysed as DNA binding agents. The DNA intercalation properties are confirmed by theoretical calculation where a preference for binding in the major groove (GG-CC and GC-CG) was observed. These complexes were tested as antimicrobial agents with strong activity in particular against C. Albicans and MRSA.

Two papers were published at the moment from this work and are attached at the end of this thesis:

- "Evaluation of in vitro and in vivo antibacterial activity of novel Cu(II)-steroid complexes", S. Barrett, S. Delaney, K. Kavanagh, D. Montagner. *Inorg. Chim. Acta* **2018**, *47*, 10721-10736

- "Anticancer activity, DNA binding and cell mechanistic studies of estrogen-functionalised Cu(II) complexes", S. Barrett, M. De Franco, A. Kellett, E. Dempsey, C. Marzano, A. Erxleben, V. Gandin, D. Montagner. *J. Biol. Inorg. Chem*. **2020**, *25*, 49-60

6   Future Work:

Future studies for chapter two in this thesis would include studying and probing the mechanism by which the drugs are interfering with the *S.* aureus on a molecular level. These studies could be carried out *via* the use of proteomics in collaboration with a suitable biologist. The reaction pathway using THF and DIPA might also be worth investigating as the ligands were isolated in pure form with much less aggressive conditions, however the yield was significantly lower. This reaction could most likely be optimised with some time to increase the yield and eliminate the use of DMF.

The biotin derived compounds studied in chapter three are still undergoing biological testing for their selectivity as anti-cancer agents and the preliminary data displayed here in section **3.16** is already very promising. It may be worth attempting to conjugate the two novel biotin ligands **3.23** and **3.24** to a gold (III) centre in the future as gold (III) displays a square planar geometry and there may be an opportunity for the chlorides on compounds **3.4** and **3.6** for a water molecule and perhaps behave in a similar manner to the famous drug cisplatin. One major drawback here would be the toxicity of the gold (III) centre. These compounds could also be screened *in vitro* as anti-microbial agents as there is some evidence that biotin analogues possess anti-microbial properties.[232] It may be a case that a combined or greater effect is observed with the copper (II) core as copper itself has anti-microbial properties.

Further work on the *Bis* – DPPZ adducts would most likely involve trying to obtain a crystal structure of one or all of these compounds. Having said this, many solvents and techniques have already been tried but not exhausted. Although the counter ion was exchanged for PF_6^- and also BF_4^- there are still some options available to increase the solubility of these

compounds. There is literature supporting the claim of a crystal structure for a non-substituted *bis* − [Cu (DPPZ)2]$^{2+}$ complex so it may be achievable with some time and patience. Further DFT studies could be carried out now that it has been identified that the preferred position in the DNA helix is in the GG - CC and GC − CG base pairs. This may reduce the load on the computation end as previously using a 10-base pair helix became a huge amount of work and very time consuming and laboursome for gaussian to perform DFT.

7   Bibliography:

[1] C. Orvig and M. J. Abrams, *Chemical Reviews* **1999**, *99*, 2201-2204.
[2] P. J. Sadler in *Inorganic chemistry and drug design*, *Vol. 36* Elsevier, **1991**, pp. 1-48.
[3] M. Linder in *Biochemistry of Copper, Ch. 6*, *Vol.* Plenum Press, New York, **1991**.
[4] K. H. Thompson and C. Orvig, *Dalton Transactions* **2006**, 761-764.
[5] M. Frezza, S. Hindo, D. Chen, A. Davenport, S. Schmitt, D. Tomco and Q. Ping Dou, *Current pharmaceutical design* **2010**, *16*, 1813-1825.
[6] C. Nardon and D. Fregona, *Current topics in medicinal chemistry* **2016**, *16*, 360-380.
[7] Y. Hu, M. Zhang, B. Lu and J. Dai, *Helicobacter* **2016**, *21*, 349-363.
[8] B. Rosenberg, L. Vancamp, J. E. Trosko and V. H. Mansour, *Nature* **1969**, *222*, 385.
[9] J. H. Burchenal, *Biochimie* **1978**, *60*, 915-923; L. H. Einhorn and S. D. Williams, *Western Journal of Medicine* **1979**, *131*, 1.
[10] G. Natile and M. Coluccia, *Coordination Chemistry Reviews* **2001**, *216*, 383-410.
[11] J. Gottlieb and B. Drewinko, *Cancer chemotherapy reports* **1975**, *59*, 621-628.
[12] M. Coluccia, A. Boccarelli, M. A. Mariggiò, N. Cardellicchio, P. Caputo, F. P. Intini and G. Natile, *Chemico-biological interactions* **1995**, *98*, 251-266.
[13] F. Ries and J. Klastersky, *American journal of kidney diseases* **1986**, *8*, 368-379.
[14] M. Reck, N. Frickhofen, S. Cedres, U. Gatzemeier, D. Heigener, H.-G. Fuhr, A. Thall, S. Lanzalone, P. Stephenson and A. Ruiz-Garcia, *Lung Cancer* **2010**, *70*, 180-187.
[15] E. Wexselblatt and D. Gibson, *Journal of inorganic biochemistry* **2012**, *117*, 220-229.
[16] D. Gately and S. Howell, *British journal of cancer* **1993**, *67*, 1171.
[17] D. Montagner, V. Gandin, C. Marzano and B. Longato, *Journal of inorganic biochemistry* **2011**, *105*, 919-926.
[18] V. Cepeda, M. A. Fuertes, J. Castilla, C. Alonso, C. Quevedo and J. M. Pérez, *Anti-Cancer Agents in Medicinal Chemistry (Formerly Current Medicinal Chemistry-Anti-Cancer Agents)* **2007**, *7*, 3-18.
[19] D. Wang and S. J. Lippard, *Nature reviews Drug discovery* **2005**, *4*, 307.
[20] J. T. Reardon, A. Vaisman, S. G. Chaney and A. Sancar, *Cancer research* **1999**, *59*, 3968-3971.
[21] T. C. Johnstone, K. Suntharalingam and S. J. Lippard, *Chemical reviews* **2016**, *116*, 3436-3486.
[22] L. Galluzzi, L. Senovilla, I. Vitale, J. Michels, I. Martins, O. Kepp, M. Castedo and G. Kroemer, *Oncogene* **2012**, *31*, 1869-1883.
[23] L. Peres and A. D. da Cunha Jr, *J Bras Nefrol* **2013**, *35*, 332-340.
[24] P. C. Dedon and R. F. Borch, *Biochemical pharmacology* **1987**, *36*, 1955-1964.
[25] J. Reedijk, *Chemical Communications* **1996**, 801-806.
[26] T. Ishibashi and S. J. Lippard, *Proceedings of the National Academy of Sciences* **1998**, *95*, 4219-4223.
[27] Y. Tanihara, S. Masuda, T. Katsura and K.-i. Inui, *Biochemical pharmacology* **2009**, *78*, 1263-1271.
[28] P. Devarajan, *Current opinion in pediatrics* **2005**, *17*, 193-199.
[29] A.-M. Florea and D. Büsselberg, *Cancers* **2011**, *3*, 1351-1371.
[30] C. Jehn, T. Boulikas, A. Kourvetaris, K. Possinger and D. Lüftner, *Anticancer research* **2007**, *27*, 471-475.
[31] E. Gaggelli, H. Kozlowski, D. Valensin and G. Valensin, *Chemical reviews* **2006**, *106*, 1995-2044.
[32] W. Sinha, M. G. Sommer, N. Deibel, F. Ehret, M. Bauer, B. Sarkar and S. Kar, *Angewandte Chemie International Edition* **2015**, *54*, 13769-13774.
[33] L. M. Gaetke and C. K. Chow, *Toxicology* **2003**, *189*, 147-163.

[34] T. Theophanides and J. Anastassopoulou, *Critical reviews in oncology/hematology* **2002**, *42*, 57-64.

[35] W. H. Koppenol, *Redox Report* **2001**, *6*, 229-234.

[36] W. Kaim and J. Rall, *Angewandte Chemie International Edition in English* **1996**, *35*, 43-60.

[37] D. Popovic, I. Leontyev, D. G. Beech and A. Stuchebrukhov, *Proteins: Structure, Function, and Bioinformatics* **2010**, *78*, 2691-2698.

[38] I. Scheiber, R. Dringen and J. F. Mercer, *Interrelations between essential metal ions and human diseases* **2013**, 359-387.

[39] C. Oswald, U. Krause-Buchholz and G. Rödel, *Journal of molecular biology* **2009**, *389*, 470-479.

[40] H. B. Leavesley, L. Li, K. Prabhakaran, J. L. Borowitz and G. E. Isom, *Toxicological Sciences* **2008**, *101*, 101-111; J. R. Alonso, F. Cardellach, S. López, J. Casademont and Ò. Miró, *Pharmacology & toxicology* **2003**, *93*, 142-146.

[41] F. Diaz, *Biochimica et Biophysica Acta (BBA)-Molecular Basis of Disease* **2010**, *1802*, 100-110.

[42] J. Richardson, K. A. Thomas, B. H. Rubin and D. C. Richardson, *Proceedings of the National Academy of Sciences* **1975**, *72*, 1349-1353.

[43] K. Keyer, A. S. Gort and J. A. Imlay, *Journal of bacteriology* **1995**, *177*, 6782-6790.

[44] J. A. Tainer, E. D. Getzoff, K. M. Beem, J. S. Richardson and D. C. Richardson, *Journal of molecular biology* **1982**, *160*, 181-217.

[45] S. J. Kaur, S. R. McKeown and S. Rashid, *Gene* **2016**, *577*, 109-118.

[46] J. A. Tainer, E. D. Getzoff, J. S. Richardson and D. C. Richardson, *Nature* **1983**, *306*, 284-287.

[47] L. McAlary, J. A. Harrison, J. A. Aquilina, S. P. Fitzgerald, C. Kelso, J. L. Benesch and J. J. Yerbury, *Analytical chemistry* **2019**, *92*, 1702-1711.

[48] H. E. Parge, E. D. Getzoff, C. Scandella, R. Hallewell and J. A. Tainer, *Journal of Biological Chemistry* **1986**, *261*, 16215-16218.

[49] V. A. Roberts, C. L. Fisher, S. M. Redford, D. E. McRee, H. E. Parge, E. D. Getzoff and J. A. Tainer, *Free radical research communications* **1991**, *12*, 269-278.

[50] S. Szpryngiel, M. Oliveberg and L. Mäler, *FEBS open bio* **2015**, *5*, 56-63.

[51] M. Ferraroni, W. R. Rypniewski, B. Bruni, P. Orioli and S. Mangani, *JBIC Journal of Biological Inorganic Chemistry* **1998**, *3*, 411-422.

[52] P. Ferenci, K. Caca, G. Loudianos, G. Mieli-Vergani, S. Tanner, I. Sternlieb, M. Schilsky, D. Cox and F. Berr, *Liver International* **2003**, *23*, 139-142.

[53] T. Wang and Z. Guo, *Current medicinal chemistry* **2006**, *13*, 525-537.

[54] A. Gaeta and R. C. Hider, *British journal of pharmacology* **2005**, *146*, 1041-1059.

[55] C. Marzano, M. Pellei, F. Tisato and C. Santini, *Anti-Cancer Agents in Medicinal Chemistry (Formerly Current Medicinal Chemistry-Anti-Cancer Agents)* **2009**, *9*, 185-211.

[56] K. M. Davies, J. F. Mercer, N. Chen and K. L. Double, *Clinical Science* **2016**, *130*, 565-574.

[57] D. E. Bredesen, *Aging (Albany NY)* **2015**, *7*, 595.

[58] Y. Nishito and T. Kambe, *Journal of nutritional science and vitaminology* **2018**, *64*, 1-7.

[59] E. Gaggelli, F. Bernardi, E. Molteni, R. Pogni, D. Valensin, G. Valensin, M. Remelli, M. Luczkowski and H. Kozlowski, *Journal of the American Chemical Society* **2005**, *127*, 996-1006.

[60] M. Klewpatinond, P. Davies, S. Bowen, D. R. Brown and J. H. Viles, *Journal of Biological Chemistry* **2008**, *283*, 1870-1881.

[61] J. W. Karr and V. A. Szalai, *Biochemistry* **2008**, *47*, 5006-5016.

[62] J. Folkman, *New england journal of medicine* **1971**, *285*, 1182-1186.

[63] J. Folkman, *Cancer Res* **1986**, *46*, 467-473.

[64] S. Brem, *Cancer Control* **1999**, *6*, 1-18; M. E. Beckner, *Cancer investigation* **1999**, *17*, 594-623.

[65] A. Parke, P. Bhattacherjee, R. Palmer and N. R. Lazarus, *The American journal of pathology* **1988**, *130*, 173.

[66] M. Ziche, J. Jones and P. M. Gullino, *Journal of the National Cancer Institute* **1982**, *69*, 475-482.

[67] S. S. Brem, D. Zagzag, A. Tsanaclis, S. Gately, M. Elkouby and S. Brien, *The American journal of pathology* **1990**, *137*, 1121; S. Brem, A. M. C. Tsanaclis and D. Zagzag, *Neurosurgery* **1990**, *26*, 391-396.

[68] G. J. Brewer, *Experimental Biology and Medicine* **2001**, *226*, 665-673.

[69] J. E. Weder, C. T. Dillon, T. W. Hambley, B. J. Kennedy, P. A. Lay, J. R. Biffin, H. L. Regtop and N. M. Davies, *Coordination Chemistry Reviews* **2002**, *232*, 95-126.

[70] J. R. Sorenson, *Progress in medicinal chemistry* **1989**, *26*, 437-568.

[71] G. Ebers, *Papyrus Ebers: die Maasse und das Kapitel über die Augenkrankheiten: erster Theil: die Gewichte und Hohlmaasse des Papyrus Ebers*, S. Hirzel, **1889**, p.

[72] H. L. Regtop and J. R. Biffin in *Divalent metal complexes of indomethacin, compositions and medical methods of use thereof*, *Vol.* Google Patents, **1995**.

[73] I. Annual, *NSW, Sydney* **1997**, 145.

[74] J. Reynolds, *Royal Pharmaceutical society of Great Britian* **1996**.

[75] J. R. Sorenson, *Journal of Medicinal Chemistry* **1976**, *19*, 135-148.

[76] J. Sorenson, *Chemistry in Britain* **1984**, *20*, 1110-1113.

[77] M. J. F.-A. Tuorkey and K. K. Abdul-Aziz, *Biomedicine & pharmacotherapy* **2009**, *63*, 194-201.

[78] M. A. Goher and T. C. Mak, *Inorganica chimica acta* **1987**, *127*, L13-L16.

[79] A. B. Caballero, A. Rodríguez-Diéguez, M. Quirós, J. M. Salas, Ó. Huertas, I. Ramírez-Macías, F. Olmo, C. Marín, G. Chaves-Lemaur and R. Gutierrez-Sánchez, *European journal of medicinal chemistry* **2014**, *85*, 526-534.

[80] E. A. Britta, A. P. B. Silva, T. Ueda-Nakamura, B. P. Dias-Filho, C. C. Silva, R. L. Sernaglia and C. V. Nakamura, *PLoS One* **2012**, *7*, e41440.

[81] D. D. Hemphill in *Trace substances in environmental health-VII*, *Vol.* University of Missouri, Columbia, MO, USA, **1973**.

[82] J. R. Sorenson, L. W. Oberley, R. K. Crouch, T. W. Kensler, V. Kishore, S. W. Leuthauser, T. D. Oberley and A. Pezeshk, *Biological trace element research* **1983**, *5*, 257-273.

[83] C. Nathan, *Nature* **2004**, *431*, 899-902.

[84] K. Morris, *The Lancet* **2008**, *372*, 1941-1942.

[85] D. R. Graham, L. E. Marshall, K. A. Reich and D. S. Sigman, *Journal of the American Chemical Society* **1980**, *102*, 5419-5421.

[86] N. S. Ng, P. Leverett, D. E. Hibbs, Q. Yang, J. C. Bulanadi, M. J. Wu and J. R. Aldrich-Wright, *Dalton transactions* **2013**, *42*, 3196-3209.

[87] R. Safaei, S. Otani, B. J. Larson, M. L. Rasmussen and S. B. Howell, *Molecular pharmacology* **2008**, *73*, 461-468.

[88] K. Bondarczuk and Z. Piotrowska-Seget, *Cell biology and toxicology* **2013**, *29*, 397-405.

[89] S. S. Hindo, M. Frezza, D. Tomco, M. J. Heeg, L. Hryhorczuk, B. R. McGarvey, Q. P. Dou and C. N. Verani, *European journal of medicinal chemistry* **2009**, *44*, 4353-4361.

[90] D. S. Sigman, *Accounts of Chemical Research* **1986**, *19*, 180-186.

[91] M. Melník and M. Kabešová, *Journal of Coordination Chemistry* **2000**, *50*, 323-338.

[92] R. R. Conry, *Encyclopedia of Inorganic and Bioinorganic Chemistry* **2011**.

[93] A. Mukherjee, A. M. Raichur, J. M. Modak and K. Natarajan, *Journal of Industrial Microbiology and Biotechnology* **2004**, *31*, 462-468.

[94] J. A. McCleverty and T. J. Meyer, *Comprehensive coordination chemistry II*, Elsevier Ltd, **2004**, p.

[95] J. D. Ranford, P. J. Sadler and D. A. Tocher, *Journal of the Chemical Society, Dalton Transactions* **1993**, 3393-3399.

[96] O. Zelenko, J. Gallagher, Y. Xu and D. S. Sigman, *Inorganic chemistry* **1998**, *37*, 2198-2204.

[97] M. Pitié, B. Donnadieu and B. Meunier, *Inorganic chemistry* **1998**, *37*, 3486-3489.

[98] B. Zhou and J. Gitschier, *Proceedings of the National Academy of Sciences* **1997**, *94*, 7481-7486.

[99] J. M. Veal and R. L. Rill, *Biochemistry* **1991**, *30*, 1132-1140.

[100] X. Cai, N. Pan and G. Zou, *Biometals* **2007**, *20*, 1-11.

[101] V. Gandin, M. Porchia, F. Tisato, A. Zanella, E. Severin, A. Dolmella and C. Marzano, *Journal of medicinal chemistry* **2013**, *56*, 7416-7430.

[102] B. C. Bales, T. Kodama, Y. N. Weledji, M. Pitie, B. Meunier and M. M. Greenberg, *Nucleic acids research* **2005**, *33*, 5371-5379.

[103] D. Galaris and A. Evangelou, *Critical reviews in oncology/hematology* **2002**, *42*, 93-103.

[104] R. Alemón-Medina, M. Breña-Valle, J. L. Muñoz-Sánchez, M. I. Gracia-Mora and L. Ruiz-Azuara, *Cancer chemotherapy and pharmacology* **2007**, *60*, 219-228.

[105] C. Trejo-Solís, D. Jimenez-Farfan, S. Rodriguez-Enriquez, F. Fernandez-Valverde, A. Cruz-Salgado, L. Ruiz-Azuara and J. Sotelo, *BMC cancer* **2012**, *12*, 1-15.

[106] A. M. Thomas, M. Nethaji, S. Mahadevan and A. R. Chakravarty, *Journal of inorganic biochemistry* **2003**, *94*, 171-178.

[107] K. Tummalapalli, C. Vasavi, P. Munusami, M. Pathak and M. Balamurali, *International journal of biological macromolecules* **2017**, *95*, 1254-1266.

[108] Z. Molphy, A. Prisecaru, C. Slator, N. Barron, M. McCann, J. Colleran, D. Chandran, N. Gathergood and A. Kellett, *Inorganic chemistry* **2014**, *53*, 5392-5404.

[109] D. Peterson and H. Murray, *Journal of the American Chemical Society* **1952**, *74*, 1871-1872.

[110] W.-Y. Tong and X. Dong, *Recent patents on biotechnology* **2009**, *3*, 141-153.

[111] P. Y. K. Yue, N. K. Mak, Y. K. Cheng, K. W. Leung, T. B. Ng, D. T. P. Fan, H. W. Yeung and R. N. S. Wong, *Chinese medicine* **2007**, *2*, 1-21.

[112] E. W. Boland, *California medicine* **1950**, *72*, 405.

[113] D. A. Grimes, M. F. Gallo, V. Grigorieva, K. Nanda and K. F. Schulz, *Contraception* **2005**, *71*, 89-94; J. Womack, S. Richman, P. C. Tien, M. Grey and A. Williams, *Journal of midwifery & women's health* **2008**, *53*, 362-375.

[114] R. Woodward, F. Sondheimer, D. Taub, K. Heusler and W. McLamore, *Journal of the American Chemical Society* **1952**, *74*, 4223-4251.

[115] J. Xu, R.-C. Wu and B. W. O'malley, *Nature Reviews Cancer* **2009**, *9*, 615-630.

[116] S. Farzaneh and A. Zarghi, *Scientia pharmaceutica* **2016**, *84*, 409-427.

[117] E. C. Chang, J. Frasor, B. Komm and B. S. Katzenellenbogen, *Endocrinology* **2006**, *147*, 4831-4842.

[118] L.-A. Haldosén, C. Zhao and K. Dahlman-Wright, *Molecular and cellular endocrinology* **2014**, *382*, 665-672.

[119] J.-X. Zhang, D. C. Labaree and R. B. Hochberg, *Chinese Chemical Letters* **2014**, *25*, 567-570.

[120] J. Griggs, J. C. Metcalfe and R. Hesketh, *The lancet oncology* **2001**, *2*, 82-87.

[121] S. Parihar, A. Kumar, A. K. Chaturvedi, N. K. Sachan, S. Luqman, B. Changkija, M. Manohar, O. Prakash, D. Chanda and F. Khan, *The Journal of steroid biochemistry and molecular biology* **2013**, *137*, 332-344.

[122] D. M. Huryn and M. Okabe, *Chemical reviews* **1992**, *92*, 1745-1768.

[123] D. R. Haines, C. K. Tseng and V. E. Marquez, *Journal of medicinal chemistry* **1987**, *30*, 943-947.

[124] M. Tuncbilek, E. Bilget Guven, T. Onder and R. Cetin Atalay, *Journal of Medicinal Chemistry* **2012**, *55*, 3058-3065.

[125] T. C. Norman, N. S. Gray, J. T. Koh and P. G. Schultz, *Journal of the American Chemical Society* **1996**, *118*, 7430-7431.

[126] M. Legraverend and D. S. Grierson, *Bioorganic & medicinal chemistry* **2006**, *14*, 3987-4006.

[127] J. C. Bressi, J. Choe, M. T. Hough, F. S. Buckner, W. C. Van Voorhis, C. L. Verlinde, W. G. Hol and M. H. Gelb, *Journal of medicinal chemistry* **2000**, *43*, 4135-4150.

[128] V. Bavetsias, J. M. Large, C. Sun, N. Bouloc, M. Kosmopoulou, M. Matteucci, N. E. Wilsher, V. Martins, J. Reynisson and B. Atrash, *Journal of medicinal chemistry* **2010**, *53*, 5213-5228.

[129] A. Boumendjel, E. Nicolle, T. Moraux, B. Gerby, M. Blanc, X. Ronot and J. Boutonnat, *Journal of medicinal chemistry* **2005**, *48*, 7275-7281.

[130] L.-H. Huang, H.-D. Xu, Z.-Y. Yang, Y.-F. Zheng and H.-M. Liu, *Steroids* **2014**, *82*, 1-6.

[131] L.-H. Huang, Y. Li, H.-D. Xu, Y.-F. Zheng and H.-M. Liu, *Steroids* **2014**, *85*, 13-17.

[132] F. Le Bideau and S. Dagorne, *Chemical reviews* **2013**, *113*, 7793-7850.

[133] O. Gandolfi, J. Blum and F. Mandelbaum-Shavit, *Inorganica chimica acta* **1984**, *91*, 257-261.

[134] K. K. W. Lo, K. Y. Zhang, C. K. Chung and K. Y. Kwok, *Chemistry–A European Journal* **2007**, *13*, 7110-7120.

[135] L. Huang, H. Zhu, Y. Zhang, X. Xu, W. Cui, G. Yang and Y.-M. Shen, *Steroids* **2010**, *75*, 905-911.

[136] X. Zhang, Z. Zuo, J. Tang, K. Wang, C. Wang, W. Chen, C. Li, W. Xu, X. Xiong and K. Yuntai, *Bioorganic & medicinal chemistry letters* **2013**, *23*, 3793-3797.

[137] A. Vellé, R. C. Maguire, K. Kavanagh, P. Sanz Miguel and D. Montagner, *ChemMedChem* **2017**, *12*, 841-844.

[138] Y. He, S. Groleau, R.-. Gaudreault, M. Caron, H.-M. Thérien and G. Bérubé, *Bioorganic & Medicinal Chemistry Letters* **1995**, *5*, 2217-2222.

[139] C. Descôteaux, J. Provencher-Mandeville, I. Mathieu, V. Perron, S. K. Mandal, É. Asselin and G. Bérubé, *Bioorganic & medicinal chemistry letters* **2003**, *13*, 3927-3931.

[140] V. Gagnon, M.-È. St-Germain, C. Descôteaux, J. Provencher-Mandeville, S. Parent, S. K. Mandal, E. Asselin and G. Bérubé, *Bioorganic & medicinal chemistry letters* **2004**, *14*, 5919-5924.

[141] V. Perron, D. Rabouin, E. Asselin, S. Parent, C. René and G. Bérubé, *Bioorganic chemistry* **2005**, *33*, 1-15.

[142] C. N. N'soukpoé-Kossi, C. Descôteaux, E. Asselin, H.-A. Tajmir-Riahi and G. Bérubé, *DNA and cell biology* **2008**, *27*, 101-107.

[143] C. Descôteaux, V. Leblanc, G. Bélanger, S. Parent, É. Asselin and G. Bérubé, *Steroids* **2008**, *73*, 1077-1089.

[144] P. Saha, C. Descôteaux, K. Brasseur, S. Fortin, V. Leblanc, S. Parent, É. Asselin and G. Bérubé, *European journal of medicinal chemistry* **2012**, *48*, 385-390.

[145] S. Fortin, K. Brasseur, N. Morin, É. Asselin and G. Bérubé, *European journal of medicinal chemistry* **2013**, *68*, 433-443.

[146] M. J. Hannon, P. S. Green, D. M. Fisher, P. J. Derrick, J. L. Beck, S. J. Watt, S. F. Ralph, M. M. Sheil, P. R. Barker and N. W. Alcock, *Chemistry–A European Journal* **2006**, *12*, 8000-8013.

[147] S. Top, H. El Hafa, A. Vessières, M. Huché, J. Vaissermann and G. Jaouen, *Chemistry–A European Journal* **2002**, *8*, 5241-5249.

[148] E. Kitteringham, E. Andriollo, V. Gandin, D. Montagner and D. M. Griffith, *Inorganica Chimica Acta* **2019**, *495*, 118944.

[149] L. A. Summers in *The phenanthrolines*, *Vol. 22* Elsevier, **1978**, pp. 1-69.

[150] P. G. Sammes and G. Yahioglu, *Chemical Society Reviews* **1994**, *23*, 327-334.

[151] H. Irving and R. Williams, *Journal of the Chemical Society (Resumed)* **1953**, 3192-3210.

[152] G. Anderegg, *Helvetica Chimica Acta* **1963**, *46*, 2813-2822.

[153] G. Anderegg, *Helvetica Chimica Acta* **1974**, *57*, 1340-1346.

[154] C. Wang, L. Lystrom, H. Yin, M. Hetu, S. Kilina, S. A. McFarland and W. Sun, *Dalton Transactions* **2016**, *45*, 16366-16378.

[155] S. Ji, H. Guo, X. Yuan, X. Li, H. Ding, P. Gao, C. Zhao, W. Wu, W. Wu and J. Zhao, *Organic letters* **2010**, *12*, 2876-2879.

[156] E. B. van der Tol, H. J. van Ramesdonk, J. W. Verhoeven, F. J. Steemers, E. G. Kerver, W. Verboom and D. N. Reinhoudt, *Chemistry–A European Journal* **1998**, *4*, 2315-2323.

[157] B. Krishnakumar, R. Velmurugan, S. Jothivel and M. Swaminathan, *Catalysis Communications* **2010**, *11*, 997-1002.

[158] Z. Molphy, C. Slator, C. Chatgilialoglu and A. Kellett, *Frontiers in chemistry* **2015**, *3*, 28.

[159] R. Chinchilla and C. Nájera, *Chemical reviews* **2007**, *107*, 874-922.

[160] L. Malatesia and M. Angoletta, *Journal of the Chemical Society (Resumed)* **1957**, 1186-1188.

[161] N. Browne, M. Heelan and K. Kavanagh, *Virulence* **2013**, *4*, 597-603.

[162] M. Brennan, D. Y. Thomas, M. Whiteway and K. Kavanagh, *FEMS Immunology & Medical Microbiology* **2002**, *34*, 153-157.

[163] M. McCann, A. L. Santos, B. A. Da Silva, M. T. V. Romanos, A. S. Pyrrho, M. Devereux, K. Kavanagh, I. Fichtner and A. Kellett, *Toxicology Research* **2012**, *1*, 47-54.

[164] P. Zheng, A. Eskandari, C. Lu, K. Laws, L. Aldous and K. Suntharalingam, *Dalton Transactions* **2019**, *48*, 5892-5896.

[165] K. J. Thomas, P. Tharmaraj, V. Chandrasekhar, C. Bryan and A. Cordes, *Inorganic Chemistry* **1994**, *33*, 5382-5390.

[166] M. M. Ngundi, O. A. Sadik, T. Yamaguchi and S.-i. Suye, *Electrochemistry communications* **2003**, *5*, 61-67.

[167] M. McCann, J. McGinley, K. Ni, M. O'Connor, K. Kavanagh, V. McKee, J. Colleran, M. Devereux, N. Gathergood and N. Barron, *Chemical Communications* **2013**, *49*, 2341-2343.

[168] L. A. Kunz-Schughart, J. P. Freyer, F. Hofstaedter and R. Ebner, *Journal of biomolecular screening* **2004**, *9*, 273-285.

[169] J. Zempleni, S. S. Wijeratne and Y. I. Hassan, *Biofactors* **2009**, *35*, 36-46.

[170] Y. M. Xu, J. Y. Du and A. T. Lau, *Proteomics* **2014**, *14*, 2047-2060.

[171] C. Staggs, W. Sealey, B. McCabe, A. Teague and D. Mock, *Journal of Food Composition and Analysis* **2004**, *17*, 767-776.

[172] M. J. Salie and J. J. Thelen, *Biochimica et Biophysica Acta (BBA)-Molecular and Cell Biology of Lipids* **2016**, *1861*, 1207-1213.

[173] C. B. Walth, L. L. Wessman, A. Wipf, A. Carina, M. K. Hordinsky and R. S. Farah, *Journal of the American Academy of Dermatology* **2018**, *79*, e121-e124.

[174] K. Balamurugan, A. Ortiz and H. M. Said, *American Journal of Physiology-Gastrointestinal and Liver Physiology* **2003**, *285*, G73-G77.

[175] P. Prasad, *Molecular and functional characterization of the intestinal Na+-dependent multivitamin transporter. Arch Biochem Biophys* **1999**, *366*, 95-106.

[176] P. D. Prasad, H. Wang, R. Kekuda, T. Fujita, Y.-J. Fei, L. D. Devoe, F. H. Leibach and V. Ganapathy, *Journal of Biological Chemistry* **1998**, *273*, 7501-7506.

[177] G. Russell-Jones, K. McTavish, J. McEwan, J. Rice and D. Nowotnik, *Journal of inorganic biochemistry* **2004**, *98*, 1625-1633.

[178] N. M. Green, *Methods in enzymology* **1990**, *184*, 51-67.

[179] O. Livnah, E. A. Bayer, M. Wilchek and J. L. Sussman, *Proceedings of the National Academy of Sciences* **1993**, *90*, 5076-5080.

[180] R. Board and R. Fuller, *Biological Reviews* **1974**, *49*, 15-49.

[181] B. Zerega, L. Camardella, S. Cermelli, R. Sala, R. Cancedda and F. Descalzi Cancedda, *Journal of cell science* **2001**, *114*, 1473-1482.

[182] W. M. Pardridge and R. J. Boado, *FEBS letters* **1991**, *288*, 30-32.

[183] X. Zeng, Y.-X. Sun, X.-Z. Zhang and R.-X. Zhuo, *Organic & biomolecular chemistry* **2009**, *7*, 4201-4210.

[184] S. Rosebrough, *Nuclear medicine and biology* **1993**, *20*, 663-668.

[185] Z. Yao, M. Zhang, H. Sakahara, T. Saga, Y. Arano and J. Konishi, *JNCI: Journal of the National Cancer Institute* **1998**, *90*, 25-29.

[186] E. De La Fuente, C. Dawson, L. Nelin, R. Bongard, T. McAuliffe and M. Merker, *American Journal of Physiology-Lung Cellular and Molecular Physiology* **1997**, *272*, L461-L470.

[187] M. Guttinger, F. Guidi, M. Chinol, E. Reali, F. Veglia, G. Viale, G. Paganelli, A. Corti and A. G. Siccardi, *Cancer research* **2000**, *60*, 4211-4215.

[188] D. Wu and W. M. Pardridge, *Proceedings of the National Academy of Sciences* **1999**, *96*, 254-259.

[189] H. Kalofonos, M. Rusckowski, D. Siebecker, G. Sivolapenko, D. Snook, J. Lavender, A. Epenetos and D. Hnatowich, *Journal of nuclear medicine: official publication, Society of Nuclear Medicine* **1990**, *31*, 1791-1796.

[190] M. H. Lee, J. L. Sessler and J. S. Kim, *Accounts of chemical research* **2015**, *48*, 2935-2946.

[191] N. Muhammad, N. Sadia, C. Zhu, C. Luo, Z. Guo and X. Wang, *Chemical Communications* **2017**, *53*, 9971-9974.

[192] J. Z. Zhang, E. Wexselblatt, T. W. Hambley and D. Gibson, *Chemical communications* **2012**, *48*, 847-849.

[193] M. S. Finnin, J. R. Donigian, A. Cohen, V. M. Richon, R. A. Rifkind, P. A. Marks, R. Breslow and N. P. Pavletich, *Nature* **1999**, *401*, 188-193.

[194] M. Marloye, H. Inam, C. J. Moore, V. Debaille, J. R. Pritchard, M. Gelbcke, F. Meyer, F. Dufrasne and G. Berger, *JBIC Journal of Biological Inorganic Chemistry* **2021**, 1-15.

[195] K. Y. Zhang and K. K.-W. Lo, *Inorganic chemistry* **2009**, *48*, 6011-6025.

[196] C.-H. Leung, H.-J. Zhong, D. S.-H. Chan and D.-L. Ma, *Coordination Chemistry Reviews* **2013**, *257*, 1764-1776.

[197] S. Kallus, L. Uhlik, S. van Schoonhoven, K. Pelivan, W. Berger, É. A. Enyedy, T. Hofmann, P. Heffeter, C. R. Kowol and B. K. Keppler, *Journal of inorganic biochemistry* **2019**, *190*, 85-97.

[198] C. E. Murar, F. Thuaud and J. W. Bode, *Journal of the American Chemical Society* **2014**, *136*, 18140-18148.

[199] M. Zheng, P. Chen, W. Wu and H. Jiang, *Chemical Communications* **2016**, *52*, 84-87.

[200] L. Gianelli, V. Amendola, L. Fabbrizzi, P. Pallavicini and G. G. Mellerio, *Rapid Communications in Mass Spectrometry* **2001**, *15*, 2347-2353.

[201] S. Barrett, S. Delaney, K. Kavanagh and D. Montagner, *Inorganica Chimica Acta* **2018**, *479*, 261-265.

[202] Z. Molphy, V. McKee and A. Kellett, *Molecules* **2019**, *24*, 4301.

[203] D.-m. Tian, J. Qiao, Y.-z. Bao, J. Liu, X.-k. Zhang, X.-l. Sun, Y.-w. Zhang, X.-s. Yao and J.-s. Tang, *Bioorganic & medicinal chemistry letters* **2019**, *29*, 707-712.

[204] S. Roy, K. D. Hagen, P. U. Maheswari, M. Lutz, A. L. Spek, J. Reedijk and G. P. van Wezel, *ChemMedChem* **2008**, *3*, 1427-1434.

[205] T. Phillips, I. Haq, A. J. Meijer, H. Adams, I. Soutar, L. Swanson, M. J. Sykes and J. A. Thomas, *Biochemistry* **2004**, *43*, 13657-13665.

[206] A. E. Friedman, J. C. Chambron, J. P. Sauvage, N. J. Turro and J. K. Barton, *Journal of the American Chemical Society* **1990**, *112*, 4960-4962.

[207] Z. Ude, K. Kavanagh, B. Twamley, M. Pour, N. Gathergood, A. Kellett and C. J. Marmion, *Dalton Transactions* **2019**, *48*, 8578-8593.

[208] T. Kiran, V. G. Prasanth, M. Balamurali, C. Vasavi, P. Munusami, K. I. Sathiyanarayanan and M. Pathak, *Inorganica Chimica Acta* **2015**, *433*, 26-34.

[209] U. Śliwińska-Hill, F. P. Pruchnik, M. Latocha, D. Nawrocka-Musiał and S. Ułaszewski, *Inorganica Chimica Acta* **2013**, *400*, 26-31.

[210] P. Kumar, R. J. Butcher and A. K. Patra, *Inorganica Chimica Acta* **2020**, *506*, 119532.

[211] A. Bolhuis, L. Hand, J. E. Marshall, A. D. Richards, A. Rodger and J. Aldrich-Wright, *European journal of pharmaceutical sciences* **2011**, *42*, 313-317.

[212] M. C. Leung, P. L. Williams, A. Benedetto, C. Au, K. J. Helmcke, M. Aschner and J. N. Meyer, *Toxicological sciences* **2008**, *106*, 5-28.

[213] X. Liu, B. Sun, R. E. Kell, H. M. Southam, J. Butler, X. Li, R. K. Poole, F. R. Keene and J. G. Collins, *ChemPlusChem* **2018**, *83*, 643-650.

[214] Z. Drulis-Kawa, J. Gubernator, A. Dorotkiewicz-Jach, W. Doroszkiewicz and A. Kozubek, *International journal of pharmaceutics* **2006**, *315*, 59-66.

[215] M. Cusumano, M. L. Di Pietro and A. Giannetto, *Inorganic chemistry* **2006**, *45*, 230-235.

[216] S. Barrett, M. De Franco, A. Kellett, E. Dempsey, C. Marzano, A. Erxleben, V. Gandin and D. Montagner, *JBIC Journal of Biological Inorganic Chemistry* **2019**, 1-12.

[217] M. Navarro, E. J. Cisneros-Fajardo, A. Sierralta, M. Fernández-Mestre, P. Silva, D. Arrieche and E. Marchán, *JBIC Journal of Biological Inorganic Chemistry* **2003**, *8*, 401-408.

[218] T. Gupta, S. Dhar, M. Nethaji and A. R. Chakravarty, *Dalton Transactions* **2004**, 1896-1900.

[219] J. P. Hall, H. Beer, K. Buchner, D. J. Cardin and C. J. Cardin, *Philosophical Transactions of the Royal Society A: Mathematical, Physical and Engineering Sciences* **2013**, *371*, 20120525.

[220] Í. P. de Souza, B. d. P. Machado, A. B. de Carvalho, I. Binatti, K. Krambrock, Z. Molphy, A. Kellett, E. C. Pereira-Maia and P. P. Silva-Caldeira, *Journal of Molecular Structure* **2019**, *1178*, 18-28.

[221] G. W. T. M. J. Frisch, H. B., G. E. S. Schlegel, M. A. Robb,, G. S. J. R. Cheeseman, V. Barone, B. Mennucci, G. A. Petersson,, M. C. H. Nakatsuji, X. Li,, A. F. I. H. P. Hratchian, J. Bloino, G. Zheng, J. L. Sonnenberg, M. Hada, M. Ehara,, R. F. K. Toyota, J. Hasegawa,, T. N. M. Ishida, Y. Honda, O. Kitao, H. Nakai, T. Vreven, J., J. A. Montgomery, J. E. Peralta,, M. B. F. Ogliaro, J. J. Heyd, E., K. N. K. Brothers, V. N. Staroverov, T. Keith, R. Kobayashi, J., K. R. Normand, A., J. C. B. Rendell, S. S. Iyengar, J. Tomasi, M. Cossi, N. Rega, J. M. Millam, M. Klene, J. E. Knox, J., V. B. B. Cross, C. Adamo, J., R. G. Jaramillo, R. E. Stratmann, O. Yazyev, A. J. Austin, R., C. P. Cammi, J. W., R. L. M. Ochterski, K. Morokuma, V. G. Zakrzewski, G. A. Voth, P. Salvador, J. J. Dannenberg, S. Dapprich,, O. F. A. D. Daniels, J. B. and J. V. O. Foresman, J. Cioslowski, D. J. Fox. in *Gaussian 09, Revision E.01, Vol. Wallingford* Gaussian Inc, **2013**.

[222] A. D. Becke, *J. Chem. Phys* **1993**, *98*, 5648-5652.

[223] C. Lee, W. Yang and R. Parr, *Phys. Rev. B* **1988**, *37*, 785-789.

[224] P. J. Stephens, F. J. Devlin, C. F. Chabalowski and M. J. Frisch, *The Journal of physical chemistry* **1994**, *98*, 11623-11627.

[225] L. Goerigk and S. Grimme, *The Journal of Chemical Physics* **2010**, *132*, 184103.

[226] J. Madureira, C. I. Ramos, M. Marques, C. Maia, B. de Sousa, L. Campino, M. G. Santana-Marques and N. Farrell, *Inorganic chemistry* **2013**, *52*, 8881-8894.

[227] A. Robertazzi, A. Magistrato, P. de Hoog, P. Carloni and J. Reedijk, *Inorganic chemistry* **2007**, *46*, 5873-5881.

[228] L. Yan, Y. Lu and X. Li, *Physical Chemistry Chemical Physics* **2016**, *18*, 5529-5536.

[229] P. Jaque, A. V. Marenich, C. J. Cramer and D. G. Truhlar, *The Journal of Physical Chemistry C* **2007**, *111*, 5783-5799.

[230] C. P. Kelly, C. J. Cramer and D. G. Truhlar, *The Journal of Physical Chemistry B* **2006**, *110*, 16066-16081.

[231] Z. Molphy, D. Montagner, S. S. Bhat, C. Slator, C. Long, A. Erxleben and A. Kellett, *Nucleic acids research* **2018**, *46*, 9918-9931.

[232] T. P. Soares da Costa, W. Tieu, M. Y. Yap, O. Zvarec, J. M. Bell, J. D. Turnidge, J. C. Wallace, G. W. Booker, M. C. Wilce and A. D. Abell, *ACS medicinal chemistry letters* **2012**, *3*, 509-514.

8 Appendix

Graduate Modules:

Chemistry Specific Modules:

CH801 – Core Skills and Research Techniques in Chemistry

CH803 – Teaching Skills in Chemistry

CH804 – Thesis Planning

CH808 – Research Supervision Training

Generic / Transferable modules:

GST1 – Professional Development & Employability

GST2 – Finding Information for Your Thesis

FM806 – Advanced Communications Skills: Conference presentation

Analytical HPLC Traces Chapter 3:

All Traces were run as RP-HPLC (C$_{18}$, 254 nm, 80:20 CH$_3$CN : H$_2$O) with any impurity less than 5%.

Compound 3.3
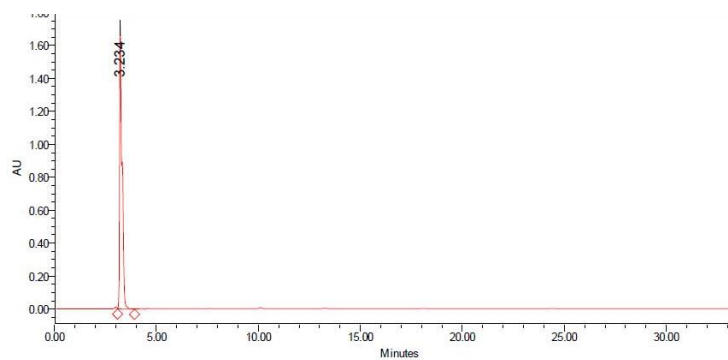
Compound 3.4
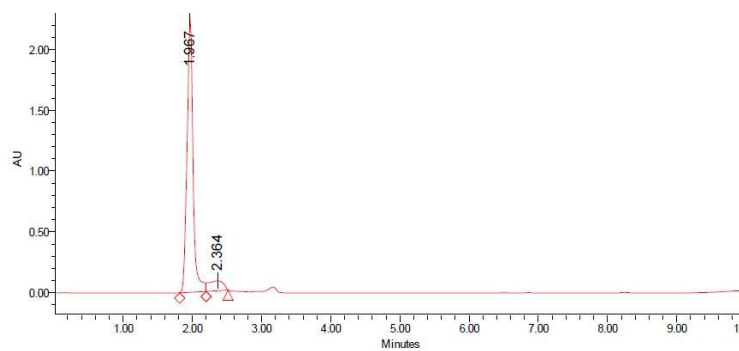
Compound 3.5
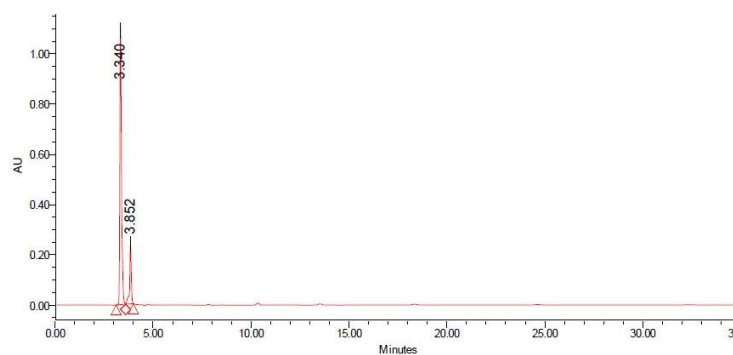
Compound 3.6
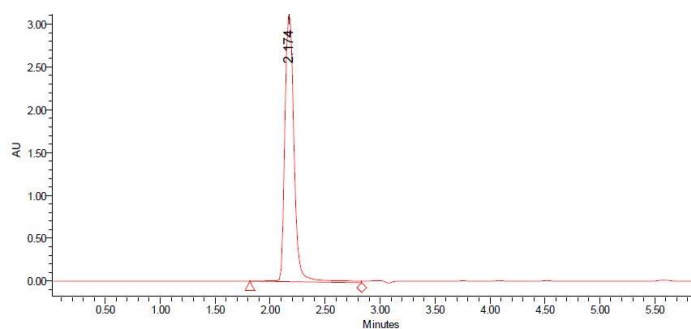
ESI HRMS Chapter 4:

Compound 4.3
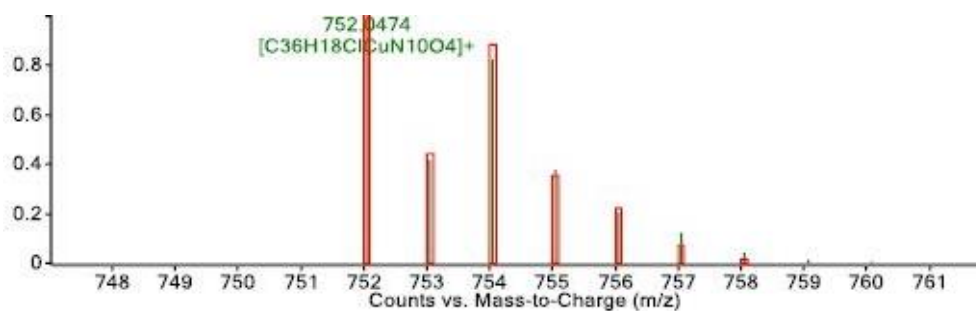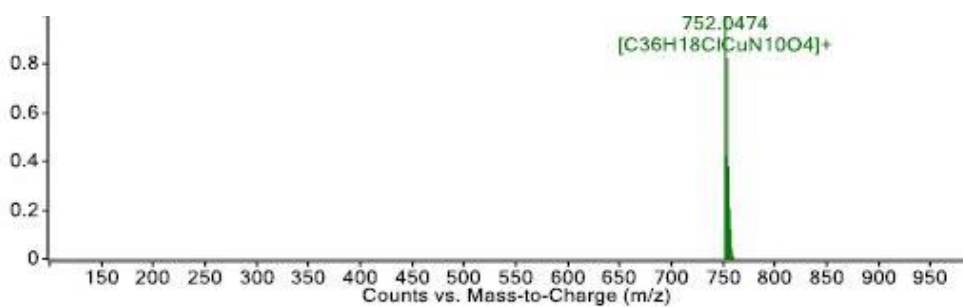
Compound 4.4
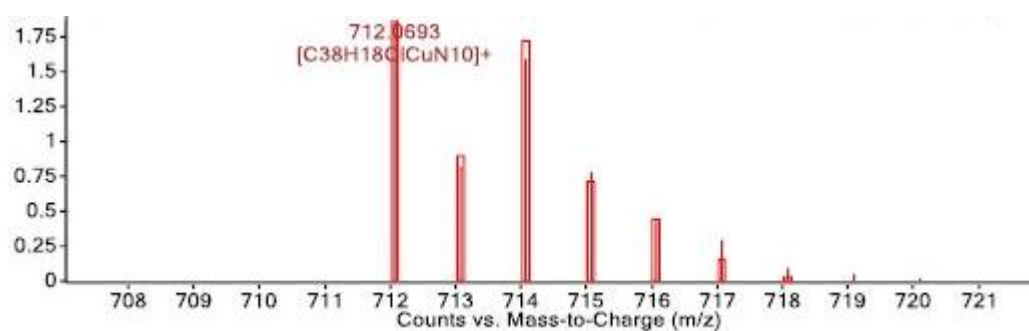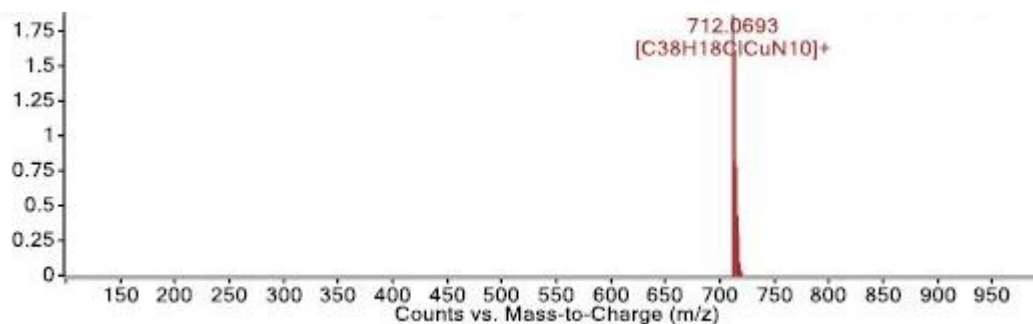
Compound 4.5
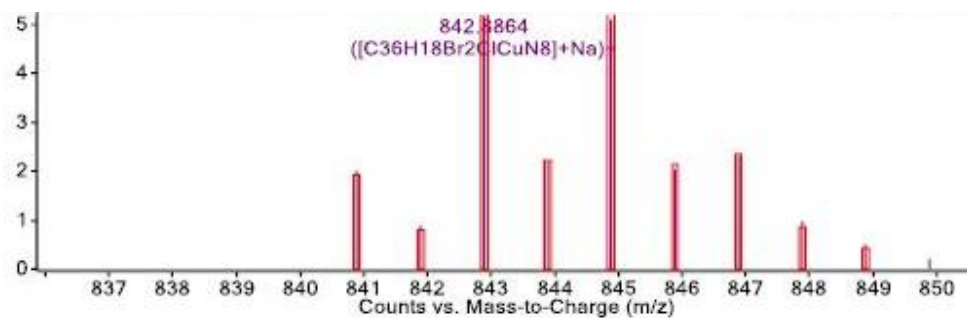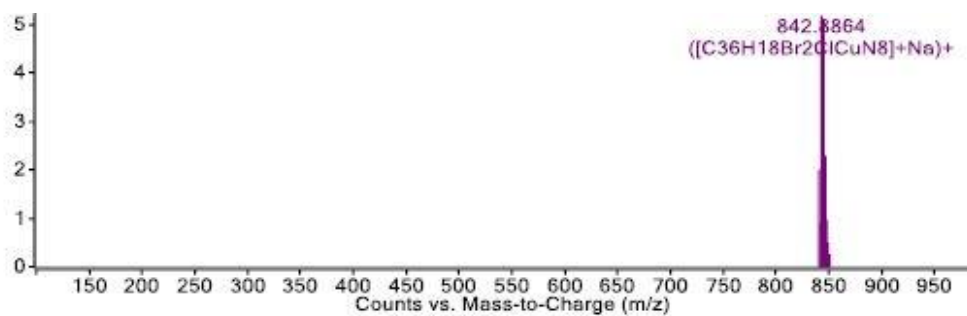
Compound 4.6
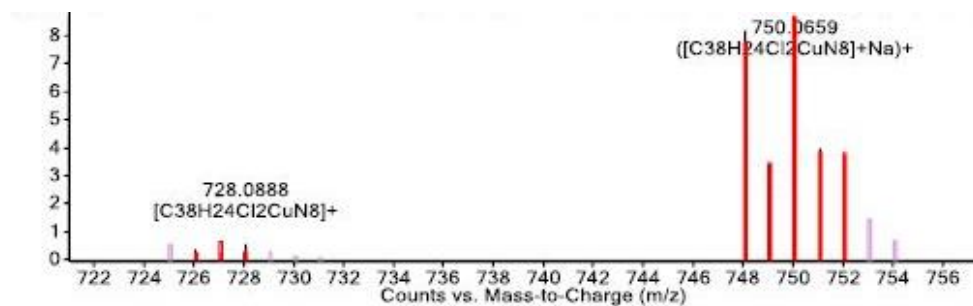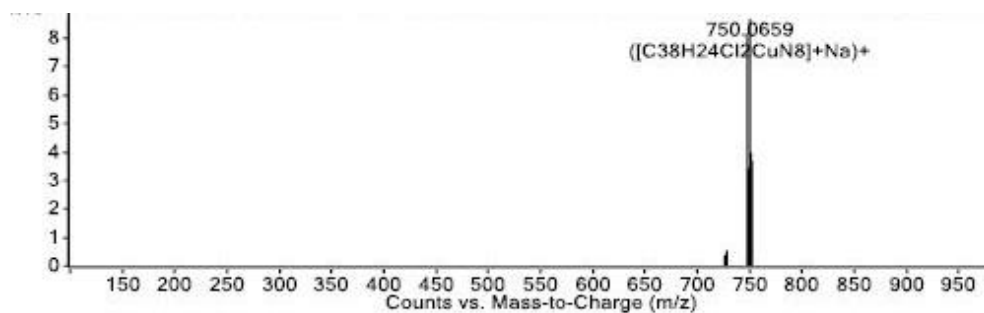
Author Publications:

Research paper

Evaluation of *in vitro* and *in vivo* antibacterial activity of novel Cu(II)-steroid complexes

Stephen Barrett [a], Stephen Delaney [b], Kevin Kavanagh [b,*], Diego Montagner [a,*]

[a] *Department of Chemistry, Maynooth University, Maynooth, Ireland*
[b] *Department of Biology, Maynooth University, Maynooth, Ireland*

ABSTRACT

A pioneer series of copper(II) complexes bearing planar phenanthroline-modified aromatic ligands and steroid (ethynylestradiol and ethisterone) with generic formula $[Cu(N \cap N)(steroid)](NO_3)_2$ where $N \cap N$ is DPQ, DPPZ and DPPN and steroid is estradiol or testosterone, were synthetized, characterised and screened *in vitro* and *in vivo* as antimicrobial agents against *Staphylococcus aureus* and methicillin resistant *Staphylococcus aureus* (MRSA). Toxicity studies revealed notable antibacterial activity of the copper – based compounds, which is significantly increased *in vivo* by the presence of the steroid moiety. Toxicity profiling was estimated *in vitro* versus Gram-positive (*Staphylococcus aureus*) and MRSA and *in vivo* in *Galleria mellonella* larvae infected with *S. aureus*. Results showed the complexes to be active against *S. aureus* and MRSA *in vitro* (MIC_{50} average value of 2.46 and 97 μM in *S. aureus* and MRSA, respectively) and to be active when larvae infected with *S. aureus* were administered the agents.

© 2018 Elsevier B.V. All rights reserved.

1. Introduction

The bacterium *Staphylococcus aureus* is a Gram positive body commensal which has the ability to survive in a wide variety of environments [1], and this contributes to its ability to induce a range of superficial and systemic infections. *S. aureus* possesses a number of virulence factors that contribute to its ability to colonise tissue including the presence of a capsule, the expression of adhesins, the secretion of a range of toxins and immunomodulators which disrupt the host's immune response [2]. This bacterium is present on approximately 30% of healthy individuals in the anterior nares and on the skin, but a skin breach resulting from surgery or trauma can result in a variety of skin infections, such as impetigo, or more serious diseases such as toxic shock syndrome and sepsis [3,4]. *S. aureus* infection can be extremely difficult to treat and up to 4% of cases can be fatal [3]. Treatment of *S. aureus* infections is hindered by the emergence of methicillin-resistant *S. aureus* (MRSA) and due to the increasing incidence of resistance to conventional antimicrobials there is a renewed interest in the development of novel metal based drugs as antimicrobial agent [5].

Despite the classic organic based antibacterial agents, metal complexes are an excellent alternative and in particular Cu(phen) derivatives. In the last twenty years the antimicrobial activity of

Cu(phen) complexes have been deeply investigated; double charged copper with planar chelating ligands exhibit growth inhibitory activity against *Staphylococcus aureus* (MIC ≥ 4.0–7.9 μM) and to a lesser extent against *Escherichia coli* [6–13]. It is still not completely clear what role the planar ligands play in the antimicrobial activity of the corresponding metal based drugs. Indeed, metal complexes with substituted planar aromatic ligands (i.e. DPQ, DPPZ and DPPN, Scheme 1) show an increased interaction via intercalation with the DNA and Cu(II) derivatives and also show artificial nuclease activity but this could not be related with the antimicrobial properties [14–16]. Mitochondrial membrane damage and p53 upregulation are also alternative possible pathways of action. Creaven et al. showed that Cu(phen) complexes functionalised with acetic acids are able to inhibit respiration, reduce level of ergosterol and alter the cytochrome c content [12]. Considering these aspects, here we report the syntheses, characterization and antimicrobial evaluation of a series of Cu(II) complexes with chelating planar ligands further functionalised with steroids (testosterone and estradiol). We recently showed that the modification of Au(I)–NHC (*N*-Heterocyclic Carbenes) with steroids derivatives is a promising strategy to enhance the antibacterial activity of the related complexes [17]. In the work presented here the Cu(II) cationic complexes were evaluated as antibacterial agents *in vitro* against *S. aureus* and MRSA and *in vivo* using *Galleria mellonella* larvae.

---

* Corresponding authors.
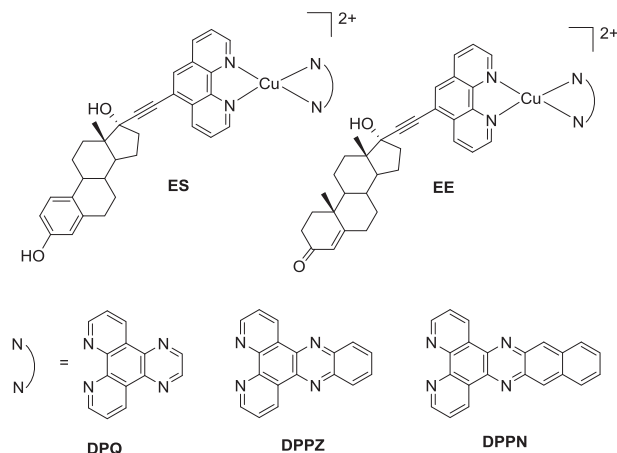
Scheme 1. Structures of [Cu(ES-5-phen)(DPQ)]²⁺ **4**, [Cu(EE-5-phen)(DPQ)]²⁺ **5**, [Cu(ES-5-phen)(DPPZ)]²⁺ **6**, [Cu(EE-5-phen)(DPPZ)]²⁺ **7**, [Cu(ES-5-phen)(DPPN)]²⁺ **8**, [Cu(EE-5-phen))(DPPN)]²⁺ **9**.

The immune system of insects shows many structural and functional similarities to the innate immune response of mammals [18–20] and consequently insects can be used to assess the virulence of microbial pathogens or the *in vivo* efficacy of antimicrobial drugs and give results similar to those obtained using mammals [21,22]. Larvae of *Galleria mellonella* are a popular choice for these types of tests and are inexpensive to purchase, and give rapid results [18]. *G. mellonella* larvae have previously been used to demonstrate the *in vivo* activity of novel metal based drugs against pathogenic bacteria and fungi [23,24] and show a strong correlation with results obtained in rats [25].

The aim of this work was to analyse the *in vitro* effects of the six metal complexes on *Staphylococcus aureus* and MRSA, to evaluate the toxicity of the compounds in *Galleria mellonella* larvae and to examine if the compounds showed any therapeutic properties when larvae had been pre-inoculated with microbial infections.

2. Material and methods

All reagents and reactants used were purchased from commercial sources. The two sources used were Sigma Aldrich and Tokyo Chemical Industry. DPQ (Dipyrido[3,2-*f*:2′,3′-*h*]quinoxaline), DPPZ (Dipyrido[3,2-*a*:2′,3′-*c*]phenazine), DPPN (Benzo[*I*]dipyrido[3,2-a:2′,3′-c]phenazine) and tetrakis triphenylphosphine Palladium(0) were synthetized as previously reported [26–29].

All solvents were used without further purification. The DMF was dried using 4 Ã... molecular sieves, it was then decanted into a round bottom flask and kept under high vacuum using a Schlenk line while immersed in liquid nitrogen. The DMF was then flushed with nitrogen gas. This step was repeated a minimum of three times for the Sonogashira coupling reaction to obtain ES-5-phen and EE-5-phen.

All NMR spectra were recorded on a Bruker Advance spectrometer with the probe at 293 K, operating at 500 MHz for the ¹H nucleus. Proton signals were assigned with the help of 2D NMR experiments (COSY). Spectra were recorded in CDCl₃ using Me₄Si as the internal standard. All chemical shifts are reported in ppm.

Infrared (IR) spectra were recorded in the region 4000 – 400 cm⁻¹ on a Perkin Elmer precisely spectrum 100 FT/IR spectrometer. The solid samples were run using ATR.

Elemental analyses (carbon, hydrogen and nitrogen) were performed with a PerkinElmer 2400 series II analyzer. ESI mass spectra were recorded in positive mode with a Waters LCT Premier XE Spectrometer.

2.1. Assessment of antibacterial activity of novel complexes

The complexes were dissolved in 1 mL DMSO to give a stock concentration of 5 mg/mL. Nutrient broth (100μL) was added to each well of a 96 well plate. Each drug was serially diluted on the plate giving a concentration range 150 – 0.59 μM. Bacteria were grown overnight and the OD_{600} was adjusted to 0.1 (equivalent to cell density of 4×10^7/ml). Bacterial cells (100 μL) were added to each well and the growth was measured at 600 nm after 24 h at 37 °C using a spectrophotometer (BioPhotometer). The MIC_{50} values were calculated as the minimum concentration of drug that inhibited growth by 50%.

2.2. Inoculation of Galleria mellonella larvae

Sixth instar larvae of *G. mellonella* (Lepidoptera: Pyralidae, the Greater Wax Moth) (Mealworm Company, Sheffield, England) were stored in the dark at 15 °C. 5 Larvae of the same age and weighing 0.3 g were inoculated with 20 μL of PBS containing cells 4×10^7 bacterial cell through the last pro-leg using a Myjector U100 insulin syringe (Terumo Europe, Leuven, Belgium).

2.3. In vivo toxicity assay

Larvae were injected with 20 μL of compound solution (150 – 0.59 μM) or 5% (v/v) DMSO through the last left pro-leg as described. Larvae were incubated at 37 °C for 24 h prior to quantifying survival after 24, 48 and 72 h.

2.4. Effect of compounds on survival of G. Mellonella larvae infected with S. aureus

Larvae were injected with *S. aureus* through the last left proleg as described. One hour post infection 20 ul of each compound solution (0.1 or 0.25 mg/ml) was administered. The control consisted of larvae inoculated with the *S. aureus*. Larvae were incubated at 37 °C and survival was assessed at 24 and 48 h.

3. Experimental

The starting [Cu(N ∩ N)(OH₂)₂](NO₃)₂ (**1–3**) complexes (where N ∩ N is DPQ (**1**), DPPZ (**2**) or DPPN(**3**), See Experimental Part in Supporting Information) where obtained by modifying a literature procedure [21–23]. Briefly, Cu(NO₃)₂·3H₂O and the corresponding N ∩ N ligand where mixed in a 1.1 to 1 ratio in methanol and refluxed for two hours. The slight excess of the Copper salt prevent the formation of the more stable bis-adduct [Cu(N ∩ N)₂](NO₃)₂. The solid was obtained by addition of Et₂O, isolated by filtration and dried in vacuum (Supporting Information).

The phen-steroid derivatives of general formula ES or EE-5-phen (where ES-5-phen and EE-5-phen are the Estradiol and Testosterone derivatives, respectively) have been obtained by Sonogashira coupling reaction between 5-Bromophenanthroline and the correspondent commercial available alkyne derivative of the steroids (See Scheme 2 and Supporting Information).

The final complexes [Cu(N ∩ N)(EE or ES-5-phen)](NO₃)₂ (**4–9**) are depicted in Scheme 1 and were obtained by mixing the corresponding [Cu(N ∩ N)(OH₂)₂](NO₃)₂ (**1–3**) and the corresponding steroid-phen in a 1 to 1 ratio in DMF at 50 °C overnight. The solids were isolated by filtration after addition of Et₂O and dried in vacuum (See Supporting Information).
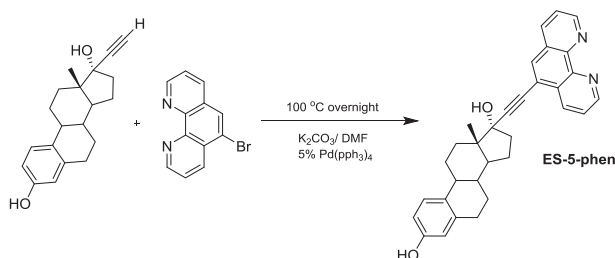
Scheme 2. Synthetic pathway to produce ES-5-Phen using Sonogashira Coupling Reaction.

Table 1
Antimicrobial activity of selected compounds. MIC_{50} [μM].

Compound	S. aureus	MRSA
4	4.7 ± 0.9	219 ± 10.4
5	1.5 ± 0.2	125 ± 9.5
6	2.1 ± 0.1	102 ± 8.9
7	2.0 ± 0.2	32 ± 3.2
8	2.5 ± 0.4	17.5 ± 1.5
9	2.0 ± 0.3	88 ± 7.8

4. Results and discussion

Recent results from our group showed that the presence of steroids (Estradiol and Testosterone) enhanced the *in vivo* antibacterial activity of Au(I)–NHC carbene complexes [17]. Since Copper and in particular Cu(II)-phenanthroline complexes are important antibacterial agents, we sought to combine these with steroid derivatives to confirm the efficacy of this approach. Furthermore, the complexes were functionalised with aromatic planar phenanthroline derivatives ligands such as DPQ, DPPZ and DPPN.

The coordination sphere of the series of Cu(II) complexes analysed in this work is composed by two modified phenanthroline scaffolds as depicted in Scheme 1. The alkyne steroids derivatives (ES Ethinyl Estradiol and EE Ethiosterone) have been covalently bound to phenathrolin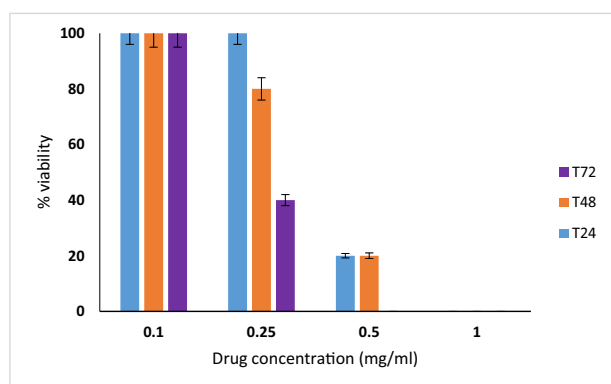e using the Sonogashira coupling reaction with 5-Bromophenanthroline as shown in Scheme 2 for the Estradiol steroid (ES-5-phen).

The success of Sonogashira coupling reactions are highly dependent upon the nature of the base and by the catalyst used as well as by the inert and degassed use of solvent. After several attempts we found that the best conditions were the use of the inorganic base K_2CO_3, the use of a freshly prepared *tetrakis*-[Pd(PPh$_3$)$_4$] catalyst, dry and degassed DMF at 100 °C overnight under nitrogen atmosphere (See Supporting Information). The success of the reaction can be easily visualised in the ^1H NMR spectrum by the disappearance of the alkyne proton of the starting EE and ES at 2.55 ppm and by the shift of the ^1H in position six of the phenathroline that moves upfield of 0.5 ppm in the ES/EE-5-Phen with respect the starting 5-Bromophenanthroline (Fig. 1S and 2S).

The final complexes have been characterised by IR, Elemental Analyses and Mass Spectrometry (Supporting Information). All the mass spectra show a clearly visible peak with the isotopical pattern of Cu in the positive region corresponding to the species $[M−NO_3]^+$ or $[M−2(NO_3)+Cl]^+$ (Figs. 3-8S). The activity of the compounds against *S. aureus* and MRSA was assessed as described and the results indicate that all drugs were active against *S. aureus* with MIC_{50} values < 5 μM (Table 1) that are in line and even smaller with most of the Cu(II) complexes reported in literature. [6–12] The free estradiol and testosterone were non-active as previously reported by us. [17] Among the series, the testosterone derivatives (**5**, **7** and **9**) are more potent (average MIC_{50} of 1.83 μM) with respect the estradiol derivatives **4**, **6** and **8** (average MIC_{50} of 3.1 μM). The planar ligand seems to play an important role because the DPPZ derivatives **6** and **7** are the most active while DPQ (**4** and **5**) are the less potent with DPPN complexes (**8** and **9**) laying between (average MIC_{50} of 2.05, 2.25 and 3.1 μM for DPPZ, DPPN and DPQ, respectively). Two important factors are important: lipophilicity and solubility. It is expected that the most lipophilic complexes would be more potent due to higher intracellular uptake; although DPPN derivatives **8** and **9** are more potent than the DPQ analogues (**4** and **5**) they are less active than the DPPZ (**6** and **7**) because solubility issues arise. Large and steric encumbered DPPN complexes are less soluble than the smaller DPQ and DPPZ and this is the reason why intermediate DPPZ complexes are the most potent. In the case of MRSA the complexes are much less active (average MIC_{50} values of 97.4 μM) with some exception such as compound **8** that has a MIC_{50} in the low micromolar region (Table 1). The complexes were found to be inactive against the Gram negative bacterium *Pseudomonas aeruginosa* and the yeast *Candida albicans* (results not presented).

These promising results prompted us to investigate the *in vivo* antimicrobial properties of these Cu-steroids complexes. MRSA was not studied *in vivo* due to the poor results *in vitro*. *G. mellonella* larvae are a useful tool in this kind of study because, as discussed in the introduction, their immune system is similar to that of mammals, they provide rapid and reliable results and there are no ethical restrictions to their use. [19] The larvae are inoculated by injecting the drug into the last left pro-leg and larval viability can be easily determined by visualisation. Melanisation and lack of movement indicates the inoculation proved fatal. (See Figs. 9 and 10S in Supporting information).

The first study analysed the toxicity of the Cu(II) series in *G. mellonella* larvae. Previous work has established a strong correlation between the toxicity of compounds in insect larvae and rats [30] and compounds such as potassium nitrate [31] and caffeine [32] are metabolised in a comparable manner in *G. mellonella* larvae and mammals. The larvae were injected with increasing concentrations of each compound and the viability was analysed after 24, 48 and 72 h. Administration of doses of 0.1 mg/ml of each drug to larvae had little or no effect on viability over 72 h. In the case of administration of the 0.25 mg/ml dose compounds **4** and **5** with DPQ ligand reduced viability by 60 and 20%, respectively, by 72 h. In the case of the DPPN derivatives **8** and **9** the reduced viability was of 20% (72 h) while no significant decrease in viability at this dose over 72 h was observed for the complexes **6** and **7** with DPPZ moiety. All drugs at a concentration of 0.5 or 1 mg/ml proved toxic to larvae and resulted in 80 – 100% death at 72 h (Fig. 1 for compound **4** and 11-16S in SI for compound **5** – **9**).

In order to determine if the drugs had *in vivo* antibacterial activity, *G. mellonella* larvae were infected with a dose of *S. aureus* (1:2
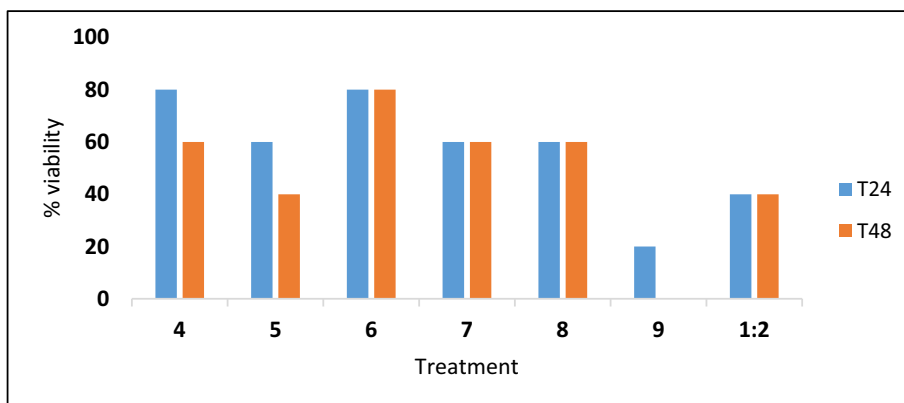

Fig. 1. Viability of *Galleria mellonella* larvae upon treatment with different concentration of complex **4**.

Fig. 2. % Viability of larvae treated with 1:2 dilution of *S. aureus* and 0.1 mg/mL of the tested complexes. Standard error was less than ± 10% of the mean in all cases.
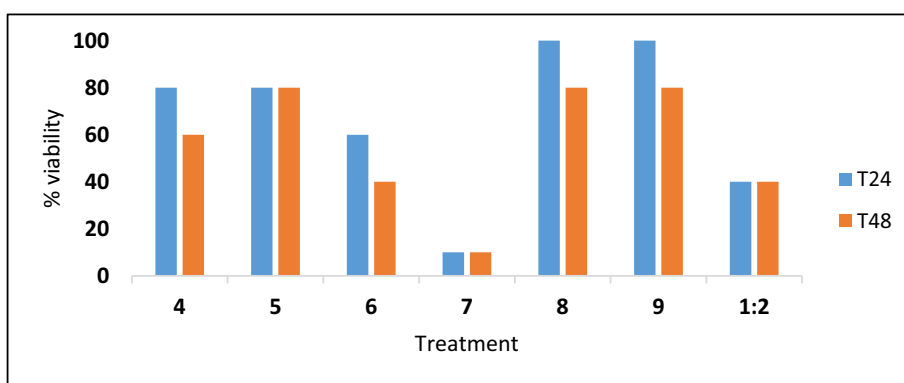

Fig. 3. % Viability of larvae treated with 1:2 dilution of *S. aureus* and 0.25 mg/mL of the tested complexes. Standard error was less than ± 10% of the mean in all cases.

dilution of OD_{600} 1.0) and one hour later administered with a non-toxic dose of each drug at a concentration of 0.1 or 0.25 mg/mL. In the first series of experiments, which used a drug dose of 0.1 mg/mL, administration of the bacteria to larvae resulted in 60% kill after 24 h (Fig. 2). In contrast those larvae administered with complexes **4** to **8** showed viability of 80 – 60% at 24 h and this did not change significantly by 48 h (Fig. 2). In a second series of experiments the ability of the complexes to prevent larvae from infection was assessed with higher concentration, 0.25 mg/mL (Fig. 3). In this experiment complexes **8** and **9** induced 100% survival of larvae at 24 h and 80% at 48 h.

DPPN derivatives **8** and **9** show very high *in vivo* activity only at higher concentration (0.25 mg/ml) while the DPPZ analogues **6** and **7** show the opposite behaviour (more active at lower concentration). The *in vivo* antimicrobial activity of the complexes does not strongly correlate with what was seen *in vitro* but this is quite common since the conditions *in vivo* are much different from those *in vitro*; the same lack of correlation was recently observed by our group with Au(I) complexes [17]. The role of the steroids and of the planar ligands in the activity of this series of Cu(II) complexes is not completely clear; the enhanced lipophlicity due to presence of the steroids that increase the bacterial uptake could explain in part the high antimicrobial activity but other mechanisms can be involved. A deeper investigation that will need the use of proteomics analyses is required and planned to clarify this aspect and will be the object of a future paper.

5. Conclusions

The six novel Cu(II)-steroid complexes showed high potency *in vitro* against *S. aureus* and MRSA and *in vivo* against *S. aureus*.

When inoculated with the complexes larval viability noticeably increased in those larvae that were previously infected with *S. aureus*. The effect of the steroids on the antimicrobial activity of the metal complexes is still not clarified and we are currently using proteomics analyses to uncover the mechanism of action. These complexes show great potential to become lead compounds which could eventually be developed into new treatments for *S. aureus* and possibly MRSA infections.

Appendix A. Supplementary data

Supplementary data associated with this article can be found, in the online version, at https://doi.org/10.1016/j.ica.2018.04.054.

References

[1] M.O. Clements, S.P. Watson, S.J. Foster, J. Bacteriol. 181 (1999) 3898–3903.
[2] M.M. Dinges, P.M. Orwin, P.M. Schlievert, Clin. Microb. Rev. 13 (2000) 16–34.
[3] J. García-Lara, M. Masalha, S.J. Foster, Drug Disc. Today 10 (2005) 643–651.
[4] C. Pichon, B. Felden, Proc. Natl. Assoc. Sci. U.S.A. 102 (2005) 14249–14254.
[5] M.M. Cortese-Krott, M. Munchow, E. Pirev, F. Hessner, A. Bozkurt, P. Uciechowski, N. Pallua, K.D. Kroncke, C.V. Suschek, Free Rad. Biol. Med. 47 (2009) 1570–1577.
[6] N.S. Ng, P. Leverett, D.E. Hibbs, Q. Yang, J.C. Bulanadi, M.J. Wu, J.R. Aldrich-Wright, Dalton Trans. 42 (2013) 3196–3209.

[7] T.S. Lobana, S. Indoria, A.K. Jassal, H. Kaur, D.S. Arora, J.P. Jasinski, Eur. J. Med. Chem. 76 (2014) 145–154.

[8] M. Geraghty, J.F. Cronin, M. Devereux, M. McCann, Biometals 13 (2000) 1–8.

[9] M. Geraghty, V. Sheridan, M. McCann, M. Devereux, V. McKee, Polyhedron 22 (1999) 2931–2939.

[10] L. Viganor, O. Howe, P. McCarron, M. McCann, M. Devereux, Current Topics, Med. Chem. 17 (2017) 1280–1302.

[11] N.S. Ng, M.J. Wu, J.R. Aldrich-Wright, J. Inorg. Biochem. 180 (2018) 61–68.

[12] B.S. Creaven, D.A. Egana, D. Karcz, K. Kavanagh, M. McCann, M. Mahone, A. Noble, B. Thati, M. Walsh, J. Inorg. Biochem. 101 (2007) 1108–1119.

[13] N.S. Ng, M.J. Wu, C.E. Jones, J.R. Aldrich-Wright, J. Inorg. Biochem. 162 (2016) 62–72.

[14] Z. Molphy, A. Prisecaru, C. Slator, N. Barron, M. McCann, J. Colleran, D. Chandran, N. Gathergood, A. Kellett, Inorg. Chem. 53 (2014) 5392–5404.

[15] L. Viganor, A.C. Galdino, A.P. Nunes, K.R. Santos, M.H. Branquinha, M. Devereux, A. Kellett, M. McCann, A.L. Santos, J. Antimic. Chemother. 71 (2016) 128–134.

[16] M.A. Zoroddu, S. Zanetti, R. Pogni, R. Basosi, J. Inorg. Biochem. 63 (1996) 291–300.

[17] A. Vellé, R. Maguire, K. Kavanagh, J.P. Sanz Miguel, D. Montagner, ChemMedChem. 12 (2017) 841–844.

[18] K. Kavanagh, E.P. Reeves, FEMS Microbiol. Rev. 28 (2004) 101–112.

[19] B.B. Fuchs, E. Mylonakis, Curr. Opt. Microbiol. 9 (2006) 346–351.

[20] N. Browne, M. Heelan, K. Kavanagh, Virulence 4 (2013) 597–603.

[21] M. Brennan, D.Y. Thomas, M. Whiteway, K. Kavanagh, Path Dis. 34 (2002) 153–157.

[22] G. Jander, L.G. Rahme, F.M. Ausubel, J. Bacteriol. 182 (2000) 3843–3845.

[23] R. Rowan, C. Moran, M. McCann, K. Kavanagh, Biometals 22 (2009) 461.

[24] N. Browne, F. Hackenberg, W. Streciwilk, M. Tacke, K. Kavanagh, Biometals 27 (2014) 745–752.

[25] M. McCann, A.L. Santos, B.A. Da Silva, M.T.V. Romanos, A.S. Pyrrho, M. Devereux, K. Kavanagh, I. Fichtner, A. Kellett, Toxicol. Res. 1 (2012) 47–54.

[26] J.G. Collins, A.D. Sleeman, J.R. Aldrich-Wright, I. Greguric, T.W. Hambley, Inorg. Chem. 37 (1998) 3133–3141.

[27] J.E. Dickeson, L.A. Summers, Aust. J. Chem. 23 (1970) 1023–1027.

[28] V.W.W. Yam, K.K.W. Lo, K.K. Cheung, R.Y.C. Kong, J. Chem. Soc. Chem. Comm. 259 (1995) 1191–1193.

[29] L. Malatesia, M. Angoletta, J. Chem. Soc. 231 (1957) 1186–1188.

[30] R. Maguire, O. Duggan, K. Kavanagh, Cell Biol. Toxicol. 32 (2016) 209–216.

[31] R. Maguire, M. Kunc, P. Hyrsl, K. Kavanagh, Comp. Biochem. Phys. Part C Toxicol. Pharmacol. 195 (2017) 44–51.

[32] R. Maguire, M. Kunc, P. Hyrsl, K. Kavanagh, Neurot. Terat. 64 (2017) 37–44.

ORIGINAL PAPER

Anticancer activity, DNA binding and cell mechanistic studies of estrogen-functionalised Cu(II) complexes

Stephen Barrett[1] · Michele De Franco[2] · Andrew Kellett[3] · Eithne Dempsey[1] · Cristina Marzano[2] · Andrea Erxleben[4] · Valentina Gandin[2] · Diego Montagner[1]

Abstract
Four estrogen-functionalised copper complexes were synthesised and investigated as electrochemical active DNA binding and cleavage agents. These complexes strategically contain a biocompatible metal centre [Cu(II)], a planar aromatic ligand as DNA intercalative agent and an estradiol-derivative moiety which acts as delivery vector to target estrogen-receptor-positive (ER+) cancer cells. Cytotoxic activity was studied over a panel of estrogen-receptor-positive (ER+) and negative (ER−) human cancer cell lines by means of both 2D and 3D cell viability studies. The complexes showed high in vitro intercalative interaction with nuclear DNA and demonstrated to be strong DNA cleaving agents. This series of Cu compounds are potent anticancer agents with low and sub-micromolar IC_{50} values and the cellular uptake follows the lipophilicity order meaning that the internalisation mainly happened via passive diffusion. Finally, the estrogen-complexes are involved in the cellular redox stress by stimulating the production of ROS (reactive oxygen species).
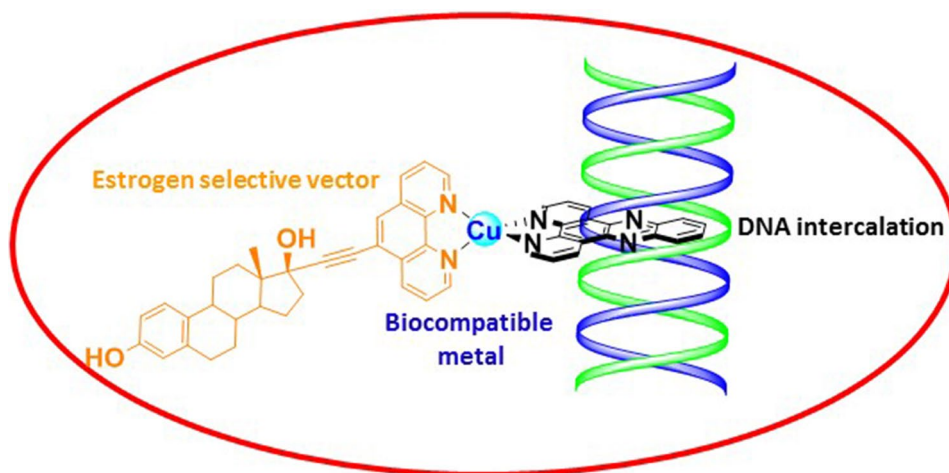
Graphic abstract

Electronic supplementary material The online version of this article (https://doi.org/10.1007/s00775-019-01732-8) contains supplementary material, which is available to authorized users.

✉ Valentina Gandin
valentina.gandin@unipd.it

✉ Diego Montagner
diego.montagner@mu.ie

Extended author information available on the last page of the article

Introduction

Copper complexes are becoming interesting developmental anticancer agents and many recent examples demonstrated the efficacy of tumour treatment with Cu-containing drugs [1, 2]. Copper complexes are considered as an alternative

to the classical platinum containing anticancer drugs (i.e., cisplatin, carboplatin, oxaliplatin) because copper, being an endogenous essential metal for most aerobic organisms, is better tolerated compared to exogenous metals. In addition, the altered copper metabolism displayed by many cancer cells as well as the differential response between normal and tumour cells to copper, laid down the rationale for the development of copper complexes as anticancer agents. Casiopeinas is the generic name of a group of copper complexes designed to be used as antineoplastics and have recently shown promising results as chemotherapeutic agents in animal models and clinical trials [3, 4]. Copper is involved in fundamental biological processes such as respiration, detoxification of ROS (reactive oxygen species) and copper-based drugs show a wide spectrum of action [5–12]. Copper is a biological redox active metal centre ($Cu^{2+} + 1e^- \rightarrow Cu^+$ $E_0 = 0.153$ V) and it is involved in the regulation of ROS ($OH^\cdot$, $O^{2-\cdot}$…) via Fenton and Haber–Weiss type reactions that are responsible for the cleavage of the DNA back-bonds [13–20]. Copper plays a major role in cancer cell oxidative stress that can result in detrimental cellular damage including lipid peroxidation, DNA damage, protein oxidation and enzyme inactivation, which in turn can lead to cell death. One of the pioneer examples of anticancer Cu(II) complexes is $[Cu(phen)_2]^{2+}$ (phen = 1,10-phenanthroline) reported by Sigman and co-workers, that showed a strong anticancer and nuclease activity in the presence of reducing agents [21, 22]. This compound also showed a strong interaction with DNA and it was able to intercalate between the DNA nucleobases due to the presence of the planar aromatic phenanthroline ligand. $[Cu(phen)_2]^{2+}$ opened the route to the synthesis of several metal complexes with DNA intercalative properties using modified phenanthroline ligands such as DPQ, DPPZ and DPPN (DPQ = dipyrido[3,2-*f*:2′,3′-*h*]

quinoxaline, DPPZ = dipyrido[3,2-*a*:2′,3′-*c*]phenazine, and DPPN = benzo[i]dipyrido[3,2-*a*:2′,3′-*c*]phenazine) [23–30]. These complexes showed great DNA binding affinity and anticancer properties but negligible selectivity for tumour tissues. One of the most desired properties for an anticancer drug is the selectivity for cancer cells and, furthermore, for some specific cancer tissues. Steroids are important delivery vectors that can be used for the selective targeting of the drugs toward the cancer cell [31]. The activity of estrogens, the primary female sex hormone, is mediated by the presence of estrogen receptors (ERs) in cells and ERs are over-expressed in breast, ovarian, colon and prostate cancers, which are termed ER+ [32, 33]. ERs therefore, represent interesting anticancer targets [34, 35]. Several cancers are estrogen-dependent (i.e., ovarian cancer) and estrogen derivatives are also used in the treatment of particular cancers. In turn, a host of strategies have been employed to date where derivatives of one of the three major endogenous estrogens (estrone, estradiol, and estriol) have been chemically linked to a platinum-containing anticancer drug [36–38] and radiopharmaceuticals [39]. Recently, we reported the antimicrobial and anticancer activity of steroid derivatives of Cu(II), Pt(II), and Au(I) complexes containing both the female (estradiol) and male (testosterone) steroids [40–42]. Here, we present the syntheses, chemical and electrochemical investigation, the DNA binding and cleavage properties together with a detailed biological study of the anticancer activity on 2D and 3D cancer cell cultures of a series of estrogen-functionalized Cu(II) complexes with the general formula [Cu(N∩N)(estradiol-phen)](NO₃)₂, where (N∩N) is phenanthroline, DPQ, DPPZ and DPPN (Fig. 1). Some of these complexes, which display the simultaneous presence of both the non-toxic metal centre [copper(II)] and of a planar ligand for DNA intercalation properties
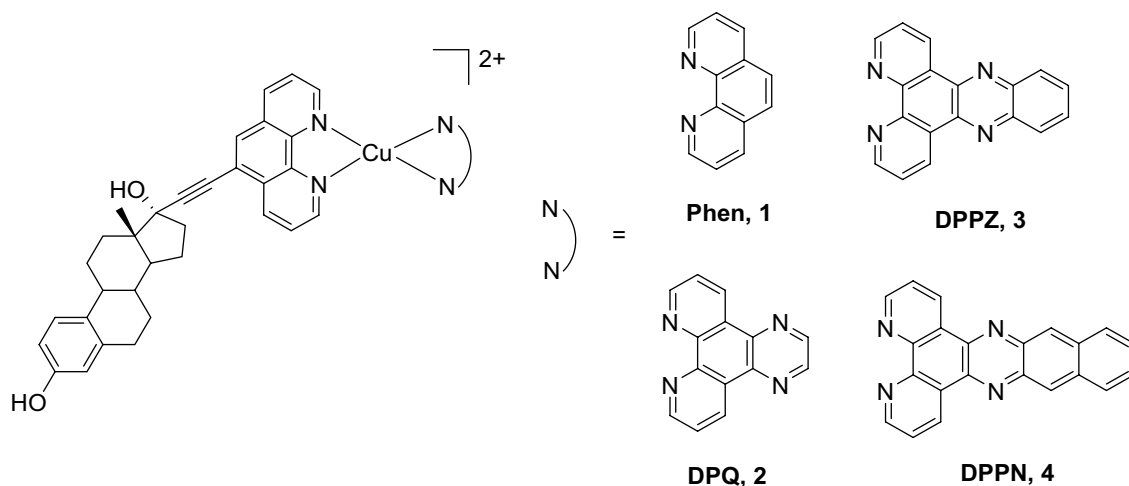

Fig. 1 Structures of the estrogen-derivatives Cu(II) complexes

(Phen, DPQ, DPPZ and DPPN), along with the presence of an estrogen-derivative as a delivery vector to target cancer cells, showed important in vitro and in vivo antimicrobial activity against *Staphylococcus aureus* [41]. The biological activity is assessed using cancer cell lines expressing estrogen receptors (ER+) and not expressing estrogen receptors (ER−) with the aim of verifying the successfulness of copper functionalization.

Materials and methods

All reagents and reactants were purchased from commercial sources. The two sources used were Sigma-Aldrich and Tokyo Chemical Industry. All solvents were used without further purification. The THF (Tetrahydrofuran) used for the Sonogashira coupling reaction, was dried using four angstrom molecular sieves, it was then decanted into a round bottom flask and kept under high vacuum using a Schlenk line while immersed in liquid nitrogen. The THF was then flushed with nitrogen gas. This step was repeated a minimum of three times for the Sonogashira coupling reaction. All NMR spectra were recorded on a Bruker Advance spectrometer with the probe at 293 K, operating at 500 MHz for the ^{1}H and at 125 MHz for ^{13}C{^{1}H} nuclei. Spectra were recorded in CDCl$_3$ using Me$_4$Si as the internal standard. All chemical shifts are in ppm. Infrared (IR) spectra were recorded in the region 4000–400 cm^{-1} on a Perkin Elmer precisely spectrum 100 FT/IR spectrometer. The solid samples were run using ATR. Elemental analyses (carbon, hydrogen and nitrogen) were performed with a PerkinElmer 2400 series II analyzer. ESI mass spectra were recorded in positive mode with a Waters LCT Premier XE Spectrometer.

Electrochemistry: Non-aqueous electrochemical analysis of 1 mM of the copper complexes **1–3** was carried out at a glassy carbon electrode (0.07 cm^2) in a three electrode configuration with Pt wire counter and non-aqueous reference Ag/Ag$^+$ reference electrode in 0.1 M LiClO$_4$/DMF (dimethylformamide). Glassy carbon electrodes were prepared by polishing with alumina suspension on a microcloth followed by sonication in deionised water. Voltammograms were generated over the range +1 to −1 or −2 V vs. Ag/Ag$^+$ in a deaerated solution (N$_2$ bubbling 10 min). Data analysis employed the third cycle of the voltammogram with cathodic scan direction at 100 mV s^{-1} in all cases.

Stability: Compound **4** was taken as reference being the most active. **4** was dissolved in DMF to obtain a 5 mM solution. 200 µL of this solution was diluted to 2.0 mL with phosphate buffer solution (pH = 7.4, [P] = 50 mM). The solution was kept at 37 °C and monitored by HPLC using a Phenomenex Luna C18 (5 µM, 100 Å, 250 mm × 4.60 mm i.d.) column at a flow rate of 1.0 mL/min with 280 nm UV detection at room temperature. The mobile phase was 80:20

acetonitrile (0.1% trifluoroacetic acid): water (0.1% trifluoroacetic acid).

DNA binding experiments

Competitive ethidium displacement

A working solution of 20.0 µM UltraPure calf-thymus DNA [CT-DNA, Invitrogen 15633-019, ε260 = 12,824 M (bp)$^{-1}$ cm^{-1}] along with 25.2 µM ethidium bromide (EtBr) in HEPES buffer (80 mM, pH = 7.2) and NaCl (40 mM) was prepared. Stock solutions of metal complexes, metal salts, and groove binding drugs were prepared at ~4.0 mM in DMSO (dimethylsulfoxide) and diluted further with ultra-pure water. 50 µL of DNA-Et working solution was placed in each well of a 96-well microplate with the exception of the blanks which contained 100 µL HEPES buffer. Serial aliquots of the tested compound were added to the working solutions and the volume was adjusted to 100 µL in each well such that the final concentration of CT-DNA and EtBr was 10.0 µM and 12.6 µM, respectively. The plate was allowed to incubate at room temperature for 1 h before being analyzed using a Bio-Tek synergy HT multi-mode microplate reader with excitation and emission wavelengths being set to 530 and 590 nm, respectively. Concentrations of the tested compounds were optimized such that fluorescence was 30–40% of the initial control (i.e., 50 µL working solution + 50 µL HEPES buffer) at their highest reading. Each drug concentration was measured in triplicate, on at least two separate occasions, and the apparent binding constants were calculated using $K_{app} = K_e \times 12.6/C50$ where $K_e = 9.5 \times 10^6$ M (bp)$^{-1}$.

DNA–ethidium fluorescence quenching

A working solution of 50.0 µM UltraPure calf-thymus DNA [CT-DNA, Invitrogen 15633 019, ε260 = 12,824 M (bp)$^{-1}$ cm^{-1}] along with either 10.0 µM ethidium bromide (EtBr) or Hoechst 33258 (Sigma) in HEPES buffer (80 *m*M, pH = 7.2) and NaCl (40 mM) was prepared. Stock solutions of metal complexes, metal salts, free ligands and groove binding drugs were prepared at ~4.0 mM in DMSO and diluted further with ultra-pure water. 50 µL of DNA-Et or DNA-Hoechst working solution were placed in each well of a 96-well microplate with the exception of the blanks which contained 100 µL HEPES buffer and 5 µM of either Hoechst or EtBr. Serial aliquots of the tested compound were added to the working solutions and the volume was adjusted to 100 µL in each well such that the final concentrations of CT-DNA and EtBr/Hoechst were 25.0 µM and 5 µM, respectively. The plate was allowed to incubate at room temperature for 5 min before being analyzed using a Bio-Tek synergy HT multi-mode microplate reader with

excitation and emission wavelengths being set to 530 and 590 nm for Et detection or 360 nm and 460 nm for Hoechst 33258 detection. Concentrations of the tested compounds were optimized such that fluorescence was 30–40% of the initial control at their highest reading. Each drug concentration was measured in triplicate, on at least two separate occasions. From a plot of fluorescence versus added drug concentration, the Q value is given by the concentration required to effect 50% removal of the initial fluorescence of bound dye.

Viscosity experiments

Fifteen mL dsDNA (deoxyribonucleic acid sodium salt from Salmon Testes, Sigma-Aldrich, D1626-1G) solution was prepared at 1×10^{-3} M in 80 mM HEPES buffer for each working sample.

Stock solutions prepared in DMSO were added according to the gradual increasing [drug]/[DNA] (r) ratios of 0.025, 0.05, 0.075, 0.1, 0.125, 0.15, 0.175 and 0.2. Viscosity values, η, (unit: cP) were directly obtained by running 0# spindle in working samples at 60 rpm via DV-II-programmable digital viscometer equipped with enhanced brookfield UL Adapter at room temperature. Data were presented as η/η_o versus [compound]/[DNA] ratio, in which η_o and η refers to viscosity of each DNA working sample in the absence and presence of complex.

Nuclease activity

Reactions were carried according to the literature procedure [29]. Briefly, in a total volume of 20 μL using 80 mL of HEPES buffer (Fisher) at pH 7.2 with 25 mM NaCl, an aliquot of the stock complex (prepared in DMSO) was mixed with 400 ng of pUC19 (Roche) and 1 μL of 20 mM Na-L-ascorbate. Samples were incubated at 37 °C for 3 h before being quenched with 6× loading dye (Fermentas), containing 10 mM Tris–HCl (pH 7.6), 0.03% bromophenol blue, 0.03% xylene cyanol, 60% glycerol and 60 mM EDTA, then loaded onto agarose gel 1% containing 2.0 μL of Gel-RedTM (10000×). Electrophoresis was completed at 80 V for 1.5 h using a wide mini-sub cell (Bio-Rad) in 1XTAE buffer (Millipore).

Biological studies

Copper complexes **1–4** were dissolved in the minimum DMSO amount prior to cell culture testing. A calculated amount of the stock drug DMSO solution was added to the cell culture media to reach a final maximum DMSO concentration of 0.5%, which had no effects on cell viability. Cisplatin was dissolved in 0.9% sodium chloride solution. MTT [3-(4,5-dimethylthiazol-2-yl)- 2,5-diphenyltetrazolium bromide], cisplatin and ImmunoPure *p*-nitrophenyl phosphate (APH) were obtained from Sigma Chemical Co, St. Louis, USA.

Cell cultures

Human colon (HCT-15) and breast (MCF-7) carcinoma cell lines were obtained from American Type Culture Collection (ATCC, Rockville, MD). Human ovarian 2008 cancer cells were kindly provided by Prof. G. Marverti (Dept. of Biomedical Science of Modena University, Italy). Human ovarian A2780 cancer cells were kindly provided by Prof. M.P.Rigobello (Dept. of Biomedical Science of Padova University, Italy). Human squamous cervical A431 carcinoma cells were kindly provided by Prof. F. Zunino (Division of Experimental Oncology B, Istituto Nazionale dei Tumori, Milan, Italy). Cell lines were maintained in the logarithmic phase at 37 °C in a 5% carbon dioxide atmosphere using RPMI-1640 medium (Euroclone) containing 10% foetal calf serum (Euroclone, Milan, Italy), antibiotics (50 units mL^{-1} penicillin and 50 μg mL^{-1} streptomycin), and 2 mM L-glutamine.

Spheroid cultures

Spheroids were initiated in liquid overlay by seeding 1.5×10^3 A2780 or HCT-15 cells/well in phenol red free RPMI-1640 medium (Sigma Chemical Co.), containing 10% FCS and supplemented with 20% methyl cellulose stock solution. A total of 150 μL of this cell suspension was transferred to each well of a round bottom non-tissue culture treated 96-well plate (Greiner Bio-one, Kremsmünster, Austria) to allow spheroid formation within 72 h.

Cytotoxicity assays

MTT assay

The growth inhibitory effect towards adherent cancer cell lines was evaluated by means of MTT assay. Briefly, $3–8 \times 10^3$ cells/well, dependent upon the growth characteristics of the cell line, were seeded in 96-well microplates in growth medium (100 μL). After 24 h, the medium was removed and replaced with fresh media containing the compound to be studied at the appropriate concentration. Triplicate cultures were established for each treatment. After 72 h, each well was treated with 10 μL of a 5 mg mL^{-1} MTT saline solution, and after additional 5 h of incubation, 100 μL of a sodium dodecylsulfate (SDS) solution in HCl 0.01 M were added. Following an overnight incubation, cell growth inhibition was detected by measuring the absorbance of each well at 570 nm using a Bio-Rad 680 microplate reader. Mean absorbance for each drug dose was expressed

as a percentage of the absorbance of the untreated control well and plotted vs drug concentration. IC_{50} values, the drug concentrations that reduce the mean absorbance at 570 nm to 50% of those in the untreated control wells, were calculated by four parameters logistic (4-PL) model. All the values are the means $\pm$ SD of not less than five measurements starting from three different cell cultures.

Acid phosphatase (APH) assay

An APH-modified assay was used for determining cell viability in 3D spheroids. Briefly, the pre-seeded spheroids were treated with fresh medium containing the compound to be studied at the appropriate concentration. Triplicate cultures were established for each treatment. After 72 h, each well was treated with 100 μL of the assay buffer (0.1 M sodium acetate, 0.1% Triton-X-100, supplemented with ImmunoPure *p*-nitrophenyl phosphate) and, following 3 h of incubation, 10 μL of 1 M NaOH solution was added. The inhibition of the cell growth induced by the tested complexes was detected by measuring the absorbance of each well at 405 nm, using a Bio-Rad 680 microplate reader. Mean absorbance for each drug dose was expressed as a percentage of the untreated control well absorbance (T/C) and plotted vs drug concentration. IC_{50} values, the drug concentrations that reduce the mean absorbance at 405 nm 50% of those in the untreated control wells, were calculated by four parameter logistic (4-PL) model. Evaluation was based on means from at least four independent experiments.

Cellular uptake and DNA binding

A2780 and HCT-15 cells (3×10^6) were seeded in 75 cm² flasks in growth medium (20 mL). After overnight incubation, the medium was replaced and the cells were treated with tested compounds for 24 h. Cell monolayers were washed twice with cold PBS, harvested and counted. Samples were than subjected to three freezing/thawing cycles at −80 °C, and then vigorously vortexed. The samples were treated with highly pure nitric acid (Cu: ≤ 0.5 μg kg^{-1}, TraceSELECT® Ultra, Sigma Chemical Co.) and transferred into a microwave Teflon vessel. Subsequently, samples were submitted to standard procedures using a speed wave MWS-3 Berghof instrument (Eningen, Germany). After cooling, each mineralized sample was analyzed for platinum using a Varian AA Duo graphite furnace atomic absorption spectrometer (Varian, Palo Alto, CA; USA) at the wavelength of 324 nm. The calibration curve was obtained using known concentrations of standard solutions purchased from Sigma Chemical Co. purchased from Sigma Chemical Co.

For DNA binding studies, DNA was extracted and purified by a commercial spin column quantification kit (Qiagen DNeasy Blood and Tissue Kit). Only highly purified samples (A260/A230·1.8 and A280/A260·2.0) were included for analysis to avoid any artefacts. The samples were completely dried and re-dissolved in 200 μL of Milli-Q water (18.2 MΩ) for at least 20 min at 65 °C in a shaking thermomixer, mineralized and analyzed for total Cu content by GF-AAS as described above.

Reactive oxygen species (ROS) production

The production of ROS was measured in A2780 cells (10^4 per well) grown for 24 h in a 96-well plate in RPMI medium without phenol red (Sigma Chemical Co.). Cells were then washed with PBS and loaded with 10 μM 5-(and-6)-chloromethyl-2′,7′-dichlorodihydrofluorescein diacetate acetyl ester (CM–H$_2$DCFDA) (Molecular Probes-Invitrogen, Eugene, OR) for 25 min, in the dark. Afterwards, cells were washed with PBS and incubated with tested compounds. Fluorescence increase was estimated utilizing the wavelengths of 485 nm (excitation) and 527 nm (emission) in a Fluoroskan Ascent FL (Labsystem, Finland) plate reader. Antimycin (3 μM, Sigma Chemical Co), a potent inhibitor of Complex III in the electron transport chain, was used as positive control.

Comet assay

About 4×10^4 A2780 cells were seeded in 25 cm² flasks in growth medium (6 mL). After 24 h, cells were incubated for 3 h with 2.5 μM of tested compounds. Cells were washed twice with cold PBS, harvested, centrifuged, and DNA fragmentation was measured by the alkaline comet assay. Low melting point agarose, 300 μL (Trevigen Inc., Gaithersburg, MD, US) was heated to 37 °C and combined with 2×10^5 cells per mL cell suspension. Each well of a 20-well CometSlide was filled with 30 μL of the cell/agarose suspension. The slides were placed in a 4 °C refrigerator in the dark for 15 min to solidify. Slides were then immersed in 50 mL of pre-chilled lysis solution containing Trizma base, Triton-X-100, DMSO and left at 4 °C for 30 min to facilitate cell membrane and histone removal. After draining excess liquid, the slides were transferred to 50 mL of freshly prepared (same day) alkaline DNA unwinding solution, (200 mmol L^{-1} NaOH, 1 mmol L^{-1} EDTA, pH > 13) and incubated at room temperature in the dark for 20 min. After the unwinding step, electrophoresis was performed at 21 V for 30 min. Slides were then rinsed with distilled water and fixed for 5 min in 70% ethanol. Slides were dried and stained for 5 min at 4 °C with SYBR Green I (Trevigen, Inc.,) diluted 1:10 000 in 10 mmol L^{-1} Tris pH 7.5, 1 mmol L^{-1} EDTA, drained to remove excess staining solution and thoroughly dried at room temperature in the dark.

Results and discussion

The complexes were synthesised as described in the Supporting Information (Scheme 1S). Phenanthroline-5-ethynylestradiol (**A**) is obtained using Sonogashira coupling reaction between 5-bromophenanthroline and ethynylestradiol (Scheme 1).

These kinds of reactions require extreme dry and degassed conditions and inert atmosphere; the reaction was optimized using milder conditions with respect to what was recently reported by us [41]. The yield and purity of the final product highly depend on the catalyst $[Pd(PPh_3)_4]$ which must be freshly prepared (See Supporting Information) and stored under argon at $-20\,^\circ\mathrm{C}$. Briefly, **A** is synthesised by coupling 5-bromophenanthroline and ethynylestradiol in dry THF with 3% of $[Pd(PPh_3)_4]$ as catalyst and diisopropylamine (DIPA) as a base. The replacement of K_2CO_3 with the DIPA for the base and of DMF with THF for the solvent, allowed the reaction to work at r.t. with the formation of less impurities. The reaction success is evident by the disappearance of the alkyne proton resonance at 2.6 ppm in the ^{1}H-NMR spectrum of **A** (Fig. 1S). Phenanthroline-5-ethynylestradiol (**A**), after purification, is mixed in a stoichiometric ratio 1:1 with the correspondent $[Cu(N\cap N)(OH_2)_2](NO_3)_2$ (**B–E**) (Scheme 1S), obtaining the final complexes **1–4** (Fig. 1, where $N\cap N = $ phen—**1**; $N\cap N = $ DPQ—**2**; $N\cap N = $ DPPZ—**3** and $N\cap N = $ DPPN—**4**), as described in detail in the SI. The complexes **1–4**, characterized with IR, El. analyses, mass spectrometry, were stable up to 1 week in saline solution (0.9% NaCl). The electrochemical behavior of complexes **1–3** was investigated and Table 1 summarises the electrochemical data generated. All compounds exhibited a quasi-reversible wave when examined over the potential range 1 to -1 V, being ascribed to the $Cu^{2+/1+}$ redox process (Fig. 1). No clear trend was evident with respect to $Cu^{2+/1+}$ $E_{1/2}$ values for the series **1–3**, all of which fell within a similar interval (-0.29 to -0.27 V vs. Ag/Ag^+) that is within the biological range (-0.2–0.4 V) and they

are likely to undergo reduction ($Cu^{2+} + 1e^- \rightarrow Cu^{1+}$) in physiological cell environment [43]. The relatively positive shift in all values for these complexes relative to that of the starting materials $[Cu(N\cap N)(OH_2)_2](NO_3)_2]$ **B–D** with $E_{1/2}$ values -0.456 V (phen), -0.363 V (DPQ) and -0.311 V (DPPZ), may reflect the electron donating contribution of the estradiol conjugate and geometric alterations upon reduction of the Cu^{2+} centres in **1–3** to the Cu^+ forms. Thus, the processes may be influenced by steric effects of the ligands which overshadow electronic effects [44, 45]. The ΔE_p values of the metal processes indicate a significant departure from a one electron reversible process, with the possibility of coupled chemical reactions and the geometric reorganisation which may accompany the $Cu^{2+/1+}$ redox system. All $I_{p(a)}/I_{p(c)}$ ratios are close to unity for the diffusion-controlled metal process. When the cathodic limit was extended to -2.0 V vs. Ag/Ag^+ the metal underwent further one electron reduction $Cu^{1+/0}$ with subsequent ligand dissociation and (in some cases) re-oxidation (stripping) of plated copper back to Cu^+ upon anodic switching [45]. The quasi reversibility of the $Cu^{2+/1+}$ metal processes (cathodic limit -1 V vs. Ag/Ag^+) indicates little structural change prior to this point, after which it is likely that the complexes undergo decomposition. In the case of compounds **1** and **2**, a significant anodic shift in the $E_{p(c)}$ values for the phenanthroline and DPQ ligands was evident (-1.99 V to -1.3 V and -1.92 V to -1.37 V, respectively). This may reflect a stabilisation of the LUMO state of the ligands, due in this case to the presence of the estradiol group, resulting in a more facile ligand reduction process. The electrochemical behaviour of natural and synthetic estrogens has been reported [46, 47] with ease of oxidation of the phenol group to the phenoxonium ion (a two electron process) being dependent on ring substitution and the solvent–electrolyte system. In these complexes, no estradiol anodic process is visible over the range examined, though clearly the presence of the steroid group influenced the phen, DPQ and DPPZ electrochemistry (Fig. 2; Table 1).

Scheme 1 Sonogashira coupling reaction for the synthesis of phenanthroline-5-ethynylestradiol **A**
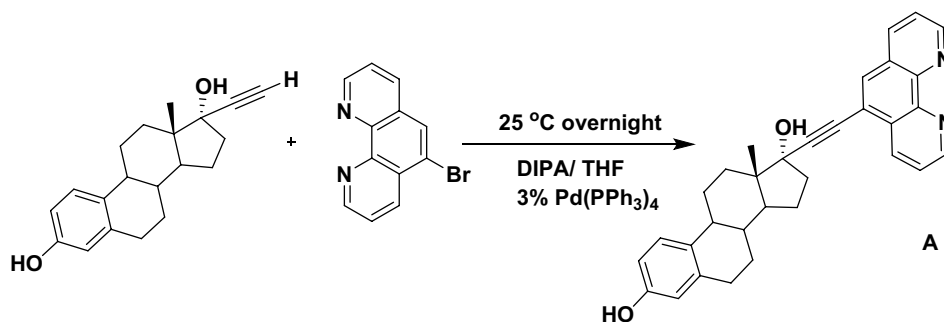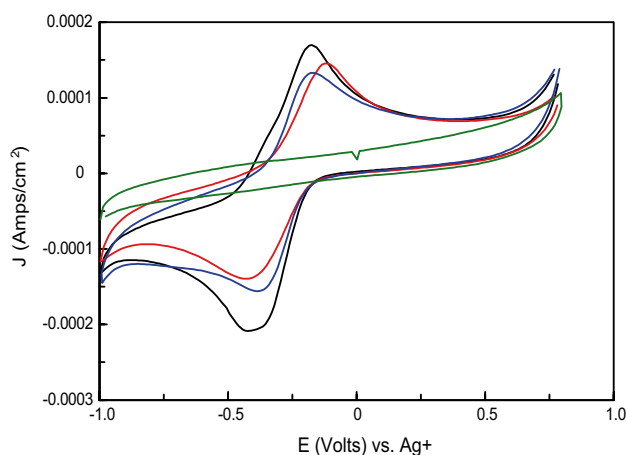
Fig. 2 Cyclic voltammogram of 1 mM solution of complexes **1–3** at a glassy carbon electrode (0.07 cm^2) in a three electrode configuration with Pt wire counter and non-aqueous reference Ag/Ag$^+$ reference electrode in 0.1 M LiClO$_4$/DMF. Scan rate 100 mV s^{-1} over the potential range $+1$ to -1 V vs. Ag/Ag$^+$. Background electrolyte (green circle), **(1)** (blue circle) **(2)** (red circle) **(3)** (black circle)

Binding affinity to calf-thymus and salmon testes DNA

The DNA binding affinity of the series of complexes was determined with calf-thymus and salmon testes duplex DNA polymers using a high throughput ethidium bromide and Hoechst 33258 fluorescence quenching assay [30], competition assay, and viscosity analyses (Fig. 3). The presence of modified phen ligands significantly enhanced the ctDNA binding affinity with K_{app} (apparent DNA binding constant) values rising from 7×10^6 M (bp)$^{-1}$ for complex **1** (phen) to $\sim 10^7$ M (bp)$^{-1}$ for complexes **2** and **3** (DPQ and DPPZ, respectively). Both phenazine complexes had a binding affinity comparable to a reference intercalating antibiotic, Actinomycin D (3×10^7 M (bp)$^{-1}$) [28]. Complex **4**, containing the extended phenazine substituent DPPN, had a lower binding constant of $\sim 5 \times 10^6$ M (bp)$^{-1}$ (Table 2), an effect previously observed with copper(II) ternary complexes [29]. Fluorescence quenching (*Q*) of limited Hoechst 33258 (minor groove binder) and ethidium
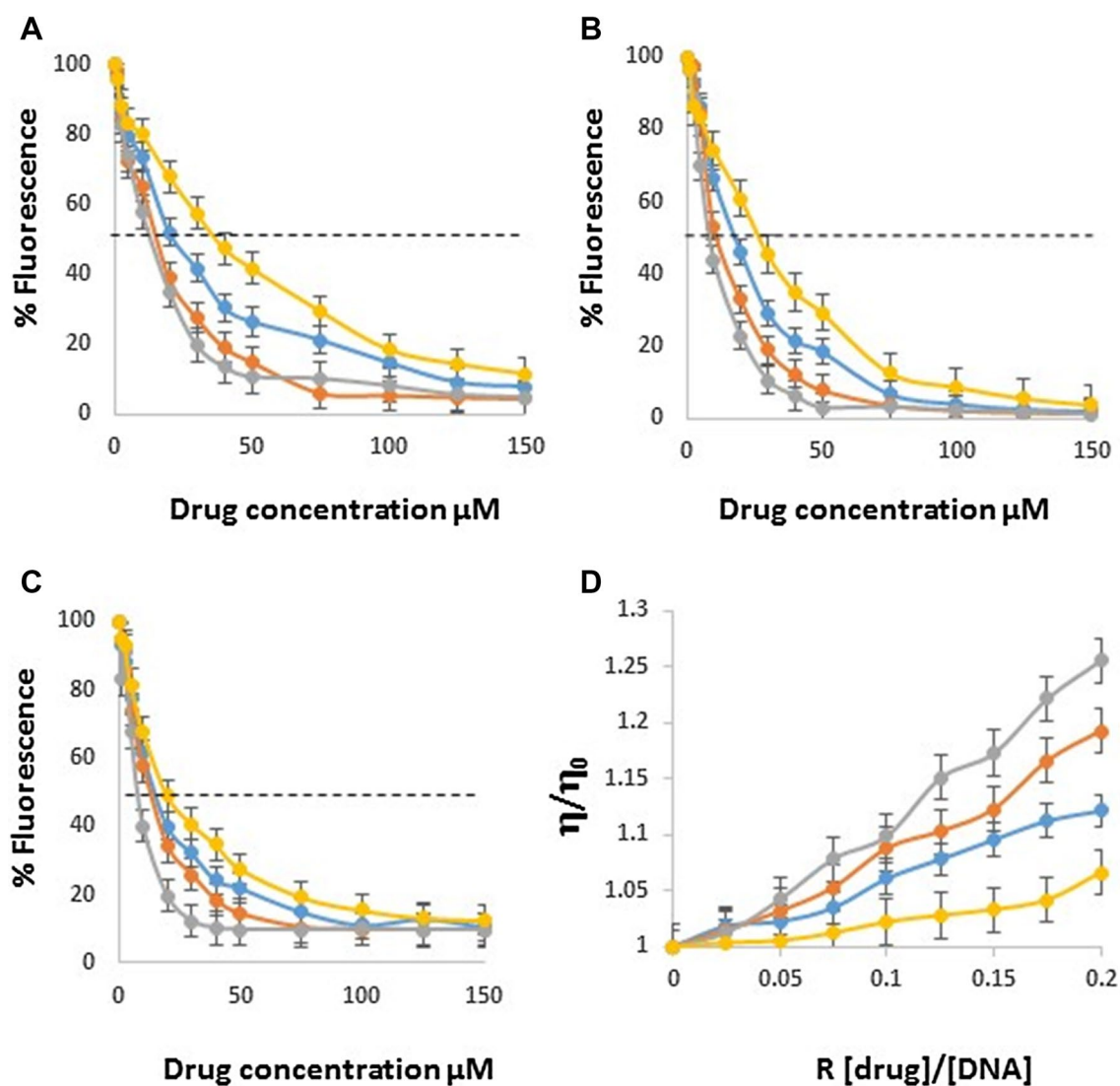
bromide (intercalator) bound ctDNA shows the complex series were not selective in displacing these fluorophores, however, a similar trend was observed in the displacement of both reporters: **3 > 2 > 1 > 4** (Table 2). Viscosity analysis with salmon testes duplex DNA confirmed complex **3**, containing the DPPZ ligand, as a strong intercalator and this hydrodynamic profile was followed by complex **2** (DPQ) and then **1** (phen, which presumably kinks DNA) [48]. Complex **4** with the larger DPPN ligand again displayed attenuated activity (Table 2). Moving from phen to DPQ and DPPZ the planarity and aromaticity of the ligands are optimized for DNA intercalation but the further modification to DPPN leads to steric hindrance thereby preventing efficient DNA binding [49, 50].

The DNA-cleavage ability of the Cu(II) complexes was measured by monitoring the conversion of SC-DNA (form I) to the nicked-circular form (NC, form II) using agarose gel electrophoresis (Fig. 4). SC pUC19 DNA (400 ng) was incubated with increasing complex concentrations (range 0.5–20 μM) in the presence of Na-L-ascorbate (1 mM) for 3 h. All complexes had the ability to convert SC-DNA into the nicked form at 1 μM but complex **3**, the DPPZ-containing complex, displayed the highest cleavage potency being able to cleave plasmid DNA already at 0.5 μM concentration. In absence of Na-L-ascorbate no detectable cleavage was observed.

With the aim of evaluating the antitumor potential of the newly developed Cu(II) complexes **1–4**, and to verify if they are more effective in targeting ER+ cell lines with respect to ER− ones, their in vitro antitumor potential was assessed in a panel of ER+ human cancer cell lines, A431 (cervical), MCF-7 (breast), 2008 (ovarian) and A2780 (ovarian) cancer cells as well as against ER- HCT-15 colon cancer cells. Cells were exposed to the tested compounds for 72 h and the IC$_{50}$ values, calculated from the dose–response curves, are reported in Table 3. The stability of complex **4** in phosphate buffer solution (37 °C, pH 7.4) was previously evaluated via HPLC to confirm that the estrogen moiety, that can be carcinogenic being a steroid, is not released from the coordination sphere of the metal centre. Figure 3S reports the chromatograms

Table 1 Electrochemical data for complexes **1–3**

Complex	Cathodic limit (V)	Cu(I/II)			Cu(0/I)	Ligand redox process			
		$E_{1/2}$ (V)	ΔE_p (V)	$I_{p(a)}/I_{p(c)}$	$E_{p(c)}$ (V)	$E_{p(a)}$ (V)	$E_{p(c)}$ (V)	$E_{1/2}$ (V)	ΔE_p (V)
1	−1	−0.2769	0.198	0.85	–	–	–	–	–
	−2	–	–	–	–	–	−1.3	–	–
2	−1	−0.272	0.296	1	–	–	–	–	–
	−2	–	–	–	–	–	−1.37	–	–
3	−1	−0.287	0.225	0.84	–	–	–	–	–
	−2				−1.17	-1.365	−1.475	−1.42	0.11
	−2						−1.845		

Fig. 3 Binding of complexes **1** (blue circle), **2** (orange circle), **3** (gray circle), and **4** (yellow circle) to **A** ethidium bromide saturated solution of dsDNA (ctDNA); **B** and **C** fluorescence quenching of limited ethidium bromide or Hoechst 33258 bound ds DNA (ctDNA) upon titration of complexes; **D** viscosity properties of complex treated salmon testes dsDNA

Table 2 DNA binding properties of complexes 1–4

Complex	C_{50} (µM)[a]	K_{app} M(bp^{-1})[b]	Q (EtBr, µM)[c]	Q (Hoechst, µM)[c]	n/n_0 ($r = 0.2$)[d]
1	16.13	7.21×10^6	21.5	16.4	1.12
2	12.70	9.43×10^6	15.1	12.9	1.19
3	8.32	1.44×10^7	12.5	9.29	1.25
4	21.50	5.57×10^6	37.6	26.1	1.06

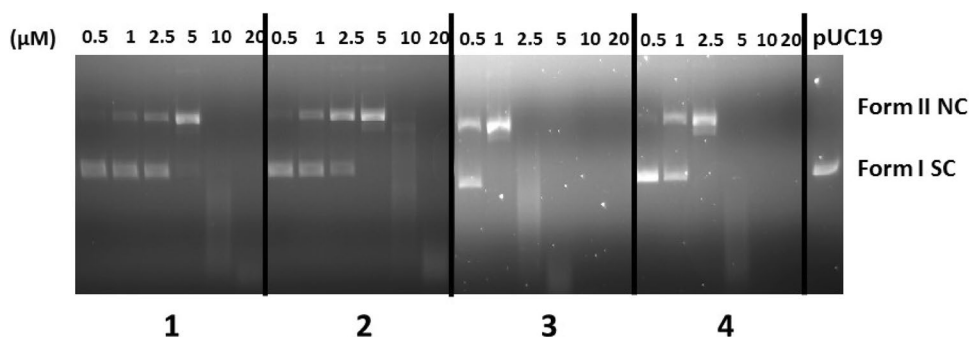[a] C_{50} = concentration required to reduce fluorescence by 50%

[b] $K_{app} = K_e \times 12.6/C_{50}$ where $K_e = 9.5 \times 10^6$ M (bp^{-1})

[c] Reduction of 50% initial fluorescence from DNA-bound dye by tested compound (µM)

[d] Relative viscosity value at $r = 0.20$

Fig. 4 DNA cleavage. Agarose gel electrophoresis patterns of SC pUC19 DNA incubated with complexes **1–4** (0.5–20 μM) in HEPES buffer at 37 °C for 3 h

Table 3 In vitro cytotoxic activity of complexes **1**-**4**

	IC$_{50}$ (μM) ± SD				
	A2780	2008	A431	MCF-7	HCT-15
1	0.6 ± 0.1	1.5 ± 0.7	1.3 ± 0.3	1.0 ± 0.2	0.8 ± 0.3
2	0.3 ± 0.02	1.6 ± 0.4	2.0 ± 0.4	1.2 ± 0.3	0.8 ± 0.1
3	0.1 ± 0.04	0.2 ± 0.1	0.1 ± 0.1	0.7 ± 0.2	0.5 ± 0.2
4	0.04 ± 0.01	0.6 ± 0.03	0.3 ± 0.03	0.9 ± 0.2	0.5 ± 0.2
Cisplatin	2.6 ± 0.8	2.2 ± 0.6	1.7 ± 0.3	7.6 ± 0.2	13.9 ± 1.7

Cells (3–8 × 10^3 mL^{-1}) were treated for 72 h with increasing concentrations of the tested compounds. Cytotoxicity is assessed by MTT test. IC$_{50}$ values (μM) were calculated by a four parameter logistic model ($p < 0.05$)

SD standard deviation

Table 4 In vitro cytotoxicity against ovarian and colon cancer cell spheroids

|	IC$_{50}$ (μM) ± SD	
	A2780	HCT15
1	10.6 ± 1.0	7.7 ± 1.6
2	7.7 ± 1.0	9.9 ± 1.0
3	4.1 ± 0.1	9.2 ± 0.6
4	3.0 ± 0.02	8.6 ± 0.5
Cisplatin	91.3 ± 5.4	68.3 ± 2.1

Spheroids (1.5 × 10^3 cells/well) are treated for 72 h with increasing concentrations of test compounds. The growth inhibitory effect was evaluated by means of the APH test. IC$_{50}$ values were calculated from the dose-survival curves by the four parameter logistic model ($p < 0.05$)

SD standard deviation

of **4** immediately upon dissolution and after 72 h where it is clearly visible that the complex is highly stable with negligible amount of steroid released.

All the complexes promoted a significant cytotoxic activity, with IC$_{50}$ values in the low-/sub-micromolar range against all cancer cell lines tested. In general, all derivatives were more effective in inducing cancer cell death with respect to the reference metallodrug cisplatin. Among the newly developed Cu(II) compounds, **3** and **4** were the most potent derivatives, with IC$_{50}$ calculated towards all tested cancer cells in the sub-micromolar range. These data indicate that by increasing the lipophilicity of the diamine ligand in turn increased the cytotoxic activity of the related copper(II) complex. On the other hand, complexes **1–3** displayed equally cytotoxic properties against ER+ and ER− cancer cells, thus suggesting the inability of these complexes to selectively target ER+ cancer cells. Conversely, **4** proved to be slightly more effective against ER+ A2780 ovarian cancer cells.

The in vitro antitumor potential of the Cu(II) complexes was also examined in 3D cell culture models of ovarian (ER+) and colon (ER−) cancers. Actually, even if the 2D cell cultures is the most used in vitro method for screening of potential therapeutics due to its simplicity, reproducibility, and low cost, this method is unable to reproduce the

properties of in vivo solid tumors. 3D cell cultures, possessing several features that more closely mimic the heterogeneity and complexity of in vivo tumors, are recognized to be more predictive for in vivo results than conventional 2D cell cultures [51]. The cancer spheroids were treated with copper(II) complexes or cisplatin for 72 h and cell viability was assessed by means of the acid phosphatase (APH) assay (Table 4).

These tested non-proliferative and very resistant tumour models, **1–4** were extremely effective, being more active than cisplatin against both A2780 ovarian and HCT-15 colon cancer cell spheroids. In particular, **3** and **4** were confirmed as the most potent derivatives, being about 30 and 9 times more effective than cisplatin in A2780 and HCT-15 3D cell cultures, respectively.

Complexes **1–3** showed a similar activity toward ER+ and ER− cancer cells, thus confirming the results obtained in the 2D system and supporting the hypothesis of their inability to selectively target ER+ cancer cells. On the contrary, in 3D systems, compound **4** again showed a certain degree of selectivity towards A2780 cancer cells, being about 3 times more effective in ER+ human ovarian cancer cells with respect to ER− human colon cancer cells. With the aim of identifying a possible correlation between cytotoxic
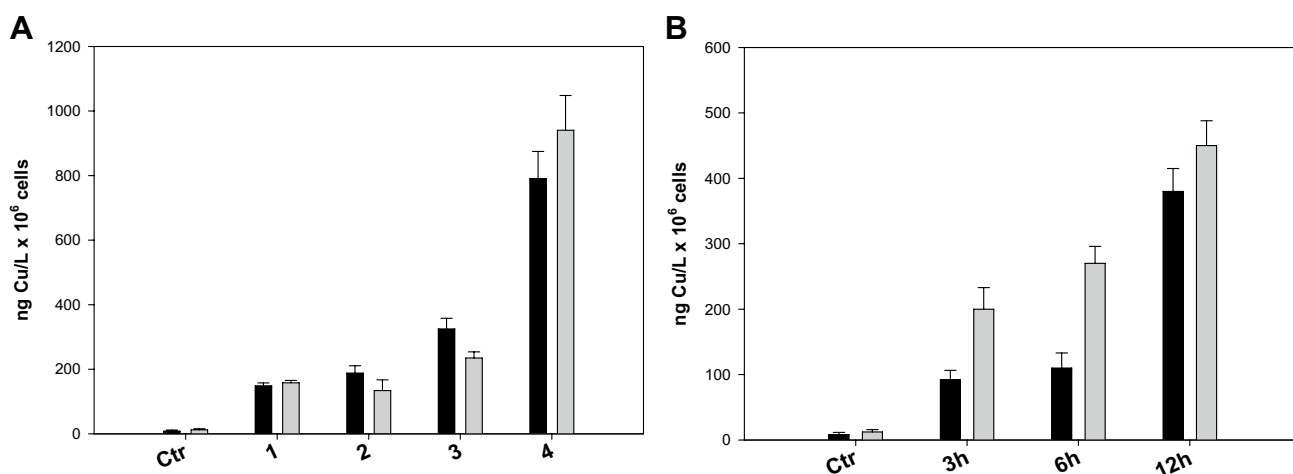
Fig. 5 Cellular uptake in A2780 (grey bars) and HCT-15 (black bars) cancer cells. **A** Cancer cells were incubated with 0.5 μM of copper complexes for 24 h, and cellular copper content was detected by GF-AAS analysis. **B** Cancer cells were incubated with 0.5 μM of copper complex **4** for 3, 6 or 12 h, and cellular copper content was detected by GF-AAS analysis. Error bars indicate the standard deviation

activity and cellular accumulation, cellular copper content was measured in ER+ A2780 and ER− HCT-15 cancer cells treated for 24 h with equimolar concentrations of the tested compounds. The cellular copper levels were quantified by means of GF-AAS analysis, and the results, expressed as ng Cu per 10^6 cells, are shown in Fig. 5A.

Although to a different extent, all derivatives were able to cross the cancer cell membrane and enter cancer cells. Complexes **1**–**3** were able to similarly accumulate into ovarian and colon cancer cells, whereas derivative **4** was significantly more effective in entering ER+ A2780 cancer cells. Interestingly, **4** accumulated in a time-dependent manner, actually both ovarian and colon cancer cells displayed a time-dependent increase in cellular copper content (Fig. 5B). By matching cytotoxic activity data with those arising from cellular uptake quantification, a linear and direct correlation is evidenced (Fig. 4S).

Copper species have been regarded as redox active compounds and it was shown that copper complexes may catalyze the reaction of hydrogen peroxide in the form of Fenton-like reactions inside the cell to produce ROS, thus altering cellular redox homeostasis and driving cells towards oxidative stress. On these bases, we evaluated cellular ROS levels in A2780 cells treated with 10 μM of the most effective complex **4**. ROS production was monitored using the peroxide-sensitive fluorescent probe CM-H$_2$DCFDA [5-(and-6)-chloromethyl-2′,7′-dichlorodihydrofluorescein diacetate, acetyl ester]. Antimycin, a classical inhibitor of the mitochondrial respiratory chain at the level of complex III, was used as a positive control.

The results, expressed as arbitrary units of fluorescence as a function of time, are shown in Fig. 6A. Interestingly, **4** was able to substantially stimulate the production of hydrogen peroxide in a time-dependent manner, to a rather
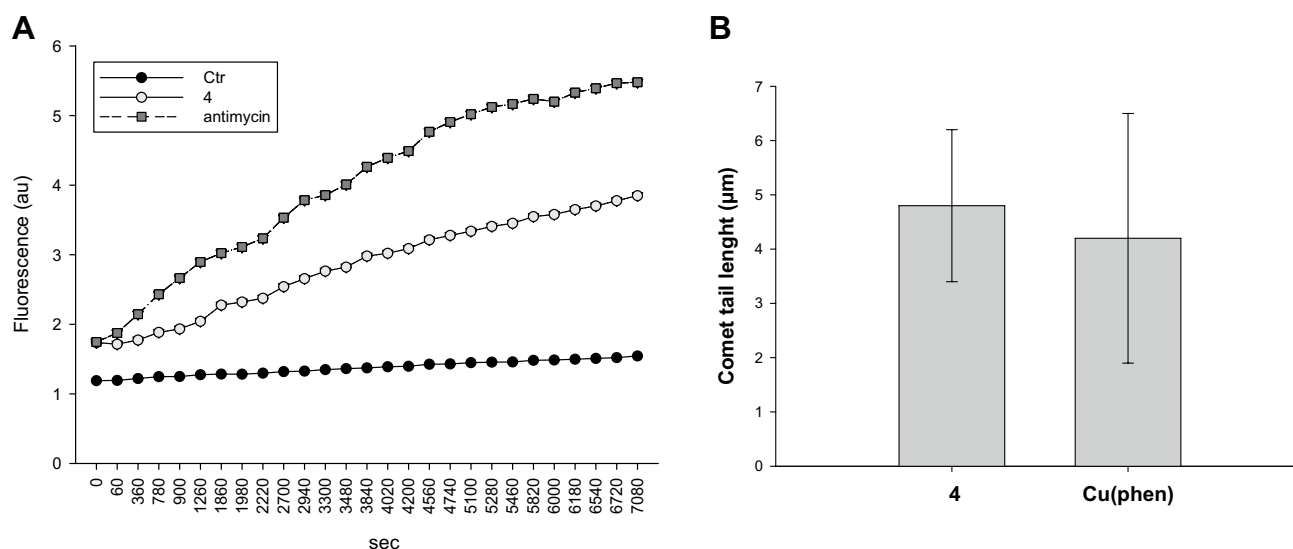
similar extent as the respiratory chain complex III inhibitor, antimycin.

In addition, we confirmed the results obtained in cell-free experiments (DNA binding, cleavage and viscosimetry studies) and we assessed the ability of the newly synthesised copper(II) complexes to bind and to damage the DNA within intact cancer cells. The DNA damage in A2780 cells was studied after treatment with **4** for 3 h, using alkaline single cell gel electrophoresis (Comet assay, Fig. 6B). The results were compared with those obtained after treatment of A2780 cells with equitoxic concentrations of dichloro(1,10-phenanthroline)copper(II), [Cu(phen)]. Similar to [Cu(phen)], the **4**-treated cells displayed a statistically significant increase in electrophoretic migration of the DNA fragments, evidenced by well-formed comets. To analyze the cellular DNA binding, cells A2780 were treated with complexes **1**–**4** for 24 h, as described in the experimental section, and the amount of copper covalently bound to the extracted DNA was determined via GF-AAS. All the complexes showed very little capacity to bind to the DNA in a covalent mode comparison to the endogenous Cu control (Fig. 5S), confirming that the interaction between the complexes and DNA is purely electrostatic (intercalation).

These results confirmed the ability of these copper(II) complexes to target DNA in intact cancer cells.

Conclusions

Four copper(II)-based complexes containing the female steroid estradiol, were synthesised with the aim to selectively target cancer cells overexpressing the estrogen receptors. The complexes proved to be very effective against all

A

B

Fig. 6 Mechanistic studies: ROS production (**a**) and DNA damage (**b**) in A2780 cancer cells. **A** Cells were preincubated in PBS/10 mM glucose medium for 20 min at 37 °C in the presence of 10 μM CM-DCFDA and then treated with derivative **4** (10 μM) or antimycin (3 μM). The fluorescence of DCF was measured as reported in the experimental section. **B** A2780 cells were treated for 3 h with 0.5 μM of compound **4** and then processed for the comet assay as reported in the experimental section. Comet tail length was calculated from the center of the cell and measured in micrometers with ImageJ software. The error bars indicate the standard deviation

the cancer cell lines examined (low and sub μM IC_{50} values), much more with respect to the reference drug cisplatin, complex **4** being the most effective one. Although no selectivity was observed for ER+ with respect to ER− cells for complexes **1–3**, for complex **4** a slight difference in anticancer potential towards ER+ cancer cells was underlined. Actually, a linear correlation was obtained in ER+ cancer cells between drug uptake and IC_{50} values. In general, the antiproliferative activity and cellular uptake increased with the lipophilic character of Cu(II) complexes, thus indicating that cellular internalisation is principally due to a passive diffusion mechanism with a minimum role of the estrogen moiety. From a mechanistic point of view, cell-free fluorescent analyses evidenced for all copper complexes strong intercalation properties but a discrimination between major and minor groove was not observed. Cu(II) complexes were redox active at the physiological range and were able to cleave DNA at very low concentrations (0.5 μM) in the presence of a reducing agent. More interestingly, cell studies confirmed their ability to target DNA and to induce ROS production in ER+ human cancer cells.

Compliance with ethical standards

Conflict of interest There are no conflicts to declare.

References

1. Santini C, Pellei M, Gandin V, Porchia G, Tisato F, Marzano C (2014) Chem Rev 114:815–862
2. Kellett A, Molphy Z, McKee V, Slator C (2019) Recent advances in anticancer copper compounds. In: Casini A, Vessieres A, Meier-Menches SM (eds) Chapter 4, Metal based anticancer agents. The Royal Society of Chemistry, pp 91–119. https://doi.org/10.1039/9781788016452-00091
3. Trejo-Solis C, Jimenez-Farfan D, Rodriguez-Enriquez S, Fernando-Valverse F, Cruz-Salgado A, Ruiz-Azuare L, Sotelo J (2012) BMC Cancer 12:156
4. Silva-Platas C, Villegas CA, Oropeza-Almazán Y, Carrancá M, Torres-Quintanilla A, Lozano O, Valero-Elizondo J, Castillo EC, Bernal-Ramírez J, Fernández-Sada E, Vega LF, Treviño-Saldaña N, Chapoy-Villanueva H, Ruiz-Azuara L, Hernández-Brenes C, Elizondo-Montemayor L, Guerrero-Beltrán CE, Carvajal K, Bravo-Gómez ME, García-Rivas G (2018) Oxid Med Cell Longev. https://doi.org/10.1155/2018/8949450 (**ID 8949450**)
5. Ming LJ (2003) Med Res Rev 23:697–762
6. Yu Y, Kalinowski DS, Kovacevic Z, Siafakas AR, Jansson PJ, Stefani C, Lovejoy DB, Sharpe PC, Bernhardt PV, Richardson DR (2009) J Med Chem 52:5271–5294
7. Chen D, Peng F, Cui QC, Daniel KG, Orlu S, Liu J, Dou QP (2005) Front Biosci 10:2932–2939
8. Chen ZF, Tan MX, Liu LM, Liu YC, Wang HS, Yang B, Peng Y, Liu HG, Liang H, Orvig C (2009) Dalton Trans 48:10824–10833

9. Laws K, Binjeva-Todd G, Eskandari A, Lu C, O'Reilly N, Suntharalingam K (2018) Angew Chem Int Ed 57:287–291
10. Lu C, Laws K, Eskandari A, Suntharalingam K (2017) Dalton Trans 46:12785–12789
11. Balzarini J, Keyaerts E, Vijgen L, Vandermeer F, Stevens M, De Clercq E, Egberink H, Van Ranst M (2006) J Antimicrob Chemother 57:472–481
12. Kellett A, Molphy Z, Slator C, McKee V, Farrell NP (2019) Chem Soc Rev 48:971–988
13. Molphy Z, Montagner D, Bhat SS, Slator C, Long C, Erxleben A, Kellett A (2018) Nucleic Acid Res 46:9918–9931
14. Fleming AM, Muller JG, Li L, Burrows CJ (2011) Org Biomol Chem 9:3338–3348
15. Buchtik R, Travnicek Z, Vanco J (2012) J Inorg Biochem 116:163–171
16. Montagner D, Gandin V, Marzano C, Erxleben A (2015) Inorg Chim Acta 145:101–107
17. Jopp M, Becker J, Becker S, Miska A, Gandin V, Marzano C, Schindler S (2017) Eur J Med Chem 132:274–281
18. Slator C, Molphy Z, McKee V, Long C, Brown T, Kellett A (2018) Nucleic Acid Res 46:2733–2750
19. Müller S, Versini A, Sindikubwabo F, Belthier G, Niyomchon S, Pannequin J, Grimaud L, Cañeque T, Rodriguez R (2018) PLoS One 13:e0208213
20. Zuin Fantoni N, Molphy Z, Slator C, Menounou G, Toniolo G, Mitrikas G, McKee V, Chatgilialoglu C, Kellett A (2019) Chem Eur J 25:221–237
21. Sigman DS, Zelenko O, Gallagher J, Xu Y (1998) Inorg Chem 37:2198–2204
22. Meijler MM, Zelenko O, Sigman DS (1997) J Am Chem Soc 119:1135–1136
23. Zhou H, Zheng C, Zou G, Tao J (2002) Gong D. Int J Biochem Cell Biol 34:678–684
24. Pitie M, Donnadieu B, Meunier B (1998) Inorg Chem 37:3486–3489
25. Trejo-Solís C, Jimenez-Farfan D, Rodriguez-Enriquez S, Fernandez-Valverde F, Cruz-Salgado A, Ruiz-Azuara R, Sotelo J (2012) BMC Cancer 12:1471–2407
26. Thomas AM, Nethaji M, Mahadevan S, Chakravarty AR (2003) J Inorg Biochem 94:171–178
27. Charefa F, Sebtia N, Arrara L, Djarmounia M, Boussoualima N, Baghiania A, Khennoufb S, Damend SAL, Mubarakd MS, Peterse DG (2015) Polyhedron 85:450–456
28. Tummalapalli K, Vasavi CS, Munusami P, Pathak M, Balamurali MM (2017) Int J Biol Macromol 95:1254–1266
29. Molphy Z, Prisecaru A, Sleitor C, Barron N, McCann M, Colleran J, Chandran D, Gathergood N, Kellett A (2014) Inorg Chem 53:5392–5404
30. McCann M, McGinley J, Ni K, O'Connor M, Kavanagh K, McKee V, Colleran J, Deveraux M, Gathergood N, Barron N, Prisecaru A, Kellett A (2013) Chem Commun 49:2431–2433
31. Le Bideau F, Dagorne S (2013) Chem Rev 113:1193–7850
32. Provencher-Mandeville J, Descoteaux C, Mandal SK, Leblanc V, Asselin E, Berube G (2008) Bioorg Med Chem Lett 18:2282–2287
33. Provencher-Mandeville J, Debnath C, Mandal SK, Leblanc V, Parent S, Asselin E, Berube G (2011) Steroids 76:94–103
34. Sanchez-Cano C, Huxley M, Ducani C, Hamad AE, Browning M, Navarro-Ranninger C, Quiroga AG, Rodger A, Hannon MJ (2010) Dalton Trans 39:11365–11374
35. Huxley M, Sanchez-Cano C, Browning MJ, Navarro-Ranninger C, Quiroga AG, Rodger A, Hannon MJ (2010) Dalton Trans 39:11353–11364
36. Altman J, Castrillo T, Beck W, Bernhardt G, Schoenenberger H (1991) Inorg Chem 30:4085–4088
37. Kenny RG, Marmion CJ (2019) Chem Rev 119:1058–1137
38. Saha P, Descôteaux C, Brasseur K, Fortin S, Leblanc V, Parent S, Asselin E, Bérubé G (2012) Eur J Med Chem 48:385–390
39. Linden HM, Peterson LM, Fowler AM (2018) PET Clin 13:415–422
40. Velle A, Maguire R, Kavanagh K, Montagner D, Sanz-Miguel PJ (2017) ChemMedChem 12:841–844
41. Barrett S, Delaney S, Kavanagh K, Montagner D (2018) Inorg Chim Acta 479:261–265
42. Kitteringham E, Andriollo E, Gandin V, Montagner D, Griffith D (2019) Inorg Chim Acta 495:118944. https://doi.org/10.1016/j.ica.2019.05.043
43. Zheng P, Eskandari A, Lu C, Laws K, Aldous L, Suntharalingam K (2019) Dalton Trans 48:5892–5896
44. Magni M, Colomba A, Dragonetti C, Mussini P (2014) Electrochim Acta 141:324–330
45. Justin Thomas KR, Tharmaraj P, Chandrasekhar V, Bryan D, Cordes AW (1994) Inorg Chem 33:5382–5390
46. Mitrofanov M, Manowong M, Rousselin Y, Brandes S, Guilard R, Bessmertbykh-Lemeume A, Chen P, Kadish KM, Goulioukina N, Beletskaya I (2014) Eur J Inorg Chem 2014:3370–3386
47. Ngundi MN, Sadik OA, Yamaguchi T, Suye SI (2003) Electrochem Commun 5:61–67
48. Niyazi H, Hall JP, O'Sullivan K, Winter G, Sorensen T, Kelly JM, Cardin CJ (2012) Nat Chem 4:621–628
49. McGivern TJP, Slator C, Kellett A, Marmion CJ (2018) Mol Pharm 15:5058–5071
50. Ude Z, Kavanagh K, Twamley B, Pour M, Gathergood N, Kellett A, Mamion CJ (2019) Dalton Trans 48:8578–8593
51. Kunz-Schughart LA, Freyer JP, Hofstaedter F, Ebner R (2004) J Biomol Screen 9:273–282

Affiliations

Stephen Barrett[1] · Michele De Franco[2] · Andrew Kellett[3] · Eithne Dempsey[1] · Cristina Marzano[2] · Andrea Erxleben[4] · Valentina Gandin[2] · Diego Montagner[1]

[1] Department of Chemistry, Maynooth University, Maynooth, Ireland

[2] Department of Pharmaceutical and Pharmacological Sciences, University of Padova, Padua, Italy

[3] School of Chemical Sciences and National Institute for Cellular Biotechnology, Dublin City University, Glasnevin, Dublin 9, Ireland

[4] School of Chemistry, National University of Ireland Galway, Galway, Ireland